Measuring Enzyme Kinetics Using Isothermal Titration Calorimetry

Justin M. Di Trani

Department of Chemistry
McGill University
Montreal, Canada

July 2018

A thesis submitted to McGill University
in partial fulfillment of the requirements of the degree of
Doctor of Philosophy

Contributions

Chapter 2: Measuring Rapid Time-scale Reaction Kinetics Using Isothermal Titration Calorimetry

Chapter 2 was reproduced with permission from: Justin M. Di Trani, Nicolas Moitessier, Anthony K. Mittermaier. Measuring Rapid Time-Scale Reaction Kinetics Using Isothermal Titration Calorimetry. *Analytical Chemistry* **83(13),** 7022-7030 (2017). I performed all the experiments, interpreted and analysed all the data with the help of Dr. Mittermaier and created all the figures. The article was co-written by myself, Dr. Moitessier and Dr. Mittermaier.

Chapter 3: Complete Kinetic Characterization of Enzyme Inhibition in a Single Isothermal Titration Calorimetry Experiment

Chapter 3 was reproduced with permission from: Justin M. Di Trani, Nicolas Moitessier and Anthony K. Mittermaier. Complete Kinetic Characterization of Enzyme Inhibition in a Single Isothermal Titration Calorimetric Experiment. *Analytical Chemistry* **90(14),** 8430-8435 (2018). I performed all the experiments, interpreted and analysed all the data with the help of Dr. Mittermaier and created all the figures. The article was co-written by myself, Dr. Moitessier and Dr. Mittermaier.

Chapter 4: Rapid Measurement of Inhibitor Binding Kinetics by Isothermal Titration Calorimetry

Chapter 4 was reproduced with permission from: Justin M. Di Trani, Stephane De Cesco, Rebecca O'Leary, Jessica Plescia, Claudia Jorge do Nascimento, Nicolas Moitessier and Anthony K. Mittermaier. Rapid Measurement of Inhibitor Binding Kinetics by Isothermal Titration Calorimetry. *Nature Communications* **9(893),** (2018). Inhibitors were synthesized by Stephane De Cesco and Jessica Plescia. Experiments were performed by Repecca O'Leary and myself. I interpreted and

analysed experiment with the help of Dr. Mittermaier and created all the figures. The article was co-written by myself, Dr. Moitessier and Dr. Mittermaier.

Abstract

Enzymes play a central role in virtually all biological processes. Consequently, mutations that lead to alterations in enzyme activity can result in diseased states. Modern drug discovery is primarily based on developing small molecule inhibitors of biological macromolecules, in order to correct their function and restore regular physiology. The properties of inhibitors are tested throughout the drug development process to help guide structural optimization making rapid approaches for quantifying enzyme activity in the presence of inhibitors imperative. There are various techniques for measuring enzyme kinetics including isothermal titration calorimetry (ITC) which works by directly measuring heat flow, a near universal feature of chemical reactions. By measuring heat flow ITC is able to perform measurements under conditions which would be inaccessible using other techniques. In addition, ITCs have become a standard instrument in biochemistry laboratories. In this thesis, we present several novel methods for measuring enzyme kinetics using isothermal titration calorimetry. In chapter 2 we demonstrate that isothermal titration calorimeters (ITCs) are capable of measuring heat flow with sub-second precision and develop a technique for quantitatively modelling rapid time-scale kinetics. Importantly, this approach is implemented into the techniques described in chapters 3 and 4 allowing for quantitative modelling of rapid kinetics throughout the thesis. Chapter 3 describes a technique for extracting both the strength and mode of enzyme inhibitors in a single experiment. In chapter 4 we present a pair of complementary tech-

niques capable of rapidly measuring association and dissociation kinetics as well the strength of enzyme-inhibitor interactions. Importantly, all of the methods presented here are time/sample efficient and possess all of the inherent advantages of ITC.

Résumé

Les enzymes jouent un rôle principal dans pratiquement tous les processus biologiques. Par conséquent, les mutations qui mènent à des changements par rapport à l'action des enzymes peuvent entraîner des conditions de maladies. La production de médicaments actuels est principalement basée sur le développement d'inhibiteurs à petites molécules de macromolécules biologiques afin de corriger leur fonction et de rétablir la physiologie normale. Les propriétés des inhibiteurs sont testées tout au long du processus de développement du médicament afin de guider l'optimisation structurale, rendant impératif des méthodes rapides pour quantifier l'activité enzymatique en présence d'inhibiteurs. Il existe diverses techniques de mesure de cinétique enzymatique, y compris la Titration Calorimétrique Isotherme (TCI) qui fonctionne en mesurant directement le flux de chaleur, une caractéristique quasi-universelle des réactions chimiques. En mesurant le flux de chaleur, la TCI dispose alors de la capacité d'effectuer des mesures dans des conditions qui seraient inaccessibles en utilisant d'autres techniques. De plus, la TCI est devenue une méthode standard dans les laboratoires de biochimie. Dans cette thèse, nous présentons plusieurs nouvelles méthodes pour mesurer la cinétique enzymatique en utilisant la Titration Calorimétrique Isotherme. Au chapitre 2, nous démontrons que la TCI permet de mesurer le flux de chaleur avec une précision sous la seconde et développons une technique de modélisation quantitative d'échelle de temps de la cinétique à taux rapide. Étant importante, cette approche est implantée dans les techniques

décrites dans les chapitres 3 et 4, impliquant la modélisation quantitative de la cinétique à taux rapide tout au long de la thèse. Le chapitre 3 décrit une technique pour déterminer le mode et la force des inhibiteurs d'enzymes dans une seule expérience. Dans le chapitre 4, nous présentons deux techniques complémentaires permettant de mesurer rapidement la cinétique d'association et de dissociation, ainsi que la force des interactions d'inhibiteurs d'enzymes. Toutes les méthodes présentées ici sont efficaces en matière de temps et d'échantillonnage, et disposent de tous les avantages inhérents à la TCI.

Acknowledgements

Firstly, I would like to take this opportunity to extend my sincerest and abundant gratitude to my supervisor Dr. Anthony Mittermaier for being a tremendous mentor throughout my doctoral studies. Tony has taught me a great deal about many aspects of scientific research including mathematical biophysical analysis, being able to clearly and precisely communicate scientific findings, approaching problems with an open mind, ways of organizing and visualizing data in order to recognize patterns/extract meaningful information from data, and always striving for a high level of scientific rigor. Tony has always been extremely patient and clear, making him an amazing teacher. Also, I have thoroughly enjoyed scientific conversations with Tony. The project Tony and I have worked on has been extremely stimulating and enjoyable. Moving forward I feel confident that the tools I have developed in Tony's lab give me a sound basis for the remainder of my scientific career.

Thank you to the members of my Ph.D. committee Dr. Hanadi Sleiman and Dr. Scott Bohle for their support and questions during my yearly meeting which served to strengthen the work I have carried out. Also, I wish to thank Dr. Nicolas Moitessier for the fruitful collaboration as well as his insight and contributions when writing the manuscripts. I am grateful to Chantal Marotte for her help in administrative matters over the years. Thank you to any other McGill faculty, students, or staff who have helped me during my time at McGill.

I would like to thank my immediate family. My mother Sharon MacCready and

father Rocco Di Trani have always encouraged me to follow my desire to pursue a Ph.D. and have provided me with the support to do so. Also, thank you to my siblings Kyle, Emily and Brittany, you have always been a huge source of inspiration for me. Also, I would like to thank all of my extended family for their interest and encouragement during my Ph.D. Thank you to all of my friends both in Montreal and Toronto for showing interest in my work and supporting me by providing a much needed outlet from the grind of a Ph.D. through sports and adventure. Also, thank you to my girlfriend Charlotte for the encouragement and inspiration during the last part of my Ph.D.

Thank you to the members of the Mittermaier group past and present. In particular, I would like to thank Robert Harkness a fellow Ph.D. student who has always been there for stimulating and inspiring discussion. Also, thank you to all the undergraduate students I have worked with over the years who have helped motivate me and provided good productivity. Lastly, thank you to the members of the Cosa lab for their help and camaraderie during the challenges of doctoral studies.

Contents

List of Figures

List of Tables

List of Abbreviations

BAEE Nα-Benzoyl-L-arginine ethyl ester hydrochloride

BSA bovine serum albumin

BTK Bruton's tyrosine kinase

CCR2 chemokine receptor 2

CDK8/CycC cyclin-dependent kinase 8/cyclin C

EDTA ethylenediaminetetraacetic acid

ERM empirical response model

hA$_3$R human adenosine A$_3$

IPTG isopropyl β-D-1-thiogalactopyranoside

ITC isothermal titration calorimetry

ITCs isothermal titration calorimeters

LWB Lineweaver-Burk

MES 2-(N-morpholino)ethanesulfonic acid

MM Michaelis-Menten

NMR Nuclear magnetic resonance

PIPES piperazine-N,N'-bis(2-ethanesulfonic acid)

POP Prolyl oligopeptidase

SAR structure affinity relationship

SKR structure kinetics relationships

SVD singular value decomposition

TRH thyrotropin-releasing hormone

ZPG-pN carboxybenzyl-Gly-Pro-nitroanilide

ZPP Z-Pro-Prolinal

Chapter 1

Introduction

"Where's Wallace?"

—D'Angelo Barksdale

1.1 Enzymes

1.1.1 Enzyme Function

1.1.1.1 Enzymes: Biological Catalysts

Enzymes are macromolecular biological catalysts that accelerate vital reactions in living organisms. In the simplest case, the enzyme catalysis mechanism involves binding of a reactant (referred to as an enzyme's substrate) in the active site where it is catalytically converted to product, followed by product release (Equation 1.1).

$$\mathrm{E} + \mathrm{S} \underset{\mathrm{k_{-1}}}{\overset{\mathrm{k_1}}{\rightleftharpoons}} \mathrm{ES} \underset{\mathrm{k_{-c}}}{\overset{\mathrm{k_c}}{\rightleftharpoons}} \mathrm{EP} \underset{\mathrm{k_{-r}}}{\overset{\mathrm{k_r}}{\rightleftharpoons}} \mathrm{E} + \mathrm{P} \tag{1.1}$$

Here E, S, P, ES and EP represent the enzyme, substrate, product, enzyme-substrate and enzyme-product complexes respectively. k_1 and k_{-1} are the association and dissociation rates of the substrate, k_c and k_{-c} are the rate of chemical conversion and the reverse rate of chemical conversion, and k_r and k_{-r} are the rates of product release and binding.

Enzymes are capable of accelerating reactions up to 10^{19} fold ($\Delta\Delta G^{\ddagger}$ = -26.9 kCal mol^{-1}).[1] In general, this is accomplished via stabilization of the transition state by electrostatic[2] or hydrogen bonding interactions.[3] However, this is a simplified view and a more detailed depiction of catalytic mechanisms has been developed in several studies.[1] For example the catalytic pocket of an enzyme may have a much lower reorganization energy relative to the solvent.[4] Furthermore, enzyme dynamics can play a critical role in catalysis as coupled motions can help substrates progress along the reaction pathway.[5] It is also important to consider that the activation barrier includes the conformational free energy of both the enzyme and the substrate, therefore synchronous enzyme motions can contribute to lowering the overall activation barrier.[6] Lastly, enzymes can cause the reaction to undergo an altogether different mechanism.[1,7] A reaction energy diagram illustrated below (Figure 1.1) shows the Gibbs free energy in the absence and presence of catalysis. Importantly,

the free energy is composed of the enthalpy and entropy, which are state functions.

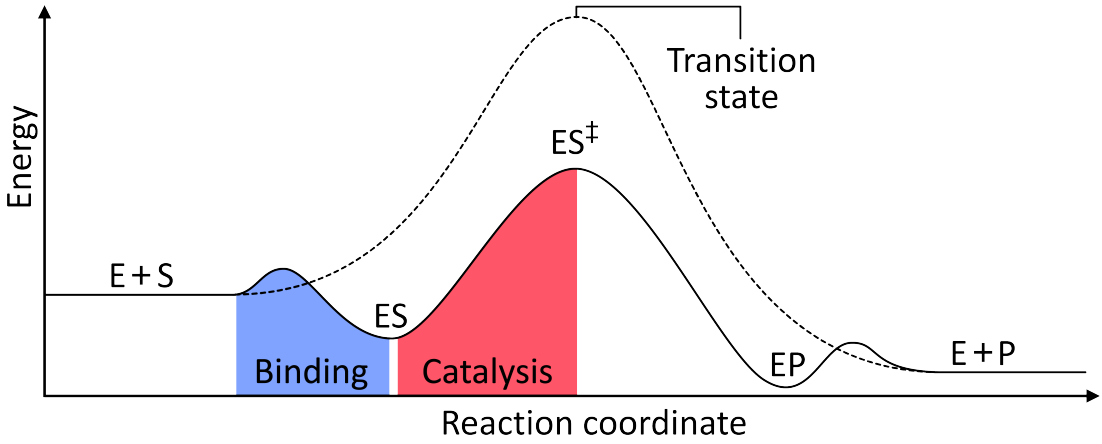

Figure 1.1. Enzyme Catalysis Energy Diagram. Adapted from Enzyme catalysis energy levels 2 by Thomas Shafee[8] under the creative common license - (CC BY 4.0).

1.1.1.2 Michaelis-Menten and Briggs-Haldane Kinetics

Quantifying enzyme activity requires a mathematical description of the reaction kinetics. Two of the most commonly used enzyme kinetics models are the Briggs-Haldane[9] and the Michaelis-Menten (MM) model.[10] In both of these models enzyme catalyzes substrate in a two step process (Equation 1.2).

$$\mathrm{E} + \mathrm{S} \underset{\mathrm{k_{-1}}}{\overset{\mathrm{k_1}}{\rightleftharpoons}} \mathrm{ES} \overset{\mathrm{k_{cat}}}{\rightharpoonup} \mathrm{E} + \mathrm{P} \tag{1.2}$$

which is a simplified version of Equation 1.1 where the catalytic conversion and product release steps are assumed to be irreversible (ie. $k_r \gg k_{-r}$ and $k_c \gg k_{-c}$) and are grouped into a single catalytic rate constant ($k_{cat} = \frac{k_r \cdot k_c}{k_r + k_c}$). In this case the rate of catalysis can be written as

$$\frac{d[P]}{dt} = k_{cat} \cdot [ES] \tag{1.3}$$

Where $[ES]$ is the concentration of the enzyme-substrate complex which can be expressed as

$$\frac{d[ES]}{dt} = k_1 \cdot [E] \cdot [S] - k_{-1} \cdot [ES] - k_{cat} \cdot [ES] \tag{1.4}$$

here $[E]$ and $[S]$ are the concentrations of enzyme and substrate respectively. Both of these models use the steady state approximation (ie. $\frac{d[ES]}{dt} = 0$) allowing for the concentration of enzyme-substrate complex to be simplified as

$$[ES] = \frac{[E_0] \cdot [S]}{[S] + K_m} \tag{1.5}$$

here $[E_0]$ is the total concentration active enzyme. In the case of the Briggs-Haldane model $K_m = \frac{k_{-1}+k_{cat}}{k_1}$, however the Michaelis-Menten model assumes that the enzyme and substrate are in rapid equilibrium (ie. $k_{-1} \gg k_{cat}$) making $K_m = K_d = \frac{k_{-1}}{k_1}$. Importantly, these two models yield identical dependencies of the rate of catalysis on substrate concentration. Substituting equation 1.5 into equation 1.3 yields

$$\frac{d[P]}{dt} = \frac{k_{cat} \cdot [E_0] \cdot [S]}{[S] + K_m} \tag{1.6}$$

This relationship implies that the rate of catalysis will have a hyperbolic dependence on the substrate concentration. For simplicity, in the remainder of this thesis hyperbolic dependence is referred to as ordinary Michaelis-Menten kinetics and K_m is referred to as the Michaelis constant. In the limit where $[S] \gg K_m$ equation 1.6 simplifies to

$$\frac{d[P]}{dt} = k_{cat} \cdot [E_0] \tag{1.7}$$

which is defined as the maximum velocity of the enzyme-substrate pair (V_{max}). Notably, at half the maximum velocity (when the enzyme is at half saturation) the substrate concentration is equal to the Michaelis constant ($[S] = K_m$). Scenarios where ($k_{cat} \gg k_{-1}$) are possible as well, in these cases the substrate is referred to as 'sticky'.[11]

1.1.1.3 Visualization Tools

There are several graphical tools for visualizing enzyme kinetics. A plot of the rate of catalysis vs. substrate concentration displays their hyperbolic relationship (Figure 1.2). This plot has an asymptote at $\frac{d[P]}{dt} = V_{max}$. Also, it is easy to graphically

interpret the K_m as $[S] = K_m$ when $\frac{d[P]}{dt} = \frac{1}{2} \cdot V_{max}$.

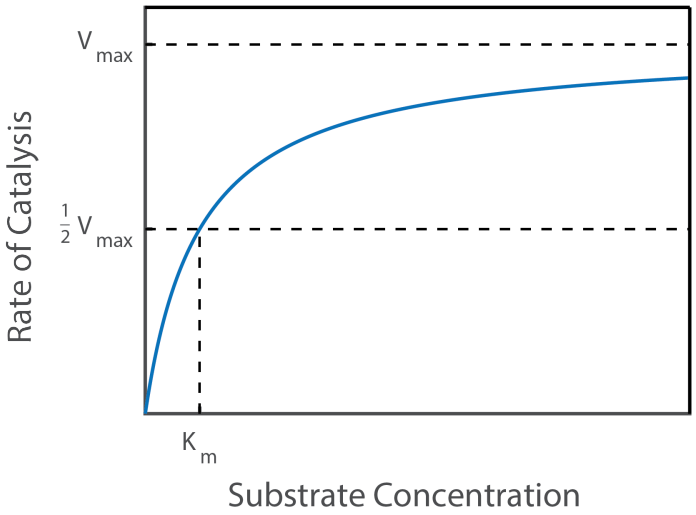

Figure 1.2. Rate of Catalysis vs. Substrate Concentration.

Another graphical tool used to visualize Michaelis-Menten kinetics is the Lineweaver-Burk (LWB) or double reciprocal plot. The equation used in this plot is arrived at by taking the reciprocal of both sides of the Michaelis-Menten equation (Equation 1.6). The reciprocal Michaelis-Menten equation can be simplified and written as

$$(\frac{d[P]}{dt})^{-1} = \frac{K_m}{V_{max}} \cdot \frac{1}{[S]} + \frac{1}{V_{max}} \tag{1.8}$$

A plot of $(\frac{d[P]}{dt})^{-1}$ vs. $\frac{1}{[S]}$ will be linear with a slope of $\frac{K_m}{V_{max}}$, a y-intercept of $\frac{1}{V_{max}}$ and an x-intercept of $-\frac{1}{K_m}$. Importantly, by plotting the data in this way it is possible to immediately tell if the reaction is following the Michaelis-Menten equation based on the linearity, furthermore, changes in the k_{cat} and K_m values are visually evident based on the slope and intercept of the plot (Figure 1.3).

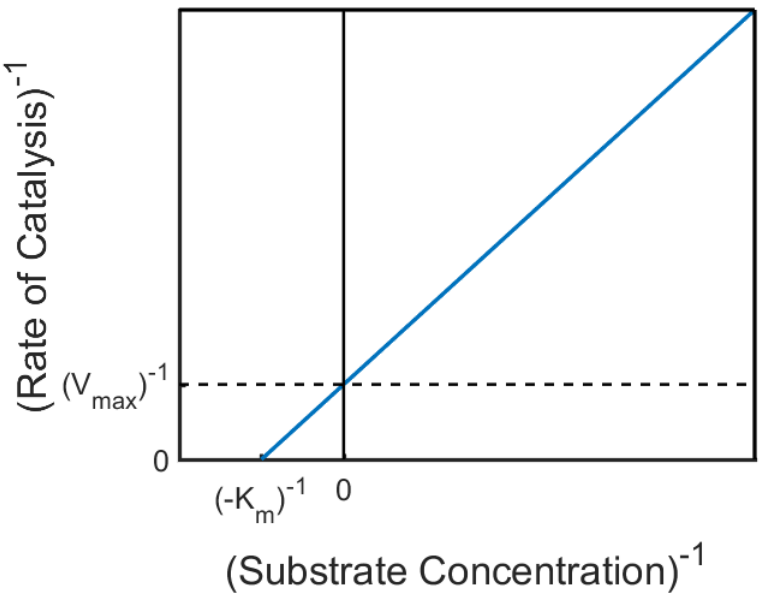

Figure 1.3. Lineweaver-Burk Plot.

1.1.1.4 Extracting Kinetic Parameters

To extract both the K_m and k_{cat} for an enzyme-substrate pair it is necessary to sample the rate of catalysis at various concentrations of substrate. Furthermore, in order to accurately extract the value of k_{cat} it is necessary to measure the rate of catalysis at a sufficiently high level of saturation (ie. $[S] \gg K_m$). When $[S] \ll K_m$ only the ratio $\frac{k_{cat}}{K_m}$ can be extracted.[12] Enzyme kinetics can be measured using discontinuous assays: where several separate rate measurements are made at different concentrations of substrate, or in a continuous assay: where an initial pool of substrate is depleted by the enzyme until completion while velocity is sampled at various concentrations of substrate. These two types of measurements along with the techniques typically used to make these measurements are discussed in detail below (see 1.1.3).

1.1.1.5 Non-Michaelis-Menten Kinetics

Although a great number of enzymes behave according to Michaelis-Menten kinetics some enzymes adhere to an entirely different mechanism or deviate from MM

kinetics under certain conditions. Situations such as these are referred to as non-Michaelis-Menten kinetics. Cooperativity is a widespread phenomenon that can cause an enzyme to deviate from ordinary MM kinetics. Due to the inherently dynamic nature of macromolecules, structural rearrangements can accompany ligand binding, altering the binding of subsequent ligands.[13] Similarly, substrates may induce structural rearrangements in enzymes and binding of a first substrate can alter the binding or catalysis of subsequent substrates. If the binding of subsequent substrates is enhanced the phenomenon is referred to as positive cooperativity, if the binding is diminished it is referred to as negative cooperativity. Typically, the Hill equation (Equation 1.9) is used to model cooperative enzyme kinetics.[14]

$$\frac{d[P]}{dt} = \frac{k_{cat} \cdot [E_0] \cdot [S]^n}{K_m + [S]^n} \tag{1.9}$$

where n is referred to as the Hill coefficient. Values above 1 represent positive cooperativity, in this regime the rate of catalysis will have a sigmoidal dependence on substrate concentration and higher positive cooperativity will lead to a curve with a higher slope at the inflection point (Figure 1.4). Importantly, when $n = 1$ there is no cooperativity present and the kinetics are of the ordinary Michaelis-Menten type (Figure 1.2). Furthermore, values below 1 represent negative cooperativity.

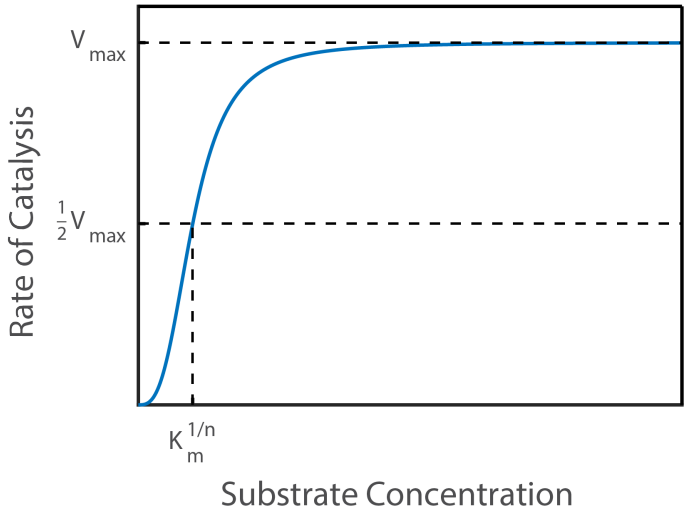

Figure 1.4. Sigmoidal Enzyme Kinetics. Simulated with $n = 3$

Interestingly, sigmoidal kinetics are not exclusive to multi-substrate enzymes, single-substrate enzymes can also demonstrate this behavior through a number of different mechanisms. One example is the mnemonic model. Here the enzyme is present in two states with high and low substrate affinities (E and E* in Figure 1.5a). The catalytic cycle involves binding of substrate inducing a conformational change to an entirely different state (E′) followed by catalysis and product release. Importantly, product release regenerates the high-affinity state (E). In the presence of high concentrations of substrate the high-affinity state can rebind substrate prior to relaxing back into the E* state. However, at low concentrations of substrate the enzyme will be more likely to relax back to the E* state. The relative amounts of E and E* at steady state results in a sigmoidal dependence of enzyme velocity on substrate concentration. Another example is the ligand-induced slow transition model. Once again the enzyme pre-exists in two different conformations with differing affinities (E and E* in Figure 1.5b) where the equilibrium of the bound form is different from that of the unbound form and both states are catalytically active. The resulting steady state velocity will be the sum of the rates for the two catalytic cycles.[14,15] In this case different combinations of microscopic rate constants can result in positive or negative cooperativity with either initial bursts or lags in enzyme velocity.[16] Importantly, enzyme cooperativity can have important biological implications, for example the cooperative nature of glucokinase makes its activity most responsive (ie. highest dependence on substrate) at physiological glucose concentrations.[14]

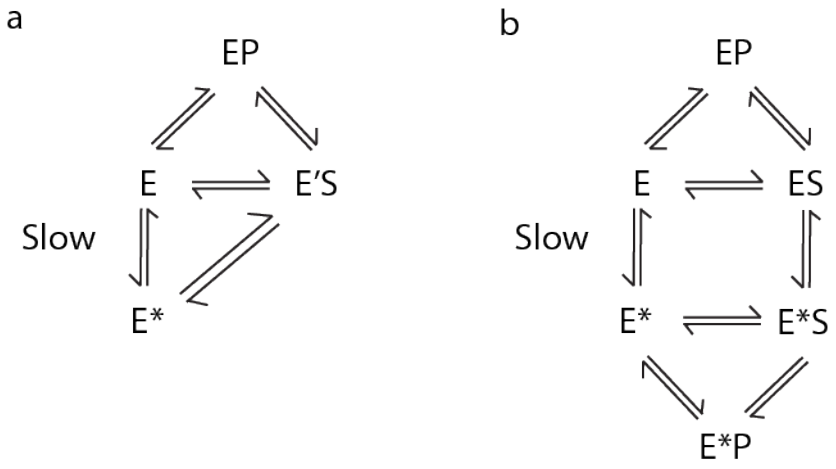

Figure 1.5. Mechanisms for Cooperativity in Monomeric Enzymes with Single Ligand-Binding Sites. (a) Mnemonic model and (b) Ligand-induced slow transition model. E and E* represent the high and low affinity states respectively. In (a) binding of substrate induces a new conformational state E′. Reproduced from Porter and Miller[14] with permission.

1.1.1.6 Enzymes in Disease

Enzymes play central roles in virtually all biological processes therefore, alterations in their activity can lead to diseased states. Modern drug discovery is mainly based on developing small molecule inhibitors of biological macromolecules to alter their function and restore regular physiology, thereby producing a therapeutic effect.[17] A 2006 pharmacological review reported that over 551 known therapeutic enzyme targets remain without a successful drug on the market[18] suggesting a large demand for the development of novel inhibitors. Furthermore, continuous advances in the technology and the development of methods for drug target identification promise to provide a continuous expansion in the list of known enzyme targets.[19]

1.1.1.7 Prolyl Oligopeptidase

Prolyl oligopeptidase (POP) is a cytosolic serine endopeptidase widely distributed in the body and brain of humans, pigs and several other organisms.[20,21] POP gained interest as a therapeutic target after several studies demonstrated potential ther-

apeutic effects from its inhibition. Firstly, POP inhibition was shown to reverse memory loss in animal models[22] and halt human gastric cancer cell growth.[23] Also, interestingly, the expression of POP is correlated with different stages of depression,[22,20] and appears to have a role in the regulation of blood pressure through participation in the renin-angiotensin system. There are several ongoing efforts towards designing inhibitors of POP in both academic and industrial settings including within the Moitessier group at McGill University where a library of bicyclic covalent and non-covalent inhibitors of POP have been designed and synthesized.

POP is a large (∼80 kDa) protein containing two main domains, the catalytic domain containing the catalytic triad; three residues necessary for carrying out catalytic function, and a seven-bladed β-propeller domain covering the active site. The latter domain functions as a gateway for the catalytic site preventing the proteolysis of large structured peptides[20,24] The lack of a primary isotope effect for POP demonstrates that the chemical step is not rate limiting, it was therefore concluded that the rate limiting step is a conformational change during the catalytic cycle.[25] This finding was supported by differential scanning calorimetry experiments demonstrating that the two domains of POP cooperatively melt in the presence of a ligand while each domain melts separately in the free form.[26,24] Biophysical characterization of proteins can have important implications when designing therapeutics.[27] Similarly, the unique properties of POP may be pertinent in future drug design efforts.

1.1.1.8 Drug Design and Development

Drug development is typically a multi-step process beginning with the identification of a druggable target and ending with thorough clinical testing. The first step is target validation, where the druggability of a predicted molecular target is confirmed (Figure 1.6). Once validated, hit compounds are identified from large libraries of molecules via high throughput screening assays.[28,29] Hits are then developed into leads by optimizing their potency: a measure of the amount of drug required to achieve a therapeutic effect, and their selectivity: the ability to discriminate between the target of interest and off-targets. Lead inhibitors are optimized further

by increasing their potency. Once an inhibitor has shown promise it can enter pre-clinical and clinical trials. If the inhibitor passes clinical trials it can be marketed as a drug.[30] According to a study carried out at the *Tufts Center for the Study of Drug Development*, a new drug costs an average of $2.6 billion to develop,[31] furthermore, only 1 in every 10 compounds that enters clinical trials becomes a drug.[32] The high cost and low success rate of the drug design process creates a large demand for methodologies to assist in rapid, inexpensive hit development and lead optimization.

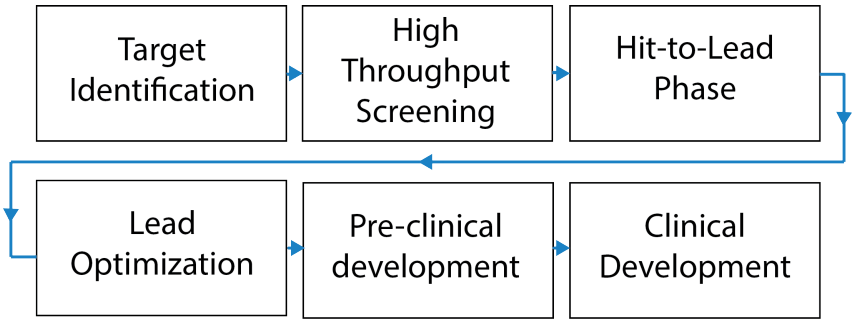

Figure 1.6. Overview of Drug Development.

Throughout the drug design and development process there are a great variety of in vitro assays performed in order to measure the thermodynamic and, less often, kinetic properties of the inhibitor-target interactions, as well as in vivo assays for measuring the efficacy and toxicity.[17] To develop a potent inhibitor the structure must be optimized towards a tight, specific interaction with the therapeutic target of interest, this is typically accomplished via a structure affinity relationship (SAR) to test correlations between the structure of the inhibitor and its affinity.[33] Furthermore, the importance of inhibitors' kinetic properties have recently been demonstrated, prompting the development of structure kinetics relationships (SKR) discussed in detail below (see 1.1.2.3). The following section gives a mathematical description of the thermodynamics/kinetics of enzyme-inhibitor interactions and discusses the importance of these measurements in the context of the drug design and development process.

1.1.2 Enzyme-Inhibitor Interactions

1.1.2.1 Strength and Mode of Inhibition

Early efforts in the drug development process are typically directed towards optimizing the affinity of inhibitors which is achieved using structure affinity relationships. To quantify the extent of binding the dissociation constant (K_d) can be extracted, which is referred to as the as the inhibition constant (K_i) for inhibitors. For a one-step reversible reaction the following equation applies.

$$\mathrm{E} + \mathrm{I} \underset{\mathrm{k_{off}}}{\overset{\mathrm{k_{on}}}{\rightleftharpoons}} \mathrm{EI} \tag{1.10}$$

where E, I and EI are the enzyme, inhibitor and enzyme-inhibitor complex respectively. k_{off} and k_{on} are the dissociation rate constant and the association rate constant. The expression for the inhibition constant in this case is.

$$K_i = \frac{k_{off}}{k_{on}} = \frac{[E] \cdot [I]}{[EI]} \tag{1.11}$$

where $[E]$, $[I]$ and $[EI]$ are the equilibrium concentrations of enzyme, inhibitor and enzyme inhibitor complex respectively. In order to extract the K_i, the extent of binding must be quantified at several known total concentrations of enzyme and inhibitor. In the case of enzyme inhibitors the Michaelis-Menten parameters change in a particular way depending on how the inhibitor binds, or the mode of inhibition. There are three main modes of inhibition: 1) competitive inhibition, where the inhibitor binds to the free enzyme (E) and blocks interactions with the substrate, 2) uncompetitive inhibition, where the inhibitor binds to the enzyme-substrate complex (ES), blocking catalysis, and 3) mixed inhibition, where the inhibitor can bind to both E and ES. The special case in which the affinities for E and ES are equal is referred to as noncompetitive inhibition. Understanding the mode of inhibition is important for structural characterization and guided optimization of the inhibitor bound form.[34] To quantitatively understand each type of inhibition mode it is conve-

nient to first consider the most general case; mixed inhibition with competitive and uncompetitive inhibition constants $K_{i,1}$ and $K_{i,2}$ respectively, furthermore, for simplicity, it is assumed that the double bound state ESI_2 does not exist ($[ESI_2] = 0$). This scenario can be expressed through the following sets of equations.

$$\mathrm{E} + \mathrm{S} \overset{\mathrm{K_m}}{\rightleftharpoons} \mathrm{ES} \overset{\mathrm{k_{cat}}}{\rightharpoonup} \mathrm{E} + \mathrm{P} \tag{1.12}$$

$$\mathrm{E} + \mathrm{I} \overset{\mathrm{K_{i,1}}}{\rightleftharpoons} \mathrm{EI} \qquad\qquad \mathrm{ES} + \mathrm{I} \overset{\mathrm{K_{i,2}}}{\rightleftharpoons} \mathrm{ESI} \tag{1.13 a,b}$$

where

$$K_m = \frac{[E]\cdot[S]}{[ES]}, \quad K_{i,1} = \frac{[E]\cdot[I]}{[EI]}, \quad K_{i,2} = \frac{[ES]\cdot[I]}{[ESI]} \tag{1.14 a-c}$$

these equations can be used in conjunction with 1.4 to obtain an expression for the rate of catalysis for mixed inhibition

$$\frac{d[P]}{dt} = \frac{k_{cat}\cdot[E_0]\cdot[S]}{[S]\cdot(1+\frac{[I]}{K_{i,2}}) + K_m\cdot(1+\frac{[I]}{K_{i,1}})} \tag{1.15}$$

Provided $[EI]$ and $[ESI] \ll [I_o]$, the free inhibitor concentration $[I]$ can be approximated by $[I_o]$; the total concentration of inhibitor. Equation 1.15 applies when inhibitor can bind to both E and ES with different affinities, however, limiting cases of this expression can be used to arrive at other types of inhibition. For competitive inhibition $1/K_{i,2} \to 0$, uncompetitive inhibition $1/K_{i,1} \to 0$ and noncompetitive inhibition $K_{i,1} = K_{i,2} = K_i$. The resulting equations in these three limits are

$$\frac{d[P]}{dt} = \frac{k_{cat}\cdot[E_o]\cdot[S]}{[S] + K_m\cdot(1+\frac{[I]}{K_{i,1}})}, \qquad \frac{d[P]}{dt} = \frac{k_{cat}\cdot[E_o]\cdot[S]}{[S]\cdot(1+\frac{[I]}{K_{i,2}}) + K_m},$$
$$\frac{d[P]}{dt} = \frac{k_{cat}\cdot[E_o]\cdot[S]}{([S]+K_m)\cdot(1+\frac{[I]}{K_i})} \tag{1.21a-c}$$

for competitive, uncompetitive and noncompetitive inhibition respectively (top left, right then bottom left). Importantly, these equations can be reparametrized in terms

of the effective K_m and k_{cat} values as

$$\frac{d[P]}{dt} = \frac{k_{cat} \cdot [E_o] \cdot [S]}{[S] + K'_m}, \qquad \frac{d[P]}{dt} = \frac{k'_{cat} \cdot [E_o] \cdot [S]}{[S] + K'_m},$$
$$\frac{d[P]}{dt} = \frac{k'_{cat} \cdot [E_o] \cdot [S]}{[S] + K_m}, \qquad \frac{d[P]}{dt} = \frac{k'_{cat} \cdot [E_o] \cdot [S]}{[S] + K''_m} \tag{1.22a-d}$$

For competitive, uncompetitive, noncompetitive and mixed inhibition respectively (top left, right, bottom left, then right). When cast in this form Equations 1.22a-d are analogous to the Michaelis-Menten equation. When the enzyme-inhibitor complex equilibrates rapidly relative to the time-scale of the measurement (see chapter 3) the enzyme will appear to undergo ordinary Michaelis-Menten kinetics with effective K_m and k_{cat} values (K'_m, K''_m, k'_{cat}) which increase or decrease with inhibitor concentration. The aforementioned Lineweaver-Burk plots are an exceptionally powerful way for monitoring the strength and mode of inhibition as the slope and intercept change according to the values of K_m and k_{cat}. Overlaying several different LWB plots at different concentrations of inhibitor will give lines that intersect at the y-axis for competitive inhibition, parallel lines for uncompetitive inhibition or lines that intersect at the x-axis for noncompetitive inhibition. Mixed inhibition on the other hand will give lines with different slopes and intercepts that depend on the relative magnitudes of $K_{i,1}$ and $K_{i,2}$ (Figure 1.7).

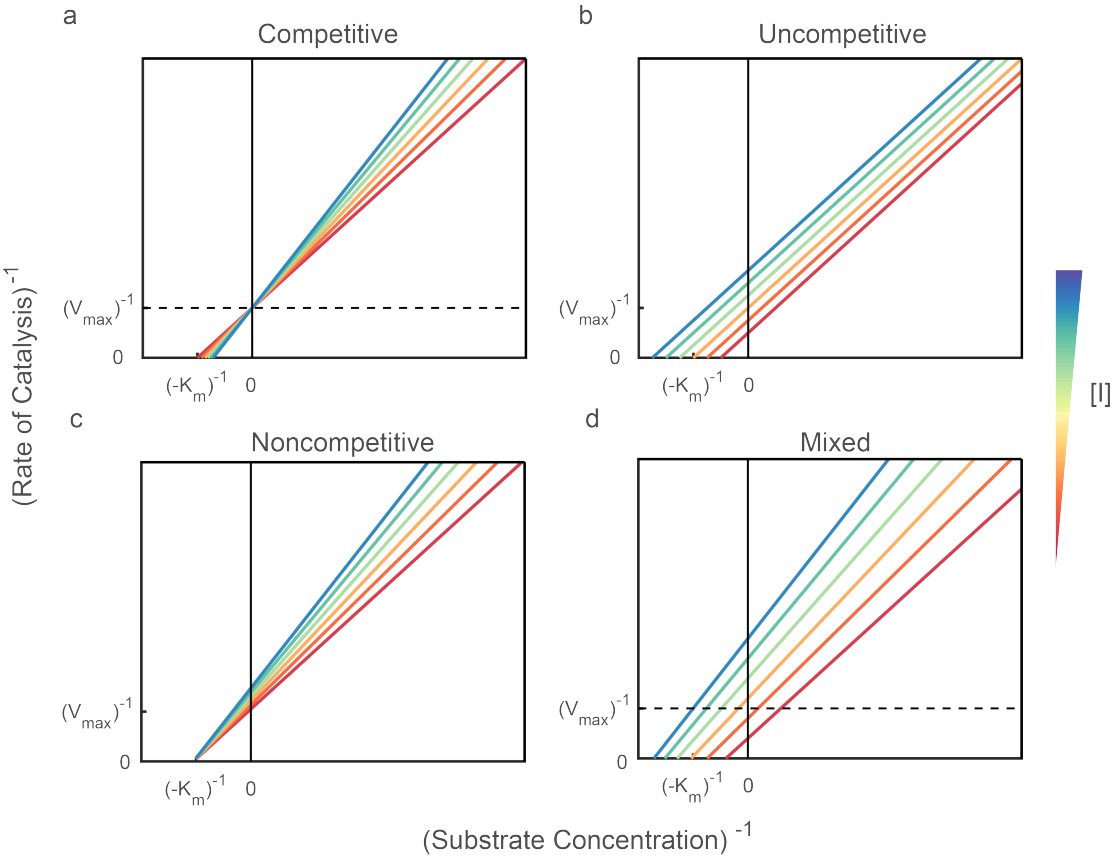

Figure 1.7. Overlay of Lineweaver-Burk Plots at Different Concentrations of Inhibitor. (a) Competitive inhibition, (b) Uncompetitive inhibition, (c) Noncompetitive inhibition, and (d) Mixed inhibition.

1.1.2.2 Measuring IC_{50}

Equations 1.22a-d also demonstrate that extracting the mode of inhibition requires measurement of both the K_m and k_{cat} at various concentrations of inhibitor. This means that n_s different substrate concentrations are required in order to extract both MM parameters at n_i different inhibitor concentrations totaling $n_i \cdot n_s$ different conditions. Alternatively, it is possible to measure the the IC_{50} which is defined as the inhibitor concentration to cause a 50% decrease in the rate of catalysis. Measuring the IC_{50} requires only n_i different measurements saving a multitude of time and sample. However, to determine the K_i from the IC_{50}, knowledge of the binding mode is required.[35]

1.1.2.3 Kinetics of Drug-Target Interactions

The majority of drug development programs place a large emphasis on the thermodynamics of drug-target interactions. The underlying basis of this emphasis is contingent on the assumption that drug-target interactions occur in a closed system. However, this is not true, as in-vivo there are constant fluctuations in drug, substrate and macromolecule concentrations making it necessary to consider the kinetic properties of the interactions as well.[36] There are numerous studies demonstrating the relationship between the kinetic properties of inhibitors and their biological effect.[37,38,39] For single step drug-target binding the following equation applies.

$$\mathrm{E} + \mathrm{I} \underset{\mathrm{k_{off}}}{\overset{\mathrm{k_{on}}}{\rightleftharpoons}} \mathrm{EI} \tag{1.18}$$

Where k_{on} and k_{off} are the association and dissociation rates of the inhibitor respectively and $K_i = \frac{k_{off}}{k_{on}}$. The residence time (the inverse of the off rate $\tau_r = \frac{1}{k_{off}} = \frac{t_{\frac{1}{2}}}{ln(2)}$) is regarded as the most important kinetic parameter to consider when optimizing an inhibitor.[38] To understand this importance consider that local concentrations of inhibitor will fluctuate at the site of the target. In the case of a drug-target system that rapidly associates and dissociates the level of inhibition will be proportional to the local concentration of the drug, therefore, as the drug diffuses away from the target, saturation will decrease and activity will return. However, in the case of an inhibitor with a large residence time even after the local concentrations of inhibitor fall, the target will remain inhibited, prolonging the therapeutic effect (Figure 1.8).[40]

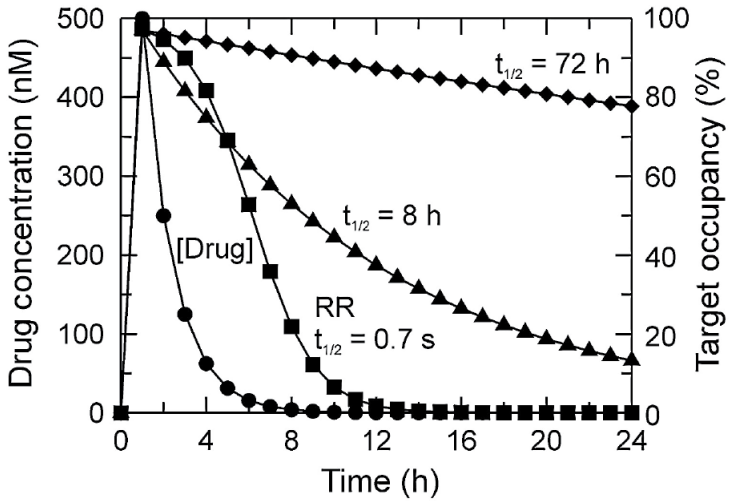

Figure 1.8. Effect of Residence Time on Enzyme Activity. Curve with overlaid circles is drug concentration with time. Curves with overlaid squares, triangles and diamonds are the target occupancy for three different targets with different half lifes shown beside curves. RR is the rapid reversible drug where the residancy was calculated directly from the K_d. Reproduced from Copeland *et al.*[36] with permission.

Another important facet of in vivo conditions to consider is the local concentration of substrate. Inhibition of an enzyme may cause the blockade of a metabolic pathway resulting in depletion of end-products and accumulation of substrates.[41] If local concentrations of substrate become high enough they may reverse the effective strength of competitive inhibitors, restoring the original flux through the inhibited reaction. This process is referred to as metabolic resistance.[42,43] However, inhibitors with large residence times will be less affected by large concentrations of substrate as reactivation requires dissociation of the drug-enzyme complex. Therefore, the enzyme's return to activity will be mainly dependent on the residence time and not local concentrations of substrate.[41]

Although the majority of emphasis is placed on the residence time, the association rate can influence the drug development process as well. This is a consequence of how enzyme activity assays are typically performed.[44] If the enzyme-inhibitor mixture is not given a sufficient amount of time to associate prior to the activity being measured, inhibitors with slow association rates might appear much less potent

then they are in reality. This may cause potentially potent inhibitors to be missed entirely or skew SAR data.[45] Therefore, when assessing inhibitors it is crucial to consider their association kinetics in addition to residence time.

The well-established importance of a drug's kinetic properties has prompted the development of many structure kinetics relationships, where the kinetic properties of inhibitors are used to optimize their structure. For example, in drug design studies targeting chemokine receptor 2 (CCR2), inhibitors with high affinity typically lacked efficacy. These difficulties prompted a combined SAR-SKR based optimization of inhibitors where affinity and residence time were simultaneously considered. This optimization yielded a high affinity compound ($K_i = 3.6$ nM) with a residence time of 135 min, however, a purely SAR based study yielded a compound with high affinity ($K_i = 6.8$ nM) except with a residence time of only 2.4 min.[46] This directly demonstrated that a combined SKR/SAR can result in different and potentially more efficacious structures than just a SAR. In another drug development program, a SKR was developed in conjunction with crystallographic data while testing inhibitors of cyclin-dependent kinase 8/cyclin C (CDK8/CycC). The structure of the inhibitor-target complex revealed hydrogen bonding between CDK8/CycC only affected the residence time if the hinge region of CDK8/CycC was involved.[47] With these findings they were able to correlate specific interactions with kinetic properties, allowing them to intelligently fine tune the residence time. Lastly, SKR's have been used to produce k_{on}-k_{off}-K_d kinetic maps of inhibitors for human adenosine A_3 (hA_3R) (Figure 1.9) allowing for quantitative clustering of inhibitors. By testing several inhibitors with the same k_{on} but different K_d and k_{off} (Group C in Figure 1.9), using a cell based assay they were able to demonstrate that compounds with higher residence times showed superior efficacies.[33] The studies described above provide structural insight into how resonance time can be tuned for specific systems, and demonstrate that affinity and resonance time don't necessarily correlate. Therefore, consideration of an inhibitor's kinetic parameters can yield different and potentially more efficacious drugs than SAR alone.

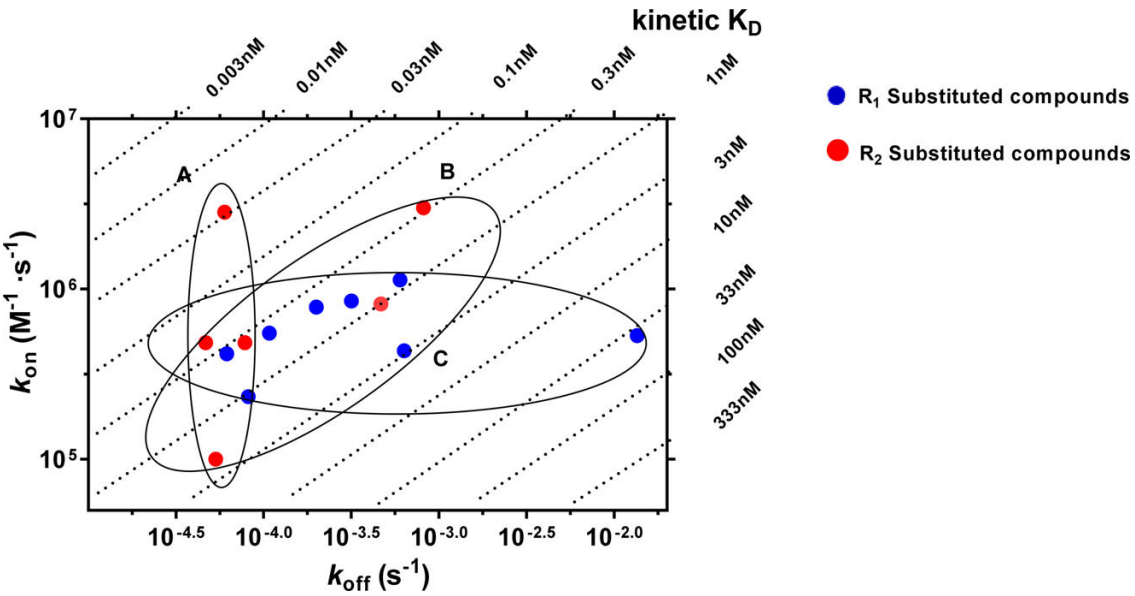

Figure 1.9. Kinetic Map for adenosine A_3 (hA_3R) Inhibitors. Group A: compounds have similar k_{off} values. Group B: compounds have similar K_d values. Group C: compounds have similar k_{on} values. Reproduced from Xia *et al.*[33] under the creative common license - (CC BY 4.0).

The kinetic parameters of enzyme inhibitors can be extracted by quantitatively modelling how enzyme activity changes in the presence of an inhibitor. A one step binding mechanism can be expressed as

$$\mathrm{EI} \underset{\mathrm{k_{on}}}{\overset{\mathrm{k_{off}}}{\rightleftharpoons}} \mathrm{E} + \mathrm{I} + \mathrm{S} \underset{\mathrm{k_{-1}}}{\overset{\mathrm{k_1}}{\rightleftharpoons}} \mathrm{ES} \overset{\mathrm{k_{cat}}}{\rightharpoonup} \mathrm{E} + \mathrm{P} \tag{1.19}$$

By assuming the enzyme-substrate complex adheres to the steady state approximation, the rate of catalysis can be expressed as

$$\frac{d[P]}{dt} = k_{cat} \cdot [ES] = \frac{k_{cat} \cdot ([E_o] - [EI]) \cdot [S]}{[S] + K_m} \tag{1.20}$$

where the kinetics of inhibition are given by

$$\frac{d[EI]}{dt} = k_{on} \cdot [E] \cdot [S] - k_{off} \cdot [EI] \tag{1.21}$$

This set of equations makes it possible to extract inhibitor kinetics by monitoring

the rate of enzyme catalysis as a function of time.

1.1.2.4 Covalent Inhibition

The majority of the drug development programs are geared towards optimizing electrostatic, hydrogen bonding and hydrophobic interactions, however, covalent interactions are more seldom pursued. This is because covalent inhibitors are associated with having high toxicity resulting from non-specific, covalent modification of important biological molecules.[48] Despite this, there are various blockbuster covalent drugs present on the market including Clopidogrel, an anti-coagulant; Lansoprazole and Esomeprazole, proton pump inhibitors; as well as Aspirin, a well-known pain killer. The former three drugs were amongst the top ten selling drugs in the United States in 2009.[49] In fact, over 30% of marketed drugs that target enzymes act as covalent inhibitors.[50] Recently, there has been a surge in the development of covalent inhibitors; the number of publications involving covalent inhibition has increased exponentially since the 1970's and many purposefully designed covalent inhibitors are being introduced into the market or are in late stage clinical trials.[49] This surge is the result of an increasing realization that covalent inhibitors have beneficial thermodynamic and kinetic properties over their non-covalent counterparts under certain circumstances.

Covalent inhibitors will interact with their target in a two-step reaction according to the following reaction

$$\mathrm{E} + \mathrm{I} \underset{\mathrm{k_{-2}}}{\overset{\mathrm{k_2}}{\rightleftharpoons}} \mathrm{EI} \underset{\mathrm{k_{-3}}}{\overset{\mathrm{k_3}}{\rightleftharpoons}} \mathrm{E{-}I} \tag{1.22}$$

Where EI and E-I are the non-covalent and covalent complex respectively. k_2, k_{-2}, k_3, and k_{-3} are the microscopic rate constants for the association and dissociation of the non-covalent complex, and the formation and cleavage of the covalent bond respectively. Note that this mechanism does not exclusively pertain to covalent inhibition, a two-step reaction can occur in other scenarios such as binding followed

by a conformational change. The overall inhibition constant in this case is

$$K_i^* = \frac{[E] \cdot [I]}{[E-I] + [EI]} = \frac{K_i}{1 + \frac{k_3}{k_{-3}}} \tag{1.23}$$

Where K_i^* is the overall affinity and $K_i = \frac{k_{-2}}{k_2}$. The high activation energy of covalent bond cleavage will lead to small values of k_{-3} causing high residence times and affinities. This has been demonstrated with a series of POP inhibitors that differ by their covalent linker functional group. The series contains inhibitors with aldehyde, nitrile or $COCH_2OH$ covalent warheads as well as non-covalent analogues. Addition of any covalent moiety was shown to increase the inhibitory potency by two orders of magnitude (from $K_i = 11$ nM to $K_i^* \approx 0.1$ nM), which was attributed to the introduction of a covalent bond. In addition, the dissociation, association rate as well as affinity were shown to be crucially dependent on the type functional group present.[51] In another study performed with the therapeutic target Bruton's tyrosine kinase (BTK) it was demonstrate that inhibitors' residence times spanned from several minutes up to 7 days. Importantly, the residence time was acutely sensitive to the steric and electronic environment of the electrophilic carbon directly involved in the covalent bond allowing for calculated adjustment of the inhibitors' kinetic properties.[52]

The beneficial properties of covalent inhibitors makes SKR of these molecules important, in turn requiring a quantitative description of the inhibition and initiation kinetics. In general when $(k_{-2} + k_3) \gg k_2 \cdot [I]$, EI does not accumulate appreciably as a kinetic intermediate and the kinetics of inhibition are indistinguishable from those of simple non-covalent inhibition.[53,54] Formation of the inhibited state (EI + E-I) follows Equation 1.24 with an apparent association rate constant:

$$k'_{on} = \frac{k_2 \cdot k_3}{k_{-2} + k_3} \tag{1.24}$$

When this kinetic condition is not met, bi-phasic kinetics is obtained, characterized by rapid formation of EI followed by gradual conversion to E-I.[53,55] Similarly, when

$k_3 \gg k_{-3}$ or $k_3 \gg k_{-2}$ dissociation is kinetically first order with an apparent rate constant:

$$k'_{off} = \frac{k_{-2} \cdot k_{-3}}{k_{-2} + k_3} \tag{1.25}$$

When $k_{-2} \gg k_3 \approx k_{-3}$, dissociation is biphasic with rapid dissociation of EI followed by gradual loss of E-I. In some cases, biphasic inhibition kinetics are observed experimentally, giving information on the microscopic parameters in equation 1.25.[56,57] In many cases, however, binding is empirically monophasic and the apparent association and dissociation represent the experimentally-accessible physical parameters.

1.1.3 Techniques for Studying Enzyme-Inhibitor Interactions

1.1.3.1 Methods for Measurement

There are a number of techniques used to measure enzyme kinetics including UV-Vis spectroscopy,[44] NMR spectroscopy,[58] chromatography,[59] electrophoresis, mass spectrometry,[44] and isothermal titration calorimetry.[60] All the techniques except ITC measure the concentration of substrate or product as a function of time and the first derivative can be taken to calculate the rate of catalysis. However, isothermal titration calorimetry measures the rate of catalysis directly (see section 1.3). As discussed above, extracting Michaelis-Menten parameters requires evaluating the rate of catalysis at various concentrations of substrate.

There are two main methods by which this is accomplished. Firstly, a continuous assay where a high concentration ($\gg K_m$) of substrate is mixed with enzyme. As the substrate is depleted over time by the reaction, the rate of catalysis can be sampled over a range of substrate concentrations (Figure 1.10a). Alternatively, discontinuous assays are used. This involves arranging several different enzyme samples each with a different concentration of substrate. Samples are quenched after various incubation periods and the amount of product or substrate is quantified. The activity can be calculated for each sample making it possible to measure the rate of catalysis over an array of substrate concentrations (Figure 1.10b).[54]

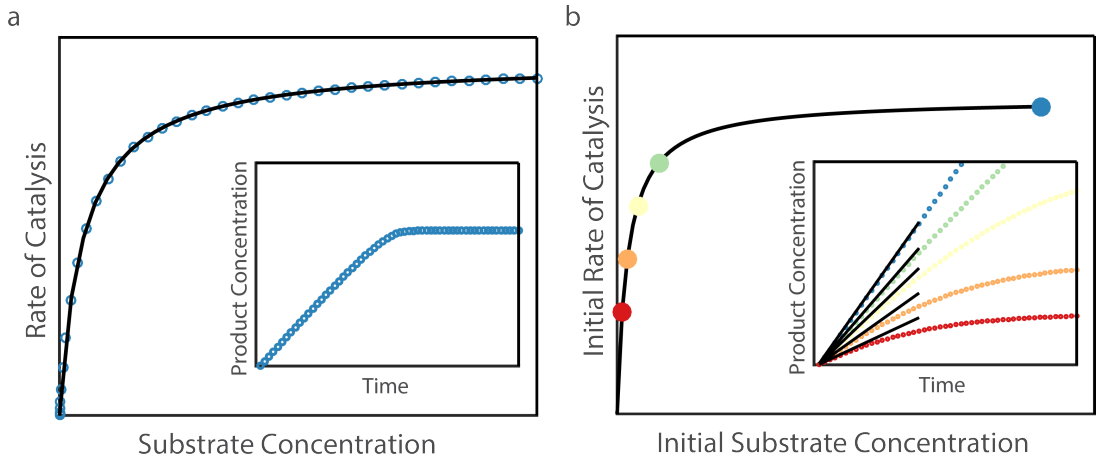

Figure 1.10. Enzyme Kinetics Measurements. (a) Continuous enzyme kinetics measurements (b) Discontinuous enzyme kinetics measurements.

Enzyme-inhibitor kinetics are quantified using either continuous assays or initial rate measurements. Association rates can be measured in continuous inhibition assays where inhibitor is added to a solution of enzyme and substrate. The enzyme will become progressively inhibited as the enzyme and inhibitor approach equilibrium causing the rate of catalysis to decrease with time according to the association rate. By analyzing the rate of catalysis vs. time curve, it is possible to extract the association rate of the inhibitor (red curve Figure 1.11a). Similarly, the dissociation rate can be extracted with a continuous initiation assay. Here enzyme-inhibitor complex is diluted into a solution containing substrate. The dilution will cause the enzyme-inhibitor complex to dissociate and the rate of catalysis will increase over time according to the dissociation rate. Once again by analyzing the rate of catalysis vs. time curve, it is possible to extract the dissociation rate of the inhibitor (orange curve Figure 1.11a). Alternatively, kinetics can be measured in a series of initial rate measurements, here inhibitor is added to enzyme and allowed to incubate. The enzyme inhibitor is added to substrate solution allowing for measurement of the rate of catalysis after various incubation periods (inset in Figure 1.11b). Enzyme-inhibitor formation will cause the rate of catalysis to decrease with time allowing for quantification of the association rate (Figure 1.11b). In a similar fashion initiation kinetics can be measured via dilution of enzyme-inhibitor complex followed by

sampling the rate of catalysis after various incubation periods.

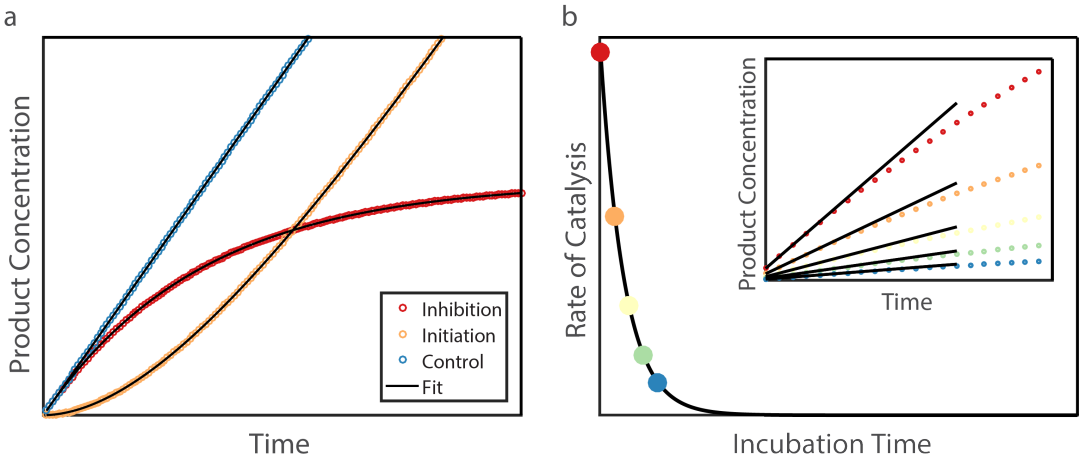

Figure 1.11. Enzyme-Inhibitor Kinetics Measurements. (a) Continuous Inhibition and Initiation Kinetics. Control (blue circles) was simulated with no inhibitor present. (b) Initial Rate Kinetics of inhibition

1.1.3.2 UV-Vis Spectroscopy

Spectroscopic techniques are amongst the most common ways for measuring enzyme kinetics and enzyme-inhibitor interactions. Ideally, to measure catalytic rates, the spectroscopic signal of the substrate will differ from the product. By monitoring the change in signal of either the substrate or product with time, it is possible to extract the rate of catalysis (see 1.1.3.1). If native substrates and products are indistinguishable, non-native substrates can be designed to undergo changes in adsorption or fluorescence when converted to products.[61,62] There are a number of known natural substrates for prolyl oligopeptidase such as angiotensin I and II, oxytocin and thyrotropin-releasing hormone (TRH) that are indistinguishable from their products by UV-Vis.[63] To circumvent this, a number of synthetic peptide substrates have been designed to undergo changes in fluorescence or absorbance upon cleavage.[64] Alternatively, coupled enzyme assays can be applied where products of catalysis are rapidly consumed in order to generate or deplete spectroscopically active compounds. These are commonly utilized with kinases where the adenosine diphosphate (ADP) is used in a series of post reaction catalytic steps, eventually

leading to the depletion of Nicotinamide adenine dinucleotide (NADH) which has a strong absorbance at 340 nm.[65] However, coupled assays must be individually optimized to ensure that the post reaction steps are not rate limiting. Furthermore, coupled assays place constraints on the conditions under which the reaction can be tested.[66] For example it is impossible to probe enzyme-ADP interactions using this technique. There are three main UV-Vis instruments used to measure the thermodynamics or kinetics of enzyme inhibitor interactions: ordinary sample cell spectrometers, well plate readers, or stopped flow instruments. The former two techniques have a dead time of up to several minutes while stopped flow systems typically have dead times of only ≈ 0.5 ms.[67]

1.1.3.3 NMR Spectroscopy

Nuclear magnetic resonance (NMR) spectroscopy can also be used to measure enzyme kinetics by monitoring signal produced by the substrate or product with or without inhibitor over time. NMR has been applied to several systems including the cleavage of sucrose by invertase[68] and the oxidation of phenolic compounds by polyphenol oxidases.[69] The advantage of this technique is that it is very sensitive to chemical structure, including stereochemistry making it applicable to many types of reactions. However, it is not applicable to fast enzyme kinetics as there is a large dead time and a minimum acquisition time between data points,[70] furthermore, NMR can be expensive and time consuming.

1.1.3.4 Chromatography, Electrophoresis and Mass Spectrometry

There are a number of post-reaction techniques for quantifying the amount of product formed/substrate depleted including liquid chromatography, gel electrophoresis and mass spectrometry. Here, enzyme is quenched after specific incubation periods followed by quantification using one or more of the techniques.[54] This approach is very general as most chemical alterations can be quantified using at least one of these techniques. However, these techniques can be time consuming and expensive

as each time point requires a large amount of work-up. Furthermore, post reaction steps can add uncertainty to the measurements.

1.1.3.5 Isothermal Titration Calorimetry

Enzyme kinetics can also be measured using isothermal titration calorimetry (ITC), which measures the heat produced or absorbed by catalysis following the mixing of substrate and enzyme. A typical ITC experiment involves making a series of automated injections from a syringe into a sample cell and measuring the heat produced or absorbed over time. There are a great number of advantages to using ITC for measuring enzyme kinetics. Firstly, ITC does not typically require synthetic substrates or coupled assays as most chemical reactions release or absorb heat, making it a near universal enzyme assay. The instrumentation enables measurement of the heat flow with virtually no dead time, as the instrument continuously makes measurements prior to, during, and following the injection.[71] Also, ITC detects heat flow directly which is proportional to the rate of catalysis, making it acutely sensitive to changes in the catalytic rate (see section 1.3). Conversely, other techniques require indirect calculation of the rate using the changes in concentrations of substrates or products with time making them significantly less sensitive. ITCs are capable of perfoming measurements under physiological conditions and are completely compatible over a wide range of salt concentrations, pH's and temperatures.[72] Additionally, conditions that lead to scattering and/or absorption of light such as high concentrations of bovine serum albumin (BSA) can hinder spectroscopic measurements, however, the sensitivity of ITC remains unchanged.[73] The generality of ITC has already been demonstrated by Matthew J Todd and Javier Gomez[60] by measuring MM parameters for all six classes of enzymes (hydrolases, oxidoreductase, transferases, lyases, isomerases and ligases) using a pair of ITC based techniques (see 1.3) similar to the continuous enzyme kinetics method and initial rate kinetics method. This study not only provided valuable techniques for studying enzyme kinetics but also demonstrated that enzymes from all six classes are capable of producing sufficient signal to be mearurable using ITC. Furthermore, ITC has been used to study systems

that were not compatible with other techniques such as cellulolytic enzymes. Previously cellulolytic enzyme assays required the use of modified substrates to increase solubility and make it possible to measure kinetics spectroscopically. However, by amplifying the heat signal using a coupled ITC assay it was possible to measure even the slowest hydrolytically active enzymes such as cellobiohydrolases with its natural substrate.[74] Also, the promiscuity of oxalate oxidase was discovered using ITC as several small molecule carboxylic compounds were found to act as substrates.[75] In addition to these distinct advantages for measuring enzyme kinetics, isothermal titration calorimeters (ITCs) have become ubiquitous instruments in biophysical laboratories, and are easy to set-up and maintain. The distinct advantages and ubiquitousness of ITCs poises them to become a popular technique for measuring enzyme kinetics and enzyme-inhibitor interactions.

1.2 Isothermal Titration Calorimetry

1.2.1 Instrumentation

1.2.1.1 Compensation Calorimetry

Calorimetry is the measurement and analysis of heat released or absorbed by a substance when it undergoes chemical or physical change. There are several different types of calorimeters including reaction calorimeters, bomb calorimeters, differential scanning calorimeters, and isothermal titration calorimeters which is a type of compensation calorimeter. In a compensation calorimeter a resistive heater supplies a feedback power to the sample cell in order to maintain it at the same temperature as a reference cell. Therefore, the feedback power supplied to the reaction cell will adjust when heat is created or absorbed by a reaction in order to maintain the two cells at the same temperature. The feedback power is recorded by the instrument, and is directly related to heat generated or absorbed by the reaction in the cell.[76]

1.2.1.2 Instrument Description

Modern isothermal titration calorimeters are designed with sample cell stirring, in order to ensure heat is generated quickly and evenly, and a compensations system allowing for rapid measurement of heat.[77] The core of the instrument contains an adiabatic shield encompassing the sample and adjacent reference cell. The cells are typically coin-shaped or cylindrical with stems open to the outside in order to allow for introduction or removal of the sample via long-needled syringes (Figure 1.12).[71] The inner surface of each cell is composed of a robust alloy such as hastelloy C.[78] Each cell has an electric heater distributed uniformly on the outer surface with an extremely sensitive thermoelectric device sandwiched between two cells which actively measures the temperature difference between them (ΔT_1). An additional thermocouple connects the circumference of the reference cell with the adiabatic jacket also measuring their temperature difference (ΔT_2) (Figure 1.13).[71] The injection syringe is a glass barrel attached to a needle followed by a stir paddle. The injection syringe is inserted in a low friction bearing assembly coupled to a stirring motor providing complete mixing following an injection. (Figure 1.12).[71]

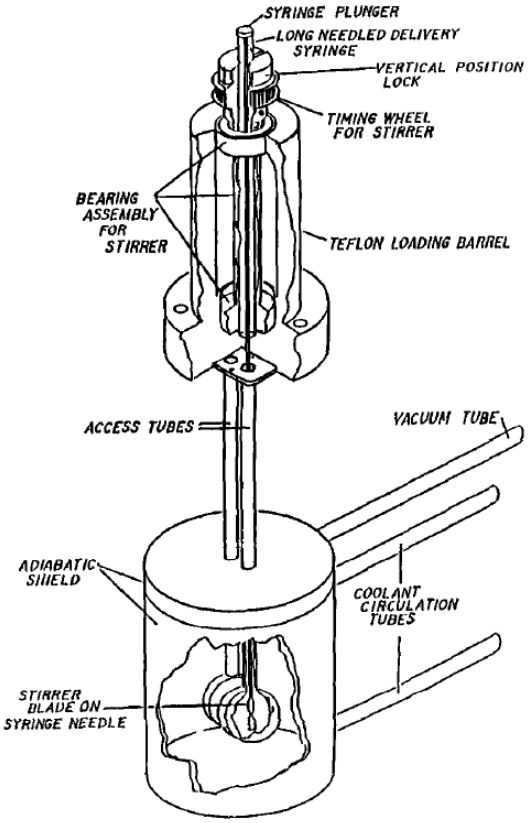

Figure 1.12. Drawing of an Isothermal Titration Calorimeter Cell. Reproduced from Wiseman *et al.*[71] with Permission.

For example suppose there are two chemical species A and B which interact to form species C while either producing or absorbing heat (equation 1.26).

$$A + B \overset{\Delta H_{react}}{\rightleftharpoons} C \tag{1.26}$$

The experiment can be arranged with species A in the syringe and B in the cell or vice versa. An injection schedule is specified by the user (with number of injections, injection volumes, injection durations and time between injections) as well as several other experimental variables (stirring speed, cell temperature, acquisition time, and pre-injection delay time). Once initiated, the experiment will proceed without further user input. Initially, the cell is equilibrated to the desired temperature and stirring begins. During the course of an experiment power is supplied to three resis-

tive heaters. The first is a feedback heater supplying power to the adiabatic jacket maintaining it at a slightly lower temperature than the reference cell $\Delta T_2 \approx 0$. In addition, a resistive heater supplies a small constant power to the reference cell. Another feedback heater supplies power to the sample cell in order to maintain $\Delta T_1 = 0$. This is the feedback power recorded by instrument and is the only feedback power referred to in the remainder of the thesis. Initially, the feedback power is allowed to stabilize, establishing a baseline, followed by the pre-injection delay, then execution of the injection schedule. In the absence of a reaction the feedback power is equivalent to the power supplied to the reference cell.[71] Species A is ejected from the syringe and mixes with the cell solution allowing for the reaction to take place which either produces or absorbs heat. The reaction heat produced/absorped occurs in the sample cell but not the reference cell creating a temperature gradient detected by the thermocouple between the two cells. The temperature gradient activates the feedback circuit which causes a change in the amount of power being supplied to the sample cell, driving the ΔT_1 back to zero (Figure 1.13).[79]

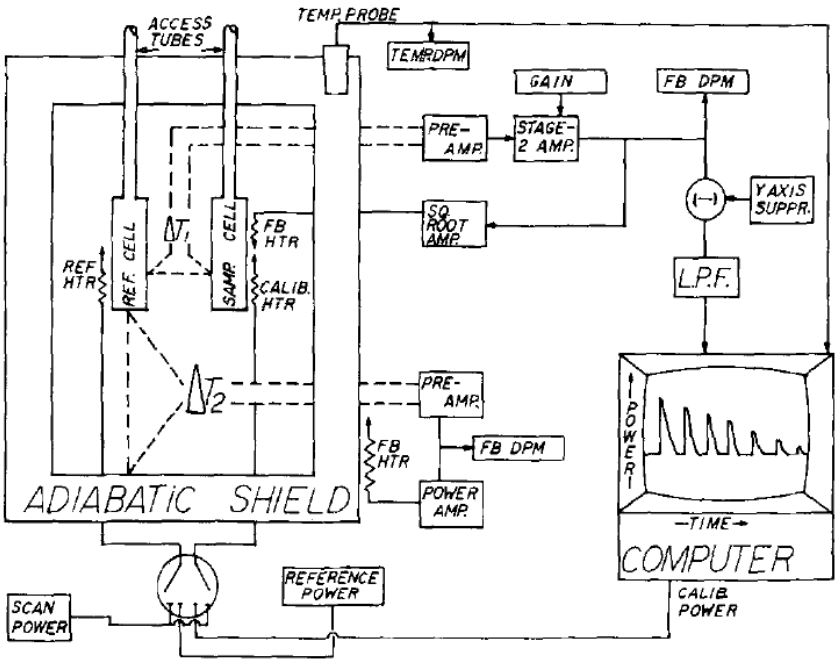

Figure 1.13. Block Diagram of an Isothermal Titration Calorimeter. Reproduced from Wiseman *et al.*[71] with permission.

The feedback power is digitally sampled and recorded by the instrument.[71] An exothermic reaction will cause the supplied feedback power to temporarily decrease (Figure 1.14a) which will appear as a downwards deflection in the baseline while an endothermic reaction will cause the supplied power to temporarily increase appearing as an upwards deflection (Figure 1.14b), once the reaction is finished the feedback power will return to baseline. The entire process will produce a spike of heat usually referred to as a peak, multiple injections can be performed in order to produce multiple peaks. Once a theoretical baseline is established (see 1.2.3.1) peaks can be integrated to quantify thermodynamics and peak shapes can be used to quantify kinetics.

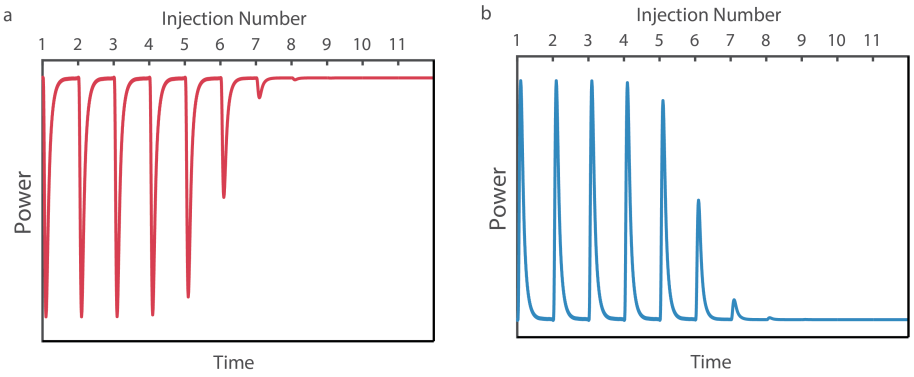

Figure 1.14. Peaks Produced by an isothermal titration calorimeter. (a) Peaks produced by and exothermic reaction (b) Peaks produced by an endothermic reaction.

1.2.1.3 Modern Isothermal Titration Calorimeters

There are a number of different isothermal titration calorimeters available from two main companies; Microcal a subsidiary of Malvern Instruments, and TA instruments. Microcal produces three main ITCs; the original VP-ITC, the ITC-200 and the recently released PEAQ-ITC (Figure 1.15). TA instruments also produce the Nano ITC and the Affinity ITC (Figure 1.16). All of these instruments work under the same principles but differ in terms of operating temperature, cell and syringe size, shape and material, baseline noise levels, stir speed and response time (Tables 1.1 and 1.2). The instrument specification can influence the physical, chemical and

electronic processes that must occur in order for heat to be measured. Therefore, instrumentation will affect the resulting shape of the instrument output.

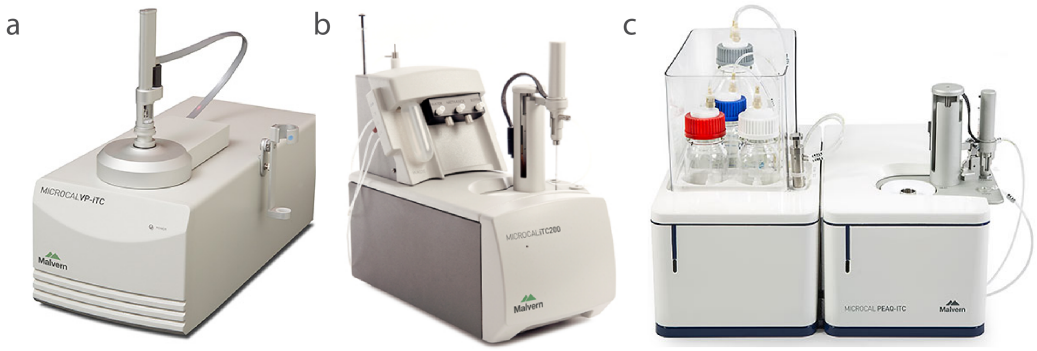

Figure 1.15. Microcal Isothermal Titration Calorimeters. (a) VP-ITC, (b) ITC-200, and (c) PEAQ-ITC

Table 1.1. Microcal Isothermal Titration Calorimeters Specifications[78,80,81]

Property	VP-ITC	ITC-200	PEAQ-ITC
Cell Material and Shape	Hastelloy, coin-shaped with stems		
Syringe Shape	Twisted rectangle		
Operating Temp	2°C to 80°C		
Cell Volume	1400μL	200 μL	200 μL
Syringe Volume	280 μL	40 μL	40 μL
Stir Speed	0RPM-1088RPM	0RPM-1500RPM	0RPM-400RPM
Baseline Noise	0.5 nCal s^{-1}	0.2 nCal s^{-1}	0.15 nCal s^{-1}
Response Time	20 s	10 s	8 s

Figure 1.16. TA Isothermal Titration Calorimeters. (a) Nano ITC and (b) Affinity ITC

Table 1.2. TA Isothermal Titration Calorimeters Specifications[82,83]

Property	Nano ITC	Affinity ITC
Cell Material and Shape	24K Gold/Hastelloy, cylindrical with stems	
Syringe Shape	Twisted rectangle	
Operating Temp	2°C to 80°C	
Cell Volume	190 μL	
Baseline Noise	0.3 nCal s^{-1}	
Response Time	11 s	
Stir Speed	0RPM-400RPM	0RPM-200RPM
Syringe Volume	50 μL	250 μL

1.2.2 ITC Standards and Applications

1.2.2.1 Standard ITC Experiments

There are several standard ITC experiments used to calibrate the instrument, ensure that the instrument is functioning properly, and for practice setting up experiments. The three most common standards are methanol injections into water, electric heater pulses, and calcium injections into ethylenediaminetetraacetic acid (EDTA) (Ca^{2+}/EDTA injections). For methanol injections the syringe is loaded

with dilute amounts of methanol in water (typically ≈ 0.5%) and pure water is loaded into the cell.[78] Injections are performed and heat is produced due to the heat of dilution of methanol. Importantly, this experiment demonstrates that even when no specific interaction is present between the syringe and cell contents, heats of dilution are still present. This adds additional complexity when performing experiments as the measured heat will be a combination of the reaction heats in addition to dilution heats. However, this can be rectified via blank subtraction (see 1.2.3.1). Another standard ITC experiment is electric heater pulses, where a user defined amount of power is supplied to a special reference heater connected to the sample cell (Figure 1.13) over a specific amount of time.[84] The heat will flow into the sample cell allowing for it to be measured like an ordinary reaction. This experiment is typically used to ensure that the instrument's compensation system is functioning correctly as total heat measured by the compensation system can be directly compared to the total heat produced by the electric heater. Lastly, Ca^{2+}/EDTA injections can be used as a standard binding experiment;[85] EDTA binds calcium in a 1:1 ratio with large enthalpies ($\Delta H \approx$ -3.5 kCal mol^{-1}), strong affinity ($K_d \approx 0.180$ μM),[86] and rapid association rates ($k_{on} \approx 5{\cdot}10^6$ M^{-1} s^{-1}).[86] Also, the reagents are inexpensive and easy to prepare making Ca^{2+}/EDTAtitrations ideal for user practice and to ensure proper calorimeter function.[85]

1.2.2.2 Single Site Binding

ITC is most commonly applied to probing single site binding, in particular drug-target interactions.[87] ITC measures the affinity, enthalpy and stoichiometry of intermolecular interactions by titrating ligand (L) into macromolecule (M).[71] Injections introduce ligand into the cell which will bind to the macromolecule producing/absorbing heat. The peak produced by the injection can be integrated in order to calculate the total heat of the process (Figure 1.17). Throughout the titration the macromolecule will become increasingly saturated with ligand and a plot of the total heat per mole of injected ligand vs. the $[L] : [M]$ will appear sigmoidal. The steepness of this sigmoid at the inflection point is related to the affinity (K_d) of

the macromolecule-ligand interaction. Furthermore, the inflection point of the sigmoid will occur when $[L] : [M] = 1$ making the experimental output sensitive to the stoichiometry (n) of the reaction.[71] Lastly, the total heat produced per mole of injected ligand is directly related to the enthalpy of binding (ΔH_{bind}). By fitting a single experimental curve with the appropriate equations (see 1.2.4) it is possible to extract all three of these parameters. This makes ITC a robust technique for directly probing single site binding interactions.

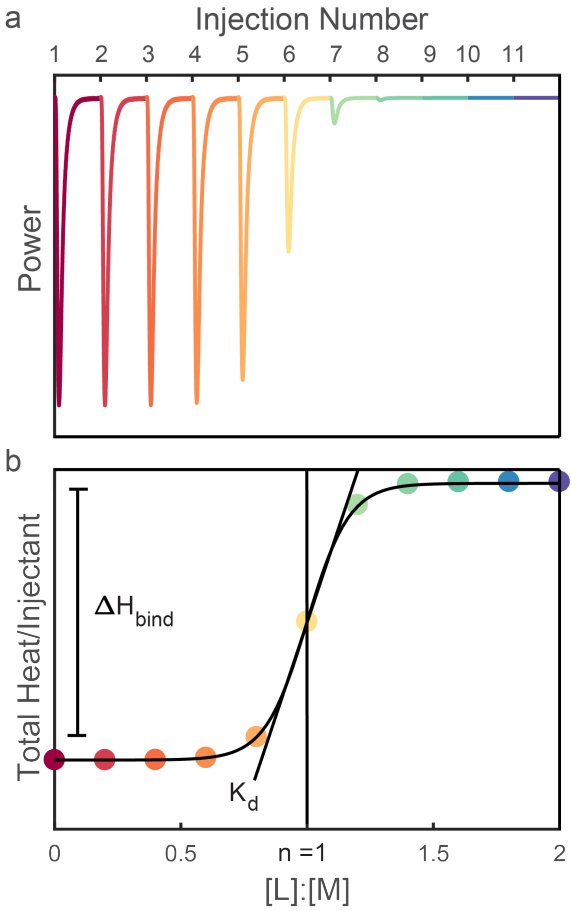

Figure 1.17. Single Site Binding Isotherm. (a) Peaks produced by titration (b) Integrated heat per injection vs. the ratio of ligand to macromolecule.

1.2.2.3 Complex Binding Interactions and Global Analysis

ITC can also be used to elucidate more complex binding interactions such as peptide self assembly[88] and aggregation,[89] protein adsorption,[88] micelle formation,[90] and

multi-site binding.[91,92] When measuring complex interactions the heat produced by each injection is often a result of several simultaneous events. Therefore, individual thermodynamic parameters can be difficult to extract depending on the affinities and enthalpies of the events.[91] One of the more powerful applications of ITC is in global fitting analysis where multiple ITC experiments with varying conditions such as temperature or concentration are simultaneously fit with a global set of parameters. ITC has become a popular technique for probing the temperature dependence of binding in order to extract heat capacities. This is because ITC is capable of directly measuring the enthalpy at each individual temperature while other techniques require indirect measurement using the van't Hoff equation.[93,94] This in part has motivated the development of several software packages designed for extracting heat capacities by group fitting sets of ITC isotherms obtained at different temperatures.[95,96,97]

1.2.2.4 Binding Kinetics

Kinetic data can also be extracted from ITC binding experiments by analyzing how the heat due to binding develops with time. The shapes of the peaks are related to the association kinetics k_{on} and the total heats of the injections can be used to extract the K_d, these values can then be used to calculate the dissociation rate ($k_{off} = K_d \cdot k_{on}$) allowing for a complete thermodynamic and kinetic characterization in a single experiment.[98] This type of analysis has been performed on a number of protein, DNA and RNA systems such as HIV-1 reverse transcriptase with small molecule inhibitors, TPP riboswitch with one of its ligands,[98] and the GAAA tetraloop with its receptor.[99] Notably, in the case of the RNA aptamer TPP riboswitch it was possible to elucidate a coupled binding then folding mechanism by performing a global fit with a set of ITC isotherms obtained at different temperatures. Interestingly, despite being information rich there are few applications of ITC to measure binding kinetics. One possibility for this scarcity is that in general large concentrations of both macromolecule and ligand are required to obtain an appreciable signal creating situations where association kinetics proceed too rapidly

to measure (see 1.2.8).

1.2.2.5 Enzyme Kinetics

The vast majority of kinetic ITC applications are to measure enzyme kinetics as there are many advantages (see section 1.1.3.5). The methods typically used are described in detail below (see section 1.3).

1.2.3 Pre-analysis Data Processing of Raw Data

1.2.3.1 Baseline Correction

Raw ITC data must undergo two main processing steps prior to analysis; 1) baseline correction, and 2) blank subtraction. As mentioned above (see 1.2.1.2) even in the absence of any reaction the feedback heater supplies power to the sample cell, this is the baseline of the experiment. Heat that is produced/absorbed by a process in the cell will cause the feedback power to deflect away from the baseline.[71] Therefore, when a reaction is taking place in the cell the theoretical baseline power must be interpolated. The difference between the measured feedback power and the baseline is a direct readout of the power being produced in the reaction cell. Therefore, after baseline correction, the baseline becomes the zero power value and any deflection from the corrected baseline will be interpreted as heat due to a process in the cell (Figure 1.18). Usually, the baseline is interpolated during a peak, however, factors such as rapid noise fluctuations, baseline drift, or slower reactions (aka. wider peaks and therefore longer interpolations) may make it difficult to accurately establish the baseline, leading to systematic errors.[100,101] Typically, a reasonable baseline can be established using algorithms integrated into the ITC analysis software, however, when data quality is poor, it is necessary to manually interpolate the baseline or use more advanced techniques. One notable method uses automated peak shape analysis in order to decipher the difference between baseline noise/drift and actual heat being produced in the cell. This is accomplished by extracting the main structural

components of a typical peak by singular value decomposition (SVD), followed by using these components as constraints while fitting the isotherms. This method makes it possible to extract accurate thermodynamic information from noisy data which would be impossible using conventional analysis.[102]

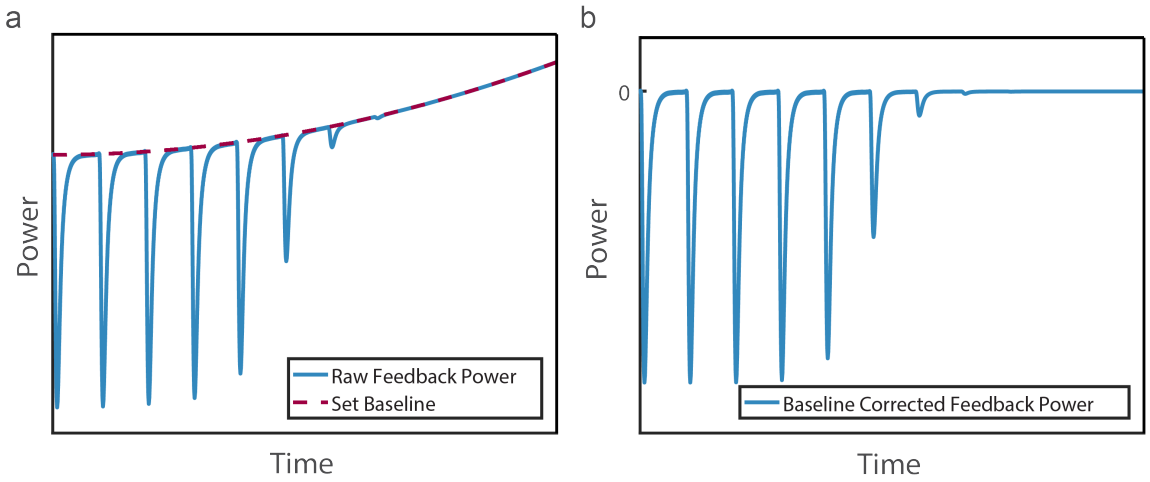

Figure 1.18. Baseline Correction of ITC Data. (a) Raw feedback power obtained from multi-injection experiment (b) Baseline corrected ITC data

1.2.3.2 Blank Subtraction

The compensation system of an isothermal titration calorimeter will measure all the heat produced/absorbed in the cell due to an injection. This means that in addition to heat from the reaction of interest, ITCs will also simultaneously measure heats of dilution of the syringe contents into the cell, mechanical heats due to the injection process, and dilution of the cell contents due to the addition of the syringe solution. The latter dilution factor is usually negligible as syringe volumes are typically much smaller than the cell volumes (see Table 1.1 and 1.2). Fortunately, by performing a blank experiment it is possible to directly measure the heat of dilution of the syringe contents as well as the mechanical heats. A blank experiment is performed with the same syringe contents as the actual experiment but the cell contents do not contain the interacting species. For example, in a single site binding experiment the syringe will contain ligand while the cell will contain only buffer. The blank experiment

can be baseline corrected in the same manner as the actual experiment and a blank subtraction can be performed by subtracting the blank experiment from the actual experiment (Figure 1.19). The resulting isotherm only includes heat for the reaction process(es) of interest.

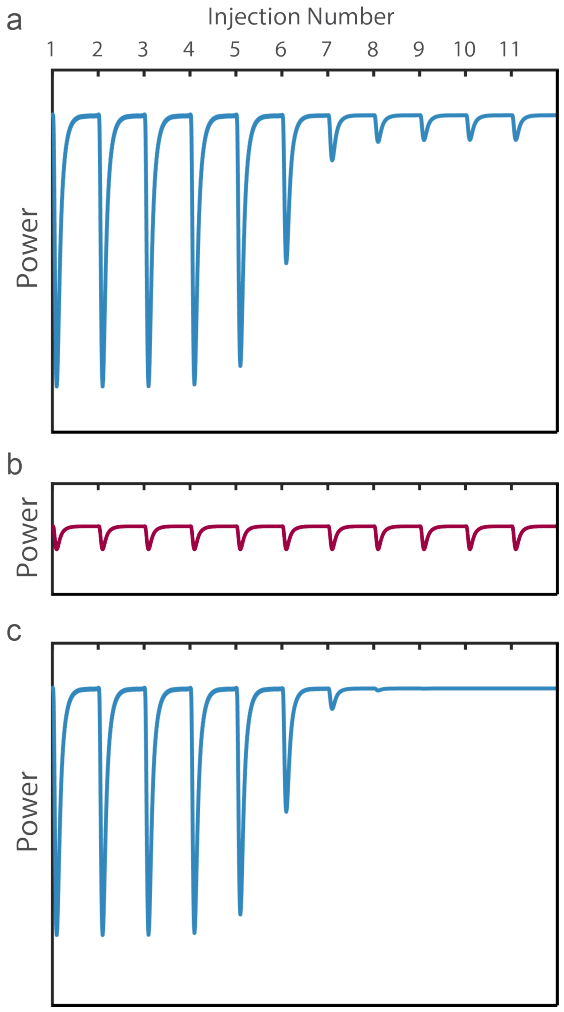

Figure 1.19. Blank Subtraction of ITC Data. (a) Raw experiment with ligand in syringe and macromolecule in cell (b) Blank experiment with ligand in syringe but only buffer in cell (c) Blank subtracted data (a)-(b).

1.2.4 Analyzing Thermodynamics Using ITC

1.2.4.1 Modelling Thermodynamic Data

To extract thermodynamic parameters each peak of the raw isotherm can be individually integrated in order to calculate the total heat per injection. The total heat per injection as a function of $[L] : [M]$ will be sensitive to the K_d, ΔH_{bind} and n and can be mathematically modelled in order to extract these thermodynamic parameters. For an experiment with ligand (L) in the syringe at a concentration $[L]_{syr}$ and macromolecule (M) in the cell at a concentration $[M]_{cell}$ the total amount of ligand and macromolecule in the cell ($[L_0]$ and $[M_0]$) after total injection volume v_{inj} can be calculated as.

$$[L_0] = [L]_{syr} \cdot (1 - f) \tag{1.27}$$

$$[M_0] = [M]_{cell} \cdot f \tag{1.28}$$

Where the dilution factor f can be expressed in terms of the total volume of the cell V_{cell} and the total injection volume.[103]

$$f = e^{-\frac{v_{inj}}{V_{cell}}} \tag{1.29}$$

By solving the appropiate binding polynomial for the model of interest it is possible to express the concentrations of all the species as a function of the injected volume and the equilibrium constant(s) of the interaction(s). In the case of single site binding ($M + L \overset{K_d}{\rightleftharpoons} ML$) the quadratic binding polynomial can be analytically solved in order calculate $[ML]_i$[104] which will be a function of both the affinity (K_d) of the interaction as well as the total concentrations of both species $[M_0]$ and $[L_0]$ (which are a function of v_{inj}, Equations 1.27-1.29). Importantly, heat is produced as a result of the dynamic formation of $[ML]$ due to an injection. Therefore, the total heat due to the ith injection (ΔQ_i) with an injection volume $v_{inj,i}$ will be the total heat produced when going from $v_{inj} = 0$ to $v_{inj} = \sum_{j=1}^{i-1} v_{inj,j}$ denoted (Q_{i-1}) subtracted from and the total heat produced when going from $v_{inj} = 0$ to

$v_{inj} = \sum_{j=1}^{i} v_{inj,j}$ denoted (Q_i).

$$\Delta Q_i = Q_i - Q_{i-1} \tag{1.30}$$

where

$$Q_i = \Delta H_{bind} \cdot [ML]_i \cdot V_{cell} \tag{1.31}$$

By fitting equation 1.30 to the experimental data it is possible to extract the K_d as well as the ΔH_{bind}. In addition, the stoichiometry of the interaction n can be extracted by allowing for $n \cdot [M]_{cell}$ sites and floating n. Alternatively, n can be fixed at 1 and $[M]_{cell}$ can be floated. Although the equations above are for single site binding they can be expanded to more complex situations such as those mentioned above (see 1.2.2.3).

1.2.5 C-value

An important metric to consider when quantifying any type of interaction between two or more species is the c-value, a unitless parameter defined as

$$c = \frac{[M]_{cell}}{K_d} \tag{1.32}$$

for a single intependent site. The c-value is directly related to the shape of an isotherm; For very high c-values ($c \gg 1000$) essentially all added ligand will bind until the macromolecule is saturated making a rectangular curve with a height of ΔH_{bind}. Moderate c-values ($1 < c < 1000$) will create sigmoid shaped isotherms that are very sensitive to small changes in c. Lastly, for a low c-value ($c < 1$) the trace will be nearly horizontal and very little of the injected ligand will bind to the macromolecule (Figure 1.20). Isotherms with moderate values of c can be analyzed to extract the affinity, enthalpy and stoichiometry. However, in the case of isotherms with high c, only the enthalpy and stoichiometry can be extracted. Furthermore, low c isotherms give accurate information on the values of K_d and ΔH_{bind} only if the values of $[M]_{cell}$ and n are fixed.[105]

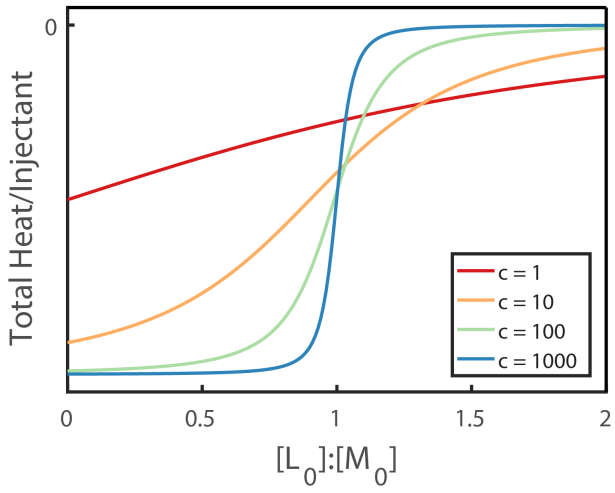

Figure 1.20. Effect of c-value on the shape of an isotherm.

1.2.6 Analyzing Kinetics Using ITC

1.2.6.1 Processes Involved in Measuring Heat

In order to extract kinetic parameters from ITC experiments it is necessary to properly model how heat produced in the reaction cell is measured by the instrument with time. This requires mathematical description of the various mechanical, chemical and electrical processes that are involved in measuring heat in an isothermal titration calorimeter. The first process is the injection, where the syringe species is injected into the cell, followed by mixing throughout the cell. As the components of the syringe and cell mix together they are able to react which produces or absorbs heat depending on the ΔH of the reaction. The heat produced or absorbed must then transfer from the site of the reaction to the solid thermocouple resulting in a temperature gradient. This causes the feedback circuitry to alter the electric power supplied to the sample cell heater, which is recorded by the instrument allowing for quantitative analysis. Figure 1.21 below summarizes the processes that must occur in order to perform the measurement of heat in a calorimeter. In the following subsections enzyme kinetics is used as an example to illustrate how reaction kinetics are typically modelled using ITC; in this example enzyme is placed in the cell at a

concentration $[E]_{cell}$ and substrate in the syringe at a concentration $[S]_{syringe}$. These equations can be expanded to different kinetic scenarios depending on the system being studied.

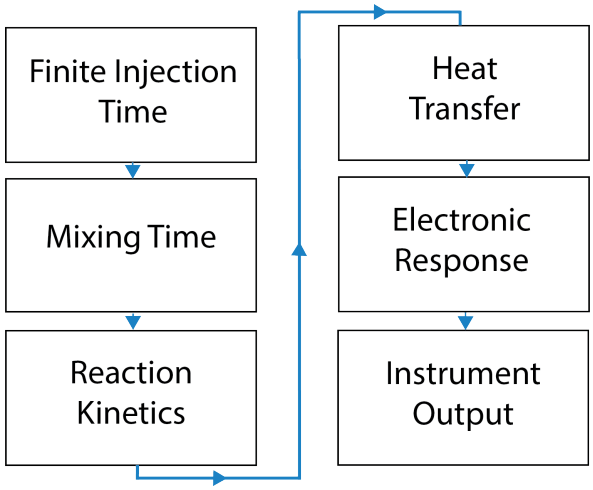

Figure 1.21. ITC Processes.

1.2.6.2 Finite Injection Time

During the finite injection, substrate from the syringe is introduced into the cell at a rate $\frac{d[S]_{cell}}{dt}$ and this can be quantified using Equation 1.33.

$$\frac{d[S]_{cell}}{dt} = [S]_{syringe} \cdot Rate_{dil} - [S]_{cell} \cdot Rate_{dil} \tag{1.33}$$

The first term in this case accounts for the appearance of substrate in the cell and the second term accounts for the substrate already in the cell which is diluted by the injection. Similarly, the dilution of the enzyme in the cell can be expressed as.

$$\frac{d[E_0]}{dt} = -[E]_{cell} \cdot Rate_{dil} \tag{1.34}$$

Where $[E]_{cell}$ is the concentration of enzyme in the cell and $Rate_{dil}$ is the dilution rate defined as $\frac{v_{inj,i}}{V_{cell} \cdot \tau_{inj}}$ where τ_{inj} is the total duration of the injection. In cases where $v_{inj,i}$ is small, the contribution of Equation 1.34 will be minute and can therefore be ignored.

1.2.6.3 Mixing Time

The pre-reaction mixing can be treated as a mass transfer step from an "unmixed" reservoir that is unavailable to react to a "mixed" reservoir that is available to react. This transfer step is typically assumed to proceed as a first order kinetic process with a characteristic mixing time τ_{mix} which depends on the viscosity of the solution, geometry of the cell and syringe paddle as well as stirring speed.[98]

$$\frac{d[S]_{mix}}{dt} = \frac{[S]_{unmix}}{\tau_{mix}} \tag{1.35}$$

$$\frac{d[S]_{unmix}}{dt} = [S]_{syringe} \cdot Rate_{dil} - \frac{[S]_{unmix}}{\tau_{mix}} \tag{1.36}$$

Where $[S]_{mix}$ is the concentration of mixed substrate and $[S]_{unmix}$ is the concentration of unmixed substrate. The time integral of these differential equations is equivalent to:

$$[S]_{mix,t} = [S]_{unmix,t} \otimes e^{-\frac{t}{\tau_{mix}}} \tag{1.37}$$

where $\otimes$ indicates the convolution (Equation 1.42).

1.2.6.4 Reaction Kinetics

The reaction kinetics and heat generation can be modelled using differential equations or integrated rate equations. In principle, any kinetic scheme with any number of heat sources can be modelled. In the case of MM kinetics the coupled set of differential equations can be written as

$$\frac{d[S]_{avail}}{dt} = \frac{d[S]_{mix}}{dt} - \frac{k_{cat} \cdot [E_0] \cdot [S]_{avail}}{[S]_{avail} + K_m} \tag{1.38}$$

$$\frac{d[P]}{dt} = \frac{k_{cat} \cdot [E_0] \cdot [S]_{avail}}{[S]_{avail} + K_m} \tag{1.39}$$

where $[S]_{avail}$ is the total concentration of substrate available to react. In this case the only appreciable source of reaction heat is from the generation of product,

therefore, $h(t)$, the instantaneous heat, can be expressed as

$$h(t) = \Delta H_{cat} \cdot V_{cell} \cdot \frac{d[P]}{dt} \tag{1.40}$$

Which can be calculated by numerically integrating differential equations 1.38-1.40. Alternatively, the differential equations are solvable for some mechanisms[98] allowing for an analytical solution.

1.2.6.5 Heat Transfer and Electronic Response

The heat transfer and electronic response processes are difficult to separate in practice; therefore they are mathematically grouped into one process. In a compensation calorimeter an infinitesimally short burst of heat produced in the cell will be measured over time by the instrument. The shape of the curve produced by the instrument due to the burst of heat is referred to as the instrument response function ($f(t)$). When a reaction is taking place in the cell, the instantaneous heat produced at every point in time is recorded by the instrument according to the instrument response function. Therefore, the heat being measured by an instrument at a given point in time has contributions from the heat produced in the cell at various points in the past. This process can be mathematically modelled as a convolution between the instantaneous heat curve and the instrument response function. Typically, a negative exponential response function with a characteristic response time τ_r is used as the response function.[98,99,84,106,107] The response time is either measured by fitting a negative exponential to the tail end of a methanol injection[98,106] or by using the response time reported by the manufacturer (see Tables 1.1 and 1.2). The instrument output can therefore be expressed as

$$g(t) = h(t) \otimes f(t) \tag{1.41}$$

Where $g(t)$ is the calculated instrument output and the convolution is defined according to:

$$h(t) \otimes f(t) = \int_0^t f(\tau) \cdot g(t-\tau) d\tau \tag{1.42}$$

The convolution can be performed using various numerical methods such as the polynomial multiplication method[108] or the convolution theorem (see 3.6.8).

The calculated instrument output $g(t)$ can be digitally resampled in order to match the time between data points of the actual instrument output. This allows for direct comparison between the calculated and measured curves, for example in a fitting routine, in order to extract kinetic data.

1.2.7 Deconvoluting ITC Data

As described above the instrument output can be modelled via a convolution between the instantaneous heat and the instrument response function. This can be quantitatively compared to the instrument output in order to extract kinetic data. An alternative way of analyzing data is by deconvoluting the instrument response from the measured instrument output in order to directly calculate the instantaneous heat. For a negative exponential response function it is possible to derive an analytic solution for the deconvolution using Laplace transforms (Equation 3.21).[84]

$$h_{deconv}(t) = g_{experimental}(t) + \tau_r \cdot \frac{dg_{experimental}}{dt} \tag{1.43}$$

Where $h_{deconv}(t)$ is the mathematically deconvoluted instantaneous heat and $g_{experimental}(t)$ is the baseline corrected, blank subtracted instrument output. The instantaneous heat obtained via deconvolution can be directly fit to a calculated instantaneous heat ($h(t)$) or qualitatively analyzed.

1.2.8 Timescale of Kinetics Measurable by ITC

All of the processes outlined above will affect the shape of a peak or curve measured by an isothermal titration calorimeter. However, the relative time scales of

each of these processes governs which process dominates in determining the shape of the peak. When the reaction kinetics are much slower than the injection time, mixing time and response function of the instrument, the instrument output can be accurately modelled by only considering the reaction kinetics. However, when reactions occur on the same time scale as the instrument processes it is necessary to model all of the processes as each one will contribute in determining the shape of the peaks.[60,98] Due to the added complexity of measuring rapid time scale kinetics, most of the kinetic applications using ITC are with slower time scale kinetics.[109,84,110,111,112,113,114,115,116]

1.3 ITC Enzyme Kinetics Applications

1.3.1 Single Injection Enzyme Kinetics

1.3.1.1 Arrangement and Analysis

Using ITC it is possible to extract both the K_m and k_{cat} values with a single injection. This is accomplished by placing a solution of enzyme in the syringe and substrate in the cell or vice versa. In the former arrangement enzyme is injected into the cell to a desired concentration and enzyme catalyzes the reaction until substrate is depleted. As a result subsequent injections do not provide additional heat due to catalysis.[84] In the latter arrangement substrate is placed in the syringe and enzyme in the cell. Substrate is injected into the cell to a desired concentration and enzyme will catalyze substrate until the substrate is completely consumed. In this arrangement multiple injections can be performed producing multiple kinetic peaks.[117] The injected substrate will reach a maximum concentration at the end of the injection (τ_{inj}) then be depleted over time. In a single injection experiment, substrate is depleted with time allowing for the rate of catalysis to be sampled over a range of substrate concentrations. Therefore a full $\frac{d[P]}{dt}$ vs. $[S]$ curve can be obtained from a single continuous experiment (Figure 1.22). By fitting the experimental curve with

enzyme kinetics models (see 1.2.6) the K_m, k_{cat} and ΔH_{cat} can be extracted. The analysis described above assumes there is no product inhibition, however, quantitative analysis is also possible when product inhibition is present (see[117] and chapter 3). Several studies (including chapter 1 and 2 below) use trypsin as a model system for developing enzyme kinetics techniques[84,60] as it is a well characterized system with a low K_m.

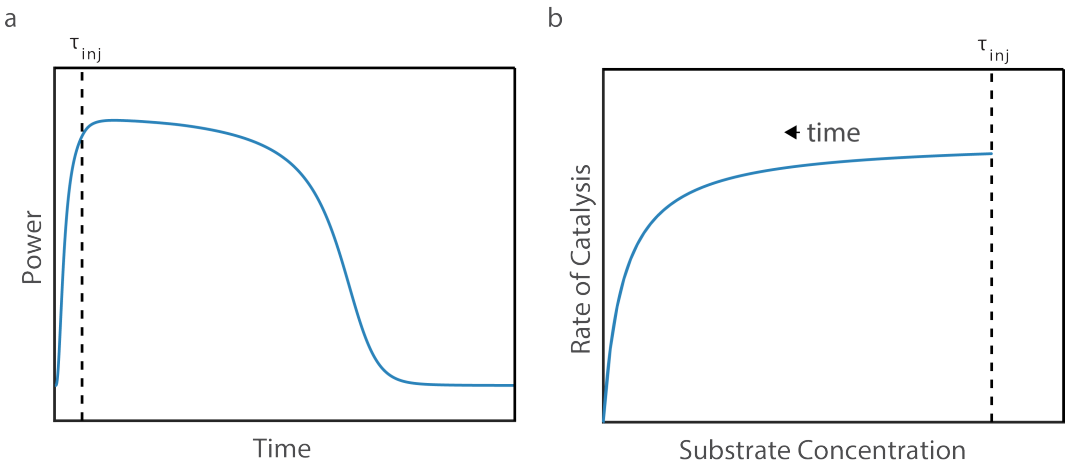

Figure 1.22. Single Injection Enzyme Kinetics Technique. Modelled with substrate in the syringe and enzyme in the cell. (a) Raw curve measured by a single injection (b) Rate of catalysis vs substrate concentration calculated from (a) starting at τ_{inj}.

1.3.1.2 Obtaining High Enough Concentration to Measure k_{cat}

As mentioned above (Section 1.1.1.4) obtaining accurate values of K_m and k_{cat} requires measurement of the enzyme velocity at a sufficiently high concentration of substrate. If this condition is not met, the Michaelis-Menten equation simplifies to $\frac{k_{cat}\cdot[E_0]\cdot[S]}{K_m}$. Therefore, only the ratio of the MM parameters can be extracted as they will have a large covariance.[12] This has implications when designing single injection experiments. When substrate is initially in the cell it must be arranged such that $[S]_{cell} \gg K_m$. In the case where substrate is placed in the syringe the dilution factor when introducing syringe species into the cell must be considered. The concentration of substrate as well as the injection volume must be adjusted such that $[S]_{syr} \cdot (1 - f(v_{inj,i})) \gg K_m$ where $f(v_{inj,i})$ is the dilution factor defined

above (Equation 1.29). This may introduce additional complications when dealing with substrates that have solubility issues.

1.3.1.3 Single Injection Experiments in the Presence of Inhibitor

An important application of the single injection method is to extract the strength and mode of inhibitors. This can be accomplished by performing multiple single injection experiments at differing concentrations of inhibitor allowing for measurement of the k_{cat} and K_m as a function of the inhibitor concentration by analysing each experiment as above.[114,115] This application is powerful as it allows for measurement of both the strength and mode of inhibition, however, multiple experiments are required. As a result these measurements can be very time consuming as it is necessary to clean and load the cell/syringe as well as wait for the baseline to equilibrate prior to each experiment.

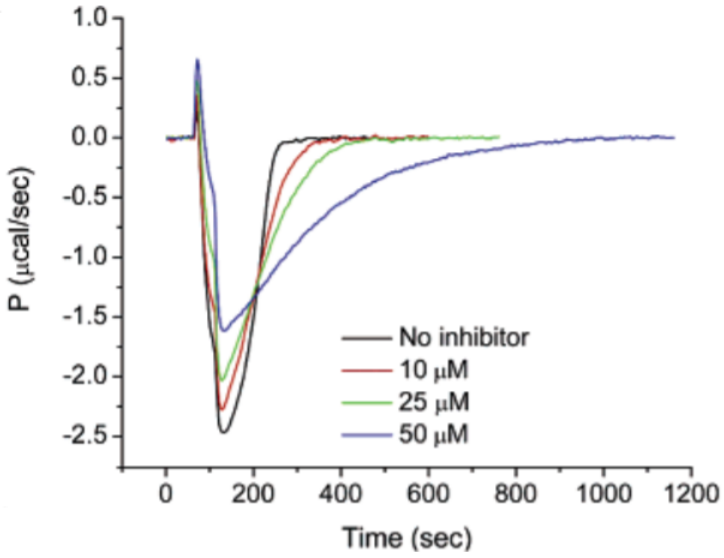

Figure 1.23. Single Injection Enzyme Kinetics Experiments with Varying Concentrations of Inhibitor. Reproduced from Poduch *et al.*[115] with permission.

1.3.2 Multiple Injection Enzyme Kinetics

In addition to measuring a MM curve in a single transient, it is also possible to measure enzyme kinetics using initial rate measurements with a single multi-injection ITC experiment.[60] In this application the concentration of enzyme in the cell must be low enough such that substrate is not depleted over long periods of time. Importantly, the rate of catalysis is proportional to the offset distance from the baseline (Figure 1.24a). Therefore, once the enthalpy of the reaction is measured (with a single injection experiment 1.3.1), it is possible to directly calculate the rate of catalysis using Equation 1.44 (Figure 1.24b).

$$\frac{d[P]}{dt} = \frac{1}{\Delta H_{cat} \cdot V_{cell}} \cdot \frac{dQ}{dt} \tag{1.44}$$

Where $\frac{dQ}{dt}$ is the measured power offset from the baseline. By performing multiple injections of substrate into enzyme, (represented by different colours in Figure 1.24a) it is possible to measure the power level at multiple concentrations of substrate which can used to calculate the rate of catalysis using Equation 1.44 and produce an entire $\frac{d[P]}{dt}$ vs. $[S]$ curve (Figure 1.24b). A large advantage to this technique is that it only requires measurement of the offset from the baseline and does not require taking into account the finite injection time, mixing time, or the response function making the analysis simple. Additionally, multiple experiments can be performed with varying amounts of inhibitor in the cell in order to extract the strength and mode of inhibition.

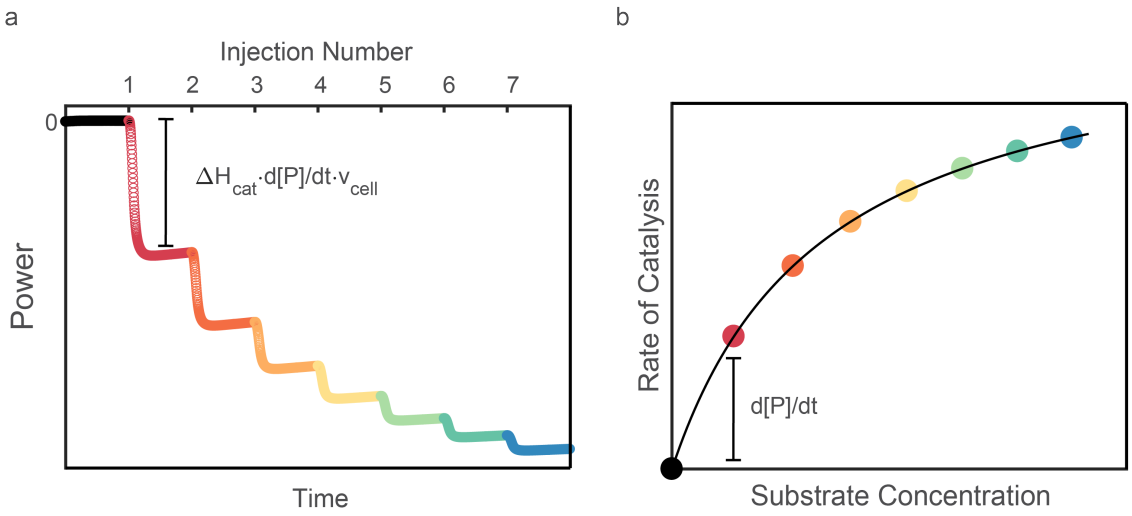

Figure 1.24. Multiple Injection Enzyme Kinetics ITC Experiments.

1.4 Thesis Objectives

The ability to rapidly measure and extract enzyme kinetics and quantify enzyme-inhibitor interactions is crucial for the drug design and development process. There are a variety of tools for measuring enzyme kinetics, however, they are accompanied by a number of drawbacks. Isothermal titration calorimetry is a robust tool for extracting enzyme kinetics as it measures heat, a near universal feature of chemical reactions. Also, ITC has become a standard instrument in biochemistry labs. The obvious advantages and ubiquitousness of ITCs makes rapid ITC based methods for measuring enzyme kinetics and enzyme-inhibitor interactions valuable for the drug design and development process.

This thesis describes the development of ITC based methods for quantifying rapid enzyme kinetics and efficiently extracting thermodynamic/kinetic parameters of enzyme-inhibitor interactions. In chapter 2, the lower time resolution limits of various ITC instruments are examined and determined to be on the sub-second scale indicating that rapid kinetics are in principle accessible using ITC. While modelling rapid enzyme kinetics we demonstrate that conventional methods are not capable of quantitatively reproducing the experimental output. In order to rectify this,

we experimentally establish a new approach for calculating an ITCs output which quantitatively agrees with experimental data. Applying this approach to another enzyme-substrate system allows us to discover unique enzyme kinetics. Furthermore, the techniques developed in subsequent chapters incorporate this approach allowing for access to rapid kinetics throughout the thesis. In chapter 3, a multiple injection method is developed which allows for the strength and mode of inhibition to be measured up to 10 times more rapidly than previous ITC based methods. This is accomplished by placing both substrate and inhibitor in the syringe and enzyme in the cell. Therefore, each injection allows for extraction of a full MM curve at a different concentration of inhibitor. In addition, a deconvolution method is presented, which enables visual assessment of the mode of inhibition and provides a model-free way of analyzing data. In chapter 4 a pair of complementary methods are developed. The first allows for rapid measurement of the association rate of enzyme inhibitors along with the affinity by titrating inhibitor into enzyme and substrate. The second allows for rapid measurement of the dissociation rate of enzyme inhibitors along with the affinity by titrating enzyme-inhibitor complex into substrate. In addition, through extensive simulations and calculations, the limitations of the complementary methods described above are explored, and guidelines are reported in order to assist users attempting to utilize them. In short, this thesis describes the development and testing of several new ITC based methods for measuring enzyme kinetics and enzyme-inhibitor interactions.

1.5 References

[1] Mireia Garcia-Viloca et al. “How Enzymes Work: Analysis by Modern Rate Theory and Computer Simulations”. In: *Science* 303.5655 (2004), pp. 186–195.

[2] Alexander Kienhöfer, Peter Kast, and Donald Hilvert. “Selective Stabilization of the Chorismate Mutase Transition State by a Positively Charged Hydrogen Bond Donor”. In: *Journal of the American Chemical Society* 125.11 (2003), pp. 3206–3207.

[3] Marie Zhang et al. “Crystal Structure of Bovine Low Molecular Weight Phosphotyrosyl Phosphatase Complexed with the Transition State Analog Vanadate”. In: *Biochemistry* 36.1 (1997), pp. 15–23.

[4] A. Shurki et al. “How Much Do Enzymes Really Gain by Restraining Their Reacting Fragments?” In: *Journal of the American Chemical Society* 124.15 (2002), pp. 4097–4107.

[5] Pratul K. Agarwal et al. “Network of coupled promoting motions in enzyme catalysis”. In: *Proceedings of the National Academy of Sciences* 99.5 (2002), pp. 2794–2799.

[6] Laura Masgrau and Donald G. Truhlar. “The Importance of Ensemble Averaging in Enzyme Kinetics”. In: *Accounts of Chemical Research* 48.2 (2015), pp. 431–438.

[7] Sharon Hammes-Schiffer. “Catalytic Efficiency of Enzymes: A Theoretical Analysis”. In: *Biochemistry* 52.12 (2013), pp. 2012–2020.

[8] Thomas Shafee. *Enzyme catalysis energy levels 2*. URL: https://commons.wikimedia.org/wiki/File:Enzyme_catalysis_energy_levels_2.svg.

[9] George Edward Briggs and John Burdon Sanderson Haldane. “A Note on the Kinetics of Enzyme Action”. In: *Biochemical Journal* 19.2 (1925), pp. 338–339.

[10] Kenneth A. Johnson and Roger S. Goody. "The Original Michaelis Constant: Translation of the 1913 Michaelis–Menten Paper". In: *Biochemistry* 50.39 (2011), pp. 8264–8269.

[11] M. Picozzi and R. De Cristofaro. "Effect of temperature on the association step in thrombin-fibrinogen interaction". In: *Biochemical Journal* 294.Pt 2 (1993), pp. 563–567.

[12] Marko Goličnik. "Exact and approximate solutions for the decades-old Michaelis-Menten equation: Progress-curve analysis through integrated rate equations". In: *Biochemistry and Molecular Biology Education* 39.2 (2011), pp. 117–125.

[13] Melanie I. Stefan and Nicolas Le Novère. "Cooperative Binding". In: *PLOS Computational Biology* 9.6 (2013), e1003106.

[14] Carol M. Porter and Brian G. Miller. "Cooperativity in monomeric enzymes with single ligand-binding sites". In: *Bioorganic Chemistry* 43 (2012), pp. 44–50.

[15] Carl Frieden. "Kinetic Aspects of Regulation of Metabolic Processes: THE HYSTERETIC ENZYME CONCEPT". In: *Journal of Biological Chemistry* 245.21 (1970), pp. 5788–5799.

[16] G. Robert Ainslie, Jonathan P. Shill, and Kenneth E. Neet. "Transients and Cooperativity: A SLOW TRANSITION MODEL FOR RELATING TRANSIENTS AND COOPERATIVE KINETICS OF ENZYMES". In: *Journal of Biological Chemistry* 247.21 (1972), pp. 7088–7096.

[17] Hughes JP et al. "Principles of early drug discovery". In: *British Journal of Pharmacology* 162.6 (2011), pp. 1239–1249.

[18] C. J. Zheng et al. "Therapeutic Targets: Progress of Their Exploration and Investigation of Their Characteristics". In: *Pharmacological Reviews* 58.2 (2006), pp. 259–279.

[19] Janet N. Y. Chan, Corey Nislow, and Andrew Emili. “Recent advances and method development for drug target identification”. In: *Trends in Pharmacological Sciences* 31.2 (2010), pp. 82–88.

[20] Vilmos Fülöp, Zsolt Böcskei, and László Polgár. “Prolyl Oligopeptidase”. In: *Cell* 94.2 (1998), pp. 161–170.

[21] Vilmos Fülöp et al. “Distribution of Immunoreactive Prolyl Oligopeptidase in Human and Rat Brain”. In: *Neurochemical Research* 32.8 (2007), pp. 1365–1374.

[22] T. Pt Männisto Pekka et al. “Prolyl oligopeptidase: a potential target for the treatment of cognitive disorders”. In: *DRUG NEWS* 20.5 (2007), pp. 293–305.

[23] Kanayo Suzuki et al. “Prolyl oligopeptidase inhibition-induced growth arrest of human gastric cancer cells”. In: *Biochemical and Biophysical Research Communications* 443.1 (2014), pp. 91–96.

[24] L. Polgár. “The prolyl oligopeptidase family”. In: *Cellular and Molecular Life Sciences CMLS* 59.2 (2002), pp. 349–362.

[25] R. Van Elzen et al. “Ligand-induced conformational changes in prolyl oligopeptidase: a kinetic approach”. In: *Protein Engineering, Design and Selection* 30.3 (2017), pp. 219–226.

[26] Zoltán Szeltner et al. “The loops facing the active site of prolyl oligopeptidase are crucial components in substrate gating and specificity”. In: *Biochimica et Biophysica Acta (BBA) - Proteins and Proteomics* 1834.1 (2013), pp. 98–111.

[27] Timothy S. Tracy. *Atypical Cytochrome P450 Kinetics*.

[28] R. Oldenburg Kevin et al. “Assay Miniaturization for Ultra-High Throughput Screening of Combinatorial and Discrete Compound Libraries: A 9600-Well (0.2 Microliter) Assay System”. In: *Journal of Biomolecular Screening* 3.1 (1998), pp. 55–62.

[29] E. Stevens Michelle et al. “Comparison of Automation Equipment in High Throughput Screening”. In: *Journal of Biomolecular Screening* 3.4 (1998), pp. 305–311.

[30] Craig A. Umscheid, David J. Margolis, and Craig E. Grossman. “Key Concepts of Clinical Trials: A Narrative Review”. In: *Postgraduate Medicine* 123.5 (2011), pp. 194–204.

[31] Joseph A. DiMasi, Henry G. Grabowski, and Ronald W. Hansen. “Innovation in the pharmaceutical industry: New estimates of R&D costs”. In: *Journal of Health Economics* 47 (2016), pp. 20–33.

[32] Katarzyna Smietana, Marcin Siatkowski, and Martin Møller. “Trends in clinical success rates”. In: *Nature Reviews Drug Discovery* 15 (2016), pp. 379–380.

[33] Lizi Xia et al. “Structure–Affinity Relationships and Structure–Kinetics Relationships of Pyrido[2,1-f]purine-2,4-dione Derivatives as Human Adenosine A3 Receptor Antagonists”. In: *Journal of Medicinal Chemistry* 60.17 (2017), pp. 7555–7568.

[34] Claudia Binda et al. “Insights into the mode of inhibition of human mitochondrial monoamine oxidase B from high-resolution crystal structures”. In: *Proceedings of the National Academy of Sciences of the United States of America* 100.17 (2003), pp. 9750–9755.

[35] R. Z. Cer et al. “IC(50)-to-K(i): a web-based tool for converting IC(50) to K(i) values for inhibitors of enzyme activity and ligand binding”. In: *Nucleic Acids Research* 37.Web Server issue (2009), W441–W445.

[36] Hao Lu and Peter J. Tonge. “Drug–target residence time: critical information for lead optimization”. In: *Current Opinion in Chemical Biology* 14.4 (2010), pp. 467–474.

[37] Robert A. Copeland. “The dynamics of drug-target interactions: drug-target residence time and its impact on efficacy and safety”. In: *Expert Opinion on Drug Discovery* 5.4 (2010), pp. 305–310.

[38] Peter J. Tummino and Robert A. Copeland. “Residence Time of Receptor−Ligand Complexes and Its Effect on Biological Function”. In: *Biochemistry* 47.20 (2008), pp. 5481–5492.

[39] D. C. Swinney. “The role of binding kinetics in therapeutically useful drug action”. In: *Current Opinion in Drug Discovery & Development* 12.1 (2009), pp. 31–39.

[40] Georges Vauquelin and Steven J. Charlton. “Long-lasting target binding and rebinding as mechanisms to prolong in vivo drug action”. In: *British Journal of Pharmacology* 161.3 (2010), pp. 488–508.

[41] John V. Schloss. “Significance of slow-binding enzyme inhibition and its relationship to reaction-intermediate analogs”. In: *Accounts of Chemical Research* 21.9 (1988), pp. 348–353.

[42] Christopherson Richard I. and Duggleby Ronald G. “Metabolic Resistance: The Protection of Enzymes against Drugs which are Tight-Binding Inhibitors by the Accumulation of Substrate”. In: *European Journal of Biochemistry* 134.2 (1983), pp. 331–335.

[43] Ronald G. Duggleby and Richard I. Christopherson. “Metabolic resistance to tight-binding inhibitors of enzymes involved in the de novo pyrimidine pathway Simulation of time-dependent effects”. In: *European Journal of Biochemistry* 143.1 (1984), pp. 221–226.

[44] Robert A. Copeland. “Kinetics of Single-Substrate Enzyme Reactions”. In: *Enzymes*. John Wiley & Sons, Inc., 2002, pp. 109–145.

[45] John F. Morrison. “The slow-binding and slow, tight-binding inhibition of enzyme-catalysed reactions”. In: *Trends in Biochemical Sciences* 7.3 (1982), pp. 102–105.

[46] Maris Vilums et al. “Structure–Kinetic Relationships—An Overlooked Parameter in Hit-to-Lead Optimization: A Case of Cyclopentylamines as Chemokine Receptor 2 Antagonists”. In: *Journal of Medicinal Chemistry* 56.19 (2013), pp. 7706–7714.

[47] Elisabeth V. Schneider et al. “Structure–kinetic relationship study of CDK8/CycC specific compounds”. In: *Proceedings of the National Academy of Sciences* 110.20 (2013), pp. 8081–8086.

[48] Douglas S. Johnson, Eranthie Weerapana, and Benjamin F. Cravatt. “Strategies for discovering and derisking covalent, irreversible enzyme inhibitors”. In: *Future medicinal chemistry* 2.6 (2010), pp. 949–964.

[49] Stephane De Cesco et al. “Covalent inhibitors design and discovery”. In: *European Journal of Medicinal Chemistry* 138 (2017), pp. 96–114.

[50] James G. Robertson. “Mechanistic Basis of Enzyme-Targeted Drugs”. In: *Biochemistry* 44.15 (2005), pp. 5561–5571.

[51] Jarkko I VenäLäInen et al. “Slow-binding inhibitors of prolyl oligopeptidase with different functional groups at the P1 site”. In: *Biochemical Journal* 382.Pt 3 (2004), pp. 1003–1008.

[52] J. Michael Bradshaw et al. “Prolonged and tunable residence time using reversible covalent kinase inhibitors”. In: *Nature Chemical Biology* 11 (2015), p. 525.

[53] Phillip A. Schwartz et al. “Covalent EGFR inhibitor analysis reveals importance of reversible interactions to potency and mechanisms of drug resistance”. In: *Proceedings of the National Academy of Sciences* 111.1 (2014), pp. 173–178.

[54] Robert A. Copeland. *Kinetics of Single-Substrate Enzyme Reactions*. Enzymes. John Wiley & Sons, Inc., 2002, pp. 109–145.

[55] Petr Kuzmič, James Solowiej, and Brion W. Murray. “An algebraic model for the kinetics of covalent enzyme inhibition at low substrate concentrations”. In: *Analytical Biochemistry* 484 (2015), pp. 82–90.

[56] Yiping Jia, Amarendra Kumar, and Smita S. Patel. “Equilibrium and Stopped-flow Kinetic Studies of Interaction between T7 RNA Polymerase and Its Promoters Measured by Protein and 2-Aminopurine Fluorescence Changes”. In: *Journal of Biological Chemistry* 271.48 (1996), pp. 30451–30458.

[57] E M Horwitz et al. “Kinetic identification of a two-state glucagon receptor system in isolated hepatocytes. Interconversion of homogeneous receptors”. In: *Journal of Biological Chemistry* 260.16 (1985), pp. 9307–9315.

[58] Franziska Exnowitz, Bernd Meyer, and Thomas Hackl. “NMR for direct determination of Km and Vmax of enzyme reactions based on the Lambert W function-analysis of progress curves”. In: *Biochimica et Biophysica Acta (BBA) - Proteins and Proteomics* 1824.3 (2012), pp. 443–449.

[59] Robert A. Copeland, David L. Pompliano, and Thomas D. Meek. “Drug-target residence time and its implications for lead optimization”. In: *Nature Review Drug Discovery* 5.9 (2006), pp. 730–739.

[60] Matthew J. Todd and Javier Gomez. “Enzyme Kinetics Determined Using Calorimetry: A General Assay for Enzyme Activity?” In: *Analytical Biochemistry* 296.2 (2001), pp. 179–187.

[61] Julius A. Goldbarg et al. “The colorimetric determination of -glutamyl transpeptidase with a synthetic substrate”. In: *Archives of Biochemistry and Biophysics* 91.1 (1960), pp. 61–70.

[62] G. Bruce Birrell et al. “Allosteric Interactions within Subsites of a Monomeric Enzyme: Kinetics of Fluorogenic Substrates of PI-Specific Phospholipase C”. In: *Biophysical Journal* 84.5 (2003), pp. 3264–3275.

[63] Janice Lawandi et al. “Inhibitors of Prolyl Oligopeptidases for the Therapy of Human Diseases: Defining Diseases and Inhibitors”. In: *Journal of Medicinal Chemistry* 53.9 (2010), pp. 3423–3438.

[64] Jarkko I. Venäläinen et al. “Substrate-dependent, non-hyperbolic kinetics of pig brain prolyl oligopeptidase and its tight binding inhibition by JTP-4819”. In: *Biochemical Pharmacology* 64.3 (2002), pp. 463–471.

[65] J. G. Nørby. “Coupled assay of Na+,K+-ATPase activity”. In: *Methods in enzymology* 156 (1988), pp. 116–9.

[66] W. R. McClure. “Kinetic analysis of coupled enzyme assays”. In: *Biochemistry* 8.7 (1969), pp. 2782–2786.

[67] Xiwei Zheng et al. “Analytical methods for kinetic studies of biological interactions: A review”. In: *Journal of Pharmaceutical and Biomedical Analysis* 113 (2015), pp. 163–180.

[68] Cheenou Her, Jaideep Singh, and V. V. Krishnan. “Effect of sucralose on the enzyme kinetics of invertase using real-time NMR spectroscopy and progress curve analysis”. In: *Carbohydrate Research* 455 (2018), pp. 5–9.

[69] E. Rodrigues et al. “Inclusion of Polyphenol Oxidase Substrates in -Cyclodextrin: A 1 H-NMR Study”. In: *Journal of inclusion phenomena and macrocyclic chemistry* 44.1 (2002), pp. 395–397.

[70] Gabriel E. Wagner et al. “Monitoring fast reactions by spatially-selective and frequency-shifted continuous NMR spectroscopy: application to rapid-injection protein unfolding”. In: *Chemical Communications* 49.30 (2013), pp. 3155–3157.

[71] Thomas Wiseman et al. “Rapid measurement of binding constants and heats of binding using a new titration calorimeter”. In: *Analytical Biochemistry* 179.1 (1989), pp. 131–137.

[72] Apiradee Wangsakan, Pavinee Chinachoti, and David J. McClements. "Isothermal titration calorimetry study of the influence of temperature, pH and salt on maltodextrin–anionic surfactant interactions". In: *Food Hydrocolloids* 20.4 (2006), pp. 461–467.

[73] Søren N. Olsen. "Applications of isothermal titration calorimetry to measure enzyme kinetics and activity in complex solutions". In: *Thermochimica Acta* 448.1 (2006), pp. 12–18.

[74] Leigh Murphy et al. "An enzymatic signal amplification system for calorimetric studies of cellobiohydrolases". In: *Analytical Biochemistry* 404.2 (2010), pp. 140–148.

[75] Hassan Rana et al. "Isothermal titration calorimetry uncovers substrate promiscuity of bicupin oxalate oxidase from Ceriporiopsis subvermispora". In: *Biochemistry and Biophysics Reports* 5 (2016), pp. 396–400.

[76] Jelesarov Ilian and Bosshard Hans Rudolf. "Isothermal titration calorimetry and differential scanning calorimetry as complementary tools to investigate the energetics of biomolecular recognition". In: *Journal of Molecular Recognition* 12.1 (1999), pp. 3–18.

[77] M. Bastos et al. "Fast titration experiments using heat conduction microcalorimeters". In: *Journal of Biochemical and Biophysical Methods* 23.3 (1991), pp. 255–258.

[78] Malvern. *MicroCal PEAQ-ITC Specifications*. 2016.

[79] P. Bäckman et al. "Heat conduction calorimeters: time constants, sensitivity and fast titration experiments". In: *Journal of Biochemical and Biophysical Methods* 28.2 (1994), pp. 85–100.

[80] Malvern. *MicroCal VP-ITC Specifications*. 2016.

[81] Microcal. *ITC-200 Microcalorimeter User's Manual*. 22 Industrial Drive East.

[82] TA Instruments. *Affinity ITC Specifications*.

[83] TA Instruments. *Nano ITC Specifications*.

[84] Mark K. Transtrum, Lee D. Hansen, and Colette Quinn. “Enzyme kinetics determined by single-injection isothermal titration calorimetry”. In: *Methods* 76 (2015), pp. 194–200.

[85] Clara Ràfols et al. “The Ca2+–EDTA chelation as standard reaction to validate Isothermal Titration Calorimeter measurements (ITC)”. In: *Talanta* 154 (2016), pp. 354–359.

[86] M. Naraghi. “T-jump study of calcium binding kinetics of calcium chelators”. In: *Cell calcium* 22.4 (1997), pp. 255–268.

[87] Ernesto Freire, Obdulio L. Mayorga, and Martin Straume. “Isothermal titration calorimetry”. In: *Analytical Chemistry* 62.18 (1990), 950A–959A.

[88] Maryam Kabiri and Larry D. Unsworth. “Application of Isothermal Titration Calorimetry for Characterizing Thermodynamic Parameters of Biomolecular Interactions: Peptide Self-Assembly and Protein Adsorption Case Studies”. In: *Biomacromolecules* 15.10 (2014), pp. 3463–3473.

[89] Tatsuya Ikenoue et al. “Heat of supersaturation-limited amyloid burst directly monitored by isothermal titration calorimetry”. In: *Proceedings of the National Academy of Sciences* 111.18 (2014), pp. 6654–6659.

[90] Watson Loh, César Brinatti, and Kam Chiu Tam. “Use of isothermal titration calorimetry to study surfactant aggregation in colloidal systems”. In: *Biochimica et Biophysica Acta (BBA) - General Subjects* 1860.5 (2016), pp. 999–1016.

[91] Chad A. Brautigam. “Fitting two- and three-site binding models to isothermal titration calorimetric data”. In: *Methods* 76 (2015), pp. 124–136.

[92] Samuel J. Darby et al. “An isothermal titration calorimetry study of phytate binding to lysozyme”. In: *Journal of Thermal Analysis and Calorimetry* 127.2 (2017), pp. 1201–1208.

[93] Ashish and R. Kishore. "Thermodynamic characterizations of an intramolecularly hydrogen bonded C5-structure across proteinogenic residue". In: *FEBS Letters* 417.1 (1997), pp. 97–100.

[94] Nicholas E. Grossoehme, Anne M. Spuches, and Dean E. Wilcox. "Application of isothermal titration calorimetry in bioinorganic chemistry". In: *JBIC Journal of Biological Inorganic Chemistry* 15.8 (2010), pp. 1183–1191.

[95] hiranmayi duvvuri hiranmayi, lucas c wheeler lucas c, and Michael Harms. "pytc: a python package for analysis of Isothermal Titration Calorimetry experiments". In: *bioRxiv* (2017), https://doi.org/10.1101/234682.

[96] Huaying Zhao, Grzegorz Piszczek, and Peter Schuck. "SEDPHAT – a platform for global ITC analysis and global multi-method analysis of molecular interactions". In: *Methods* 76 (2015), pp. 137–148.

[97] Chad A. Brautigam et al. "Integration and global analysis of isothermal titration calorimetry data for studying macromolecular interactions". In: *Nature Protocols* 11 (2016), p. 882.

[98] Dominique Burnouf et al. "kinITC: a new method for obtaining joint thermodynamic and kinetic data by isothermal titration calorimetry". In: *Journal of the American Chemical Society* 134.1 (2011), pp. 559–565.

[99] Kirk A. Vander Meulen and Samuel E. Butcher. "Characterization of the kinetic and thermodynamic landscape of RNA folding using a novel application of isothermal titration calorimetry". In: *Nucleic Acids Research* 40.5 (2012), pp. 2140–2151.

[100] Joel Tellinghuisen and John D. Chodera. "Systematic errors in isothermal titration calorimetry: Concentrations and baselines". In: *Analytical Biochemistry* 414.2 (2011), pp. 297–299.

[101] Joel Tellinghuisen. "Optimizing Experimental Parameters in Isothermal Titration Calorimetry". In: *The Journal of Physical Chemistry B* 109.42 (2005), pp. 20027–20035.

[102] Sandro Keller et al. “High-Precision Isothermal Titration Calorimetry with Automated Peak-Shape Analysis”. In: *Analytical Chemistry* 84.11 (2012), pp. 5066–5073.

[103] Bent W. Sigurskjold. “Exact Analysis of Competition Ligand Binding by Displacement Isothermal Titration Calorimetry”. In: *Analytical Biochemistry* 277.2 (2000), pp. 260–266.

[104] Sonia Vega, Olga Abian, and Adrian Velazquez-Campoy. “A unified framework based on the binding polynomial for characterizing biological systems by isothermal titration calorimetry”. In: *Methods* 76 (2015), pp. 99–115.

[105] Joel Tellinghuisen. “Isothermal titration calorimetry at very low c”. In: *Analytical Biochemistry* 373.2 (2008), pp. 395–397.

[106] Krishna Rajarathnam and Jörg Rösgen. “Isothermal Titration Calorimetry of Membrane Proteins – Progress and Challenges”. In: *Biochimica et biophysica acta* 1838.1 (2014), 10.1016/j.bbamem.2013.05.023.

[107] A. Velázquez-Campoy, O. López-Mayorga, and M. A. Cabrerizo-Vílchez. “Determination of the Rigorous Transfer Function of An Isothermal Titration Microcalorimeter with Peltier Compensation”. In: *Journal of Thermal Analysis and Calorimetry* 57.1 (1999), pp. 343–359.

[108] Michael T. Heideman. “Convolution and Polynomial Multiplication”. In: *Multiplicative Complexity, Convolution, and the DFT*. Ed. by Michael T. Heideman. New York, NY: Springer New York, 1988, pp. 27–60.

[109] Brent A. Williams and Eric J. Toone. “Calorimetric evaluation of enzyme kinetic parameters”. In: *Journal of Organic Chemistry* 58.13 (1993), pp. 3507–3510.

[110] P. E. Morin and E. Freire. “Direct calorimetric analysis of the enzymatic activity of yeast cytochrome c oxidase”. In: *Biochemistry* 30.34 (1991), pp. 8494–8500.

[111] G. D. Watt. “A microcalorimetric procedure for evaluating the kinetic parameters of enzyme-catalyzed reactions: kinetic measurements of the nitrogenase system”. In: *Analytical biochemistry* 187.1 (1990), pp. 141–146.

[112] Nurul Karim, Hirofumi Okada, and Shun-ichi Kidokoro. “Calorimetric evaluation of the activity and the mechanism of cellulases for the hydrolysis of cello-oligosaccharides accompanied by the mutarotation reaction of the hydrolyzed products”. In: *Thermochimica Acta* 431.1-2 (2005), pp. 9–20.

[113] Nurul Karim and Shun-ichi Kidokoro. “Precise and continuous observation of cellulase-catalyzed hydrolysis of cello-oligosaccharides using isothermal titration calorimetry”. In: *Thermochimica Acta* 412.1-2 (2004), pp. 91–96.

[114] Heiko Poppe et al. “Cyclic nucleotide analogs as probes of signaling pathways”. In: *Nature Methods* 5.4 (2008), pp. 277–278.

[115] Ewa Poduch et al. “Design of Inhibitors of Orotidine Monophosphate Decarboxylase Using Bioisosteric Replacement and Determination of Inhibition Kinetics”. In: *Journal of Medicinal Chemistry* 49.16 (2006), pp. 4937–4945.

[116] Richard J. Willson et al. “Determination of Thermodynamic and Kinetic Parameters from Isothermal Heat Conduction Microcalorimetry: Applications to Long-Term-Reaction Studies”. In: *Journal of Physical Chemistry* 99 (1995), pp. 7108–7113.

[117] Lifeng Cai, Aoneng Cao, and Luhua Lai. “An Isothermal Titration Calorimetric Method to Determine the Kinetic Parameters of Enzyme Catalytic Reaction by Employing the Product Inhibition as Probe”. In: *Analytical Biochemistry* 299.1 (2001), pp. 19–23.

Chapter 2

Measuring Rapid Time-scale Reaction Kinetics Using Isothermal Titration Calorimetry

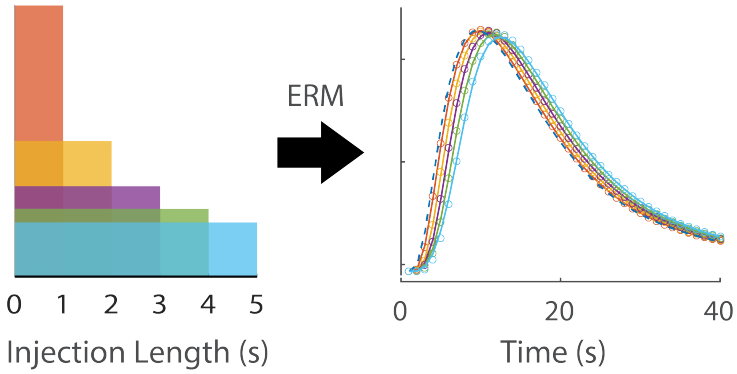

Preface

The design and development of inhibitors for therapeutic targets requires high throughput, accurate methods for assessing the thermodynamics and kinetics of target-inhibitor interactions. There are several techniques for measuring enzyme kinetics including UV-Vis spectroscopy, nuclear magnetic resonance, chromatography, electrophoresis, and mass spectrometry. However, these techniques have several inherent drawbacks and in some cases, it is not possible to extract kinetic information using these techniques. Isothermal titration calorimetry (ITC) is another technique for measuring kinetics, which can be used to measure the activity of an enzyme by measuring heat generation, a near universal property of reactions. One drawback of ITC is that measuring rapid kinetics requires mathematical consideration the physical, chemical, and electronic instrument processes that must occur to measure heat. As a result, most kinetic application of ITC are towards slowly evolving reactions. In this chapter, we demonstrate that standard commercial instruments are capable of second time-scale resolution. However, for rapid kinetics standard mathematical approaches for reproducing the instrument output lead to inherent deviations from the experimental output. Here we develop a new approach for modelling the instrument output which is capable of accurately reproducing the instrument output. This allows us to uncover unique enzyme dynamics. Our approach allows for accurate analysis of rapidly evolving kinetics with all the inherent advantages of ITC. In addition, the ability to rapidly characterize enzymes provides a foundation for the development of high throughput methods for testing enzyme inhibitor interactions.

2.1 Abstract

Isothermal titration calorimetry (ITC) is a powerful tool for acquiring both thermodynamic and kinetic data for biological interactions including molecular recognition and enzymatic catalysis. ITC-based kinetics measurements typically focus on reactions taking place over long timescales (tens of minutes or hours) in order to avoid

complications due to the finite length of time needed to detect heat flow in the calorimeter cell. While progress has been made towards analyzing more rapid reaction kinetics by ITC, the capabilities and limitations of this approach have not been thoroughly tested to date. Here, we report that the time resolution of commercial instruments is on the order of 0.2 seconds or less. We successfully performed rapid ITC kinetics assays with durations of just tens of seconds using the enzyme trypsin. This is substantially shorter than previous ITC enzyme measurements. However we noticed that for short reaction durations, standard assumptions regarding the isothermal titration calorimeter's instrument response led to significant deviations between calculated and measured ITC peak shapes. To address this issue, we developed an ITC empirical response model (ITC-ERM) that quantitatively reproduces ITC peak shapes for all reaction durations. Applying the ITC-ERM approach to another enzyme prolyl oligopeptidase, we unexpectedly discovered non-Michaelis-Menten kinetics in short time-scale measurements that are absent in more typical long time-scale experiments and are obscured in short time-scale experiments when standard assumptions regarding the instrument response are made. This highlights the potential of ITC measurements of rapid timescale kinetics in conjunction with the ITC-ERM approach to shed new light on biological dynamics.

2.2 Introduction

Isothermal titration calorimetry (ITC) is a powerful tool for determining thermodynamic and kinetic parameters for a range of biological reactions.[1,2] The instrument makes periodic injections of a macromolecule, ligand, or substrate solution into a sample cell containing a molecule of interest while recording how much power must be supplied to maintain a constant temperature. Exothermic reactions result in transient decreases in power, relative to the baseline, while endothermic reactions result in transient increases in the power supplied to the sample cell. ITC is commonly used to measure binding thermodynamics. In these applications, each peak in the ITC isotherm is integrated to yield the total amount of heat released or absorbed

during and following each injection. The resultant series of integrated heats can be fit to variety of equations to yield the affinity, enthalpy, entropy, and stoichiometry of binding interactions.[3] ITC can also be used to measure reaction kinetics. This is accomplished by analyzing the shapes of the peaks themselves, which are related to the timescale of heat generation during and following each injection. Rapid reactions lead to sharp ITC peaks that are complete in seconds or tens of seconds while slow reactions lead to broad peaks that may be minutes or even hours in length.[4,5] Quantitative ITC peak shape analysis has been used to characterize the kinetics of a wide variety of reactions including the chemical reactions of small molecules,[6] enzyme catalysis,[7,8,9,10,11,12,13,14,15,16,17] and biomolecular binding.[17,18,19,20,21,22]

ITC offers several advantages over other experimental kinetics methods such as surface plasmon resonance,[23] UV-vis spectrophotometry,[24,25,26] and nuclear magnetic resonance spectroscopy.[27] It can be performed entirely in solution under physiological conditions, does not require spectroscopically-active (eg. fluorescent) molecules, it is compatible with spectroscopically opaque solutions,[7] and can be applied to relatively dilute samples.[4] Despite its long history and technical advantages, kinetic applications of ITC remain fairly rare. A potential factor is the challenge of accurately modeling ITC peak shapes. This requires accounting for the various mechanical, chemical, and electrical processes that are involved in the measurement of an ITC isotherm. In practice, an instantaneous release of heat in the isothermal titration calorimeiter's cell is detected over a period of seconds or tens of seconds. When reactions take place on similar time scales to these processes, it is challenging to separate the kinetics of the reaction from the kinetics of the instrument response itself.[11,19] In contrast, for slower reactions taking place on the timescale of minutes to hours, the kinetics of the instrument response can essentially be ignored. Nevertheless, many interesting and biologically important reactions take place on the seconds timescale. Progress has been made towards modelling the isothermal titration calorimeter's instrument response and in measuring rapid reaction kinetics by ITC.[19] However to date the accuracy of the instrument response models has not been thoroughly tested, nor has the upper limit for reaction rates in ITC experiments been systematically

explored.

In this study, we have used a combination of electric heater pulses, Ca^{2+}/EDTA binding experiments, and enzyme assays with trypsin and prolyl oligopeptidase to map out the capabilities and limitations of rapid kinetics experiments using common benchtop ITC instruments, focusing mainly, but not exclusively, on the VP-ITC produced by MicroCal/Malvern. We found that this instrument is capable of extracting reaction times with sub-second accuracy (as is the MicroCal ITC-200 and the TA Instruments Nano ITC). Motivated by this result, we performed trypsin enzymatic reactions in which all of the injected substrate was exhausted in under a minute, which is more rapid than previous ITC enzyme assays by about a factor of 20. Using a previously-published kinetic ITC analysis technique,[9] we extracted enzyme parameters in agreement with literature values. However, the modeled ITC peak shapes were not well reproduced, potentially obscuring useful kinetic information. We therefore developed an ITC Empirical Response Model (ITC-ERM), which accurately reproduces both ITC peak shapes and kinetic parameters. Applying the ITC-ERM approach to rapid reactions of prolyl oligopeptidase, we observed surprising non-Michaelis-Menten kinetics that are completely obscured by previous ITC and spectroscopic analysis methods.

2.3 Results

2.3.1 Background

There are several related physical and chemical processes that must be considered when calculating the time-dependent ITC signal. Firstly, there is the user-selected finite injection time, during which some of the contents of the syringe are introduced to the sample cell, typically on the order of 1-500 seconds. Subsequently, during the pre-reaction mixing time, the injected solution is mixed homogeneously throughout the cell.[19] As the contents of the injection and sample cell are mixed, they can interact according to their intrinsic chemical kinetics,[19,4] leading to the release or

absorption of heat and the local heating or cooling of the solution at the site of reaction. This is followed by a heat transfer delay, the length of time necessary for the solid phase thermocouple to detect the small change in sample cell temperature, relative to the reference cell.[28,29,30,31] In an ITC feedback calorimeter this temperature difference activates the electronic response feedback circuit which causes a change in the amount of power being supplied to the sample cell, driving the temperature gradient back to zero.[30] Together, these processes determine the ultimate shape of the instrument output, i.e. the time-dependent signal (usually in μCal s^{-1}) that is recorded by the isothermal titration calorimeter. The preceding processes can all potentially contribute to the shape of a peak, however, the relative contribution and importance of each step has not been the subject of much attention to date.

Typically, the finite injection time, pre-reaction mixing, and chemical kinetic processes are combined to calculate the time-dependent rate at which heat is generated in the isothermal titration calorimeter cell, which we refer to as the instantaneous heat or $h(t)$ (see 1.2.6).[19] The post-reaction heat transfer and electronic response are usually modelled as a single function, which we refer to as $f(t)$. In most applications published to date, $f(t)$ has been expressed as a single- or bi-exponential decaying function.[19,20,29,32,33,34] When $f(t)$ is modelled as single-exponential, $f(t) = e^{-\frac{t}{\tau_r}}$, the constant τ_r is referred to as the time constant of the ITC instrument and is typically taken to be on the order of 5 to 15 seconds.[19] The instrument output, $g(t)$, is then calculated as the convolution of the instantaneous heat and the instrument response, $g(t) = h(t) \otimes f(t)$ (see 2.6). Physically, this implies that an instantaneous burst of heat in the calorimeter cell produces a signal with the shape of the response function, i.e. if $h(t)$ is the Dirac delta function, then $g(t) = f(t)$.

2.3.2 Rapid Injection Experiments

In order to test the ITC instrument outputs resulting from known inputs, we used EDTA and Ca^{2+} as a model host/guest binding reaction. This system has the advantage of very strong affinity ($K_d \approx 0.180$ μM)[35] providing tight control over

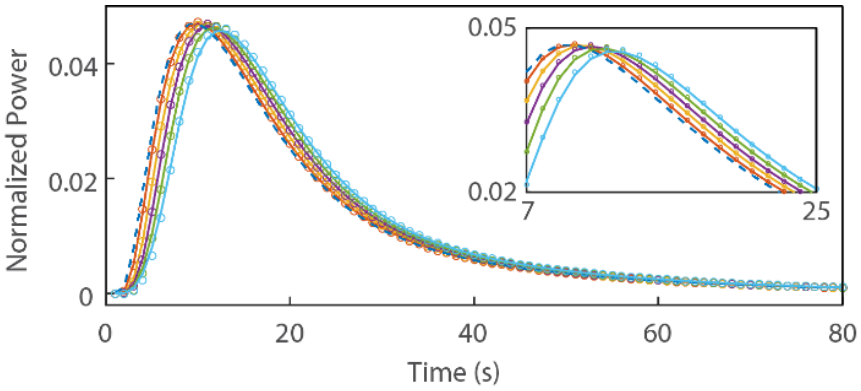

Figure 2.1. Rapid injections into EDTA using the VP-ITC. $CaCl_2$ (18 mM in syringe) was injected (1 μL injections) into the cell containing 1.8 mM EDTA. Area-normalized peaks (averages of 10 replicates) are shown for 0.2s (dashed blue line), 1s (orange circles), 2s (yellow circles), 3s (purple circles), 4s (green circles) and 5s (cyan circles) injections. The solid lines show the fit to the experimental peaks using the ERM approach (see below) while floating the injection length. Extracted lengths for the injections are plotted in Figure 2.S1

reaction stoichiometry, high reaction enthalpy ($\Delta H \approx$ -3.5 kCal M^{-1}) giving large heat signals, and extremely rapid association rates ($k_{on} \approx 5{\cdot}10^6$ M^{-1} s^{-1}),[35] meaning that the shapes of ITC peaks are dominated by factors other than the reaction kinetics, as desired for characterizing the instrument response. The pseudo first order time constant ($\tau_{react} = (k_{on}[EDTA])^{-1}$) for all Ca^{2+}/EDTA reactions recorded in this study are less than 2.5 ms. We performed a series of injections of Ca^{2+} into EDTA lasting between 0.2 and 5 seconds. During and following each injection we observed a deflection in the power due to the heat released by the Ca^{2+}/EDTA binding reaction, as shown in Figure 2.1. Although the heat signals are tens of seconds in length, the longer injections nevertheless give rise to peaks that are noticeably wider; the injections differ from each other by only 1 second but produce peaks that are clearly distinct. This demonstrates that a typical ITC instrument has sub-second time-resolution, as required for measuring rapid kinetic processes.

2.3.3 Rapid Time-Scale Enzyme Kinetics

The ITC traces obtained from injections of Ca^{2+} into EDTA, described above, suggest that short bursts of heat are detected over approximately 40 seconds by the VP-ITC instrument. We therefore aimed to test whether enzymatic reactions occurring on similar timescales can be accurately characterized by this calorimeter. We selected the well-studied enzyme trypsin and the substrate Nα-Benzoyl-L-arginine ethyl ester hydrochloride (BAEE) as a model system. Initial experiments were performed by injecting BAEE into the cell containing relatively low concentrations of trypsin, on the order of 10 nM (Figure 2.2). The observed heat signal from the instrument output is about 150 seconds in duration, indicating that the total duration of the enzyme reaction is slightly greater than 100 seconds, as the heat generated by the enzyme is detected with up to a roughly 50 second delay. The data were fit using a recently-developed approach in which the instantaneous heat, $h(t)$, is calculated according to the Michaelis-Menten (MM) equation, the instrument response, $f(t)$, is assumed to be single-exponential, and the enzyme kinetic parameters are extracted while simultaneously fitting an effective value for the instrument response time, τ_r.[9] In what follows, we refer to this as the variable-τ approach. The modelled curve closely follows the experimental data and the fitted parameters ($K_m = 3.42 \pm 0.08$ μM; $k_{cat} = 20.0 \pm 0.3$ s^{-1}; $\tau_r = 23.9 \pm 0.34$ s) are in good agreement with previously reported values ($K_m = 4$ µM; $k_{cat} = 15$ s^{-1}).[36,4] Next, more rapid transients were produced using higher concentrations of enzyme, on the order of 60 nM (Figure 2.2B). In this case, the instrument signal is roughly 70 seconds length, which is only 20 seconds longer in duration than the signal produced by a rapid injection of Ca^{2+} into EDTA. In other words, this enzymatic reaction occurs on a timescale equal to or less than the instrument response time. Once again, the data were fit using the variable-τ procedure. The extracted parameters ($K_m = 4.24 \pm 0.05$ μM; $k_{cat} = 16.7 \pm 0.1$ s^{-1}; $\tau_r = 16.4 \pm 0.16$ s) agreed well with reported values, however the modelled curve deviated substantially from the experimental data. Trypsin has been shown to follow Michaelis-Menten kinetics in numerous studies. This strongly suggests that the variable-τ procedure used to model the isothermal titration calorimeter's

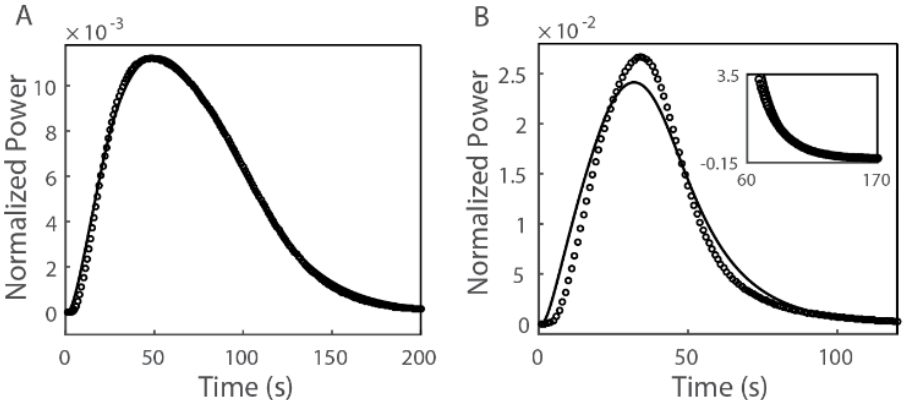

Figure 2.2. Single Injection Enzyme Kinetics for Trypsin using the VP-ITC fit with variable-τ approach. (A) Single injection (30 μL over 20 s) of BAEE (400 μM in syringe) into the cell containing trypsin 10 nM (open circles). Best fit according to the variable-τ approach.[11] (solid line). (B) Single injection of BAEE (1100 μM in syringe) into the cell containing trypsin 60 nM (open circles). Best fit according to the variable-τ approach.[11] (solid line).

response yields distorted peak shapes, at least for rapid reactions, potentially obscuring important kinetic information.

2.3.4 Factors Affecting ITC Peak Shapes

In order to develop an analytical approach that more closely reproduces ITC kinetic peak shapes, we re-examined the assumptions of the variable-τ method used above to analyze trypsin kinetics. These are 1) that pre-reaction mixing is effectively instantaneous and 2) that the post-reaction response of the calorimeter ($f(t)$ in Equation 2.10) is a single exponential decaying function. Inspection of the Ca^{2+}/EDTA traces in Figure 2.1 reveals that either one or both of these assumptions must be false. A short injection (0.2 s) produces a heat signal that increases up to the 9-second mark. For instantaneous mixing with a single-exponential response function, the maximum heat flow is necessarily at the end of the injection period. In this case, the maximum heat flow is obtained 9 seconds after the end of the injection.

One possible explanation for this delayed response is that it takes several seconds for the injected Ca^{2+} to mix with the EDTA in the cell. Note that the rate constant

for this reaction ($5{\cdot}10^6$ M^{-1} s^{-1})[35] is sufficiently large that it may be assumed that Ca^{2+} and EDTA react instantaneously once mixed. We tested the mixing time by performing a series of Ca^{2+} injections into a highly concentrated solution of EDTA (Figure 2.3), with a c-value ([EDTA]/K_d) of roughly 500. In the second of these injections (the first injection is ignored due to pre-titration diffusion from the syringe), there is sufficient EDTA to fully react with injected Ca^{2+} in 7 μL of the cell solution, i.e. just 5% of the total cell volume. In this case, one would expect that sufficient mixing of the two components would occur very rapidly. With subsequent injections, as free EDTA is converted to the bound form, the amount of mixing required for each injection increases. By the 20th injection, the Ca^{2+} must fully mix with at least 630 μL of the partly-saturated EDTA solution (45% of the cell volume) in order to react to completion. In this case we would expect that sufficient mixing would require more time than for the first injection. Notably, all Ca^{2+} injections, from the second to the 20th give superimposable peak shapes, although the amount of mixing required for each injection can vary by up to about 90-fold. This strongly suggests that pre-reaction mixing is not rate-limiting for generation and detection of heat in the isothermal titration calorimeter under these conditions. We note that the signal from the 21st Ca^{2+} injection is substantially broader than that of the previous injections. In this case, mixing with at least 79.5% of the cell volume is required to reach completion, and it seems likely that in this case, the pre-reaction mixing step becomes at least partially rate-limiting. Nevertheless, the assumption of instantaneous mixing appears to be valid for a broad range of free EDTA concentrations.

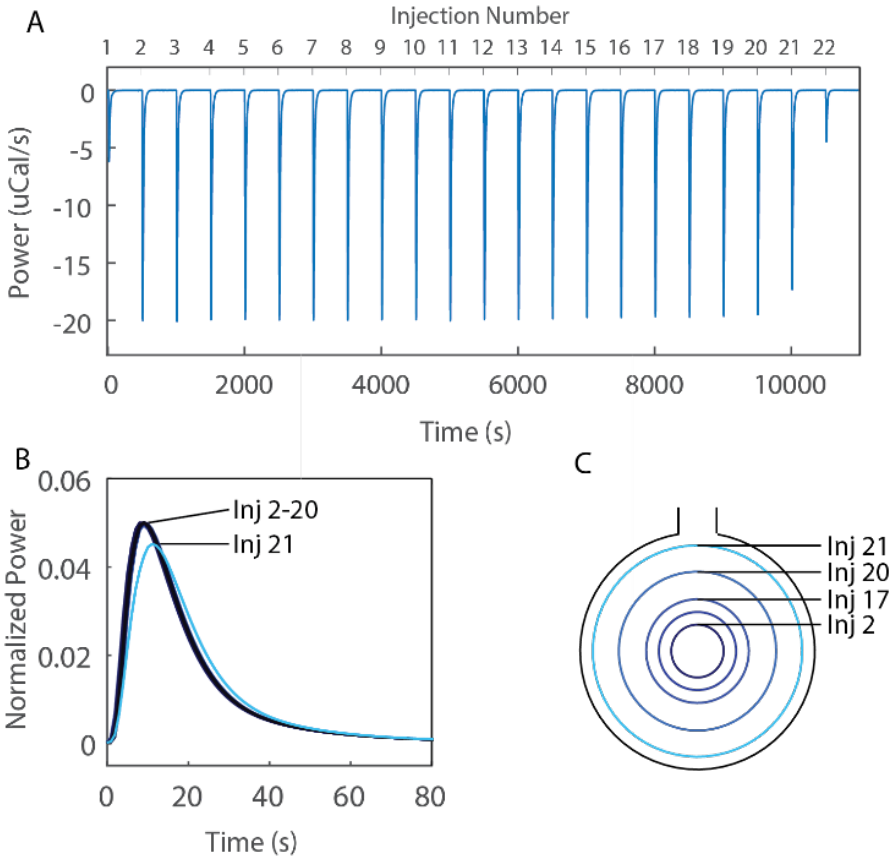

Figure 2.3. Ca^{2+} EDTA saturation experiments using the VP-ITC. (A) Titration of $CaCl_2$ 11 mM into EDTA 1.8 mM until saturation form a single experiment. (B) Overlay of area-normalized peaks 2-20 and 21. (C) Representation of coin shaped cell (outer ring with neck). The area of each inner disk is proportional to the volume of cell solution which contains enough unbound EDTA to bind all $CaCl_2$ provided in that injection. The first injection small (5 μL over 10s) is not shown in panel B or C due to pre titration diffusion form the tip of the syringe into the cell all subsequent injections are 10 μL over 2s.

Another possible explanation for the observed ITC peak shapes is that the post-reaction heat transfer and electronic response do not combine to give a single exponential response function. In order to examine these steps more closely, we measured the ITC signals resulting from short impulses of the electrical heater used to calibrate the sample cell. Here again, we observed heat signals that continued to build for roughly 9 seconds following the end of the heater pulse, despite the fact that no mixing of reactants is required (Figure 2.S3). We repeated these experiments with

the water-filled syringe present in the cell rotating at different stirring speeds. Notably, we observed broader peaks at slower stirring speeds. Furthermore, the stirring speed dependences of ITC peaks obtained from heater pulses and Ca^{2+}/EDTA injections are very similar. This strongly suggests that stirring affects the post-reaction heat transfer step, and that this together with the electronic feedback mechanism largely governs the isothermal titration calorimeter's peak shapes measured here.

2.3.5 Empirical Response Model

We have a developed an approach for analyzing ITC peak shapes based on an empirical response model. The approach treats pre-reaction mixing as effectively instantaneous, as outlined above, and subsumes all post-reaction heat transfer and electronic response into a single empirical response function, $f(t)$, which obeys the convolution relationship in Equation 2.11. We took advantage of the property of convolutions, wherein an infinitesimally short burst of heat in the calorimeter cell ($h(t) = \delta(0)$) produces $g(t)$ as the instrument output. Here, we approximated an instantaneous burst of heat with a 0.1 to 0.5 second injection of Ca^{2+} into EDTA, and took the resulting peak as the empirical response function, $f(t)$. ITC peak shapes were then simulated by numerically convoluting the instantaneous heat profile ($h(t)$) with the empirical response function ($f(t)$) thus obtained. We tested the ITC-ERM by fitting Ca^{2+}/EDTA injections of varying durations and comparing the known injection lengths with those extracted from the peak shapes. This approach reproduced the experimental ITC peaks with remarkable fidelity (Figure 2.1), and the extracted injection lengths closely match the set values with a root-mean-square deviation of only 0.2 s (Figure 2.S1). We then repeated the kinetic analysis of trypsin using the ITC-ERM approach and assuming Michaelis-Menten enzyme kinetics, obtaining very close agreement between the simulated and experimental peak shapes (Figure 2.4), and kinetic parameters that match the literature values ($K_m = 2.848 \pm 0.001$ μM; $k_{cat} = 16.69 \pm 0.02$ s^{-1}). This is in contrast with the variable-τ method (Figure 2.2B), where simulated ITC peak shapes show large systematic deviations from the

experimental data. These results give us confidence that the ITC-ERM approach quantitatively reproduces ITC peaks of arbitrarily short duration with a high degree of accuracy.

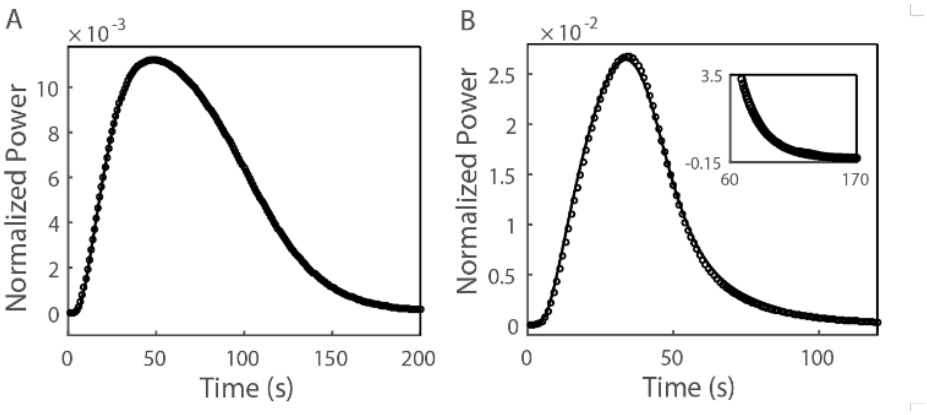

Figure 2.4. Single Injection Enzyme Kinetics for Trypsin using the VP-ITC fit with ITC-ERM. (A) Single injection of BAEE (400 μM in syringe) into the cell containing trypsin 10 nM (open circles). Curve produced using ITC-ERM method. (solid line). (B) Single injection of BAEE (1100 μM in syringe) into the cell containing trypsin 60 nM (open circles). Curve produced using ITC-ERM method. (solid line).

2.3.6 Prolyl Oligopeptidase

Prolyl oligopeptidase (POP), is a post-proline cleaving enzyme implicated in cancer and neurodegenerative disorders.[37,38] POP cleaves thyrotropin-releasing hormone, a modified tri-peptide with the sequence (pyro)Glu-His-Pro-NH_2, among other substrates. ITC traces obtained from injections of TRH into the reaction cell containing varying concentrations of POP are shown in Figure 2.5. The ITC-ERM approach was used to fit each transient using the Michaelis-Menten equation. At low enzyme concentrations, the calculated peak shapes agree well with the experimental data (Figure 2.5A), as seen for trypsin, above. However, at higher enzyme concentrations, the peak shapes are no longer well fit by this model. Instead, the data agree with an empirical formula, previously used to describe non-Michaelis-Menten enzymes with cooperative substrate binding,[39] according to:

$$\frac{d[P]_t}{dt} = \frac{k_{cat} \cdot [E] \cdot [S]_t^n}{K_m + [S]_t^n} \tag{2.1}$$

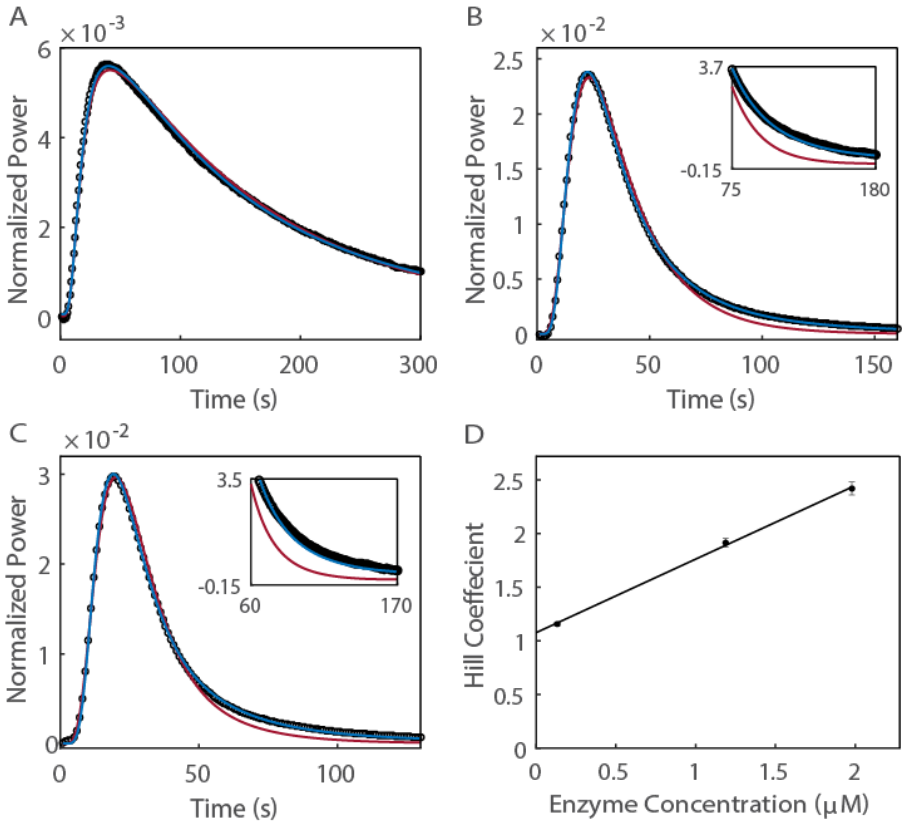

Figure 2.5. Single Injection Enzyme Kinetics for POP using the VP-ITC. All three panels show data for a single injection (20 μL over 6 s) of TRH (690 μM in syringe) made into a cell containing 132 nM POP (A), 1.8 μM POP (B), and 2.37 μM (C) (open circles). Fits using the ITC-ERM approach and Michaelis-Menten kinetics (Equation 2.5) and cooperative kinetics (Equation 2.1) are shown in red and blue lines, respectively at each concentration. Resulting Hill coefficients (n) plotted against enzyme concentration with line obtained by linear regression (D).

2.3.7 Maximum Reaction Rates

Chemical reactions that take place on roughly the same timescale as the instrument response can be quantified by ITC-ERM, while those that occur much more rapidly (eg. short Ca^{2+}/EDTA injections) are indistinguishable from instantaneous bursts

of heat and yield little or no kinetic information. In order to estimate rough upper rate limits for this technique, we performed a series of Monte Carlo calculations in which molecular binding and enzyme catalytic data were computed with simulated random errors. The synthetic data were analyzed using the ITC-ERM method and the fitted kinetic parameters were compared to the ones used to generate the data sets. For molecular recognition, we fixed K_d and ΔH to the Ca^{2+}/EDTA-derived values (0.180 μM and -3.5 kCal mol^{-1}, respectively) and varied k_{on} between 10^4 and 10^6 M^{-1} s^{-1}. The agreement between the true and fitted k_{on} values was excellent for the slower on-rates, but the error increased rapidly after 1 $\cdot 10^5$ M^{-1} s^{-1}, reaching more than 50% after about 4 $\cdot 10^5$ M^{-1} s^{-1}(Figure 2.S10). Association rates faster than this lead to signals that are essentially indistinguishable from instantaneous bursts of heat. Note that the k_{on} values for Ca^{2+}/EDTA are about 10 times this value. Thus k_{on}= 10^5 M^{-1} s^{-1} represents an approximate upper limit for association rates, under these conditions. Interestingly this is slightly faster than the ITC-derived rate constant of $3 \cdot 10^4$ M^{-1} s^{-1} reported by the Dumas lab for the TPP riboswitch.[19] For the enzyme simulations, we fixed k_{cat} and K_m to the trypsin-derived values (15 s^{-1} and 4 μM, respectively) and varied the total enzyme concentration between 5 and 1000 nM. The agreement between the true and fitted k_{cat} and K_m values was excellent for the lower enzyme concentrations, where heat is generated more slowly. In contrast, for concentrations greater than about 400 nM (V_{max} > 6 μM s^{-1}), the errors in the extracted k_{cat} and K_m values were larger than 20% and 50%, respectively, marking the approximate upper limit for this technique under these conditions (Figure 2.S11).

2.3.8 Application to Other ITC Instruments

In order to test the generality of the ITC-ERM approach, we repeated Ca^{2+}/EDTA reference experiments using the MicroCal ITC-200, which has a cell size approximately seven-fold smaller than the VP-ITC, and the Nano ITC from TA instruments, which has a cell roughly the same size as that of the ITC-200, but cylindrical

in shape, in contrast to the coin-shaped cells employed in the MicroCal instruments. In all cases, injection lengths varying between 1 and 5 seconds are clearly distinguishable, indicating that these instruments also have sub-second time resolution (Figure 2.6). The variable-length injections were then fitted using the ITC-ERM approach, as described above for the VP-ITC. Interestingly, for both the ITC-200 and the Nano ITC, the fits deviated systematically, such that injection lengths were consistently under-estimated (Figure 2.S1). We suspected that the programmed 0.2s pulses were not serving as an accurate model of the instrument response function, $f(t)$. In order to circumvent this problem, we reanalyzed the data using a longer (1 second) injection to model the instrument response and adjusting the experimental data accordingly. Briefly, we define a modified response function, $f\acute{}(t)$ as the area-normalized instrument output following a 1 second injection, and the adjusted data, $g\acute{}(t)$ to be the instrument output numerically convoluted with a 1 second square pulse, $s(t) = 1, 0 \leq t \leq 1$ and $s(t) = 0, t < 0, t > 1$. The modified response function can be used to fit the adjusted data just as the true response function is used to fit the unadjusted instrument output. The modified response function and adjusted data are described by the equations

$$f'(t) = s(t) \otimes f(t) \tag{2.2}$$

$$g'(t) = s(t) \otimes g(t) \tag{2.3}$$

where $f(t)$ is the true response function and $g(t)$ is the unadjusted instrument output. From Equations 2.10, 2.2, 2.3, and the commutative property of convolutions it therefore follows that:

$$h(t) \otimes f'(t) = g'(t) \tag{2.4}$$

This approach yields quantitative agreement between true and fitted injection lengths for all calorimeters tested here (Figure 2.6), confirming that the ITC-ERM accurate reproduces peak shapes for a range of cell sizes and geometries. Furthermore, Ca^{2+}/EDTA saturation experiments performed with the both ITC-200 and

Nano ITC show essentially superimposable peak shapes over a broad range of stoichiometric volumes (up to about 50% for both ITC-200 and Nano ITC) (Figure 2.S2). This indicates that the assumption of instantaneous mixing holds for the ITC-200 and Nano ITC under conditions similar to those we found for the VP-ITC.

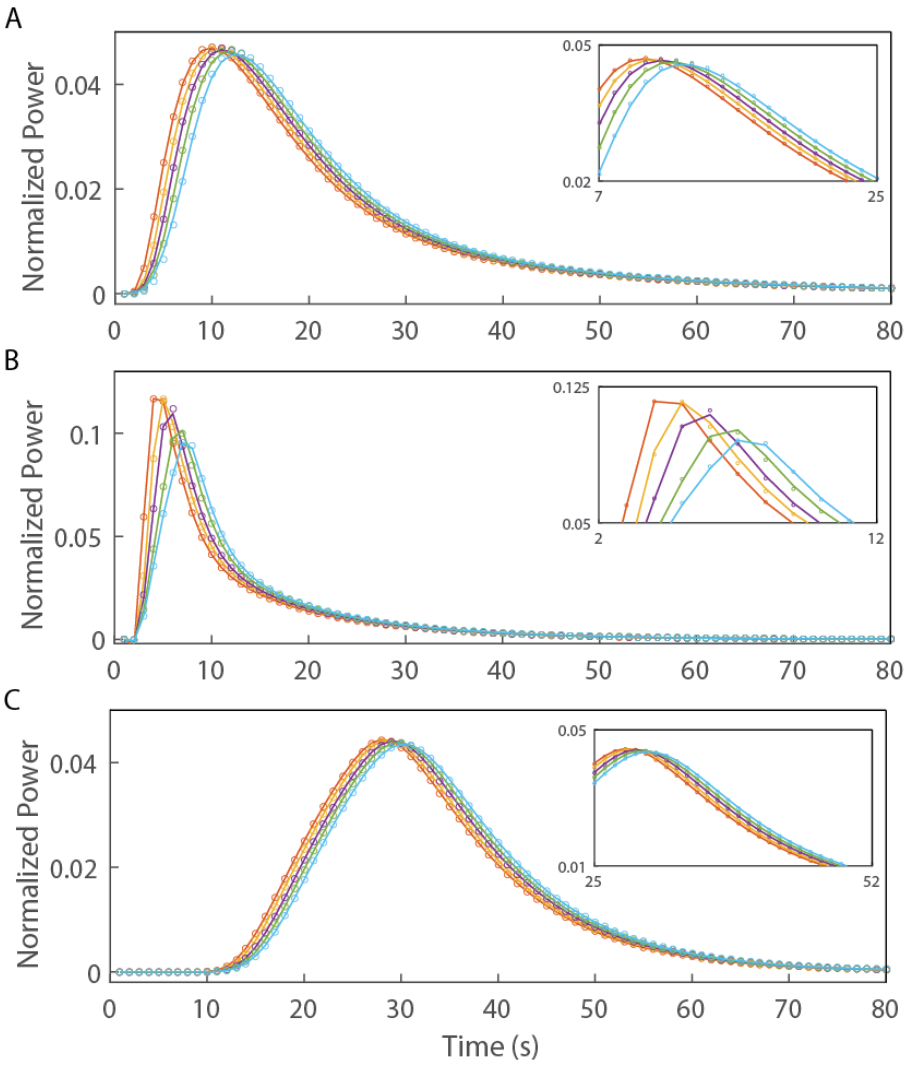

Figure 2.6. Rapid injection experiments using multiple compensation calorimeters. Normalized peaks from 1s (orange circles), 2s (yellow circles), 3s (purple circles), 4s (green circles) and 5s (cyan circles) injections of $CaCl_2$ (18 mM in syringe) into the cell containing 1.8 mM EDTA using the (a) VP-ITC, (b) ITC-200 and (c) Nano ITC. All data were convoluted with a 1s square pulse (see main text). Injections are 1 μL for the VP-ITC, 0.4 μL for the ITC-200, and 1.49 μL for the Nano ITC. 8 of each injection were carried out in series for a total of 40 injections in a single experiment for the VP-ITC. For the Nano ITC and ITC 200 each set of 10 injections was carried out in a separate experiment. The lines show ERM fits, using a 1s injection as the empirical response function while floating the injection length. Results of the fits can be found in supporting information (Figure 2.S1)

2.4 Discussion

The advantages of using ITC to measure chemical reactions, particularly enzyme kinetics, have long been recognized and there is varied literature on the subject going back several decades.[4,12,5] Most of these studies have focused on reactions taking place over tens of minutes to avoid complications of the finite instrument response time. Here we demonstrate experimentally that accurate Michaelis-Menten parameters can be extracted from ITC peaks just tens of seconds in length. Computer simulations had previously predicted that accurate enzyme kinetic parameters could be extracted from ITC peaks on this timescale. However, to our knowledge, this had not been tested experimentally. The ITC reaction times utilized in this study are about a 20-fold shorter than those of previous ITC enzyme kinetic studies, and thus represent an important experimental validation of the theoretical predictions.[9,19] Rapid ITC kinetic experiments (seconds) offer several advantages compared to longer-timescale (minutes) approaches. Firstly, they allow the same number of kinetic traces to be obtained in much less time, which is advantageous both in terms of throughput, and for substrates that degrade or enzymes that steadily lose activity under catalytic conditions, such as Cytochrome P450 and NADPH-cytochrome P450 reductase.[40] Secondly, they are well suited to small injections of dilute substrates that are consumed rapidly by the enzyme, which is desirable for expensive or sparingly soluble reagents. This is also beneficial for systems that experience product inhibition, as operating at lower substrate concentrations means generating less product. Lastly, a compensation calorimeter measures reaction rates in terms of the displacement of the heat flow from the value. However, the isothermal titration calorimeter's baseline fluctuates slowly with time and must be interpolated between the beginning of the injection and the end of the reaction.[34,11] Shorter reactions allow for smaller regions of interpolation and thus fewer errors due to baseline fluctuations.

We found that a previously published (variable-τ) approach for analyzing ITC kinetic traces yielded accurate enzyme parameters, even for short reactions on the order of tens of seconds. However, for rapid reactions (less than about 80 seconds),

the inherent assumption of a mono-exponential instrument response led to large systematic distortions of the calculated ITC peaks shapes. These distortions were eliminated by replacing the mono-exponential response function with an empirical response function that is derived experimentally from very short burst injections using a rapidly-reacting host/guest system (or 1-second reference injections and suitably adjusted data, as described above). We term this the ITC-ERM approach. Most kinetic ITC studies to date have assumed mono-exponential[9,11,19,20,34] or bi-exponential[29,33,32] instrument response functions. However the empirical response generated by a short burst of heat in the calorimeter cell is not well approximated by mono-, bi-, or tri-exponential functions (Figure 2.S5 and 2.S6) and good agreement is obtained with sums of about 14 exponential terms or more (Figure 2.S7). In principle, it would be possible to fit the experimental instrument response with a multi-exponential function, which could then be used in subsequent ITC-ERM calculations. However the experimental instrument response curves are visually extremely smooth to begin with and we did not find the additional smoothing provided by a multi-exponential function to be necessary. We therefore averaged and area-normalized the experimental data for 5-10 short injections, and used these values directly in numerical convolutions to simulate ITC data.

The ability of the ITC-ERM approach to quantitatively reproduce the fine features of ITC peaks opens the door to novel investigations of biological kinetics, particularly for systems where the kinetic mechanism is not known a priori. For instance, the ITC-ERM method clearly showed that the POP enzyme deviates from Michaelis-Menten kinetics in a concentration-dependent manner. This behavior appears only at enzyme concentrations too large to study by standard spectrometric assays, and is completely obscured by the ITC peak-shape distortions produced in the variable-τ approach. In other words, the ITC-ERM approach offers a unique opportunity to extract detailed enzyme kinetic information inaccessible using other experimental techniques. Furthermore, ITC-ERM approach is applicable not only to enzyme kinetics but to all kinetic ITC applications. For instance, kinetics of macromolecular ligand binding and coupled folding/binding reactions can be mea-

sured by ITC.[19] Many association reactions take place in seconds or tens of seconds under ITC conditions, meaning that methods to accurately reproduce rapid kinetic ITC peak shapes are quite important for these studies.

There are several caveats to the ITC-ERM approach. Firstly, as with any ITC-based kinetics method, both the affinity and the enthalpy must be large enough to permit detection of the interaction at relatively low concentrations (see 4.7 for further discussion of the minimal heat production required for accurate analysis). For instance, we found that for the Ca^{2+}/EDTA interaction, 10^5 M^{-1} s^{-1} represents an approximate upper limit for measurable association rate constants, under the conditions of this study. This corresponds to roughly 11 μCal of heat released per injection and a pseudo-first order time constant of 2 s. To achieve similar results with another system, the concentration of the injectant would have to be adjusted to yield similar heats, while the concentration in the cell would have to be adjusted to maintain association times at or slower than 2 s. For weak interactions with low enthalpies, this may not always be possible. Secondly, pre-reaction mixing is effectively ignored in the method as implemented here. This is justified based on the excellent agreement we find for trypsin kinetic ITC peaks using this approach, as well as our observation that mixing occurs at a much faster rate than the post-reaction heat transfer and detection steps, at least with a large excess concentration of host molecules (eg. EDTA) in the cell. For injections near the stoichiometric saturation of a host or kinetic saturation of an enzyme, we might expect this approximation to break down. Finite pre-reaction mixing has previously been modelled in ITC kinetic studies as a first-order exponential process.[19] This could easily be included in the ITC-ERM approach as an additional step in calculating the instantaneous heat ($h(t)$). However this does not appear to be necessary to accurately model the ITC data presented here, and details of this additional calculation are beyond the scope of this work. A second caveat is that we have found that the empirical instrument response varies as a function of temperature, stirring speed, and solvent viscosity (Figures 2.S3, 2.S8, 2.S9), and solution density and thermal conductivity are likely also important.[9] Thus burst injection host/guest experiments must

be performed under conditions as similar as possible to those of the actual kinetic data set. Note that for ITC-200 and Nano ITC calorimeters, short (∼1 s) reference injections should be performed instead of burst (∼0.2 s) injections and the instrument output adjusted prior to analysis, as described above. A temperature series of binding kinetics will require a temperature series of burst or reference injection measurements to measure the empirical response function as its shape will change under varying conditions. The ITC-ERM approach is consequently more costly in terms of experiment time than methods where a simplified mono exponential response function is either optimized on the fly, such as in the variable-τ method,[9] or approximated identically for all conditions. We note that in our hands, analyses using simplified mono-exponential response functions yield accurate enzymatic parameters, even when the fitted curves deviate substantially from the experimental data (as in Figure 2.3B). Thus when the kinetic mechanism is known a priori and only the model parameters are of interest, there are time-saving advantages to using a simplified ITC response function. However in cases where the kinetic mechanism is not known with certainty, the distortions inherent in using a simplified mono-exponential response function completely obscure the level of agreement or disagreement between any given model and the experimental data, when ITC peaks are shorter than about 150 seconds. In contrast, the ITC-ERM reproduces such short ITC peak shapes quantitatively, allowing the appropriate mechanistic model to be selected based on goodness of fit. For example, the mono-exponential variable-τ approach gives poor agreement when rapid kinetic ITC traces from either trypsin or POP are analyzed according to the Michaelis-Menten mechanism. In contrast, the ITC-ERM approach shows that trypsin data follow the Michaelis-Menten model closely, while those of POP do not, and instead follow a concentration-dependent cooperative mechanism. Thus the ITC-ERM represents a new and valuable analytical tool for extracting mechanistic information from rapid timescale ITC kinetic data and shedding new light on the function of biological macromolecules.

2.5 Conclusion

The present study demonstrates that ordinary calorimeters are capable of measuring heat flow with sub-second precision. However, conventional ITC data analysis approaches produce systematic deviations from experimental data when modelling rapid enzyme kinetics. We have developed an ITC-ERM approach that quantitatively reproduces ITC peak shapes, providing a simple way to study rapid reaction kinetics in detail. An application of ITC-ERM to prolyl oligopeptidase uniquely identified unexpected non-Michaelis-Menten kinetics, demonstrating its utility.

2.6 Methods

2.6.1 ITC Experiment Conditions

All ITC experiments were performed using a MicroCal VP-ITC in high-feedback mode with a 1 second signal-averaging window and stirring rate of 806 rpm, unless otherwise specified. Pre-injection delays of 500 seconds were employed to allow baselines to fully stabilize. Electrical Heater Pulses. Electrical heater pulses were executed using the 'pulse-off' command in the VP-Viewer2000 Thermostat/Calibration tab during a 2000s pre-titration delay with stirring. The peaks produced by the electric heater pulses were normalized by the total area of the peak (Equation 2.12).

2.6.2 Enzymes and Substrate Preparation

Trypsin (EC 3.4.21.4) was purchased in the form of (TrypZean®) from Sigma-Aldrich. The lyophilized powder was dissolved into 200 mM Tris-HCl, pH 8.0, 50 mM $CaCl_2$, and 0.2% PEG-8000 buffer. The concentration of Trypsin was measured using the extinction coefficient at 280 nm (ε= 30057 M^{-1} cm^{-1}).[41] The substrate Nα-Benzoyl-L-arginine ethyl ester hydrochloride (BAEE) (EC 220-157-0) was purchased from Sigma-Aldrich and dissolved into the same buffer.

POP was purified as previously described.[42] E. coli BL21 competent cells were transformed with pETM10 hPOP. A starter culture of LB medium (100 mL) containing kanamycin (50 mg mL^{-1}) was inoculated with one colony and was incubated overnight at 37°C with shaking. After 16 h, four cultures of LB (4 · 1000 mL) containing kanamycin (50 mg mL^{-1}) were inoculated with the overnight culture (20 mL). The inoculated cultures were incubated at 37°C and 220 rpm until the OD600 was between 0.3 and 0.5 (3 h). The temperature was lowered to 18°C, after one hour of temperature equilibration isopropyl β-D-1-thiogalactopyranoside (IPTG) was added (final concentration of 0.5 mM), and induction was allowed to proceed for 5 h. Cells were harvested by centrifugation (4000 g, 15 min, 4°C), and the pellet was resuspended in suspension buffer (50 mL) [Tris-HCl (10 mM), NaCl (300 mM), β-mercaptoethanol (5 mM), imidazole (1 mM), and 5% glycerol, pH 8] and sonicated for four cycles (2 min of sonication/2 min of rest; pulse, 0.5 intensity; duty, 0.5), while the sample was kept on ice (Branson sonifier 450, Emerson industrial automation, United States). After sonication, the sample was centrifuged (40000 g, 30 min, 4°C), and the supernatant was used immediately for POP purification. An affinity column was used (10 mL, Toyopearl, AF-Chelate-650M) for purification. The supernatant was applied at a flow rate of 0.5 mL min^{-1} to a column previously equilibrated with 2 column volumes of $NiSO_4$ (0.2 M) followed by 5 column volumes of suspension buffer. The column was then washed with 5 column volumes of suspension buffer, then 5 column volumes of washing buffer [Tris-HCl (20 mM), NaCl (300 mM), β-mercaptoethanol (5 mM), imidazole (15 mM), and 5% glycerol, pH 8]. The elution was then performed with 4 column volumes of elution buffer [Tris-HCl (20 mM), NaCl (300 mM), β-mercaptoethanol (5 mM), imidazole (500 mM), and 5% glycerol, pH 8]. Fractions (4 mL) were collected during the entire elution. Fractions testing positive for POP activity were analyzed by SDS−PAGE and stained with phastgel blue R (GE Healthcare, sweden). POP-containing fractions were combined and subjected to size exclusion chromatography (HiLoad 16/60 Superdex75 prep grade on a GE Healthcare Äkta Avant system) with [Tris-HCl (20 mM), NaCl (150 mM), benzamidine (5 mM), EDTA (1 mM), β-mercaptoethanol

[5 mM], and 5% glycerol, pH 8] as the running buffer. The purified enzyme was dialyzed in a buffer containing 20mM sodium phosphate pH 8, 150 mM sodium chloride, and 10% (w/v) glycerol. Recombinant hPOP was quantified by measuring the absorbance at 280 nm using an extinction coefficient calculated by the following equation (ε = nTrp*5000 + nTyr*1490 + nCys*125, 129090 L mol^{-1} cm^{-1} for POP).[43] POP was flash frozen in 300 μL aliquots at $\approx$ 4 μM in liquid nitrogen and stored at –80°C. Kinetic experiments were carried out with freshly thawed POP in the same buffer (above) with bovine serum albumin (BSA, 0.5 mg mL^{-1}) added to help stabilize POP. The substrate thyrotropin releasing hormone (TRH) was purchased from BACHEM international (product H-4915) and dissolved into the same buffer as POP for kinetics experiments.

2.6.3 Ca^{2+}/EDTA Titrations

All Ca^{2+}/EDTA measurements in the main text (except saturation experiments) were performed at 25°C in 10 mM 2-(N-morpholino)ethanesulfonic acid (MES) buffer pH 6. The Ca^{2+}/EDTA saturation titrations were performed at 25°C in 20 mM piperazine-N,N'-bis(2-ethanesulfonic acid) (PIPES) buffer pH 7. The peaks generated by the Ca^{2+}/EDTA injections were normalized (equation 2.12).

2.6.4 Enzyme Kinetics Fitting Scripts

All fitting was performed in MATLAB. Differential equations shown below (equations 2.5-2.8) describing Michaelis-Menten kinetics were integrated numerically using Euler's method in 0.01s integration steps (dt in equations 2.5-2.8) according to:

$$\frac{d[P]_t}{dt} = \frac{k_{cat} \cdot [E] \cdot [S]_t}{K_m + [S]_t} \tag{2.5}$$

$$[P]_{t+dt} = [P]_t + \frac{d[P]_t}{dt} \cdot dt \tag{2.6}$$

$$\frac{d[S]_t}{dt} = -\frac{d[P]}{dt} - [S]_{syringe} \cdot Rate_{dil} \tag{2.7}$$

$$[S]_{t+dt} = [S]_t + \frac{d[S]_t}{dt} \cdot dt \tag{2.8}$$

where k_{cat} and K_m are the catalytic rate and the Michaelis constant respectively, $[E]$ is the total concentration of enzyme in the cell and $[S]_t$ and $[P]_t$ are the concentrations of substrate and product at time = t. $Rate_{dil}$ is the rate of the dilution from the syringe to the cell in (s^{-1}) which is calculated as the injection rate divided by V_{cell}; the total volume of the reaction cell and $[S]_{syringe}$ is the concentration of substrate in the syringe. Note that on MicroCal instruments the beginnings of injections are indicated with an '@' sign in the raw data file. On the TA Nano instrument, injection start times are specified in advanced. This was verified visually by the user. The instantaneous heat $h(t)$ is calculated using the enthalpy of the reaction ΔH_{react} and the total volume of the cell (equation 2.9).

$$h(t) = \Delta H_{react} \cdot V_{cell} \cdot \frac{d[P]_t}{dt} \tag{2.9}$$

The instantaneous heat curve is numerically convoluted with the instrument response function according to:

$$g(t) = h(t) \otimes f(t) \tag{2.10}$$

where $f(t)$ is either a mono-exponential response function or the empirical response function (obtained from reference injections, see 2.3.5), $g(t)$ is the resulting calculated signal, and the convolution is defined according to

$$h(t) \otimes f(t) = \int_0^t h(\tau) f(t - \tau) d\tau \tag{2.11}$$

The calculated instrument output, $g(t)$, was digitally resampled in second intervals to match the experimental calorimeter output and normalized by the total area of the peak using trapezoidal integration according to

$$g_{norm}(t_m) = \frac{g(t_m)}{\sum_{n=0}^{N} [g(t_{n+1}) + g(t_n)] \cdot dt/2} \tag{2.12}$$

where N is the total number of time points, t_n and t_m are the nth and mth timepoint, dt is the time increment (1 second in all cases here) and g_{norm} is the normalized peak. Enzyme kinetic parameters as well as a scaling factor for the modelled curve N_g were fit by minimizing the target function (equation 2.13)

$$RSS = \sum_{n=0}^{N} (N_g \cdot g_{norm}(t_n) - b_{norm}(t_n))^2 \tag{2.13}$$

where RSS is the residual sum of squared differences, $b_{norm}(t)$ is experimental data which has been normalized according to equation 2.12.

2.6.5 Statistical Analysis of Errors

All enzyme experiments were performed in triplicate. Errors in the fitting parameters were calculated using the variance-covariance matrix (Equation 2.14) given by

$$\mathbf{V} = \frac{RSS}{DF} \cdot (\mathbf{XWX^T})^{-1} \tag{2.14}$$

Where RSS is the residual sum of squared differences between experimental and fitted data points, DF is the degrees of freedom of the fit (N total data points minus φ parameters of the fit), $\mathbf{W}$ is the diagonal matrix of fitting weights, in this case taken to be identity $\mathbf{I_N}$. $\mathbf{X}$ is a matrix of the first derivatives of the differences between the experimental and calculated data points (A^{exp} and A^{calc}), with respect to increments in each of the adjustable parameter (φ_i). The element corresponding to the ith adjustable parameters and jth data point is thus.

$$X_{i,j} = \frac{\partial(A_j^{exp} - A_j^{calc})}{\partial \varphi_i} \equiv \frac{\partial a_i}{\partial \varphi_i} \tag{2.15}$$

Where A_j^{calc} is evaluated at the optimized set of parameters, φ. The elements were evaluated numerically according to

$$X_{i,j} = \frac{(A_j^{exp} - A_j^{calc})(+\Delta) - (A_j^{exp} - A_j^{calc})(-\Delta)}{2\Delta} \tag{2.16}$$

Where A_j^{calc} $(+\Delta)$ is the jth data point calculated with all adjustable parameters set to their optimized values except, for the ith parameter, which is incremented by $(\pm\Delta)$. For a fit with N data points and P adjustable parameters this gives

$$\mathbf{X} = \begin{bmatrix} \frac{\partial a_1}{\partial \varphi_1} & \cdots & \frac{\partial a_N}{\partial \varphi_1} \\ \vdots & \ddots & \vdots \\ \frac{\partial a_1}{\partial \varphi_P} & \cdots & \frac{\partial a_N}{\partial \varphi_P} \end{bmatrix}$$

The diagonal elements in $\mathbf{V}$ are the variances of the optimized fit parameters the square root of which were taken to be the experimental error, while the off diagonal elements are the covariance between the errors of the optimized parameters. Parameter correlation coefficients were calculated according to

$$Corr_{i,j} = \frac{\sigma_{i,j}}{\sigma_{i,i} \cdot \sigma_{jj}} \tag{2.17}$$

In the case where there is a high degree of correlation between the k_{cat} and K_m, ie. correlation coefficients >0.95 the error of the ratio of the parameters were calculated according to

$$\sigma^2_{k_{cat},K_m} = \left(\frac{k_{cat}}{K_m}\right)^2 \cdot \left[\frac{\sigma_{k_{cat}}}{k_{cat}} + \frac{\sigma_{K_m}}{K_m} - 2 \cdot \frac{\sqrt{Corr_{i,j} \cdot \sigma_{i,i} \cdot \sigma_{j,j}}}{k_{cat} \cdot K_m}\right] \tag{2.18}$$

2.7 Supplementary Information

2.7.1 Supplementary Results

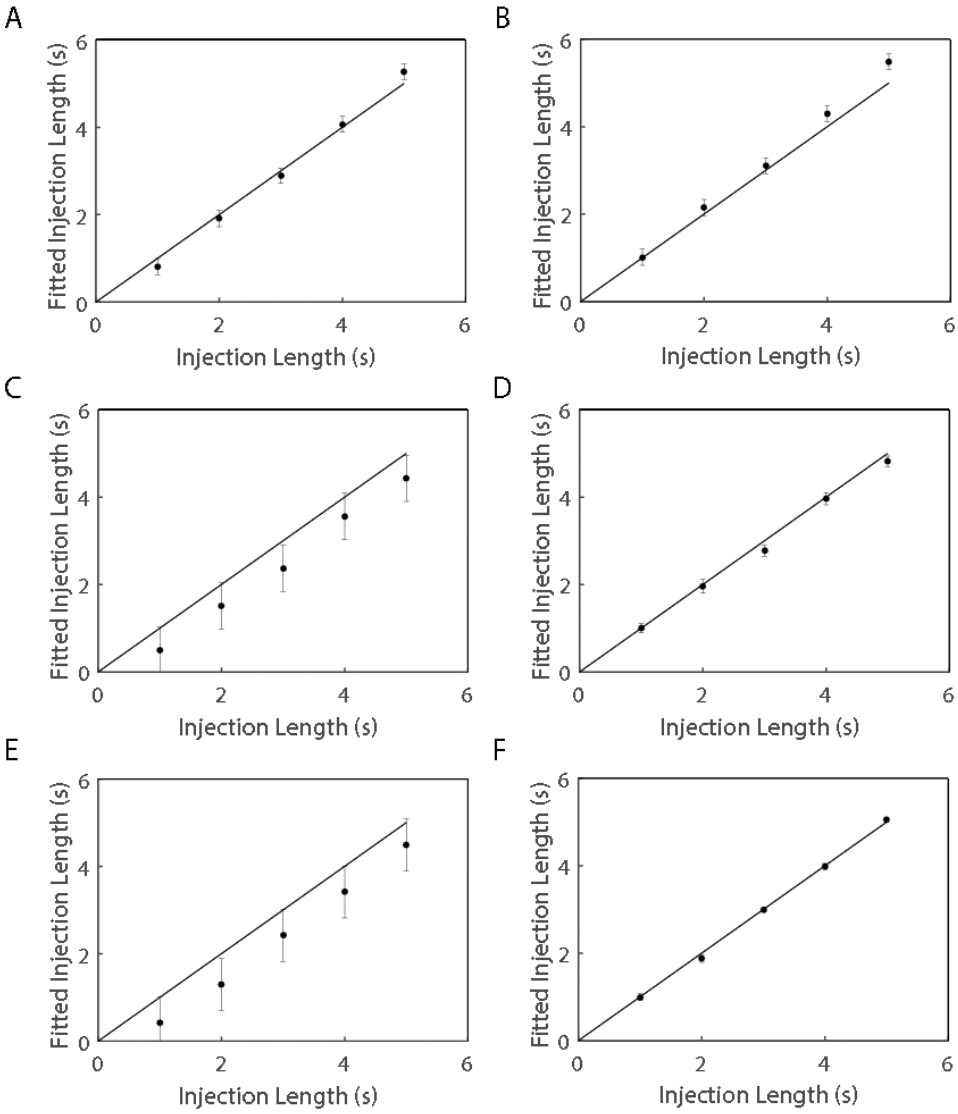

Figure 2.S1. Caption on next page

Figure 2.S1. Fitted vs. actual injection lengths for rapid injection experiments. Fitted injection length using the ERM approach for (A/B) VP-ITC, (C/D) ITC-200, (E/F) Nano ITC. Fits are shown in Figure 2.6. For A, C and E 0.2 s reference injections were used as empirical response functions and experimental data were left unmodified. For B, D and F, 1 s reference injections were used as modified empirical response functions, and the experimental data were adjusted by convoluting them numerically with a 1 s square pulse prior to analysis. Error bars are the standard deviations calculated using the bootstrap method. The RMSD (accuracy) for each fit is A) 0.16 s, B) 0.18 s, C) 0.53 s, D) 0.15 s, E) 0.59 s, and F) 0.06 s.

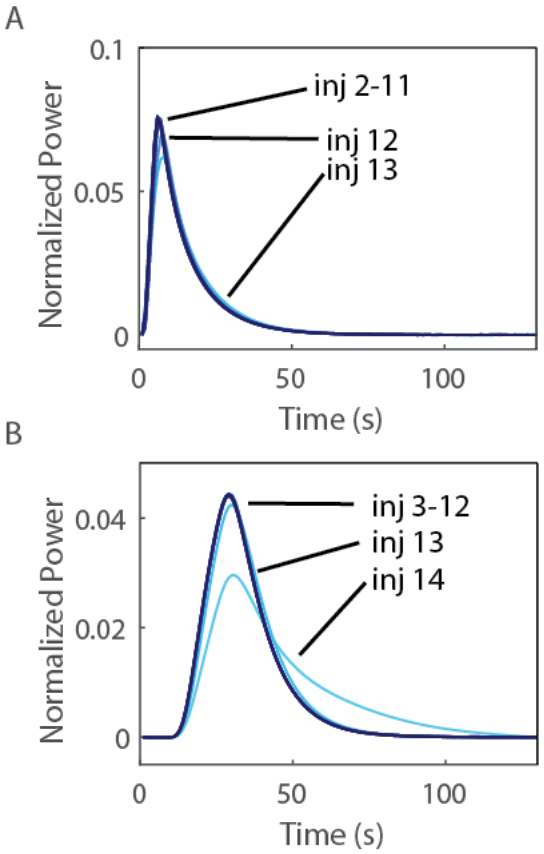

Figure 2.S2. Ca^{2+} EDTA saturation experiments using ITC-200 and Nano ITC. A) Overlay of normalized peaks 1-11, 12 and 13 from titration (2 μL injections over 4 s) of $CaCl_2$ 11 mM into EDTA 1.8 mM until saturation using the ITC-200 at a stirring rate of 1500 rpm. B) Overlay of normalized peaks 3-12, 13 and 14 from titration (1.962 μL injections over 2.7 s) of $CaCl_2$ 11 mM into EDTA 1.8 mM until saturation using the TA Nano ITC as a stirring rate of 400 rpm. All data shown is from single experiments.

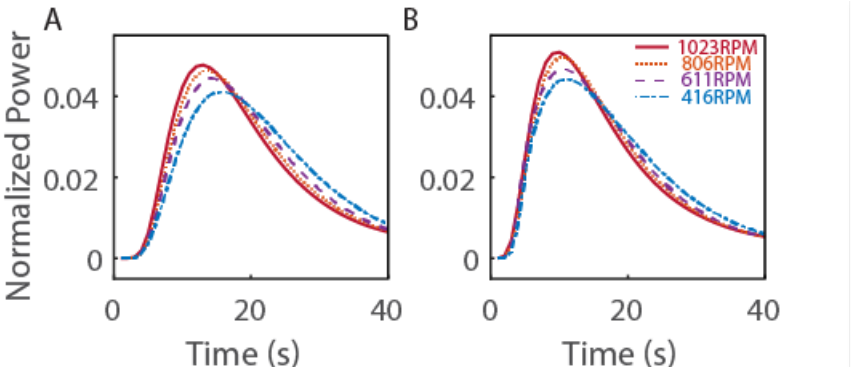

Figure 2.S3. Effect of stirring speed on peak shape for the VP-ITC. (A) 2 s electrical heater pulses at different stirring speeds. (B) 2 s injections of $CaCl_2$ (6 mM in syringe) into EDTA (9 mM in cell) at different stirring speeds in the VP-ITC. All peaks shown are an average of 3 heater pulses then normalized by area.

Table 2.S1. Summary of fitting Results for injections of BAEE into Trypsin. Errors are calculated using the variance-covariance matrix (see 2.6.5). The error in the k_{cat}/K_m is also presented which was calculated using Equation 2.18.

	Variable-τ Method		ERM	
Enzyme Concentration (nM)	10	60	10	60
k_{cat} (s^{-1})	20.0 ± 0.3	16.7 ± 0.1	15.83 ± 0.04	16.69 ± 0.02
K_m (μM)	3.42 ± 0.08	4.24 ± 0.05	2.44 ± 0.01	2.848 ± 0.001
τ_i (s)	23.9 ± 0.34	16.4 ± 0.16	–	–
N_g [a]	1.01 ± 0.01	1.01 ± 0.01	0.997 ± 0.01	1.02 ± 0.04
k_{cat}/K_m (μM^{-1} s^{-1}) [b]	5.85 ± 0.07	3.94 ± 0.03	6.49 ± 0.01	5.860 ± 0.001

[a] Scaling parameter, Equation 2.13.
[b] Error calculated using Equation 2.18

Table 2.S2. Results of fits shown in Figure 2.5. Errors are calculated using the variance-covariance matrix (see below).

Enzyme Concentration (μM)	2.37	1.8	0.132
k_{cat} (s^{-1})	1.04 ± 0.01	1.25 ± 0.05	51.33 ± 0.03
K_m (μM)	7.98 ± 0.06	10.9 ± 0.3	484.1 ± 0.2
N (Hill Coefficient)	2.42 ± 0.02	1.91 ± 0.06	1.16 ± 0.04
N_g [a]	1.001 ± 0.001	1.011 ± 0.004	1.01 ± 0.01
k_{cat}/K_m(μM^{-1} s^{-1}) [b]	1.303 ± 0.005	1.16 ± 0.07	1.06 ± 0.45

[a]Scaling parameter, equation 2.13.
[b]Error calculated using Equation 2.18

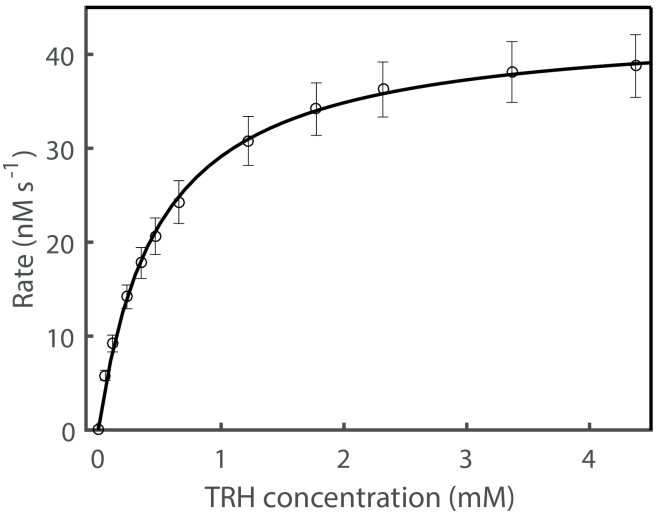

Figure 2.S4. Steady state kinetics of POP with TRH. 11 injections of TRH (27.5 mM in syringe) of 3, 3, 6, 6, 6, 10, 30, 30, 30, 60, 60 μL were made into the cell containing POP (1.8 nM). Data are the average of 3 experiments which were analyzed according to Gomez and Todd.[19]

2.7.2 Exponential Fits to Empirical Response Function

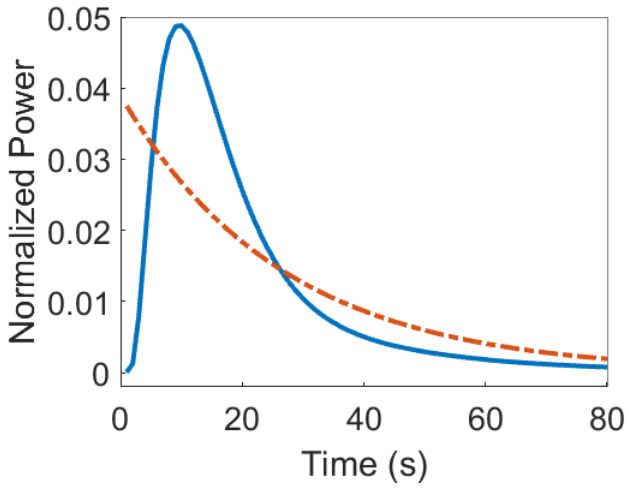

Figure 2.S5. Mono-Exponential fit to Empirical Response Function. Empirical Response Function (solid blue line) fit with Mono-Exponential Function (red dashed line).

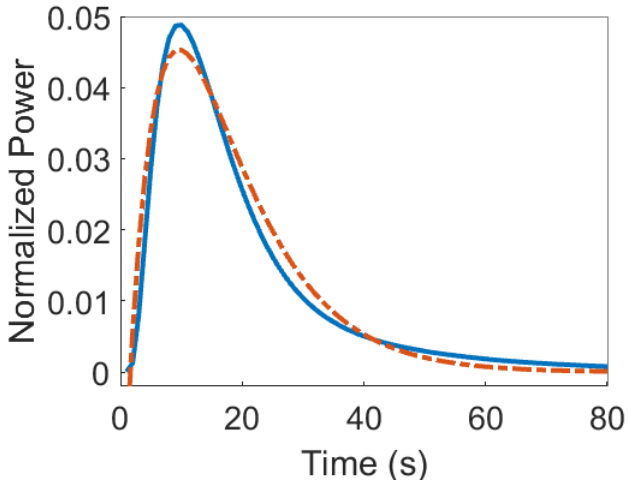

Figure 2.S6. Bi-Exponential fit to Empirical Response Function. Empirical Response Function (solid blue line) fit with Bi-Exponential Function (red dashed line).

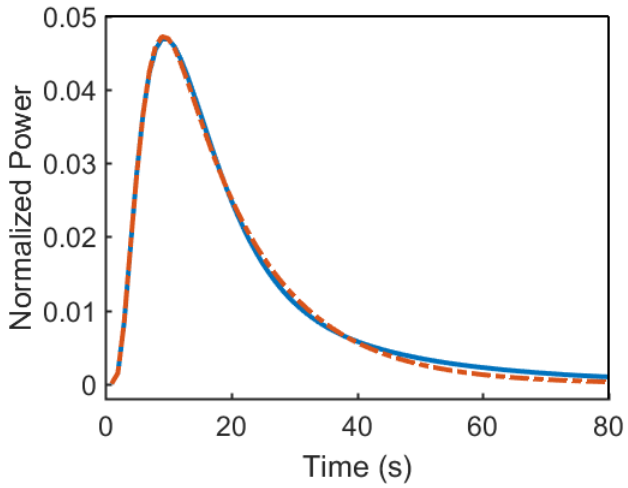

Figure 2.S7. Multi-Exponential fit to Empirical Response Function. Empirical Response Function (solid blue line) fit with Sum of 14 Exponential Functions (red dashed line).

2.7.3 Effect of experimental conditions on peak shape

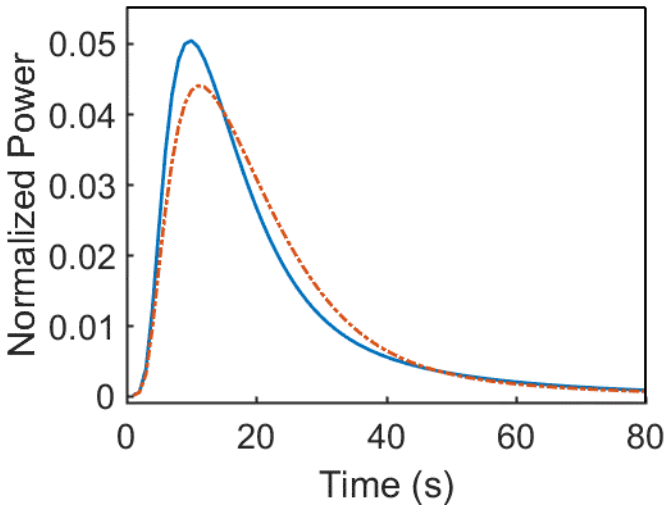

Figure 2.S8. Effect of viscosity on peak shape. 2 s injections of $CaCl_2$ (11 mM in syringe) into Cell containing EDTA (1.8 mM). Peaks shown are the average of 10 injections which were carried out in 20 mM MES buffer at 15°C pH 6 with 0% glycerol (blue solid line) or 30% glycerol (red dashed line).

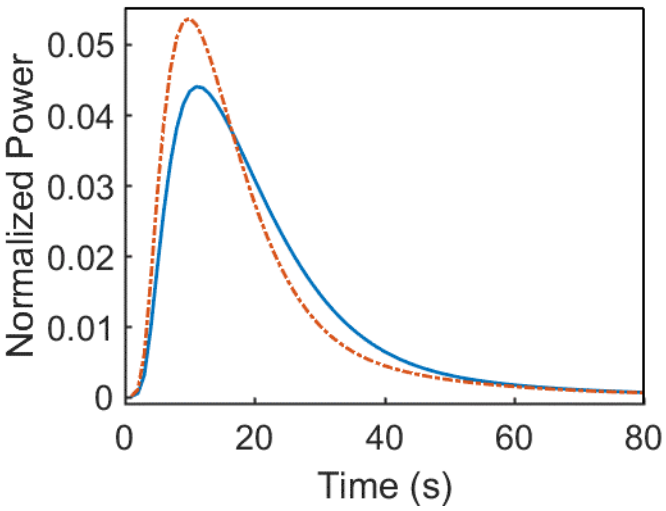

Figure 2.S9. Effect of temperature on peak shape. 2 s injections of $CaCl_2$ (11 mM in syringe) into Cell containing EDTA (1.8 mM). Peaks shown are the average of 10 injections which were carried out in 20 mM MES buffer pH 6 with 30% glycerol at 15°C (blue solid line) and 50°C (red dashed line).

2.7.4 Binding Rate Simulations

Monte Carlo simulations were carried out by modeling 10 sets of simulated data with random error at each of several association rates (k_{on}), according to:

$$\frac{d[C]_{t,i}}{dt} = [A]_{t,i} \cdot [B]_{t,i} \cdot k_{on} - [C]_{t,i} \cdot k_{off} \tag{2.19}$$

$$[C]_{t+1,i} = [C]_{t,i} + \frac{d[C]_{t,i}}{dt} \cdot dt - [C]_{t,i} \cdot Rate_{dil} \cdot dt \tag{2.20}$$

$$[B]_{t+1,i} = [B]_{t,i} - \frac{d[C]_{t,i}}{dt} \cdot dt - [B]_{t,i} \cdot Rate_{dil} \cdot dt \tag{2.21}$$

$$[A]_{t+1,i} = [A]_{t,i} - \frac{d[C]_{t,i}}{dt} \cdot dt + [A]_{syringe} \cdot Rate_{dil} \cdot dt - [A]_{t,i} \cdot Rate_{dil} \cdot dt \tag{2.22}$$

$$h(t) = \Delta H_{react} \cdot V_{cell} \cdot \frac{d[C]_{t,i}}{dt} \tag{2.23}$$

$$g(t) = h(t) \otimes f(t) \tag{2.24}$$

Here $[A]_{t,i}$ is the concentrations of Ca^{2+} in the cell at time t for injection i, $[A]_{syringe}$ is the concentration of Ca^{2+} in the syringe $[B]_{t,i}$ is the concentration of EDTA in the cell at time t for injection i, $[C]_{t,i}$ is the concentration of the EDTA-Ca^{2+} complex in the cell at time t for injection i. k_{on} and k_{off} are the association and dissociation rate of the reaction with $K_d = k_{off}/k_{on}$. The $Rate_{inj}$ is the injection rate and V_{cell} is the volume of the cell. The initial conditions for the first injection were $[A]_{t=1,i=1} = 0$, $[B]_{t=1,i=1} = [B]_{cell}$, and $[C]_{t=1,i=1} = 0$ the initial conditions for subsequent injections were $[A]_{t=1,i} = [A]_{t=N,i-1}$, $[B]_{t=1,i} = [B]_{t=N,i-1}$, $[C]_{t=1,i} = [C]_{t=N,i-1}$ where N is the total time between injections. The last terms in Equations 2.20-2.22 account for dilution of the cell solution during the injection. The simulations were performed with 18 μM EDTA in the cell and 110 μM Ca^{2+} in the syringe. The response function, $f(t)$ used for each of the simulated curves was calculated by averaging 3 randomly selected peaks from a set of 10 rapid Ca^{2+} EDTA injections. We found that uncertainty in the response function is the largest source of error. By averaging three individual instrument responses selected at random, we approximated the errors associated with experiments performed in triplicate. 23 Injections of 10 μL were simulated in series until EDTA was completely saturated. The thermodynamic constants were fixed at (K_d = 0.18 μM, ΔH_{react} = -3.5 kCal mol^{-1}). The 10 sets of simulated data were then analyzed according to the ITC-ERM approach as described in the main text and the average relative errors in the extracted k_{on} values were calculated as:

$$\sigma_{relative,k_{on}} = \frac{k_{on}}{\sigma_{k_{on}}} \tag{2.25}$$

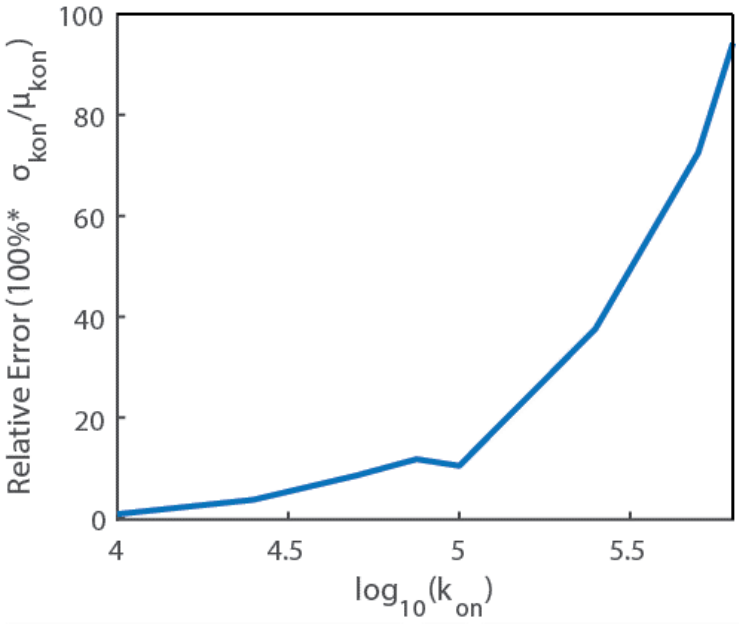

Figure 2.S10. Plot of Relative Error vs. the $\log_{10}$ of the association rate

2.7.5 Enzyme Kinetics Simulations

Monte Carlo simulations were carried out by modelling 30 sets of simulated data with random error at each of several enzyme concentrations as follows:

$$\frac{d[P]_t}{dt} = \frac{k_{cat} \cdot [E_0]_t \cdot [S]_t}{[S]_t + K_m} \tag{2.26}$$

$$[E_0]_{t+1} = [E_0]_t - [E_0]_t \cdot Rate_{dil} \cdot dt \tag{2.27}$$

$$[S]_{t+1} = [S]_t - \frac{d[P]_t}{dt} \cdot dt - [S]_t \cdot Rate_{dil} \cdot dt + [S]_{syringe} \cdot Rate_{dil} \cdot dt \tag{2.28}$$

$$h(t) = \Delta H_{react} \cdot V_{cell} \cdot \frac{d[P]_t}{dt} \tag{2.29}$$

$$g(t) = h(t) \otimes f(t) \tag{2.30}$$

Here $[S]_t$ is the concentration of BAEE in the cell at time t, $[E_0]_t$ is the concentration of trypsin in the cell at time t, and $[P]_t$ is the concentration of the product of catalysis at time t. k_{cat} and K_m are the Michaelis-Menten parameters for trypsin and BAEE.

The $Rate_{inj}$ is the injection rate and V_{cell} is the volume of the reaction cell. The initial conditions were $[E_o]_{t=0} = [E]_{cell}$, $[P]_{t=0} = 0$, and $[S]_{t=0} = 0$. $[E]_{cell}$ is the initial concentration of trypsin in the cell and $[S]_{syringe}$ is the concentration of BAEE in the syringe (1.1 mM). The response function, $f(t)$, used for each of the simulated curves was calculated by averaging 3 randomly selected peaks from a set of 10 rapid Ca^{2+} EDTA injections, as described above. ΔH_{cat} is the apparent enthalpy of the reaction. Injections were simulated as 20 μL. The enzyme parameters were fixed at ($k_{cat} = 15$ s^{-1}, $K_m = 4$ μM, $\Delta H_{cat} = -6.8$ kCal mol^{-1}), as determined for trypsin. The 30 sets of simulated data were then analyzed according to the ITC-ERM approach as described in the main text and the average fractional errors in the extracted k_{cat} and K_m values were calculated as:

$$\sigma_{relative,k_{cat}} = \frac{k_{cat}}{\sigma_{k_{cat}}} \tag{2.31}$$

$$\sigma_{relative,K_m} = \frac{K_m}{\sigma_{K_m}} \tag{2.32}$$

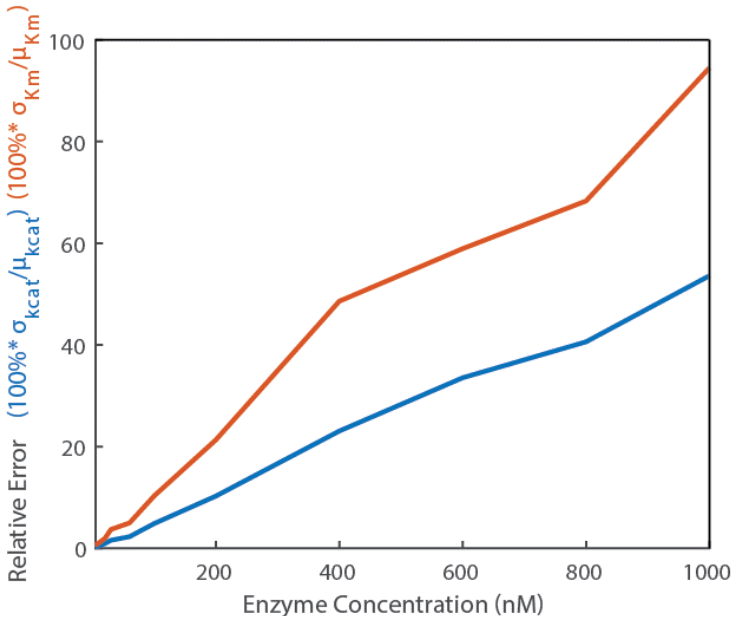

Figure 2.S11. Plot of Relative Error in the k_{cat} and K_m vs. the enzyme concentration.

2.8 References

[1] Matthew W. Freyer and Edwin A. Lewis. "Isothermal Titration Calorimetry: Experimental Design, Data Analysis, and Probing Macromolecule/Ligand Binding and Kinetic Interactions". In: *Methods in Cell Biology* Volume 84 (2008), pp. 79–113.

[2] Robert J. Falconer. "Applications of isothermal titration calorimetry – the research and technical developments from 2011 to 2015". In: *Journal of Molecular Recognition* 29.10 (2016), pp. 504–515.

[3] Stephanie Leavitt and Ernesto Freire. "Direct measurement of protein binding energetics by isothermal titration calorimetry". In: *Current Opinion in Structural Biology* 11.5 (2001), pp. 560–566.

[4] Matthew J. Todd and Javier Gomez. "Enzyme Kinetics Determined Using Calorimetry: A General Assay for Enzyme Activity?" In: *Analytical Biochemistry* 296.2 (2001), pp. 179–187.

[5] Anne Buzzell and Julian M. Strutevant. "A New Calorimetric Method". In: *Journal of the American Chemical Society* 73.6 (1951), pp. 2454–2458.

[6] Richard J. Willson et al. "Determination of Thermodynamic and Kinetic Parameters from Isothermal Heat Conduction Microcalorimetry: Applications to Long-Term-Reaction Studies". In: *Journal of Physical Chemistry* 99 (1995), pp. 7108–7113.

[7] Søren N. Olsen. "Applications of isothermal titration calorimetry to measure enzyme kinetics and activity in complex solutions". In: *Thermochimica Acta* 448.1 (2006), pp. 12–18.

[8] Brent A. Williams and Eric J. Toone. "Calorimetric evaluation of enzyme kinetic parameters". In: *Journal of Organic Chemistry* 58.13 (1993), pp. 3507–3510.

[9] Neil A. Demarse et al. “determining enzyme kinetics via isothermal titration calorimetry”. In: *Enzyme Engineering: Methods and Protocols*. Ed. by James C. Samuelson. Totowa, NJ: Humana Press, 2013, pp. 21–30.

[10] P. E. Morin and E. Freire. “Direct calorimetric analysis of the enzymatic activity of yeast cytochrome c oxidase”. In: *Biochemistry* 30.34 (1991), pp. 8494–8500.

[11] Mark K. Transtrum, Lee D. Hansen, and Colette Quinn. “Enzyme kinetics determined by single-injection isothermal titration calorimetry”. In: *Methods* 76 (2015), pp. 194–200.

[12] G. D. Watt. “A microcalorimetric procedure for evaluating the kinetic parameters of enzyme-catalyzed reactions: kinetic measurements of the nitrogenase system”. In: *Analytical biochemistry* 187.1 (1990), pp. 141–146.

[13] Nurul Karim and Shun-ichi Kidokoro. “Precise and continuous observation of cellulase-catalyzed hydrolysis of cello-oligosaccharides using isothermal titration calorimetry”. In: *Thermochimica Acta* 412.1-2 (2004), pp. 91–96.

[14] Nurul Karim, Hirofumi Okada, and Shun-ichi Kidokoro. “Calorimetric evaluation of the activity and the mechanism of cellulases for the hydrolysis of cello-oligosaccharides accompanied by the mutarotation reaction of the hydrolyzed products”. In: *Thermochimica Acta* 431.1-2 (2005), pp. 9–20.

[15] Heiko Poppe et al. “Cyclic nucleotide analogs as probes of signaling pathways”. In: *Nature Methods* 5.4 (2008), pp. 277–278.

[16] Ewa Poduch et al. “Design of Inhibitors of Orotidine Monophosphate Decarboxylase Using Bioisosteric Replacement and Determination of Inhibition Kinetics”. In: *Journal of Medicinal Chemistry* 49.16 (2006), pp. 4937–4945.

[17] Lee D. Hansen et al. “Enzyme-catalyzed and binding reaction kinetics determined by titration calorimetry”. In: *Biochimica et Biophysica Acta (BBA) - General Subjects* 1860.5 (2016), pp. 957–966.

[18] Tsuyoshi Egawa et al. “Method for determination of association and dissociation rate constants of reversible bimolecular reactions by isothermal titration calorimeters”. In: *Analytical chemistry* 79.7 (2007), pp. 2972–2978.

[19] Dominique Burnouf et al. “kinITC: a new method for obtaining joint thermodynamic and kinetic data by isothermal titration calorimetry”. In: *Journal of the American Chemical Society* 134.1 (2011), pp. 559–565.

[20] Kirk A. Vander Meulen and Samuel E. Butcher. “Characterization of the kinetic and thermodynamic landscape of RNA folding using a novel application of isothermal titration calorimetry”. In: *Nucleic Acids Research* 40.5 (2012), pp. 2140–2151.

[21] Robert E. Johnson and Rodney L. Biltonen. “Determination of reaction rate parameters by flow microcalorimetry”. In: *Journal of the American Chemical Society* 97.9 (1975), pp. 2349–2355.

[22] Iva Navratilova et al. “Thermodynamic benchmark study using Biacore technology”. In: *Analytical Biochemistry* 364.1 (2007), pp. 67–77.

[23] J. Homola, S. S. Yee, and G. Gauglitz. “Surface plasmon resonance sensors: review”. In: *Sensors and Actuators B-Chemical* 54.1-2 (1999), pp. 3–15.

[24] Hans Bisswanger. “Binding Measurements”. In: *Practical Enzymology*. Wiley-VCH Verlag GmbH and Co. KGaA, 2011, pp. 265–296.

[25] Meseret Ashenafi et al. “Purification and Characterization of Aminoglycoside Phosphotransferase APH(6)-Id, a Streptomycin Inactivating Enzyme”. In: *Molecular and cellular biochemistry* 387.0 (2014), pp. 207–216.

[26] X. W. Zheng et al. “Analytical methods for kinetic studies of biological interactions: A review”. In: *Journal of Pharmaceutical and Biomedical Analysis* 113 (2015), pp. 163–180.

[27] Franziska Exnowitz, Bernd Meyer, and Thomas Hackl. “NMR for direct determination of Km and Vmax of enzyme reactions based on the Lambert

W function-analysis of progress curves". In: *Biochimica et Biophysica Acta (BBA) - Proteins and Proteomics* 1824.3 (2012), pp. 443–449.

[28] Kourosh Ebrahimi et al. "Accurate label-free reaction kinetics determination using initial rate heat measurements". In: *Scientific reports* 5 (2015), p. 16380.

[29] Luis García-Fuentes, Carmen Barón, and Obdulio L. Mayorga. "Influence of Dynamic Power Compensation in an Isothermal Titration Microcalorimeter". In: *Analytical Chemistry* 70.21 (1998), pp. 4615–4623.

[30] Thomas Wiseman et al. "Rapid measurement of binding constants and heats of binding using a new titration calorimeter". In: *Analytical Biochemistry* 179.1 (1989), pp. 131–137.

[31] Ernesto Freire, Obdulio L. Mayorga, and Martin Straume. "Isothermal titration calorimetry". In: *Analytical Chemistry* 62.18 (1990).

[32] Mayorga Lopez, P. L. Mateo, and M. Cortijo. "The use of different input signals for dynamic characterisation in isothermal microcalorimetry". In: *Journal of Physics E: Scientific Instruments* 20 (1987).

[33] A. Velazquez-Campoy, O. LÛpez-Mayorga, and M. O. Cabrerizo-VÌlchez. "Determination of the Rigorous Transfer Function of an Isothermal Titration Microcalorimeter With Peltier Compensation". In: *Journal of Thermal Analysis and Calorimetry* 57 (1999).

[34] Clifford W. Hansen et al. "Correction for instrument time constant and baseline in determination of reaction kinetics". In: *International Journal of Chemical Kinetics* 43.2 (2011), pp. 53–61.

[35] M. Naraghi. "T-jump study of calcium binding kinetics of calcium chelators". In: *Cell calcium* 22.4 (1997), pp. 255–268.

[36] Tadashi Ingami. "The Mechanism of the Specificity of Trypsin Catalysis". In: *Journal of Biological Chemistry* 239.2 (1963), pp. 1388–1394.

[37] Thomas Kelly. “Fibroblast activation protein- and dipeptidyl peptidase IV (CD26): Cell-surface proteases that activate cell signaling and are potential targets for cancer therapy”. In: *Drug Resistance Updates* 8.1–2 (2005), pp. 51–58.

[38] L. Polgár. “The prolyl oligopeptidase family”. In: *Cellular and Molecular Life Sciences CMLS* 59.2 (2002), pp. 349–362.

[39] Carol M. Porter and Brian G. Miller. “Cooperativity in monomeric enzymes with single ligand-binding sites”. In: *Bioorganic Chemistry* 43 (2012), pp. 44–50.

[40] F. Peter Guengerich et al. “Measurement of cytochrome P450 and NADPH-cytochrome P450 reductase”. In: *Nat. Protocols* 4.9 (2009), pp. 1245–1251.

[41] Elliott Shaw, Marcos Mares-Guia, and William Cohen. “Evidence for an Active-Center Histidine in Trypsin through Use of a Specific Reagent, 1-Chloro-3-tosylamido-7-amino-2-heptanone, the Chloromethyl Ketone Derived from N-Tosyl-L-lysine*”. In: *Biochemistry* 4.10 (1965), pp. 2219–2224.

[42] Gaëlle Mariaule et al. “3-Oxo-hexahydro-1H-isoindole-4-carboxylic Acid as a Drug Chiral Bicyclic Scaffold: Structure-Based Design and Preparation of Conformationally Constrained Covalent and Noncovalent Prolyl Oligopeptidase Inhibitors”. In: *Journal of Medicinal Chemistry* 59.9 (2015), pp. 4221–4234.

[43] Stanley C. Gill and Peter H. von Hippel. “Calculation of protein extinction coefficients from amino acid sequence data”. In: *Analytical Biochemistry* 182.2 (1989), pp. 319–326.

Chapter 3

Complete Kinetic Characterization of Enzyme Inhibition in a Single Isothermal Titration Calorimetric Experiment

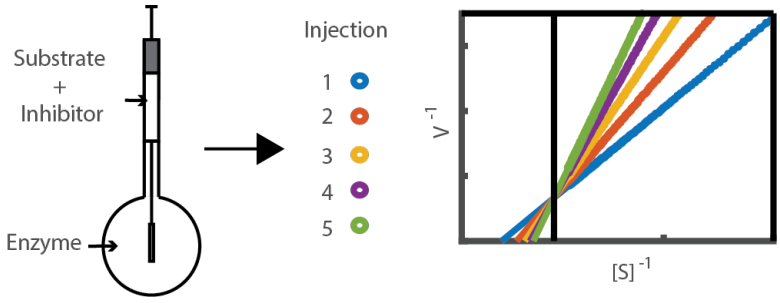

Preface

Complete characterization of enzyme inhibitors for drug design and development requires measurement of both the strength of the enzyme-inhibitor interaction and the mode of inhibition. This characterization involves measuring the enzyme activity at different concentrations of inhibitor and substrate, which can be very time consuming as several experiments must be performed. Using ITC it is possible to measure enzyme activity at different concentrations of substrate with a single injection of substrate into enzyme. In chapter 1 we also demonstrate that it is possible to perform these single injection experiments under conditions where the reaction proceeds quickly allowing for a high throughput analysis. Here we present a method where we perform multiple injections of substrate and inhibitor into enzyme enabling measurement of the activity at several different concentrations of both substrate and inhibitor in a single experiment. This allows for a high throughput, complete characterization of enzyme inhibitors.

3.1 Abstract

Techniques for rapidly measuring both the strength and mode of enzyme inhibitors are crucial to lead generation and optimization in drug development. Isothermal titration calorimetry (ITC) is emerging as a powerful tool for measuring enzyme kinetics with distinct advantages over traditional techniques. ITC measures heat flow, a feature of nearly all chemical reactions, and gives an instantaneous readout of enzyme velocity, eliminating the need for artificial substrates or post-reaction processing. In principle, ITC is an ideal method for characterizing enzyme inhibition. However existing ITC experiments are not well-suited to rapid throughput and few studies to date have employed this approach. We have developed a new ITC experiment, in which substrate and inhibitor are premixed in the injection syringe, that yields the complete kinetic characterization of an enzyme inhibitor in an hour or less. This corresponds to savings in time and material of 5-fold or greater compared

to previous ITC methods. We validated the approach using the trypsin inhibitor benzamidine as a model system, recapitulating both its competitive inhibition mode and binding constant. Our approach combines the rapid throughput of optimized spectroscopic assays with the universality and precision of ITC-based methods, providing substantially improved inhibitor characterization for biochemistry and drug development applications.

3.2 Introduction

Biophysical characterization of enzyme inhibitors is crucial to lead generation and optimization in drug development.[1] Inhibitors are typically evaluated based on their affinities and their modes of inhibition, of which there are three main types:[2] 1) competitive inhibition, where the inhibitor binds to the free enzyme (E) and blocks interactions with the substrate, 2) uncompetitive inhibition, where the inhibitor binds to the enzyme-substrate complex (ES), blocking catalysis, and 3) mixed inhibition, where the inhibitor can bind to both E and ES. The special case in which the affinities for E and ES are equal is referred to as noncompetitive inhibition. Information on both the affinity and mode of inhibition is critical to drug development since tight binding is required for efficacy while the mode reveals the nature of the inhibited state(s). In what follows, we refer to the determination of both the affinity and mode of inhibition as the complete kinetic characterization of an inhibitor. Additional parameters, such as association and dissociation rates, can also play important roles in drug development,[3] and ITC is suitable for their measurement which is developed in chapter 4, however binding kinetics are outside the aims of the current chapter and will not be considered further.

Both the strength and mode of inhibition can be determined by measuring Michaelis-Menten enzyme kinetic parameters while varying the inhibitor concentration. Different modes of inhibition lead to different patterns of changes in K_m and k_{cat} as a function of inhibitor concentration. However, the development of a simple and effective enzyme kinetic assay is not always straightforward, depending on

the enzyme of interest. In favourable cases, substrates and products are distinguishable spectroscopically and the reaction velocity can easily be monitored as catalysis proceeds.[4] Non-native substrates can be designed to undergo changes in colour or fluorescence when converted to products.[5,6] Alternatively, coupled enzymatic assays can be used to rapidly convert reaction products to spectroscopically active derivatives,[7] although this places constraints on the reaction conditions.[8] Nevertheless, direct detection is frequently impossible and post-reaction ancillary techniques, such liquid chromatography, gel electrophoresis, or mass spectrometry are required to quantify the depletion of substrates and accumulation of products.[9] These additional steps add time, expense, and uncertainty to the measurement process. In some cases, inhibitor development is substantially hampered by the lack of a rapid and reliable enzymatic assay.[10,11]

Isothermal titration calorimetry (ITC) is emerging as a powerful tool for measuring the kinetics of challenging enzyme systems. Rather than tracking the concentrations of substrates and products over time, it detects the heat that is released or absorbed during catalysis in real time. Since nearly all chemical reactions release or absorb heat (i.e. $\Delta H_{cat} \neq 0$), ITC can be applied nearly universally. ITC experiments can be performed under dilute conditions in physiological buffers, even those that are spectroscopically opaque.[12] ITC has been successfully used to characterize enzymes that were recalcitrant to traditional analyses including cellbiohydrolases,[13] oxalate oxidase,[14] heparinase-I,[15] and systems that require complex mixtures of macro-molecules.[12] One drawback of the ITC method is that the workflow cannot be easily parallelized. In order to measure how inhibitors influence enzyme kinetic parameters, a series of reactions must be performed with different inhibitor concentrations. In the ITC studies performed to date, this has meant setting up numerous (5-10) separate experiments, emptying, cleaning, refilling, and re-equilibrating the instrument before each measurement is taken.[15,16,17] This is costly both in terms of time and material, resulting in total measurement times of several days for the kinetic characterization of single inhibitor. Here, we present and validate a simple method for performing enzyme reactions with a range of inhibitor concentrations in

a single ITC experiment. This allows the complete kinetic characterization of an inhibitor in under an hour, yielding substantial reductions in the amount of time and sample required for analysis.

3.3 Results

3.3.1 Inhibitor-Free Enzyme Kinetics

Our method builds upon the single-injection ITC enzyme kinetics experiment,[15,18] in which the sample cell contains the enzyme of interest and the automated injection syringe contains the substrate. An injection of substrate into the sample cell initiates the reaction, which is detected as a change in heat flow. The signal continues for roughly as long as the reaction proceeds, returning to the baseline once all the substrate has been consumed. Rapid catalysis gives tall narrow peaks, slow catalysis gives low broad peaks, and the total area of each peak depends on the amount of substrate injected and the enthalpy change of the catalyzed reaction. The shape of each peak is governed by the concentration of enzyme and its Michaelis-Menten parameters, as well as the rate of substrate injection and the intrinsic response function of the calorimeter (see chapter 2). The peaks can be modelled quantitatively, yielding the values of k_{cat} and K_m from a single injection (see chapter 2 and[18]), as described in the methods section. We have used the enzyme trypsin and one of its substrates, N-Benzoyl-L-arginine ethyl ester (BAEE), as a model system for this study. Figure 3.1 shows the normalized ITC output produced by three injections of BAEE into trypsin. The peaks are virtually superimposable, with minuscule reductions in the heights of successive peaks coming from the slight dilution of the enzyme that occurs with each injection. The values of k_{cat} and K_m extracted from the three peaks are nearly identical (Table 3.S1) with average values of 16.01 $\pm$ 0.02 s^{-1} and 2.45 $\pm$ 0.05 μM respectively, which agree well with previous studies.[15,19]

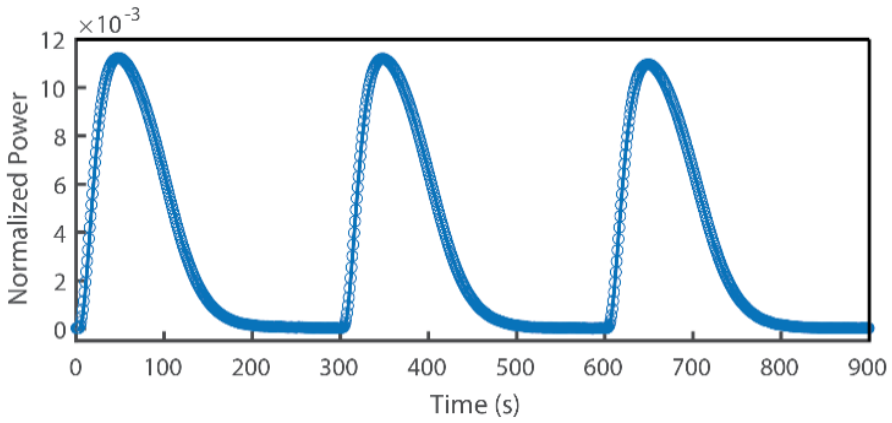

Figure 3.1. ITC data for injections of BAEE into trypsin. Normalized data from injections 2, 3, 4 are shown above (open circles) with fits according to Michaelis-Menten kinetics (lines).

3.3.2 Progressive Inhibition Enzyme Kinetics

We have adapted the approach above by filling the syringe with a combination of inhibitor and substrate. A series of injections is then made, similar to those of Figure 3.1, with the difference that inhibitor accumulates in the sample cell with each successive injection. Thus, the Michaelis-Menten parameters obtained for the second peak correspond to twice the inhibitor concentration compared to the first peak and those of the third peak correspond to three times the inhibitor concentration, etc. In order to test this method, we used the trypsin inhibitor benzamidine, together with substrate BAEE. Figure 3.2A shows ITC data for a series of five injections, corresponding to a five-fold variation of inhibitor concentration. Each peak is substantially lower and broader than the previous one due to increasing inhibition of the enzyme and thus slower catalysis. As before, we modelled the peak shapes to extract the Michaelis-Menten parameters (Table 3.S2). The values of k_{cat} are similar for each injection, while the value of K_m increases along with the concentration of inhibitor. This is consistent with competitive inhibition, in agreement with benzamidine's reported mode of action;[20] a competitive inhibitor increases K_m, a noncompetitive inhibitor decreases k_{cat}, and an uncompetitive inhibitor reduces both K_m and k_{cat}.[2] These data also yield the inhibition constant, K_i. For a competitive inhibitor, a plot of the apparent K_m (K'_m) versus inhibitor concentration (Figure

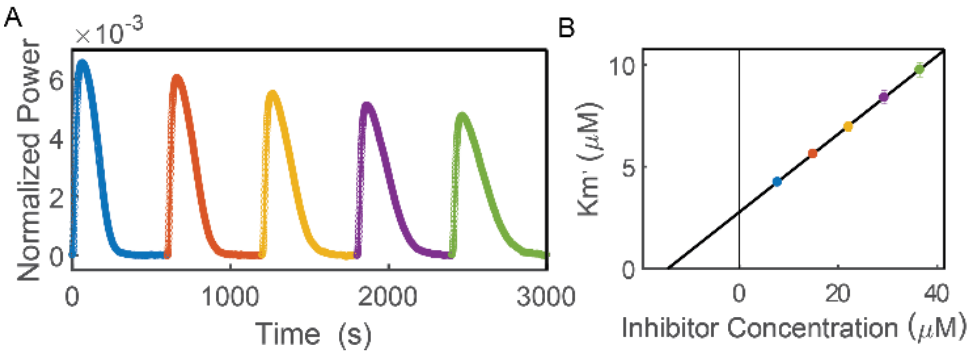

Figure 3.2. Multiple injections of BAEE and benzamidine into trypsin. (A) Normalized data from injections 2-6; open blue, orange, yellow, purple and green circles respectively overlaid with fits using Michaelis-Menten kinetics (lines). (B) Secondary plot of the total inhibitor concentration immediately following the injection vs. the apparent Km for each injection with line of bests fit (black line).

3.2B) is linear with a y-intercept of the true K_m and a slope of $\frac{K_m}{K_i}$. In this case, the y-intercept (2.77 $\pm$ 0.03 μM) agrees closely with the value of obtained in the absence of benzamidine, while the value of K_i extracted from the slope of the line (14.5 $\pm$ 0.1 μM) matches literature values (16-18 μM[15,19]). Note that this analysis (Equations 3.1-3.6) assumes that the inhibitor concentration is constant throughout the measurement of each peak, despite the fact the inhibitor concentration increases during the injection period (i.e. first $\approx$ 20 s of each peak). This simplification was made since explicitly modelling the effects of changing inhibitor concentrations requires prior knowledge of the mode of inhibition which is generally unavailable. We find that this approximation has little effect on the extracted parameters, provided the injection length (τ_{inj}) is kept below 20% of the total length of the first peak used in the analysis. Longer injection lengths produce systematic deviation in the kinetic parameters extracted by direct fitting (Figure 3.S7 and Table 3.S3) although deconvolution approaches may still be rigorously applied (see below).

3.3.3 Visual Assessment of Inhibition Mode

As an alternative to the direct modelling of ITC peak shapes assuming Michaelis-Menten kinetics, the data can be analysed by numerical deconvolution and double-

reciprocal or Lineweaver-Burk plots (see 3.6). This has the advantage of providing an opportunity to visually assess the mode of inhibition and the extent to which the enzyme kinetics follow the Michaelis-Menten paradigm. First, the effect of the finite response time of the ITC instrument is removed from the data. This can be achieved using Tian's equation,[21] which assumes a single-exponential instrument response. Alternatively, deconvolution using a full empirical instrumental response function may be performed in the frequency domain (see 3.6.8). We found the second approach agrees better with direct fitting, particularly for rapid reactions (Figure 3.S1) and is preferred. These calculations yield the true rates of heat generation in the sample cell as a function of time, which are directly proportional to the instantaneous enzyme velocities, V_0. Second, the concentration of substrate, $[S]$, remaining at each instant is calculated using Equations 3.18-3.20. For enzyme kinetics that follow the Michaelis-Menten Equation, a plot of $\frac{1}{V_0}$ versus $\frac{1}{[S]}$ is linear with a y-intercept of $\frac{1}{V_{max}} = \frac{1}{[E_0] \cdot k_{cat}}$, an x-intercept of $\frac{-1}{K_m}$, and a slope of $\frac{K_m}{k_{cat}}$. Double-reciprocal plots obtained for different concentrations of competitive inhibitors produce lines that intersect at the y-axis. For noncompetitive inhibitors, the lines intersect at the x-axis, and for uncompetitive inhibitors, the lines are parallel.[2] A double reciprocal plot for benzamidine inhibition of trypsin is shown in Figure 3.3, where each line is calculated from the post-injection portion of each peak in Figure 3.2. The data are all nearly perfectly linear, confirming that they follow the Michaelis-Menten equation. The slope increases for each successive injection, reflecting the progressive inhibition of the enzyme. Notably, the intersection of the lines occurs precisely at the y-axis, providing strong validation for the robustness of the progressive inhibition method and deconvolution approach.

In addition to its use as a visual assessment tool, linear regression analysis of the double reciprocal plots yields k_{cat} and K_m at each concentration of inhibitor. Because the data are deconvoluted and only the post-injection portions analyzed, no approximations regarding inhibitor concentrations during the injection are required and there are no limits imposed on suitable τ_{inj} values, in contrast to direct fitting (Figure 3.S7). The ERM-deconvolution can therefore be used as an internal consis-

tency check. Both direct fitting and deconvolution with Lineweaver-Burk analysis should yield the same k_{cat}, K_m, and K_i values. Importantly, we find that the values extracted using these two approaches are in excellent agreement (Figure 3.S3).

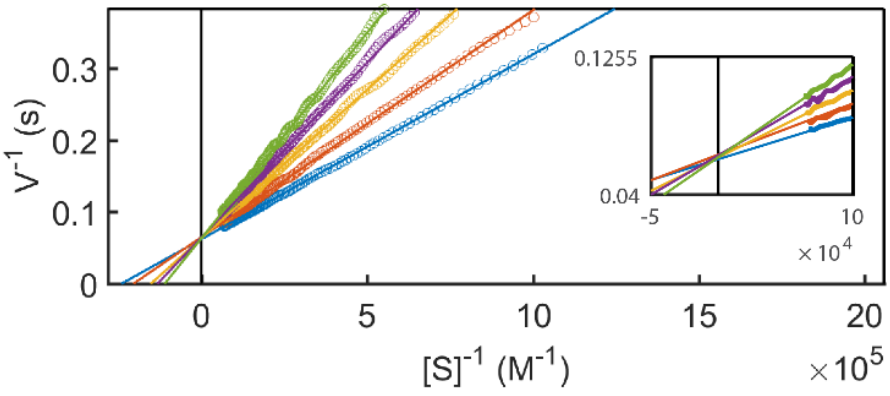

Figure 3.3. Lineweaver-Burk plot. ERM-Deconvoluted, Linearized data of the multiple injection data from Figure 3.2 (injections 2-6; open blue, orange, yellow, purple and green circles respectively). Lines correspond best linear fits.

3.4 Discussion

These results demonstrate that Michaelis-Menten parameters can be determined for multiple inhibitor concentrations in a single ITC experiment with a high level of accuracy. This contrasts with previous ITC studies in which separate experiments were performed for each concentration of inhibitor tested.[15,16] The multi-injection method thus provides a reduction in the required time and material that is proportional to the number of different inhibitor concentrations used. In our estimation, five different inhibitor concentrations provide good sampling of the K_m and k_{cat} variation and are sufficient to unambiguously identify the mode of inhibition. This then corresponds to a five-fold improvement in efficiency compared to previous methods. We note that the number of injections can be increased substantially without greatly extending the experiment time or amount of enzyme required. The bulk of the experiment time is occupied by cleaning, filling, and equilibrating the instrument, prior to data collection. Thus, time and material savings of ten-fold or more

are easily accessible (see 3.7.3).

In our hands, a multi-injection ITC inhibition experiment can be performed start to finish in approximately for 1.2 hours for a large volume instrument (eg. MicroCal VP-ITC, 1.4 mL) or 1 hour for a small volume instrument (eg. Mi-croCal ITC-200, 0.2 mL). This is on par with the length of time needed to perform complete kinetic characterization of an inhibitor using conventional spectrophotometry and a multi-well plate reader. Even in this case, there are distinct advantages to the ITC method. Conventionally, the initial enzyme velocity is measured for separate reaction mixtures with various concentrations of substrate and inhibitor.[22] This requires the preparation of $n_s \cdot n_i$ individual reaction mixtures, where n_s and n_i are the number of different substrate and inhibitor concentrations, respectively. Pipetting errors can introduce non-negligible uncertainty in the resultant data. In contrast, a multi-injection ITC experiment obtains all data from the same enzyme sample. Different values of $[S]$ are produced by the action of the enzyme itself, determined directly from the ITC peak shape, and sampled in much smaller intervals than is possible with conventional techniques (600 different values for ITC compared to approx. 5-20 spectrophotometrically).[22] In many cases, direct photometric detection of substrates and products is possible only with unnatural colorigenic or fluorogenic substrates.[5,6] Since these form ES complexes that differ chemically from those containing the native substrate, values obtained for uncompetitive and mixed inhibitors, which interact with ES, may be affected. In contrast, the natural substrate can always be used with the ITC method so this issue is non-existent. Finally, many enzymes lack a spectrophotometric assay altogether and require additional steps to separate and quantify substrates and products from each separate reaction, such as mass spectrometry, chromatography, or electrophoresis.[9] These additional steps add time, cost, and uncertainty to the measurements. The ITC kinetics method presented here thus has the potential to provide substantial improvements in efficiency and accuracy for these systems.

One way to streamline conventional assays is to measure IC_{50} rather than true K_i values and binding modes. The IC_{50} is the concentration of inhibitor necessary

to produce a 50% decrease in enzyme activity at an arbitrary concentration of substrate, and thus requires only n_i separate reactions, as opposed to $n_s \cdot n_i$. It must be emphasized that IC_{50} values are relatively information-poor, as they do not reveal the inhibition mode which is essential knowledge for structural characterization and optimization of the inhibitor-bound form (E, ES, or both)[23,24] as well as for discriminating amongst different enzymatic mechanisms for multi-substrate enzymes.[25] Furthermore, IC_{50} values cannot be quantitatively interpreted in terms of binding affinity unless the inhibition mode is known a priori. In contrast, information on the mode and affinity(s) of an inhibitor is obtained rapidly using the multi-injection ITC kinetics approach presented here.

Despite its overall versatility, there are nevertheless some caveats for employing this ITC method. Firstly, in order to extract reliable k_{cat} and K_m values from individual injections, the enzyme must be sufficiently saturated at the maximum of each peak, implying that concentration of substrate must reach roughly 1.5-fold the K_m. This requirement is true for all single-injection type ITC enzyme kinetics experiments,[18] with the added complication that the apparent K_m increases as competitive inhibitors are added, increasing the concentration of substrate required. Conversely, the addition of uncompetitive inhibitors decreases the apparent K_m, reducing the amount of substrate that is required in successive injections. Secondly, the concentration of inhibitor needed in the syringe is about 5-fold greater than the final concentration of inhibitor present in the sample cell. This demands that the inhibitor be well soluble in water, as injections of aggregated molecules can produce large artefactual heats of dilution. Additionally, slow inhibitor binding kinetics can lead to distortions in the ITC data that appear as aberrant curvature in Lineweaver-Burk plots (Figure 3.S8), or as apparent K_m and k_{cat} values that vary depending on the concentration of substrate in the syringe (Figure 3.S9). Our simulations show that these artefacts begin to appear when the bound half-life of the inhibitor is approximately equal to or greater than the length of the first peak (Figure 3.S8). In other words, when kinetics are slow, it is preferable to increase substrate and reduce enzyme concentrations in order to extend the widths of the peaks. In principle, the

kinetic information encoded in such distorted ITC data could be accessed by fitting models that explicitly include association and dissociation rates, although such an analysis is beyond the scope of the this work. Furthermore, in the next chapter we develop ITC methods tailored to measuring association and dissociation rates, that are more suitable when kinetic characterization is desired. Finally, some enzymes are inhibited by their reaction products, which also accumulate in the sample cell with successive injections of substrate. This would lead to progressive lowering and broadening of ITC peaks in the inhibitor-free multiple-injection experiment, in contrast to the results obtained for trypsin/BAEE where the peaks are virtually superimposable (Figure 3.1). While this complicates the analysis, such datasets are information-rich. We have simulated this scenario and find that the strength and mode of product inhibition can be extracted from a multi-injection experiment (Figure 3.S10). Such an application to the study of product inhibition can be considered a powerful variant of this approach. Furthermore, with this information in hand, it is possible to quantify the affinity and mode of additional (non-product) inhibitors from multiple injections of substrate+inhibitor, similar to Figure 3.2.

3.5 Conclusion

Our multi-injection approach combines the versatility of ITC-based enzyme assays with rapid throughput on par with spectrophotometric experiments, yielding savings in time and material of 5-10 fold compared to previous ITC studies. We have demonstrated experimentally that it is effective and straightforward using trypsin, a single-substrate enzyme that follows Michaelis-Menten kinetics with no product inhibition. However, in principle the method applies equally well to enzymes with multiple substrates and/or product inhibition (Figure 3.S10). Thus ITC has great potential to become a general tool for rapidly and economically characterizing enzyme inhibition.

3.6 Methods

3.6.1 ITC Experiment Conditions

All ITC experiments were performed using a MicroCal VP-ITC in high-feedback mode with a 1 second signal-averaging window and stirring rate of 806 rpm. Pre-injection delays of ≈500 s were employed to allow baselines to fully stabilize.

3.6.2 Enzymes, Substrate and Inhibitor Preparation

Trypsin (EC 3.4.21.4) was purchased in the form of (TrypZean^{TM}) from Sigma-Aldrich. The lyophilized powder was dissolved into 200 mM Tris-HCl, pH 8.0, 50 mM $CaCl_2$, and 0.2% PEG-8000 buffer. The concentration of Trypsin was measured using the extinction coefficient at 280 nm (ε= 30057 M^{-1} cm^{-1}).[26] The substrate Nα-Benzoyl-L-arginine ethyl ester hydrochloride (BAEE) (EC 220-157-0) was purchased from Sigma-Aldrich and dissolved into the same buffer. The inhibitor benzamidine hydrochloride, anhydrous (CAT# 02005) was purchased from Chem-Impex International, Inc. and dissolved in the buffer described above immediately prior to use.

3.6.3 Multiple Injections of BAEE into Trypsin

Trypsin was placed in the cell at 10 nM with BAEE in the syringe at 400 μM. There were a total of four injections (first injection 2 μL over 4 s, subsequent three injections 30 μL over 20 s) using the Microcal VP-ITC.

3.6.4 Multiple Injections of BAEE and Benzamidine into Trypsin

Trypsin was placed in the cell at 10 nM with BAEE and benzamidine in the syringe at 800 μM and 336 μM respectively. There were a total of 6 injections (first injection 2 μL over 6.3 s, subsequent five injections 30 μL over 25 s) using the VP-ITC.

3.6.5 Enzyme Kinetics Fitting Scripts

All fitting was performed using MATLAB. Differential equations shown below (Equations 3.1-3.6) describing Michaelis-Menten kinetics were integrated numerically using Euler's method in 0.01 s integration steps (dt in the equations below) according to:

$$\frac{d[P]_t}{dt} = \frac{k_{cat} \cdot [E_0]_t \cdot [S]_t}{K_m + [S]_t} \tag{3.1}$$

$$[P]_{t+dt} = [P]_t + \frac{d[P]_t}{dt} \cdot dt \tag{3.2}$$

$$\frac{d[S]_t}{dt} = -\frac{d[P]_t}{dt} + [S]_{syringe} \cdot Rate_{dil} - [S]_t \cdot Rate_{dil} \tag{3.3}$$

$$[S]_{t+dt} = [S]_t + \frac{d[S]_t}{dt} \cdot dt \tag{3.4}$$

$$\frac{d[E_0]_t}{dt} = -[E_0]_t \cdot Rate_{dil} \tag{3.5}$$

$$[E_0]_{t+dt} = [E_0]_t + \frac{d[E_0]_t}{dt} \cdot dt \tag{3.6}$$

where k_{cat} and K_m are the catalytic rate and the Michaelis constant respectively, and $[E]_t$, $[S]_t$ and $[P]_t$ are the total concentrations of enzyme, substrate and product at time = t. $Rate_{dil}$ is the rate of dilution (in s^{-1}) calculated as $\frac{v_{inj}}{Vcell \cdot \tau_{inj}}$ during the injection and 0 otherwise, where v_{inj} is the volume of the injection, V_{cell} is the total volume of the reaction cell and τ_{inj} is the total time of the injection. $[S]_{syringe}$ is the concentration of substrate in the syringe. The second last term of Equation 3.3 accounts for dilution of the syringe species into the cell while the last term of Equation 3.3 and 3.5 account for dilution of species already in the cell due to the injection. The instantaneous heat $h(t)$ is calculated using the enthalpy of the reaction ΔH_{cat} and the total volume of the cell (Equation 3.7).

$$h(t) = \Delta H_{cat} \cdot V_{cell} \cdot \frac{d[P]_t}{dt} \tag{3.7}$$

The instantaneous heat curve is numerically convoluted with the instrument response function according to:

$$g(t) = h(t) \otimes f(t) \tag{3.8}$$

where $f(t)$ is the empirical response function, $g(t)$ is the resulting calculated signal, and the convolution is defined according to

$$h(t) \otimes f(t) = \int_0^t h(\tau) f(t - \tau) d\tau \tag{3.9}$$

The calculated instrument output, $g(t)$, was digitally resampled in 1 s intervals to match the experimental calorimeter output and normalized by the total area of the peak using trapezoidal integration according to

$$g_{norm}(t_m) = \frac{g(t_m)}{\sum_{n=0}^{N} [g(t_{n+1}) + g(t_n)] \cdot dt/2} \tag{3.10}$$

where N is the total number of time points, t_n and t_m are the nth and mth timepoint, dt is the time increment (1 s in all cases here) and g_{norm} is the normalized peak. Enzyme kinetic parameters were fit by minimizing the target function (Equation 3.11)

$$RSS = \sum_{n=0}^{N} (N_g \cdot g_{norm}(t_n) - b_{norm}(t_n))^2 \tag{3.11}$$

where RSS is the residual sum of squared differences, $b_{norm}(t)$ is experimental data which has been normalized according to Equation 3.10. Errors of fits were calculated using the variance-covariance matrix (see 2.6.5). All enzyme experiments were performed in triplicate. The first injection of each experiment was ignored due to diffusion from the syringe during the equilibration period.

3.6.6 Floating ΔH_{cat} in Enzyme Kinetics Fitting Scripts

Note that the normalization procedure above eliminates the need to fit the value of ΔH_{cat} in Equation 3.7, as this is essentially a scaling parameter. Alternatively, the

normalization steps may be skipped, and the value of ΔH_{cat} may be optimized. In this case, the normalization step (Equation 3.10) is not used and the residual sum of squares (RSS) is calculated as

$$RSS = \sum_{n=0}^{N} (N_g \cdot g(t_n) - b(t_n))^2 \tag{3.12}$$

where $g(t)$ and $b(t)$ are the raw calculated instrument output and the raw experimental instrument output respectively. The RSS is minimized while adjusting the enzyme kinetic parameters and the enthalpy of the reaction (in Equation 3.1 and 3.7). Importantly, we obtain essentially identical enzyme kinetic parameters using either fitting procedure and the enthalpy values extracted from the fits (ΔH_{cat}) are close to those calculated via direct integration of the curve (data not shown).

3.6.7 Secondary Plots

Secondary plots were produced by plotting the apparent K_m (K'_m) as a function of the inhibitor concentration which was calculated using an exponential dilution factor.[27] Linear regression was performed in order to extract the slope and the intercept. The inverse of the slope was take to be the $\frac{K_i}{K_m}$, and the y-intercept to be the K_m.

3.6.8 Deconvolution Using an Empirical Response Function

In the previous chapter we showed that peaks produced by an isothermal titration calorimeter can be quantitatively modelled using an empirical response function. However, such a response function is incompatible with the typical deconvolution approach employing Tian's equation.[21] We have therefore developed a numerical method that can be used to deconvolute experimental curves produced by ITC using an empirical response function (ERM-deconvolution). We find that this approach produces curves that agree closely with direct fitting, and allows for analysis of the entire curve including the portion where the injection is taking place. The

deconvolution procedure can be performed in several steps: 1) measurement and normalization of the empirical response function, 2) Fourier transformation of experimental curve and empirical response function and deconvolution in the frequency domain using the convolution theorem, 3) frequency domain filtering of the deconvoluted data using a window function, and 4) Fourier transform back to time domain taking only the real portion of the data.

Measurement and normalization of empirical response function Measurement of the empirical response function should be performed under conditions as similar to those of the actual experiment as possible using Ca^{2+}/EDTA injection or other standards (see 2.3.5). Acquiring a smooth empirical response function may require averaging of several (≈10) replicate injections. The resulting curve can then be normalized using trapezoidal integration (Equation 3.10).

Fourier transform and deconvolution using deconvolution theorem Once the experimental data and normalized empirical response function are obtained the curves are zero filled and Fourier transformed into the frequency domain. Zero filling involves adding zeros to the end of both data vectors until their total length is 2^n where n is an integer (typically between 9-12 but depends on the length of the experimental data) specified by the user. The calorimeter instrument output ($g(t)$) can be modelled as the convolution of the instantaneous heat ($h(t)$) and the response function ($f(t)$) (Equation 3.8). These curves therefore adhere to the convolution theorem which states that the Fourier transform of a convolution of two functions is the product of the Fourier transforms of the two functions (Equation 3.13).

$$\mathscr{F}\{h(t) \otimes f(t)\} = \mathscr{F}\{h(t)\} \cdot \mathscr{F}\{f(t)\} \tag{3.13}$$

Where $\mathscr{F}\{\}$ is the Fourier transform of the function contained in the brackets. The domain of the Fourier transformed experimental data and response function will be between 0 and $\nu_{max} = \frac{1}{t_f}$ where ν_{max} is the maximum frequency and t_f is the sam-

pling time (or filter time) for the calorimeter. By substituting Equation 3.8 from the main text into Equation 3.13 above and dividing through by the Fourier transform of the response function the instantaneous heat is obtained in the frequency domain (Equation 3).

$$h(\nu) = \mathscr{F}\{h(t)\} = \frac{\mathscr{F}\{g(t)\}}{\mathscr{F}\{f(t)\}} \tag{3.14}$$

Frequency domain filtering of the deconvoluted data using a window function. Once the data are stripped of the response function the higher frequency components of the data must be filtered out in order to remove artifacts remaining from the deconvolution. Here we used a Band-stop (low-high-pass) filter window function that is symmetric about $\nu = \frac{1}{2 \cdot t_f}$ (Equation 3.15).

$$W(\nu) = \begin{cases} 1 & 0 < \nu < A_w \\ e^{-\left(\frac{\nu - A_w}{\tau_{decay}}\right)} & A_w < \nu < \frac{\nu_{max}}{2} \\ e^{-\left(\frac{\nu - (\nu_{max} - A_w)}{\tau_{decay}}\right)} & \frac{\nu_{max}}{2} < \nu < \nu_{max} - A_w \\ 1 & \nu_{max} - A_w < \nu < \nu_{max} \end{cases} \tag{3.15}$$

The parameters A_w and τ_{decay} are the apodization width and decay constant respectively which can be optimized by the user in order to remove noise from the deconvolution to the desired level. The optimal values of these parameters will depend on the experimental data being used and should therefore be individually adjusted for each experiment (Figure 3.4). The pair-wise product between the window function and the deconvoluted data can then be calculated (Equation 3.16).

$$h_{filtered}(\nu) = W(\nu) \cdot h(\nu) \tag{3.16}$$

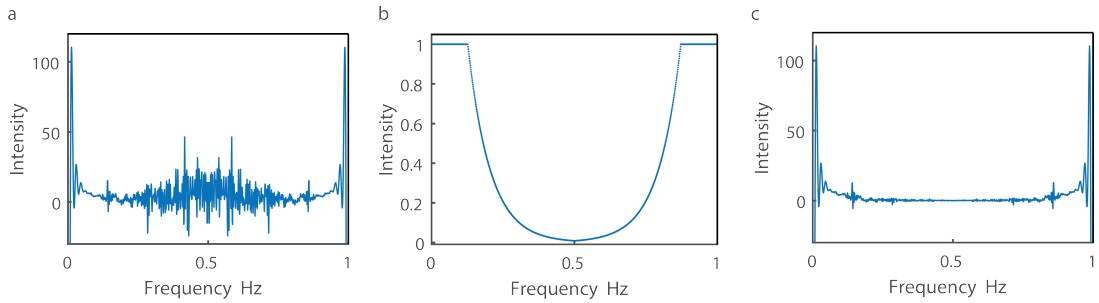

Figure 3.4. Applying window function to deconvoluted data. (a) $h(\nu)$, (b) $W(\nu)$ and (c) $h_{filtered}(\nu)$ for rapid trypsin kinetic data (see below). Adjustable parameters n, A_w and τ_{decay} were set to 10, 0.13 Hz and 0.078 Hz respectively.

Fourier transform back to time domain. The filtered instantaneous heat data $h_{filtered}(t)$ can then be Fourier transformed back to the time domain (Equation 3.17).

$$b_{deconv}(t) = \Re e\Big[\mathscr{F}\{h_{filtered}(\nu)\}\Big] \tag{3.17}$$

Where $b_{deconv}(t)$ is the deconvoluted data in the time domain and $\Re[]$ is the real portion of the data contained in the brackets. It is usually necessary to renormalize the deconvoluted data such that the total area is the same as the original data.

3.6.9 Lineweaver-Burk Plots

The deconvoluted signal ($b_{deconv}(t)$) was used to calculate the experimental rate of product formation ($\frac{d[P]_{t,exper}}{dt}$) using

$$\frac{d[P]_{t,exper}}{dt} = \frac{b_{deconv}(t)}{\Delta H_{react} \cdot V_{cell}} \tag{3.18}$$

The experimental rate of product formation and the injection rate were then used to calculate the substrate concentration as a function of time using equation 3.19 and 3.20

$$\frac{d[S]_{t,exper}}{dt} = -\frac{d[P]_{t,exper}}{dt} + [S]_{syringe} \cdot Rate_{dil} - [S]_t \cdot Rate_{dil} \tag{3.19}$$

$$[S]_{t+dt,exper} = [S]_{t,exper} + \frac{d[S]_{t,exper}}{dt} \cdot dt \tag{3.20}$$

with 1 s time increments ($dt = 1$ s). Lineweaver-Burk plots were then produced by plotting the $\frac{1}{[S]_{t,exper}}$ vs. $\frac{d[P]_{t,exper}}{dt} \cdot \frac{1}{[E]_{cell}}$ starting from immediately after the injection until a maximum $\frac{1}{[S]_{t,exper}}$ value of $1{\cdot}10^6$ M^{-1}.

3.7 Supplementary Information

3.7.1 Supplementary Results

Table 3.S1. Results of fits for multiple injections of BAEE into trypsin.

Injection	k_{cat} (s^{-1})	K_m (μM)
2	15.62 ± 0.01	2.40 ± 0.05
3	15.76 ± 0.02	2.40 ± 0.09
4	15.58 ± 0.03	2.38 ± 0.01

Table 3.S2. Results of fits for multiple injections of BAEE and benzamidine into trypsin.

Injection	k_{cat} (s^{-1})	K_m (μM)
2	16.38 ± 0.01	4.25 ± 0.01
3	16.47 ± 0.01	5.63 ± 0.02
4	16.32 ± 0.02	6.97 ± 0.02
5	16.37 ± 0.02	8.40 ± 0.02
6	16.43 ± 0.03	9.76 ± 0.03

3.7.2 ERM-Deconvolution Testing and Application

ERM-deconvolution of rapid trypsin kinetics. In order to test the deconvolution procedure presented above, injections of BAEE into high concentrations of trypsin

were performed in order to produce rapid enzyme kinetics. The experimental peaks were deconvoluted using both the ERM-deconvolution and Tian's Equation[21] (equation 7).

$$b_{deconv}(t) = g_{experimental}(t) + \frac{dg_{experimental}(t)}{dt} \cdot \tau_r \tag{3.21}$$

Where $g_{experimental}(t)$ is the experimental output and τ_r is the response time of the instrument. Michaelis-Menten curves were plotted using both deconvolution procedures (Figure 3.S1).

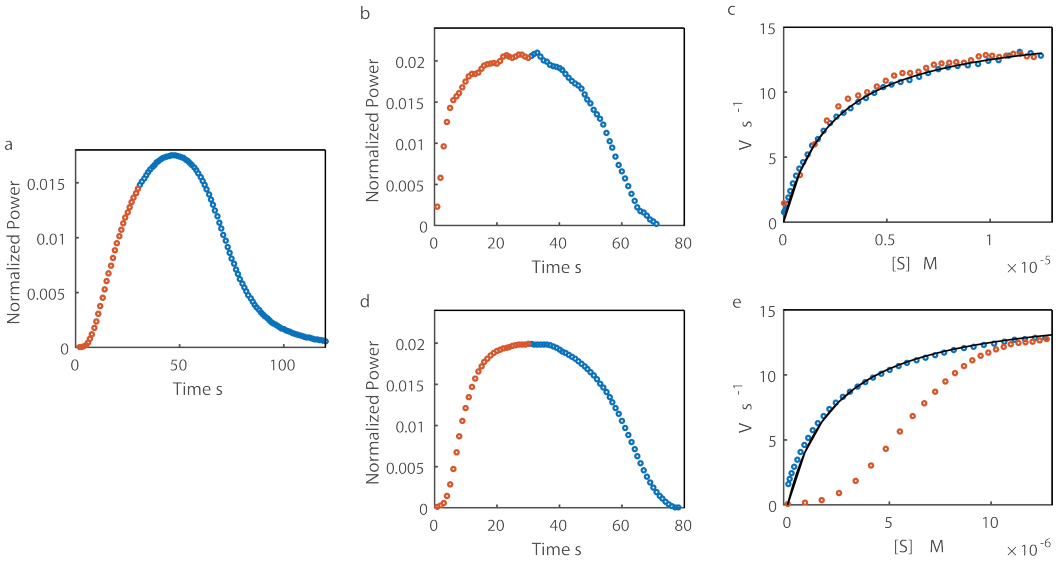

Figure 3.S1. Deconvolution of trypsin kinetics with BAEE. (a) BAEE (1.2 mM in syringe) was injected (30 μL over 30 s) into trypsin (40 nM in cell). (b) deconvolved data ($b_{deconv}(t)$) using ERM-deconvolution presented above (Figure 3.4). (c) Michaelis-Menten plot using ERM-deconvoluted data. (d) deconvoluted data ($b_{deconv}(t)$) using Tian's equation with a 15 s response time (τ_r). (e) Michaelis-Menten plot from data deconvoluted using Tian's equation. Black lines in c/e are the Michaelis-Menten curve using the parameters from direct fitting (Figure 3.1 and Table 3.S1). Data during the injection process is shown in orange (first 30 s of data points) while the remainder of the peak after the injection has ended is shown in blue.

The ERM-deconvolution provides a curve that is more consistent with the curve obtained by direct fitting than the deconvolution using Tian's equation (Figure 3.S1). The deconvolution using Tian's equation has large systematic deviations

during the injection (shown in orange) as well as small deviations at low substrate concentrations (at the end of the peak).

ERM-Deconvolution to produce LWB plots. The ERM-deconvolution procedure was applied to the multiple injection data with both BAEE and trypsin in the syringe in order to produce LWB plots (Figure 3.3). Adjustable parameters n, A_w and τ_{decay} were set to 10, 0.048 Hz and 0.2 Hz respectively. In order to further compare two deconvolution techniques Tian's equation was used to deconvolute the progressive inhibition enzyme kinetics multiple injection data with substrate+inhibitor in the syringe (Figure 3.S2).

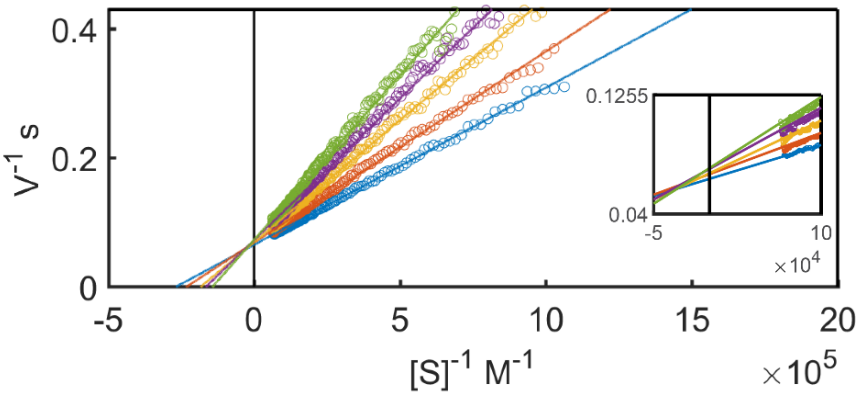

Figure 3.S2. Lineweaver-Burk plot using Tian's equation. Deconvoluted, Linearized data of the multiple injection data from Figure 3.2 (injections 2-6; open blue, orange, yellow, purple and green circles respectively). Lines correspond to lines of best fit to the corresponding ERM-deconvolution treated, linearized data. The response time τ_r was set to 15 s.

The LWB plot produced using the ERM-deconvolution is much less noisy than the one produced using Tian's equation. Also, all of the curves intersect at the y-axis much more closely than the curves produced using Tian's equation. Lastly, the apparent K_m values extracted using the ERM approach match those extracted by direct fitting much more closely than those obtained using Tian's equation (Figure 3.S3).

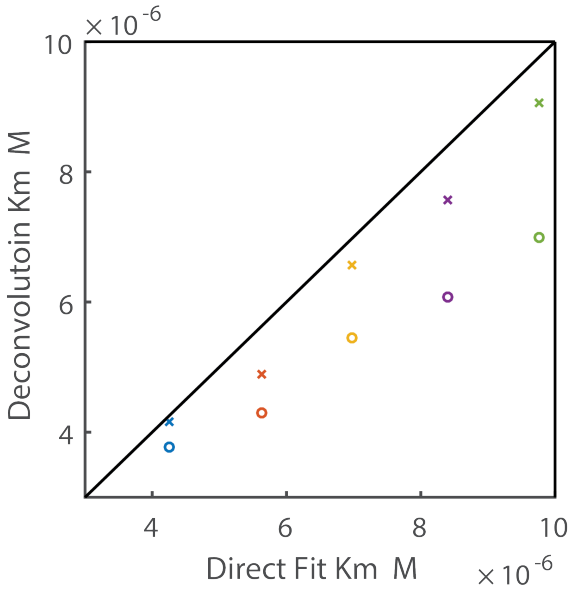

Figure 3.S3. MM parameters extracted via LWB plot using Tian's equation vs. ERM-deconvolution. Parameters extracted by direct fitting (black line) vs. those extracted by linear regression of LWB plots by Tian's equation (open circles), and ERM-deconvolution (x's). Injections 2-6 are blue, orange, yellow, purple and green respectively.

Limitations of ERM-deconvolution. In general, we have found that the ERM-Deconvolution produces accurate instantaneous curves for heat flows that change smoothly with time, as is usually the case for experimental data with normal injection lengths. However, when instrument output data are simulated for instantaneous heats that contain sharp (eg. square-pulse) transitions, the resulting ERM-deconvoluted data display ringing artifacts as illustrated in Figure 3.S4 below. Therefore we recommend that extremely rapid injections (less than about 5 seconds) are avoided when Fourier transform-based deconvolution is applied.

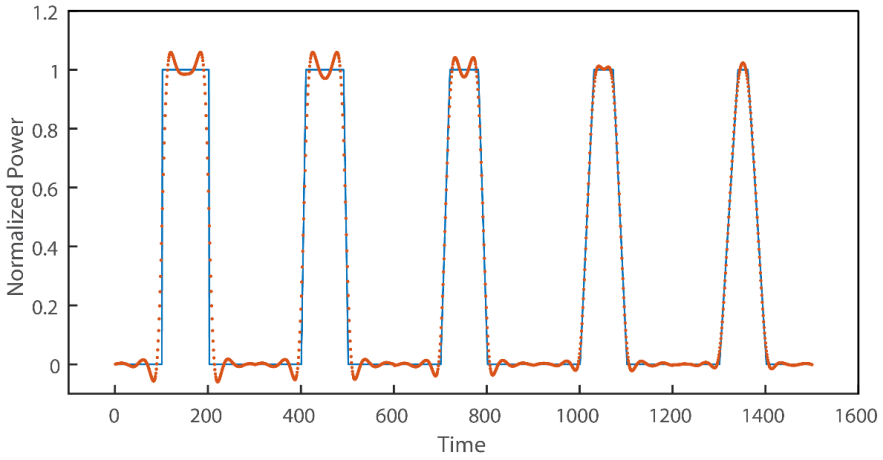

Figure 3.S4. ERM-Deconvolution limitations. Simulated instantaneous heat data for several trapezoidal pulses are shown in blue. Instantaneous heat data was convoluted with the empirical response function (Equation 3.8-3.9). Resulting data was ERM-deconvoluted and overlaid (orange circles). Adjustable parameters n, A_w and τ_{decay} were set to 10, 0.019 Hz and 0.0097 Hz respectively.

3.7.3 Ten Injection Experiment with Substrate and Inhibitor in the Syringe

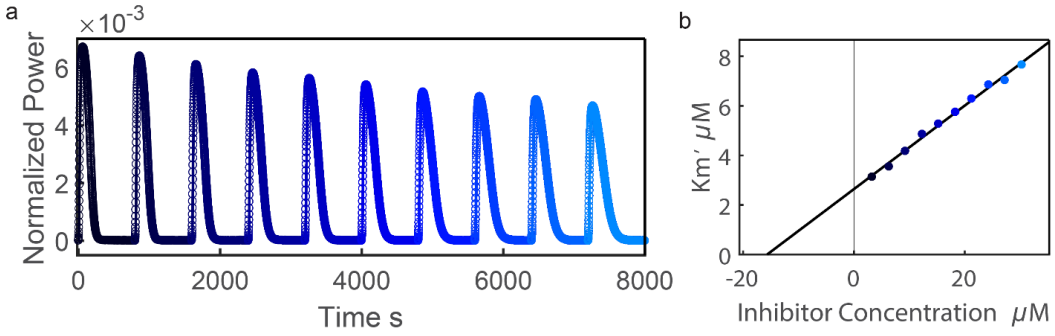

Figure 3.S5. Ten injections of BAEE and Benzamidine into trypsin. (a) Normalized multiple injection data (open circles) with fit (lines) for second injection (black peak) to eleventh injection (light blue peak). First injection is 2 μL over 4 s while subsequent 10 injections are 25 μL over 21 s. Experimental setup with 10 nM trypsin in the cell and 960 μM BAEE and 168 μM Benzamidine in the syringe. (b) Secondary plot with inhibitor concentration vs. apparent K_m for each injection and line of best fit (black line). The K_i was calculated to be 15.6 $\pm$ 0.4 μM using the reciprocal of the slope.

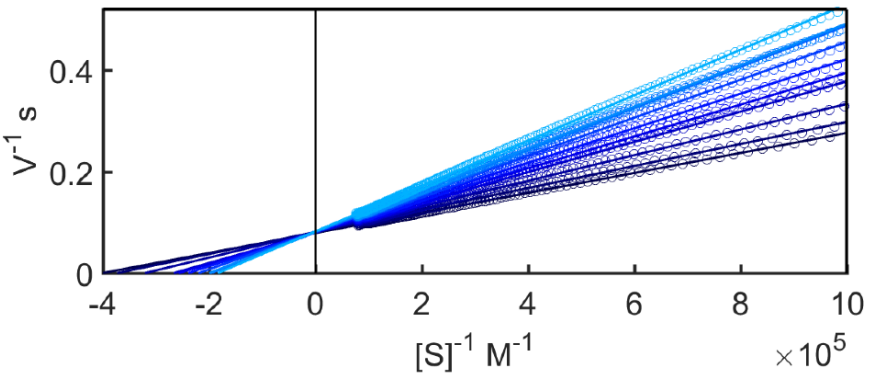

Figure 3.S6. Lineweaver-Burk plot for 10 injection experiment. Deconvoluted, Linearized data of the multiple injection data from Figure S6 (injections 2-11; ranging from black to light blue). Lines are the lines of best fit to the corresponding deconvoluted, linearized data. Data was deconvoluted using the ERM-Deconvolution. Adjustable parameters n, Aw and τ_{decay} were set to 10, 0.019 Hz and 0.19 Hz respectively.

3.7.4 Effect of Changing Inhibitor Concentration During the Injection

Equations 3.30-3.40 below were used to simulate multiple injection competitive inhibition enzyme kinetics curves with no product inhibition (Equation 3.29 with $\frac{1}{K_{iu}} = \frac{1}{K_{ip}} = 0$) and variable injection length (τ_{inj}). Substrate concentrations were set at 800 μM for τ_{inj} = 25 s, 960 μM for τ_{inj} = 75 s and 1.22 mM for τ_{inj} = 150 s which were selected in order to obtain a consistent maximum substrate concentration in the cell regardless of injection length. Inhibitor concentration was set at 336 μM and enzyme concentration in the cell was set to 10 nM. k_{cat}, K_m, and K_{ic} were set at 16 s^{-1}, 2.4 μM, and 16 μM respectively. Simulated curves were fit using equations 3.1-3.11.

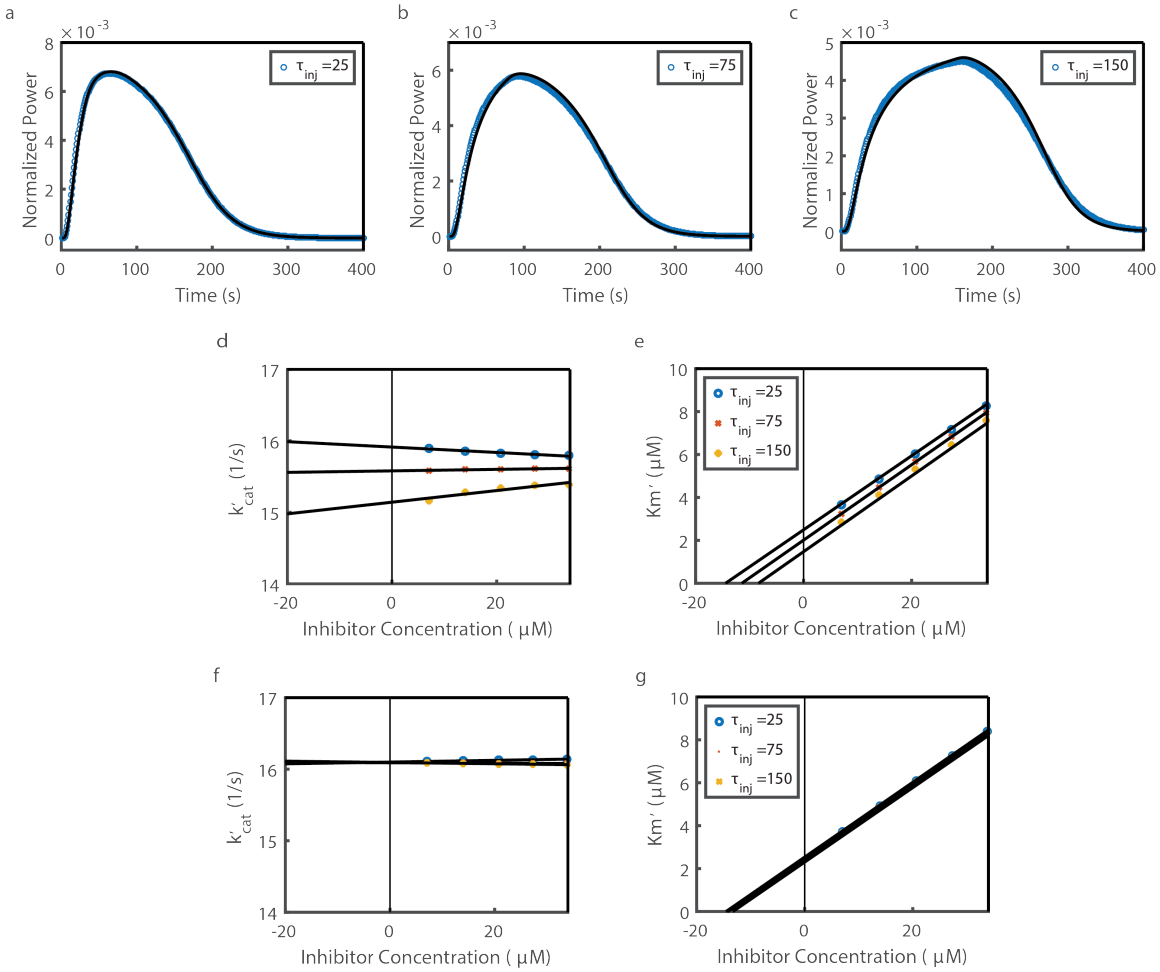

Figure 3.S7. Effect of injection length. (a)-(c) First injections for each multiple injection experiment with variable injection length (open blue circles). Fits to the first injection of each set of multiple injection experiments (black lines). (d) Effective catalytic rate (k_{cat}') obtained from MM fit to each simulated peak against inhibitor concentration in cell immediately after injection (colored points). (e) Effective MM constant (K_m') obtained from MM fit to each simulated peak against inhibitor concentration in cell immediately after injection (colored points). (f) Effective catalytic rate (k_{cat}') obtained from linear regression of LWB plots produced via ERM-deconvolution of each simulated peak. (g) Effective MM constant (K_m') obtained from linear regression of LWB plots produced via ERM-deconvolution of each simulated peak. Black lines are lines of best fit for each multiple injection experiment.

Table 3.S3. Results of secondary plots obtained from direct fits Figure 3.S7d,e.

τ_{inj}	k_{cat} (s^{-1})	K_m (μM)	K_i (μM)
25	15.9	2.46	14.1
75	15.6	2.01	11.4
150	15.1	1.62	9.2

3.7.5 Progressive Inhibition With Slow Binding Kinetics

In the progressive inhibition experiments presented in this study, the substrate and inhibitor concentrations change throughout the injection, as do the amounts of E, ES, and EI, which may affect the shapes of peaks produced. We simulated multiple injection progressive inhibition experiments with varying association and dissociation rates in order to estimate the effects on the resultant data, particularly the appearance of double-reciprocal plots. We found that there are systematic deviations from linearity in the LWB plots that can be used to visually assess whether slow binding kinetics affect the shapes of the peaks. When the half-life of the enzyme inhibitor complex ($t_{1/2} = \frac{ln(2)}{k_{off}}$) is less than the length of the length of each peak (in this case ~800 s) the LWB plots appear ordinary and the experiments can be analyzed normally (Figure 3.S8a, b). We note that the data obtained during the injection itself (x's below) lie below the post-injection data (circles), since the inhibitor is not fully injected during these periods. When $t_{1/2}$ is on the same order as the length of the peaks, the LWB plots curve in a characteristic way (Figure 3.S8c,d,e), where the injection data (x's) lie above the post-injection data (circles), due to slow dissociation of the EI complex in response to the rapid increase in substrate concentration and concomitant artifactually lower enzyme velocities. In principle these peaks can be analyzed in order to extract the kinetics of inhibition however, this is beyond the scope of this study. Lastly, when $t_{1/2}$ is much longer than the length of the peak we find that a competitive inhibitor produces a plot characteristic of noncompetitive inhibition (Figure 3.S8f). In order to discern whether slow kinetics

are at play or an inhibitor is simply noncompetitive, we suggest performing a repeat experiment with a different concentration of substrate (Figure 3.S9). The plots will be different for the two substrate concentrations if the inhibitor is competitive with slow kinetics, while the plots will be similar if the inhibitor is noncompetitive with rapid kinetics.

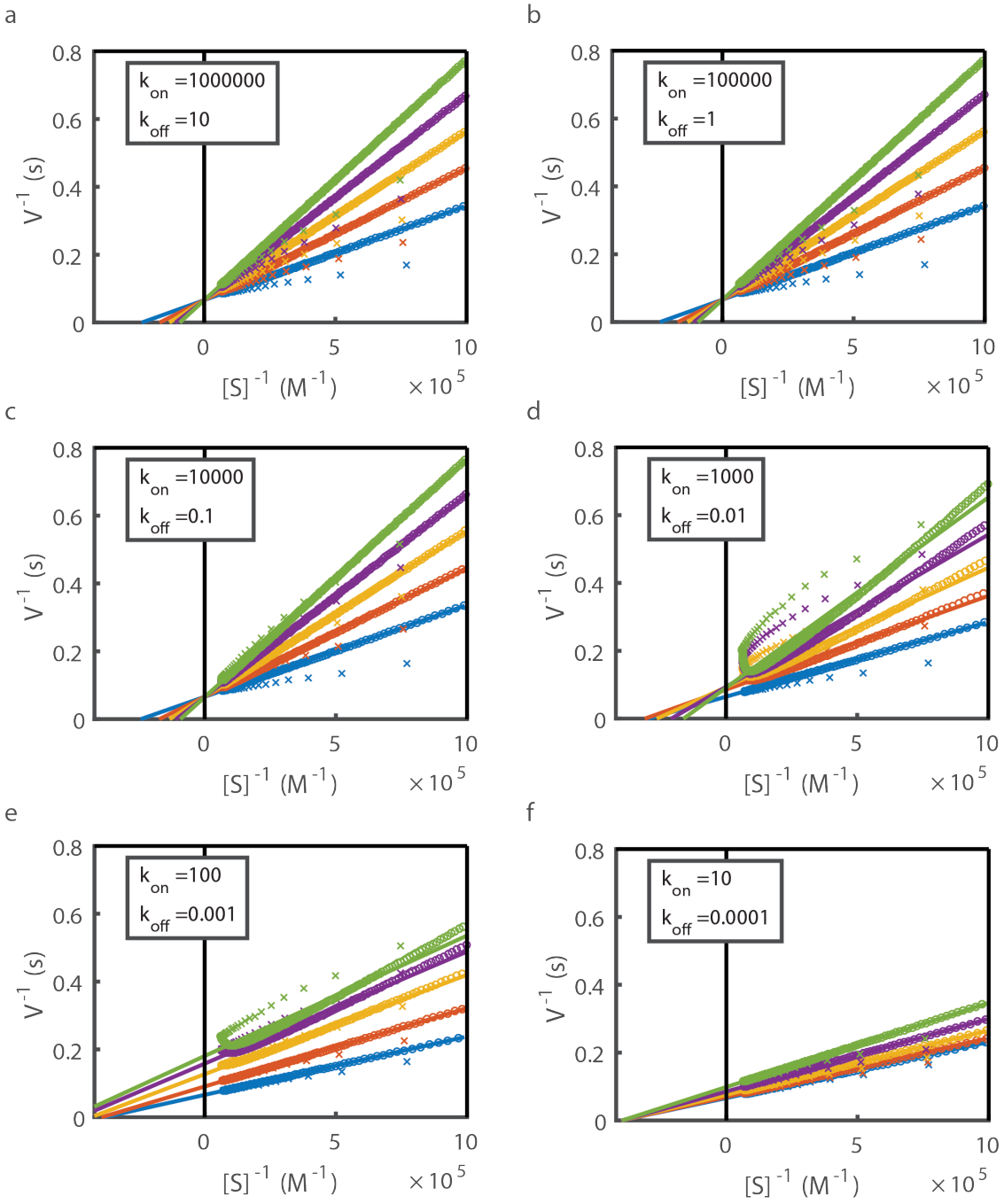

Figure 3.S8. Competitive inhibition with varying kinetic rates. Lineweaver-Burk plots produced from simulated multiple injection experiments of substrate (800 μM) and inhibitor (336 μM) in the syringe and enzyme (10 nM) in the cell for a competitive inhibitor with varying association and dissociation rates. Plots for all five injections are overlaid (blue, orange, yellow, purple and green respectively). 'x' points are for during the injection ($t \leq \tau_{inj}$), open circles are after the injection ($t > \tau_{inj}$) lines are the line of best fit of all data after the injection.

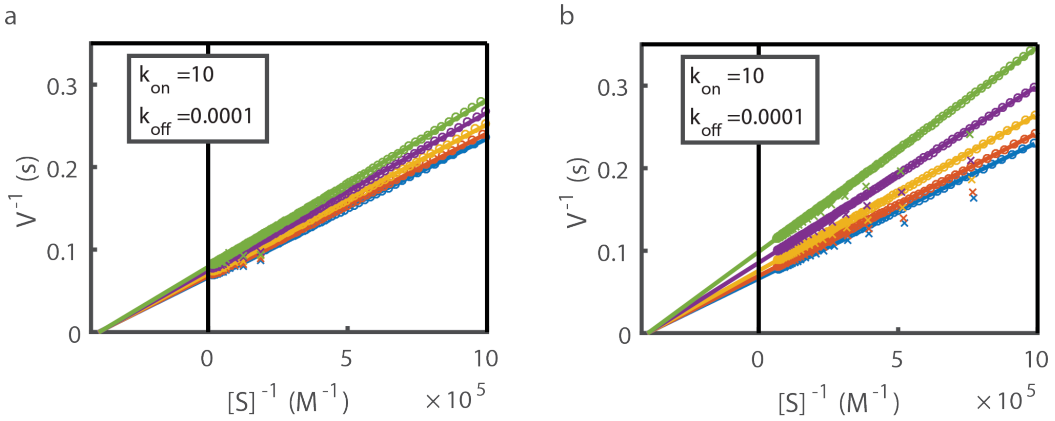

Figure 3.S9. Competitive inhibition with slow dissociation rates performed with different substrate concentrations. Lineweaver-Burk plots produced from simulated multiple injection experiments of substrate (800 μM and 3200 μM for (a) and (b) respectively) and inhibitor (336 μM) in the syringe and enzyme (10 nM) in the cell for a competitive inhibitor. Plots for all five injections are overlaid (blue, orange, yellow, purple and green respectively). 'x' points are for during the injection ($t \leq \tau_{inj}$), open circles are after the injection ($t > \tau_{inj}$) solid lines are from regression analysis for each peak after the injection ($t > \tau_{inj}$).

Simulations for progressive inhibition kinetics with slow binding kinetics. All simulations were performed in MATLAB. Differential equations shown below (Equations 3.22-3.27) describing Michaelis-Menten kinetics with competitive inhibition with inhibitor kinetics were integrated using the MATLAB ODE solver (ode23) due to the high precision required. The output $[P]_t$ was obtained in dt increments of 0.1 and was numerically differentiated in order to obtain $\frac{d[P]}{dt}$.

$$[ES]_t = \frac{([E_0]_t - [EI]_t) \cdot [S]_t}{K_m + [S]_t} \tag{3.22}$$

$$\frac{d[P]_t}{dt} = k_{cat} \cdot [ES]_t \tag{3.23}$$

$$\frac{d[EI]_t}{dt} = k_{on} \cdot ([E_0]_t - [ES]_t - [EI]_t) \cdot [I]_t - k_{off} \cdot [EI]_t - [EI]_t \cdot Rate_{inj} \tag{3.24}$$

$$\frac{d[I]_t}{dt} = -k_{on}\cdot([E_0]_t - [ES]_t - [EI]_t)\cdot[I]_t + k_{off}\cdot[EI]_t + [I]_{syringe}\cdot Rate_{inj} - [I]_t\cdot Rate_{inj} \tag{3.25}$$

$$\frac{d[S]_t}{dt} = -\frac{d[P]_t}{dt} + [S]_{syringe}\cdot Rate_{inj} - [S]_t\cdot Rate_{inj} \tag{3.26}$$

$$\frac{d[E]_t}{dt} = -[E_0]_t\cdot Rate_{inj} \tag{3.27}$$

Here $[EI]_t$ and $[ES]_t$ are the concentrations of enzyme-inhibitor complex and enzyme-substrate complex respectively, $[I]_{syringe}$ and $[I]_t$ are the concentrations of inhibitor in the syringe and cell respectively, k_{on} and k_{off} are the association rate and dissociation rate of the inhibitor, all other variables are the same as the experimental section in main text. The instantaneous heat $h(t)$ is calculated using the enthalpy of catalysis ΔH_{cat} and the total volume of the cell (Equation 3.7). For the simulations V_{cell} = 1.4 mM, v_{inj} = 30 μM, τ_{inj} = 25 s, ΔH_{cat} = −5 kCal mol^{-1}were used. k_{on} and k_{off} were systematically altered to produce peaks with different kinetics (Figure 3.S8). The instantaneous heat curve was numerically convoluted with the instrument response function according to Equation 3.8 in the main text in order to produce the calculated instrument output. For the first injection initial conditions were $[E]_t$ = 10 nM, $[S]_{t=0} = [I]_{t=0} = [EI]_{t=0} = [ES]_{t=0} = [P]_{t=0} = 0$. For subsequent injections the initial values of all the species were calculated as the final values from the proceeding injection. The signal was then resampled in 1 second intervals to match the output of the calorimeter and random Gaussian noise was added according to

$$g_{sim}(t) = g(t) + P_G(t) \tag{3.28}$$

Where $P_G(t)$ is random number from a gaussian probability density function (μ= 0, σ= 0.0017 μCal s^{-1}). The simulated curves were deconvoluted using the ERM-deconvolution. Adjustable parameters n, A_w and τ_{decay} were set to 12, 0.19 Hz and 0.0197 Hz respectively. The deconvoluted data was used to produce LWB plots using Equations 3.18-3.20 (Figure 3.S8 and 3.S9).

3.7.6 Product Inhibition in the Presence of Substrate and Inhibitor

As mentioned in the main text, mixed inhibition is a combination of both competitive and uncompetitive inhibition. The general rate of product formation for mixed inhibition in the presence of competitive product inhibition can be written as

$$\frac{d[P]}{dt} = \frac{k_{cat} \cdot [E_0] \cdot [S]}{[S] \cdot (1 + \frac{[I]}{K_{iu}}) + K_m \cdot (1 + \frac{[I]}{K_{ic}} + \frac{[I]}{K_{ip}})} \tag{3.29}$$

Where $[S]$, $[P]$ and $[E]$ are the concentration of substrate product and total enzyme respectively, $[I]$ is the concentration of inhibitor. K_{ic}, K_{ip} and K_{iu} are the inhibition constants for a competitive, product and uncompetitive inhibition respectively. Equation 3.29 represents the case of mixed inhibition but limiting cases of this equation can be used to model competitive inhibition (where $\frac{1}{K_{iu}} = 0$), uncompetitive inhibition (where $\frac{1}{K_{ic}} = 0$), as well as only product inhibition (where $\frac{1}{K_{iu}} = \frac{1}{K_{ic}} = 0$).

Extracting the product inhibition constant. First, multiple injections of only substrate into enzyme were simulated with competitive product inhibition and added instrument noise. These data were fit using the competitive product inhibition model in order to extract the k_{cat}, K_m and K_{ip}. We found in every case that the fit converged on the correct solution indicating that the k_{cat}, K_m and K_{ip} can be extracted from a multiple injection experiment of only substrate into enzyme.

Injecting substrate and inhibitor in the presence of product inhibition. In order to analyze data where inhibitor+substrate are injected into enzyme in the presence of product inhibition it is necessary to directly fit data using a model which includes both product inhibition and inhibition due to the injected inhibitor. We have simulated multiple injection experiments with competitive, uncompetitive and mixed inhibition and fit them with each model using the fitting procedure presented below. We find that the goodness of fit for each model (RSS) can be used to assess the

mode of inhibition, and the strength can be extracted from the fit (Figure 3.S10). In some cases it is possible to extract all of the parameters (k_{cat}, K_m and K_{ip} and K_i('s)) by only fitting the experiment with substrate+inhibitor. In all cases, the mode and strength of inhibition can be accurately extracted by first analyzing data for an experiment with only substrate in the syringe (yielding k_{cat}, K_m and K_{ip}) and then subsequently analyzing data for the experiment with inhibitor+substrate in the syringe to obtain the K_i value(s). Alternatively data for both types of experiments can be globally fit to extract all 4-5 parameters simultaneously.

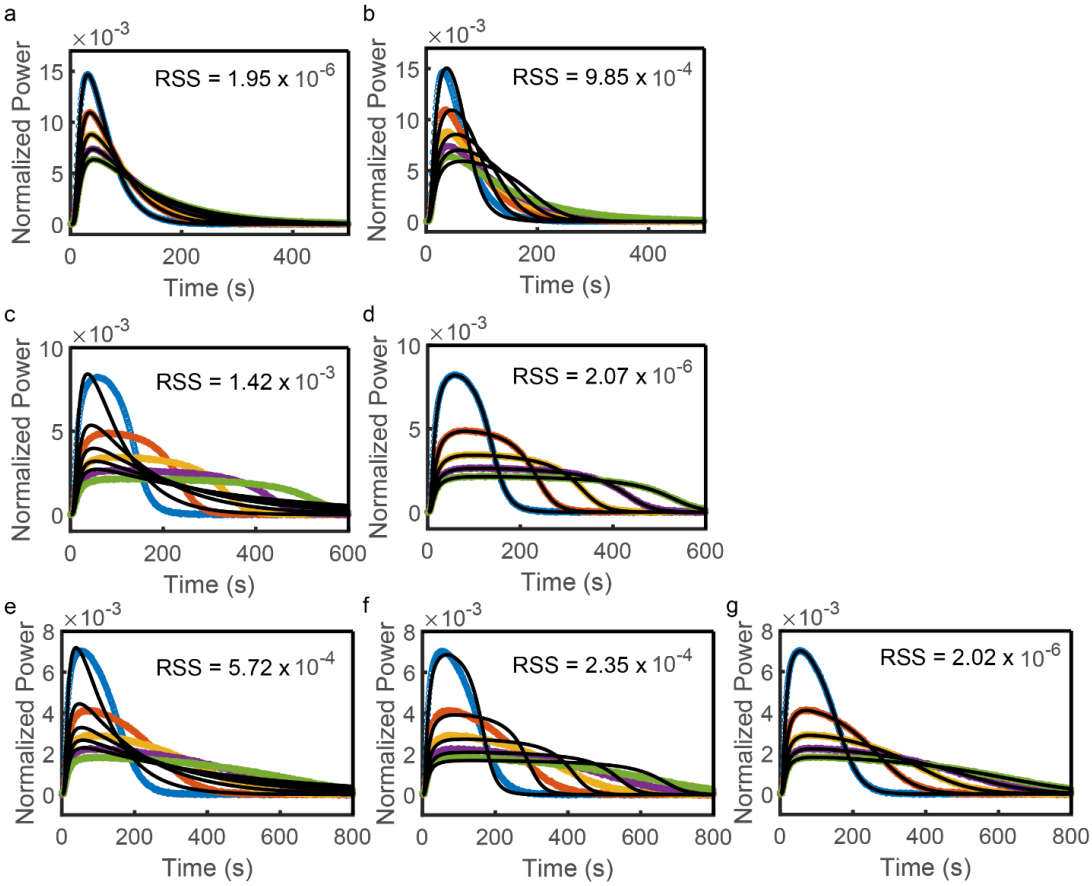

Figure 3.S10. Fits for various inhibition modes in the presence of product inhibition. Blue, orange, yellow and red curves are the first, second, third and fourth injection of the simulated isotherms for multiple injections of substrate and inhibitor (800 μM and 600 μM in syringe respectively) into enzyme (30 nM in cell) for (row 1:a,b) competitive inhibition, (row 2:c,d) uncompetitive inhibition and (row 3:e,f,g) mixed inhibition. k_{cat}, K_m, and K_{ip} were set at 20 s^{-1}, 5 μM, and 30 μM respectively. K_i('s) were set at 5 μM for competitive inhibition, 2 μM for uncompetitive inhibition and both of these values for mixed inhibition. Simulations were fit with competitive inhibition (column 1:a,c,e), uncompetitive inhibition (column 2:b,d,f), or mixed inhibition (column 3:g). Residual sum of squares from fits can be found in the top right corner of each panel. Competitive inhibitor and uncompetitive inhibition were not fit with mixed inhibition model as they are just limiting cases of mixed inhibition (see above).

Simulations for product inhibition in the presence of substrate and inhibitor.

All simulations were performed in MATLAB. Differential equations shown below

(Equations 3.30-3.37) describing Michaelis-Menten kinetics with product inhibition and in the presence of inhibitor were integrated numerically using Euler's method in 0.01 s integration steps (dt in Equations 3.30-3.37) according to:

$$\frac{d[P]_t}{dt} = \frac{k_{cat} \cdot [E_0]_t \cdot [S]_t}{[S]_t \cdot (1 + \frac{[I]_t}{K_{iu}}) + K_m \cdot (1 + \frac{[I]_t}{K_{ic}} + \frac{[I]_t}{K_{ip}})} \tag{3.30}$$

$$[P]_{t+dt} = [P]_t + \frac{d[P]_t}{dt} \cdot dt \tag{3.31}$$

$$\frac{d[S]_t}{dt} = -\frac{d[P]_t}{dt} + [S]_{syringe} \cdot Rate_{inj} - [S]_t \cdot Rate_{inj} \tag{3.32}$$

$$[S]_{t+dt} = [S]_t + \frac{d[S]_t}{dt} \cdot dt \tag{3.33}$$

$$\frac{d[I]_t}{dt} = [I]_{syringe} \cdot Rate_{inj} - [I]_t \cdot Rate_{inj} \tag{3.34}$$

$$[I]_{t+dt} = [I]_t + \frac{d[I]_t}{dt} \cdot dt \tag{3.35}$$

$$\frac{d[E]_t}{dt} = -[E]_t \cdot Rate_{inj} \tag{3.36}$$

$$[E]_{t+dt} = [E]_t + \frac{d[E]_t}{dt} \cdot dt \tag{3.37}$$

Here $[I]_{syringe}$ is the concentration of inhibitor in the syringe all other variables are as above (see 3.6.5). Different limiting cases of Equation 3.30 were used depending on the type of inhibition being modelled. For the first injection initial conditions were $[E]_t = 30nM$, $[S]_t = [I]_{t=0} = [EI]_{t=0} = [ES]_{t=0} = [P]_t = 0$. For subsequent injections the initial values of all the species were calculated as the final values from the proceeding injection. The instantaneous heat $h(t)$ is calculated using the enthalpy of the reaction $\Delta H_{cat}$and the total volume of the cell (Equation 3.38).

$$h(t) = \Delta H_{cat} \cdot V_{cell} \cdot \frac{d[P]_t}{dt} \tag{3.38}$$

For the simulations V_{cell} = 1.4 mM, v_{inj} = 20 μM, τ_{inj} = 5 s, ΔH_{cat} = -5 kCal mol^{-1} were used. The instantaneous heat curve is numerically convoluted with the

instrument response function according to equation 3.39:

$$g(t) = h(t) \otimes f(t) \tag{3.39}$$

Where $f(t)$ is the empirical response function and $g(t)$ is the resulting calculated signal. The signal was then resampled in 1 s intervals to match the output of the calorimeter and random Gaussian noise was added according to

$$g_{sim}(t) = g(t) + P_G(t) \tag{3.40}$$

Where $P_G(t)$ is random number from a gaussian probability density function (μ= 0, σ= 0.0017 μCal s^{-1}).

Analyzing product inhibition in the presence of substrate and inhibitor. In order to fit to simulated product inhibition data, differential Equations 3.30-3.37 above were numerically integrated in 0.01 second time intervals (dt in Equations 3.30-3.37). The instantaneous heat curve was then calculated and numerically convoluted using Equation 3.38-3.40. The reminder of the fitting procedure was carried out as described in the main text (Equations 3.10-3.11). When fitting to the experiments with only substrate in the syringe the K_m, k_{cat} and K_{ip} were floated while minimizing the residual sum of squares (RSS). Once these three parameters were extracted they were used as constants while fitting experiments with both substrate and inhibitor in the syringe where the inhibition constant(s) were floated (K_{iu} and/or K_{ic}) depending on which model was being used (Figure 3.S10).

3.8 References

[1] Jean-Paul Renaud et al. “Biophysics in drug discovery: impact, challenges and opportunities”. In: *Nature Reviews Drug Discovery* 15 (2016), pp. 679–698.

[2] Robert A. Copeland. “Reversible Inhibitors”. In: *Enzymes*. John Wiley & Sons, Inc., 2002, pp. 266–304.

[3] Robert A. Copeland, David L. Pompliano, and Thomas D. Meek. “Drug-target residence time and its implications for lead optimization”. In: *Nature Review Drug Discovery* 5.9 (2006), pp. 730–739.

[4] Evangelia Morou et al. “A Simple Colorimetric Assay for Specific Detection of Glutathione-S Transferase Activity Associated with DDT Resistance in Mosquitoes”. In: *PLoS Neglected Tropical Diseases* 4.8 (2010), e808.

[5] Julius A. Goldbarg et al. “The colorimetric determination of -glutamyl transpeptidase with a synthetic substrate”. In: *Archives of Biochemistry and Biophysics* 91.1 (1960), pp. 61–70.

[6] G. Bruce Birrell et al. “Allosteric Interactions within Subsites of a Monomeric Enzyme: Kinetics of Fluorogenic Substrates of PI-Specific Phospholipase C”. In: *Biophysical Journal* 84.5 (2003), pp. 3264–3275.

[7] J. G. Nørby. “Coupled assay of Na+,K+-ATPase activity”. In: *Methods in enzymology* 156 (1988), pp. 116–9.

[8] W. R. McClure. “Kinetic analysis of coupled enzyme assays”. In: *Biochemistry* 8.7 (1969), pp. 2782–2786.

[9] Robert A. Copeland. “Kinetics of Single-Substrate Enzyme Reactions”. In: *Enzymes*. John Wiley & Sons, Inc., 2002, pp. 109–145.

[10] Donmienne Leung et al. “Discovering potent and selective reversible inhibitors of enzymes in complex proteomes”. In: *Nature Biotechnology* 21 (2003), pp. 687–691.

[11] Prabhavathi B. Fernandes. “Technological advances in high-throughput screening”. In: *Current Opinion in Chemical Biology* 2.5 (1998), pp. 597–603.

[12] Søren N. Olsen. “Applications of isothermal titration calorimetry to measure enzyme kinetics and activity in complex solutions”. In: *Thermochimica Acta* 448.1 (2006), pp. 12–18.

[13] Leigh Murphy et al. “An enzymatic signal amplification system for calorimetric studies of cellobiohydrolases”. In: *Analytical Biochemistry* 404.2 (2010), pp. 140–148.

[14] Hassan Rana et al. “Isothermal titration calorimetry uncovers substrate promiscuity of bicupin oxalate oxidase from Ceriporiopsis subvermispora”. In: *Biochemistry and Biophysics Reports* 5 (2016), pp. 396–400.

[15] Matthew J. Todd and Javier Gomez. “Enzyme Kinetics Determined Using Calorimetry: A General Assay for Enzyme Activity?” In: *Analytical Biochemistry* 296.2 (2001), pp. 179–187.

[16] Ewa Poduch et al. “Design of Inhibitors of Orotidine Monophosphate Decarboxylase Using Bioisosteric Replacement and Determination of Inhibition Kinetics”. In: *Journal of Medicinal Chemistry* 49.16 (2006), pp. 4937–4945.

[17] Heiko Poppe et al. “Cyclic nucleotide analogs as probes of signaling pathways”. In: *Nature Methods* 5.4 (2008), pp. 277–278.

[18] Mark K. Transtrum, Lee D. Hansen, and Colette Quinn. “Enzyme kinetics determined by single-injection isothermal titration calorimetry”. In: *Methods* 76 (2015), pp. 194–200.

[19] Tadashi Ingami. “The Mechanism of the Specificity of Trypsin Catalysis”. In: *Journal of Biological Chemistry* 239.2 (1963), pp. 1388–1394.

[20] Marcos Mares-Guia and Elliott Shaw. “Studies on the Active Center of Trypsin: THE BINDING OF AMIDINES AND GUANIDINES AS MODELS OF THE SUBSTRATE SIDE CHAIN”. In: *Journal of Biological Chemistry* 240.4 (1965), pp. 1579–1585.

[21] P. Bäckman et al. “Heat conduction calorimeters: time constants, sensitivity and fast titration experiments”. In: *Journal of Biochemical and Biophysical Methods* 28.2 (1994), pp. 85–100.

[22] Masanori Sono and Susan G. Cady. “Enzyme kinetic and spectroscopic studies of inhibitor and effector interactions with indoleamine 2,3-dioxygenase. 1. Norharman and 4-phenylimidazole binding to the enzyme as inhibitors and heme ligands”. In: *Biochemistry* 28.13 (1989), pp. 5392–5399.

[23] Christopher E. Heise et al. “Mechanistic and Structural Understanding of Uncompetitive Inhibitors of Caspase-6”. In: *PLoS ONE* 7.12 (2012), e50864.

[24] Apurba Kumar Sau, Madhu Sudan Mondal, and Samaresh Mitra. “Mixed inhibition of the oxidoreductase activity of xanthine oxidase by Pd2+ ion”. In: *Journal of the Chemical Society, Chemical Communications* 13 (1994), pp. 1547–1548.

[25] “Steady-State Kinetics of Bisubstrate Reactions”. In: *Comprehensive Enzyme Kinetics*. Ed. by Vladimir Leskovac. Boston, MA: Springer US, 2003, pp. 139–170.

[26] Elliott Shaw, Marcos Mares-Guia, and William Cohen. “Evidence for an Active-Center Histidine in Trypsin through Use of a Specific Reagent, 1-Chloro-3-tosylamido-7-amino-2-heptanone, the Chloromethyl Ketone Derived from N-Tosyl-L-lysine*”. In: *Biochemistry* 4.10 (1965), pp. 2219–2224.

[27] Bent W. Sigurskjold. “Exact Analysis of Competition Ligand Binding by Displacement Isothermal Titration Calorimetry”. In: *Analytical Biochemistry* 277.2 (2000), pp. 260–266.

Chapter 4

Rapid Measurement of Inhibitor Binding Kinetics by Isothermal Titration Calorimetry

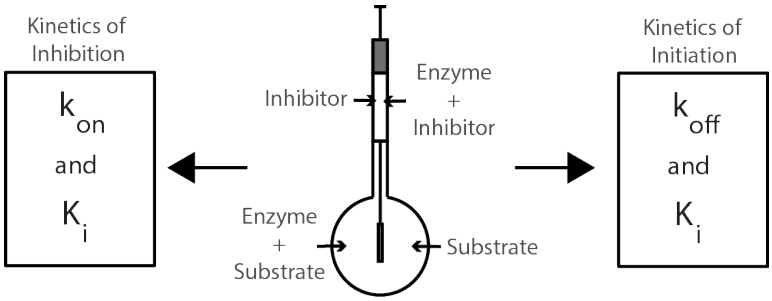

Preface

In addition to the strength and mode of inhibition, the kinetic properties of an inhibitor have been shown to correlate with their efficacy. This makes measurement of an inhibitors association and dissociation rates important for the drug design and development process. In chapter 2 we present a robust ITC based method for characterizing the strength and mode of enzyme inhibitors, however, this method is not ideal for extracting inhibitor kinetics. In this chapter, we present a pair of rapid, accurate techniques for measuring the association and dissociation rates of enzyme inhibitors using ITC. We test these methods using covalent and non-covalent inhibitors of a known therapeutic target, allowing us to make novel discoveries about the nature of covalent inhibition. The pair of methods are ideal for developing structure kinetics relationships during the hit-to-lead, and lead optimization phases of drug development.

4.1 Abstract

Although drug development typically focuses on binding thermodynamics, recent studies suggest that kinetic properties can strongly impact a drug candidate's efficacy. Robust techniques for measuring inhibitor association and dissociation rates are therefore essential. To address this need, we have developed a pair of complementary isothermal titration calorimetry (ITC) techniques for measuring the kinetics of enzyme inhibition. The advantages of ITC over standard techniques include speed, generality, and versatility; ITC also measures the rate of catalysis directly, making it ideal for quantifying rapid, inhibitor-dependent changes in enzyme activity. We used our methods to study reversible covalent and non-covalent inhibitors of prolyl oligopeptidase (POP). We extracted kinetics spanning three orders of magnitude, including those too rapid for standard methods, and measured sub-nM binding affinities, below the typical ITC limit. These results shed light on the inhibition of POP and demonstrate the general utility of ITC-based enzyme inhibition kinetic

measurements.

4.2 Introduction

There is mounting evidence that the efficacy of a therapeutic is closely related to the kinetics of interactions with its target,[1] particularly its residence time. Systemic drug concentrations fluctuate according to administration and excretion/metabolism and substrates of inhibited enzymes tend to accumulate. Long residence times allow targets to remain inhibited even when systemic drug concentrations drop[2,3,4,5,6] or substrate concentrations rise to a level that would otherwise overwhelm the effect of the drug.[7] On the other hand, molecules with slow association kinetics are disfavored in typical drug screens with short pre-incubation steps,[8] and potentially efficacious molecules may be missed altogether unless care is taken. This has prompted an interest in structure kinetics relationships to better understand the relationship between the structures of small molecule drug candidates and their kinetic properties.[9,10,11]

Enzyme kinetic studies typically employ spectroscopic[12,13] chromatographic,[3,13] or electrophoretic[13] techniques to monitor the concentrations of products or substrates as a function of time, thereby yielding rates of catalysis. To measure the strength of inhibition, K_i or IC_{50}, the enzyme (E) is allowed to equilibrate thoroughly with an inhibitor (I), such that concentration of the inhibited complex (EI) can be considered time-invariant. To characterize the inhibitor association (k_{on}) and dissociation (k_{off}) rate constants, the pre-equilibration time with the inhibitor is varied,[14] or substrate and product concentrations are measured while the concentration in EI gradually changes due to inhibitor binding and release.[15] Using traditional enzyme assays to probe inhibition kinetics has several drawbacks. For instance, experiments must be repeated multiple times with different pre-equilibration delays and/or inhibitor concentrations. Also, it can be difficult to detect small changes in catalytic rate by simply measuring substrate and concentrations over time. New biophysical methods to quickly and efficiently assess the binding kinetics of drug candidates are needed to improve screening and optimization efforts and to better

understand the fundamental mechanisms underlying enzyme inhibition.

Enzyme kinetics can also be characterized by isothermal titration calorimetry (ITC), which measures the heat generated by catalysis following the rapid mixing of enzyme and substrate.[16] An ITC experiment consists of making a series of automated injections from a syringe into a sample cell and monitoring the subsequent heat flow. There are many advantages to ITC-based enzyme measurements: they can be performed under dilute, physiological solution conditions, even those that are spectroscopically opaque.[17] The approach is completely general, since most chemical reactions produce or consume heat; ITC can be applied equally well to virtually any enzyme,[16] and does not require the development of a customized assay based on fluorogenic or colorigenic substrates, or the post-reaction separation of products and substrates by chromatography or electrophoresis.[16,18] Unlike standard spectroscopic measurements where enzyme, substrate, and inhibitor solutions are combined with delays of tens of seconds or more prior to the start of the measurement, ITC measures heat flow while the reagents are mixed rapidly with little dead time giving it time sensitivity close to stopped flow with all the inherent advantages of ITC. Furthermore, in contrast to other techniques that infer rates of catalysis indirectly from the concentrations of substrates and products, ITC detects heat flow in real time, giving a direct read-out of enzyme activity and how it varies in response to inhibitors. Despite the great potential of ITC to characterize the kinetics of enzyme inhibition, to our knowledge no study has employed it in this manner to date.

Here we present a pair of rapid, complementary ITC methods that simultaneously measure inhibitor association and dissociation rates and the inhibitory constant K_i, for enzyme inhibitors in an hour or less. We used these methods to characterize several covalent and non-covalent inhibitors (Figure 4.1) of prolyl oligopeptidase (POP), a post-proline cleaving enzyme implicated in cancer and neurodegenerative disorders.[19,20] Compounds 2 and 4 bind non-covalently to POP, while 1, 3, and 5 form reversible covalent bonds with the catalytic serine in the POP active site via aldehyde (1 and 5) or nitrile (3) moieties. Covalent inhibitors are promising as long-acting drugs, while fine-tuning the reactivity of the warhead offers an opportunity

for optimizing kinetics. Relatively little is currently known about SKR for covalent inhibitors since they have historically been disfavored in drug development due to concerns regarding specificity and off-target effects. Nevertheless, many over-the-counter and blockbuster drugs are covalent,[21,22] and the advantages of this class of compounds, including high specificity, potency, and favorable kinetics of inhibition, are increasingly being recognized.[21,23] The typically slow kinetics of covalent drugs makes them ideal candidates for developing new biophysical methods and elucidating new structure-activity relationships for the kinetics of inhibition. Application of the ITC kinetics methods presented here to POP inhibitors has provided proof-of-principle for this approach and has yielded insights into fundamental mechanisms underlying covalent and non-covalent enzyme inhibition.

4.3 Results

4.3.1 Covalent Inhibition

One complication of covalent inhibitors is that their binding mechanisms are usually considered to have at least two distinct steps.[12,13,24,25] The enzyme and inhibitor first interact non-covalently (EI) and subsequently form a covalent bond (E-I, equation 4.1).

$$\mathrm{E} + \mathrm{I} \rightleftharpoons \mathrm{EI} \rightleftharpoons \mathrm{E{-}I} \tag{4.1}$$

Depending on the rates of covalent bond formation and the association and dissociation of EI, the kinetics of inhibition can be either biphasic, characterized by rapid formation of EI followed by gradual conversion to E-I[12,24] or monophasic, such that they are indistinguishable from the kinetics of simple, one-step non-covalent inhibitors, as further discussed in the Supplementary methods.[12,13] Importantly, the time-resolution of our ITC experiments allows us to discriminate between these two possibilities (monophasic versus biphasic inhibition).

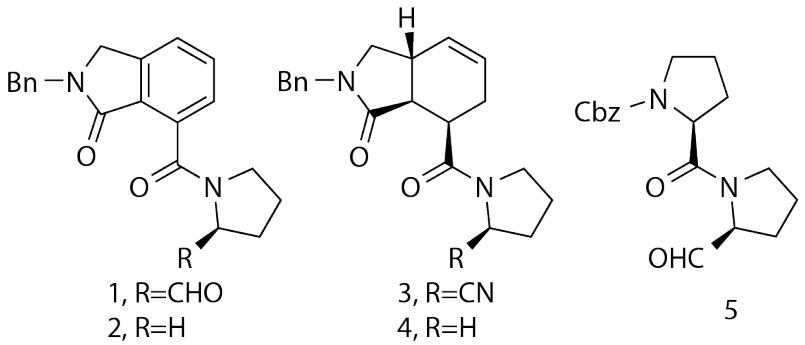

Figure 4.1. POP inhibitors employed in this study. Bn and Cbz indicate benzoyl and carboxybenzyl groups, respectively.

4.3.2 Kinetic ITC Techniques

ITC kinetic data for the POP enzyme associating with compound 1 and 4 (Figure 4.2a,b,c,d) and dissociating from compound 1 and 4 (Figure 4.2e,f,g,h) are shown in Figure 4.2. In what follows, we will refer to these two types of experiments as kinetics of inhibition and kinetics of initiation. In both experiments, the heat flow or power (y-axis) is plotted as a function of time (x-axis). Exothermic and endothermic reactions deflect the ITC signal downwards and upwards, respectively. The power is linearly related to the enzyme velocity, with larger deflections corresponding to higher velocities. In the kinetics of inhibition experiments, the ITC cell contained POP and the substrate thyrotropin releasing hormone (TRH). POP cleaves TRH producing the free acid form of TRH and ammonia as well as heat, which is detected by the ITC instrument. The rate of catalysis was initially constant, giving a horizontal line. Compounds 1 and 4 were added to the cell in a series of four (Figure 4.2a) and seven (Fig. 4.2c) injections (note that the first injections are omitted from plots in most cases). In each case, the enzyme was increasingly inhibited and the power values shifted upward, since the rate of (exothermic) catalysis and downward deflection was reduced after each injection. As highlighted in Figure 4.2b,d, this shift occurred gradually over tens to hundreds of seconds, which corresponds to the time required for compounds 1 and 4 to bind in the active site. Furthermore, each subsequent injection led to a smaller upward shift of the ITC signal, as the enzyme

became increasingly saturated with inhibitor. The decrease in the sizes of the steps is related to the inhibition constant, K_i. Data for a series of injections were fitted simultaneously to yield k_{on} and K_i (see 4.5.6). The fitted curves are in excellent agreement with the experimental ITC signal (Figure 4.2b,d). The dissociation rate was then calculated as $k_{off} = k_{on} \cdot K_i$. In the kinetics of initiation experiments, the cell contained the substrate TRH and the syringe contained a solution of POP saturated with the compounds 1 (Figure 4.2e,f) or 4 (Figure 4.2g,h), which was added to the cell in five or six injections. Immediately following each injection there was no change in the rate of catalysis in the sample cell as the added enzyme was fully inhibited. However, the large dilution (>20-fold) experienced by the injectant led to a net dissociation of the inhibitor and a gradual downward shift of the ITC signal as the freshly released enzyme began to act on the substrate (Figure 4.2e,g). Each subsequent injection led to a smaller downward shift of the ITC signal, as the inhibitor accumulated in the sample cell and the net dissociation of each injection diminished. The decrease in the sizes of the steps is governed by the value of K_i. Data for the series of injections were fitted simultaneously to yield k_{off} and K_i (see 4.5.6), giving excellent agreement (Figure 4.2f,h). The association was then calculated as $k_{on} = k_{off}/K_i$. Note that concentrations of enzyme are so low in these experiments (10 nM) that ITC detects only heats of catalysis, while heats of inhibitor/enzyme binding can be safely ignored (see 4.6.2).

4.3.3 Kinetic Characterization of Prolyl Oligopeptidase Inhibitors by ITC

In order to test the applicability of these ITC kinetic methods, they were applied to characterize the panel of POP inhibitors illustrated in Figure 4.1. The extracted thermodynamic and kinetic values are listed in Table 4.1, while the raw fits are shown in Figures 4.S5-4.S14. Most experiments were performed in under an hour, and replicate experiments were highly reproducible. For compounds 1 and 4, both the initiation and inhibition kinetics methods yielded the full set of k_{on}, k_{off}, and K_i, parameters, as described above. Notably the values obtained from the two

methods are in excellent agreement, differing by at most about a factor of two. Global fits of combined initiation and inhibition datasets are in good agreement with experiment signals and yield similar kinetic and thermodynamic parameters to the individual fits (See 4.6.3). For compound 2, the affinity of the interaction was quite weak and the residence time quite short. Consequently, both association and dissociation processes went nearly to completion during each injection and kinetic

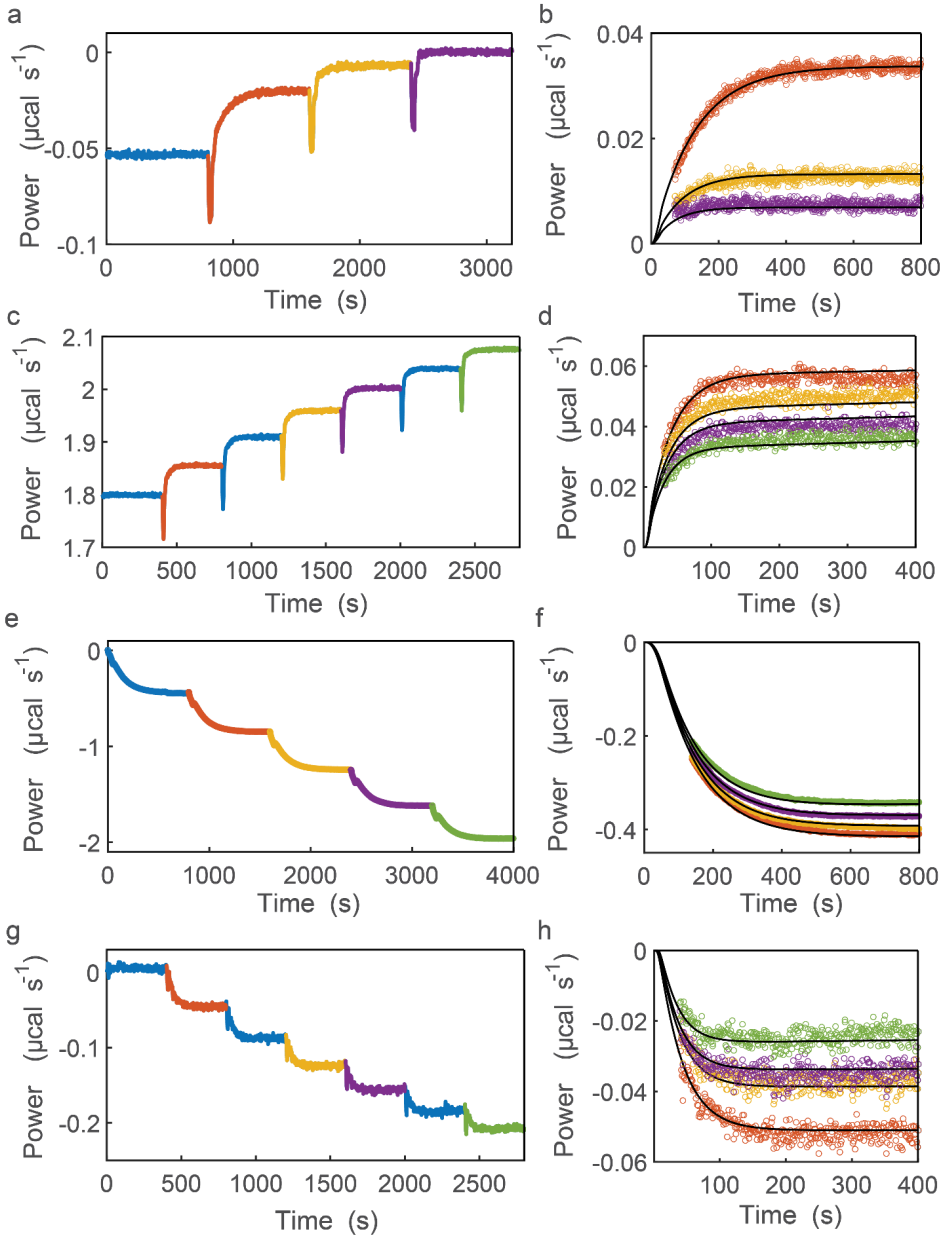

Figure 4.2. Caption on next page

Figure 4.2. Kinetics of inhibition and initiation experiments. a) Kinetics of inhibition experiment with compound 1 using a Malvern ITC-200 calorimeter. Compound 1 is titrated into cell containing POP and TRH. b) Overlay of injections 2, 3 and 4 (orange, yellow and purple circles) with fit (black line). c) Kinetics of inhibition experiment with compound 4 using a Malvern ITC-200 calorimeter. Compound 4 is titrated into cell containing POP and TRH. d) Overlay of injections 2, 4, 5, 7 (orange, yellow, purple and green circles) with fit (black line). e) Kinetics of initiation experiment of compound 1 with a Malvern VP-ITC calorimeter. Compound 1 and POP are titrated in the cell containing TRH. f) Overlay of injections 2, 3, 4 and 5 (orange, yellow, purple and green circles) with fit (black lines). g) Kinetics of initiation experiment with compound 4 using a Malvern ITC-200 calorimeter. Compound 4 and POP are titrated into cell containing TRH. h) Overlay of injections 2, 4, 5, 7 (orange, yellow, purple and green circles) from C with fit (black lines). See 4.6.3 for additional experimental details.

parameters could not be extracted with great confidence. Nevertheless, both ITC methods yielded K_i values which agreed well with each other. For compounds 3 and 5, dissociation occurred very slowly compared to the rate of ITC baseline drift and k_{off} could not be accurately measured using the initiation experiment (see 4.7). In both cases, however, the inhibition experiment provided well-defined k_{on} values, illustrating the complementary nature of the two ITC approaches. In the case of 3, this experiment also gave K_i. For 5, the k_{on} rate was very low (30-fold less than 3), meaning that in order to achieve measurable kinetics a high concentration of inhibitor was used. This saturated the enzyme in a single step and only upper bounds for the K_i and k_{off} could be determined (see 4.7). It should be mentioned that for some covalent inhibitors of other enzymes, association kinetics are markedly biphasic, due to accumulation of non-covalent binding intermediates.[12,24] In our case, all association and dissociation traces are clearly monophasic, implying that non-covalent binding intermediates are not highly populated and that association and dissociation are well-described by the k_{on} and k_{off} rate constants (see 1.1.2.4).

4.3.4 Validation of ITC-based Techniques

The fact that the inhibition and initiation ITC kinetics experiments gave matching values of k_{on}, k_{off}, and K_i gives us confidence in these methods, as the two types of measurements were performed completely independently. In order to further test their reliability, we selected representative inhibition and initiation experiments for validation using standard spectroscopic techniques. For compound 5, we used NMR to measure the loss of enzyme activity after addition of the inhibitor. We mixed enzyme, substrate, and inhibitor, placed the sample in the spectrometer, and monitored a peak present in the ^{1}H NMR spectrum of the TRH substrate but not in that of the free acid product, using the signal intensity to calculate the concentration of TRH as a function of time. The curvature of the resulting plot in Figure 4.3b is proportional to the association rate. Note that the final non-zero slope of the curve in Figure 4.3b is due to remaining uninhibited POP. Increasing the amount of 5 added would make this portion of the curve more horizontal, but would also increase the rate of inhibition (early curvature) beyond values accessible by this method, highlighting some of the challenges of measuring inhibition kinetics by non-ITC methods. The extracted value of k_{on} Table 4.1 is within error of that determined using the ITC inhibition experiment (Figure 4.3a). For compound 1, we used absorbance spectroscopy and a commercially-available colorigenic substrate Cbz-Gly-Pro-pNA (ZGP-pNA) to measure the rate at which the inhibited enzyme regained activity following dilution. POP was pre-equilibrated with a saturating concentration of inhibitor, diluted into a solution of ZGP-pNA, and the spectroscopic absorbance was used to calculate product concentration as a function of time (Figure 4.3d). The slight curvature of the resulting plot (see inset) is proportional to the inhibitor dissociation rate, k_{off}. The fitted value (Table 4.1) is consistent (within a factor two) of the results of the ITC initiation experiment (Figure 4.3c). It must be emphasized that while we have used spectroscopic methods to validate the ITC kinetics measurements, the range of applicability of the ITC kinetics experiments is far greater, due to the shorter delay between mixing and detection and the greater sensitivity to changes in catalytic rate.

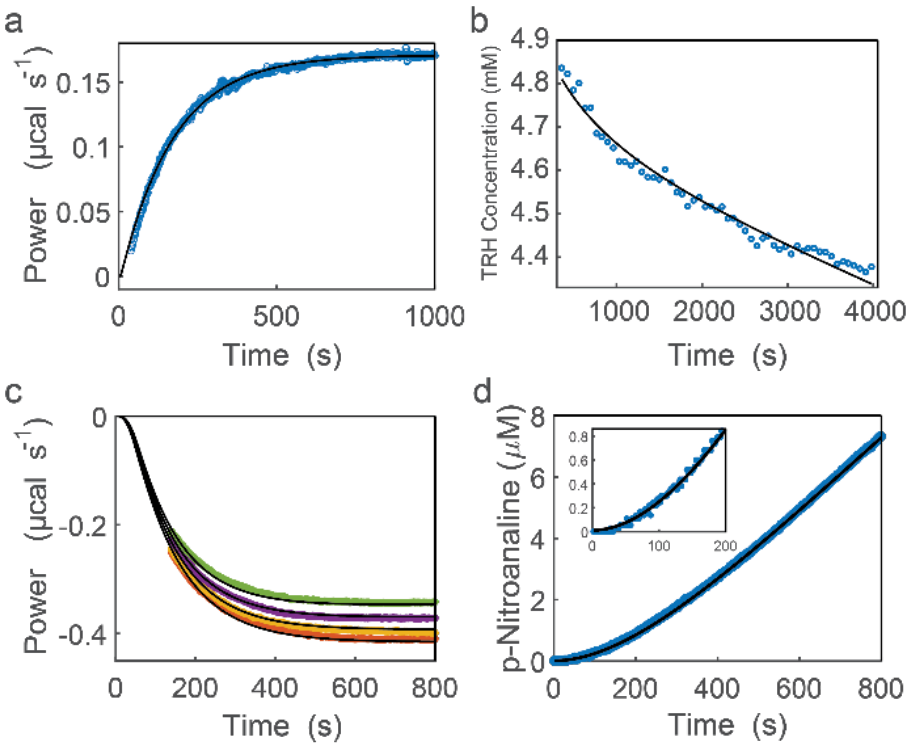

. See Table 4.1 for results of fits.

Figure 4.3. Validation using absorbance spectroscopy and ^{1}H NMR. a) Inhibition experiment with compound 5 using a Malvern ITC-200 calorimeter. Compound 5 is injected into the cell containing POP and TRH (blue circles). b) Inhibition with compound 5 using NMR. Compound 5 is added to POP and TRH. Intensity of peak for TRH was used to calculate a concentration (blue circles). Note that a and b display inhibition using the same compound with different techniques. c) Initiation experiment with compound 1 using a Malvern ITC-200 calorimeter. POP and compound 1 are injected into the cell containing TRH (second injection; orange circles, third injection; yellow circles, fourth injection; purple circles, and fifth injection; green circles). d) Initiation experiment with compound 1 using UV-Vis spectroscopy. POP and compound 1 are injected into buffer containing ZGP-pNA. The intensity of the peak at 405 nm was converted to a concentration of pNA (blue circles). Note that a and b display inhibition using the same compound with different techniques. Fits to experimental data are overlaid (black lines) using models presented in 4.5.11

4.3.5 SKR for POP Inhibitors

There is currently not much information available on how the structures of covalent inhibitors relate to their binding kinetic behavior, thus the data in Table 4.1 shed new light on this important relationship. Of particular interest is the effect of adding a reactive warhead on the association and dissociation rate constants of a given scaffold. 1 differs from the non-covalent inhibitor 2 by virtue of an aldehyde moiety. This results in about a 10-fold increase in affinity, as expected, since the enzyme complex with 1 is stabilized by an additional covalent bond. The dissociation rate also shows a substantial decrease. For the non-covalent inhibitor 2, k_{off} is too rapid to measure, i.e. larger than about 0.1 s^{-1}, while for the covalent inhibitor 1, the dissociation rate is reduced to about 60 $\cdot 10^{-4} s^{-1}$, likely due to the added kinetic barrier of breaking a covalent bond. Similarly, 3 differs from 4 by a reactive nitrile group, and binds about 100-fold more tightly. This is largely due to the 25-fold decrease in the dissociation rate, similar to what was seen for 1 and 2. Interestingly, the association rate for 3 is about 3.5-fold higher than that of the non-covalent 4. This is unexpected, since the rate of non-covalent complex formation represents an upper bound for the kinetics of inhibition (Equation 1.24) The nitrile moiety may somehow speed the E+I $\rightarrow$ EI step although how this would occur is unclear. Alternatively, it is believed that the vast majority of molecular collisions between proteins and their ligands are unproductive, in the sense that the binding partners diffuse apart again before a tight complex can form.[26] The reaction of the nitrile group with the catalytic serine may effectively trap some collisions that would otherwise be unproductive, thereby enhancing the association rate. This possibility is provocative, as it would imply that the reaction pathway towards the covalently inhibited complex could circumvent the non-covalent intermediate, to some extent. Regardless of the underlying mechanism, these results suggest that covalent warheads can have multiple beneficial effects on the kinetics of binding, simultaneously increasing the rate of association and the residence time.

Table 4.1. Kinetic and thermodynamic parameters.

Cpd	Experiment	$k_{on} \cdot 10^5$ M^{-1} s^{-1}	$k_{off} \cdot 10^{-4}$ s^{-1}	K_i nM	ΔH_{cat}[a] kCal mol^{-1}
1	ITC inhib	1.12 ± 0.02	43.1[b] ± 0.9	38.4 ± 0.4	-6.69 ± 0.02
	ITC init	1.21[a] ± 0.01	82.1 ± 0.4	58.7 ± 0.5	-5.86 ± 0.01
	UV-VIS	1.43 ± 0.02	31.4 ± 0.3	947[a] ± 2	–
2	ITC inhib	–	–	597 ± 28	-6.79 ± 0.03
	ITC init	–	–	744 ± 16	-10.88 ± 0.06
3	ITC inhib	155.5 ± 0.4	9[a] ± 1.5	0.063 ± 0.01	-9.91 ± 0.03
4	ITC inhib	44 ± 1	249[a] ± 7	5.6 ± 0.1	-5.33 ± 0.03
	ITC init	20[a] ± 1	261 ± 9	13.1 ± 0.4	-7.19 ± 0.04
5	ITC inhib	4.18 ± 0.04	< 1.05	< 2.5	-7.97 ± 0.01
	NMR	5.4 ± 0.7	–	–	–
	Lit[27]	0.7	3	0.5	–

[a] ΔH_{cat} are floated in order account for uncertainties in enzyme concentration as the magnitude of the heat flow is directly proportional to $[E_0] \cdot \Delta H_{cat}$.

[b] calculated using $K_i = k_{off}/k_{on}$

4.4 Discussion

There is a rich literature on the use of ITC to study enzyme kinetics,[17,16] and to a lesser extent on the kinetics of ligand binding.[28,29] This study brings the power of ITC, as a near-universal enzyme assay, to bear on the important problem of inhibitor dynamics. It must be emphasized that, although we have focused on covalent inhibition here, these ITC techniques can be equally well applied to non-covalent inhibitors, for instance compounds 4 and 2. We estimate that inhibitor residence times from roughly 10 seconds to 30 minutes, association rates from 10^3 to 10^7 M^{-1} s^{-1}, and K_i values down to about 1 pM are accessible using this approach under typical conditions (see 4.7). This work also demonstrates some specific advantages of ITC compared to existing methods. For instance, since ITC measures enzyme catalytic rates directly, the signatures corresponding to inhibition and initiation are much more pronounced than those of methods that rely on measuring substrate or

product concentrations. This is well illustrated in Figure 4.3, where ITC data show large exponential changes in heat flow (a, c) while the corresponding spectroscopic experiments (b, d) show only slight curvature. This provides an opportunity for deep mechanistic analysis, as deviations from first-order kinetics could be clear in ITC data and largely obscured in product or substrate concentration measurements. The information-rich ITC data also allows full thermodynamic and kinetic characterization in a single hour-long experiment, simultaneously yielding k_{on}, k_{off}, and K_i. In contrast, spectroscopic techniques require multiple separate enzyme assays to be performed over a range of inhibitor concentrations to provide the same information. Furthermore, the ITC instrument rapidly mixes enzyme, substrate, and inhibitor solutions and records heat flow with little dead time. It is therefore ideal for characterizing inhibitors that associate or dissociate rapidly. The most rapidly-dissociating inhibitor in this study (compound 4) has a residence time of just 40 s. We have recently used ITC to extract enzyme kinetics from reactions that go to completion in just 20 seconds,[30] and anticipate that inhibition kinetics on those timescales would be accessible as well. This is well beyond the limits of conventional benchtop spectroscopy and begins to approach the times scales of stop flow instruments. Finally, these methods also represent a novel approach for applying ITC to extremely tightly-interacting inhibitors. In order to obtain reliable information, the concentration of enzyme in the ITC cell is ideally no more than 500-fold the equilibrium dissociation constant, which is generally taken as equal to the K_i.[31] Thus, very tight inhibitors require the use of very dilute enzyme solutions and produce extremely weak signals, if the heats of binding are measured directly, as is usually the case. This problem can be circumvented by using higher concentrations of enzyme and performing competitive binding assays with a known ligand that binds weakly to the same site.[32] Our experiments provide an alternative by detecting the heat generated by catalysis. Even very low (1.32 nM) enzyme concentrations produce large heat signals due to multiple substrate turnovers. This allowed the measurement of a K_i as low as 63 pM in this study (compound 3), which would not have been attainable by standard ITC titration methods, with an estimated lower limit of about

1 pM. These ITC kinetics experiments thus provide a robust and versatile approach for measuring inhibitor binding kinetics and thermodynamics, with the potential to more clearly reveal how inhibitors, both covalent and non-covalent, dock against their targets, how they dissociate, and how this relates to their chemical structures.

4.5 Methods

4.5.1 Prolyl Oligopeptidase Purification

Human prolyl oligopeptidase was purified as described above (see section 2.6.2).

4.5.2 Experimental Conditions

All experiments were carried out in 20 mM sodium phosphate, 150 mM sodium chloride, 10% glycerol, 0.5 mg mL^{-1} BSA, 0.1% (v/v) DMSO, pH 8 buffer. Ligands were dissolved into DMSO then diluted into buffer immediately prior to the experiment.

4.5.3 ITC Data Collection

ITC data collection. All experiments were performed at 30°C on high feedback mode with a stirring speed of 806 RPM (Malvern VP-ITC) or 750 RPM (Malvern ITC-200) and a filter time of 1 s. Long pre injection delays (∼1000 seconds) were used in order to establish a flat baseline. Kinetics of inhibition ITC experiments were carried out with POP and TRH in the reaction cell and inhibitor in the syringe. POP was added to the cell solution immediately prior to loading the sample cell and initializing the experiment to avoid depletion of the substrate. Kinetics of initiation ITC experiments were carried out with TRH in the reaction cell and POP/inhibitor in the syringe. The syringe solution was allowed to equilibrate at 30°C for ∼2 hours prior to starting the experiment. Ligands were dissolved into DMSO then diluted into buffer immediately prior to the experiment. DMSO was added to the cell solution in order to match the syringe solution to minimize the heats of dilution.

4.5.4 Baseline Correction

In order to correct for sloped baselines, a common artifact in ITC experiments, a baseline correction procedure was implemented for both kinetics of inhibition and initiation experiments. This procedure involves fitting lines to the final flat (usually last ∼200 s) portion of each injection (Figure 4.4a). Each of these lines is extrapolated back to the beginning of the respective injection in order to establish a full baseline for each injection. The full baseline is then subtracted from the raw data for each injection to give the baseline-corrected data (Figure 4.4b).

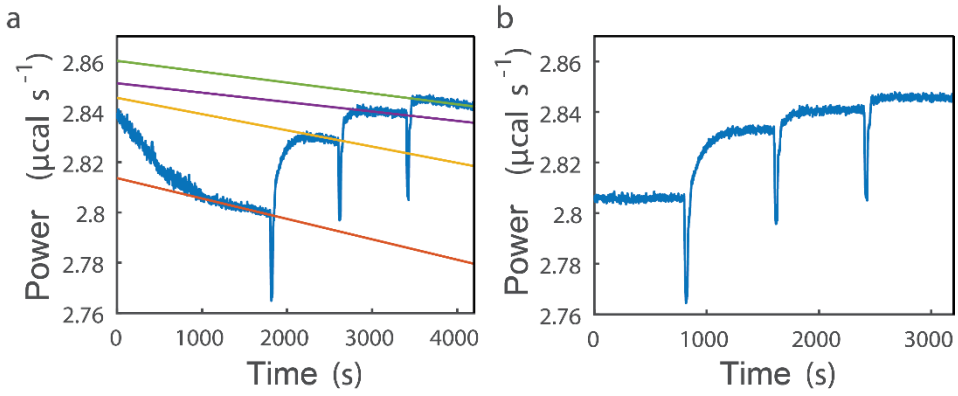

Figure 4.4. Baseline correction of raw data for inhibition experiment using compound 1. a) Raw data including pre injection delay (0-1000 s) and 4 injections (1st injection 0.4 μL over 0.8 s, subsequent 3 injections 13 μL over 26 s) of compound 1 (7 µM in syringe) into cell containing POP and TRH (1.32 nM and 13 mM) using a Malvern ITC-200 (blue line). Orange, yellow, purple and green lines show the baselines for injections 1, 2 3 and 4 respectively. b) Baseline corrected ITC kinetics of inhibition data.

4.5.5 Blank Subtraction

ITC injections are accompanied by heat produced due to the dilution of the contents of the syringe into the cell as well as the mechanical injection process itself. This heat is detected during and immediately following the injection, partially obscuring the desired signal for an amount of time that depends on the response function of the calorimeter. We have found that the most robust way to circumvent these injection artifacts is to employ a blank experiment performed identically to the

actual experiment except without either no enzyme or no substrate. The blank experiment is used to determine when the injection artifact ends (τ_{blank}) and is used as the starting point for the data analysis of each injection (see ITC kinetics fitting scripts). Note that τ_{blank} is approximately given by $\tau_{inj} + 3{\cdot}\tau_r$, where τ_{inj} is the length of the injection and τ_r is the empirical calorimeter response time (≈10 s for a Malvern ITC-200 and ≈20 s for a Malvern VP-ITC), although the best estimate is obtained directly from the blank injections (Figure 4.5).

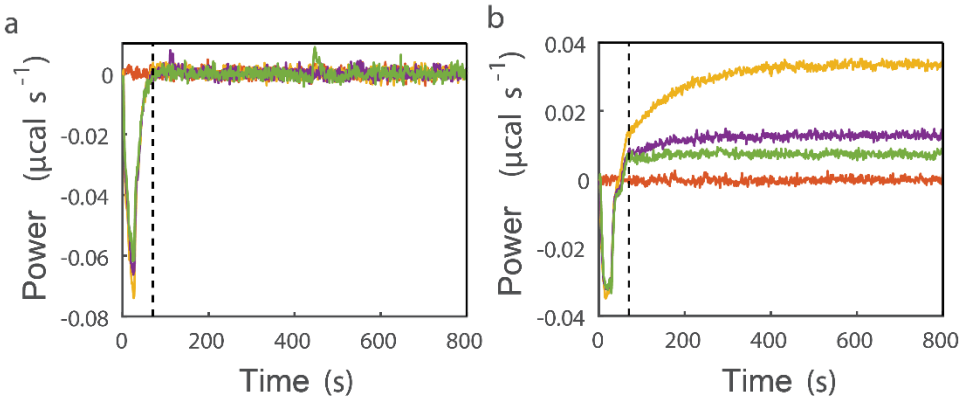

Figure 4.5. Determination of τ_{blank} for inhibition experiment using compound 1. a) Blank experiment injections for inhibition experiment of compound 1. This experiment is performed under exactly the same conditions as actual experiment except with no POP. τ_{blank} is determined to be time it takes the signal to return to baseline after an injection (dashed line at 70 s). b) Overlay of injections from inhibition experiment of compound 1 black dashed line represents the value for τ_{blank}.

4.5.6 ITC Data Fitting

POP was assumed to follow Michaelis-Menten kinetics according to:

$$\frac{d[P]}{dt} = -\frac{d[S]}{dt} = \frac{k_{cat} \cdot [S] \cdot ([E_o] - [EI])}{[S] + K_m} \tag{4.2}$$

where $[P]$, $[S]$, $[E_0]$, and $[EI]$ are the concentrations of product, substrate, total enzyme, and enzyme/inhibitor complex, respectively, k_{cat} is the catalytic rate constant and K_m is the Michaelis constant. Inhibition was assumed to follow first-order

kinetics according to:

$$\frac{d[EI]}{dt} = k_{on} \cdot [E] \cdot [I] - k_{off} \cdot [EI] \tag{4.3}$$

where $[E]$ is the concentration of free enzyme, and k_{on} and k_{off} are the association and dissociation rate constants (see 1.1.2.3). The heat flow, $Q(t)$, generated by catalysis was calculated according to:

$$Q(t) = \Delta H_{cat} \cdot V_{cell} \cdot \frac{d[P]}{dt} \tag{4.4}$$

where ΔH_{cat} is the enthalpy of catalysis and V_{cell} is the volume of the cell, followed by convolution with the empirical instrument response function. The corrected data were fitted using numerical integration of the full set of coupled differential equations, as described in the Supplementary Methods. All calculations were performed using MATLAB.

4.5.7 ITC Kinetics Fitting Scripts

All fitting routines were performed using in-house MATLAB scripts. Differential equations were integrated numerically in 0.01 s integration steps. For kinetics of inhibition experiments:

$$[ES]_{t,i} = \frac{[S]_{t,i} \cdot ([E_0]_{t,i} - [EI]_{t,i})}{[S]_{t,i} + K_m} \tag{4.5}$$

$$\frac{d[P]_{t,i}}{dt} = k_{cat} \cdot [ES]_{t,i} \tag{4.6}$$

$$[ES]_{t,i} = [E_0]_{t,i} - [EI]_{t,i} - [ES]_{t,i} \tag{4.7}$$

$$\frac{d[EI]_{t,i}}{dt} = k_{on} \cdot [E]_{t,i} \cdot [I]_{t,i} - k_{off} \cdot [EI]_{t,i} - [EI]_{t,i} \cdot Rate_{dil,i} \tag{4.8}$$

$$[EI]_{t+dt,i} = [EI]_{t,i} + \frac{d[EI]_{t,i}}{dt} \cdot dt \tag{4.9}$$

$$\frac{d[I]_{t,i}}{dt} = -k_{on} \cdot [E]_{t,i} \cdot [I]_{t,i} + k_{off} \cdot [EI]_{t,i} - [I]_{t,i} \cdot Rate_{dil,i} + [I]_{syringe} \cdot Rate_{dil,i} \tag{4.10}$$

$$[I]_{t+dt,i} = [I]_{t,i} + \frac{d[I]_{t,i}}{dt} \cdot dt \tag{4.11}$$

$$\frac{d[S]_{t,i}}{dt} = -[S]_{t,i} \cdot Rate_{dil,i} - \frac{d[P]_{t,i}}{dt} \tag{4.12}$$

$$[S]_{t+dt,i} = [S]_{t,i} + \frac{d[S]_{t,i}}{dt} \cdot dt \tag{4.13}$$

$$\frac{d[E_0]_{t,i}}{dt} = -[E_0]_{t,i} \cdot Rate_{dil,i} \tag{4.14}$$

$$[E_0]_{t+dt,i} = [E_0]_{t,i} + \frac{d[E_0]_{t,i}}{dt} \cdot dt \tag{4.15}$$

For kinetics of initiation experiments:

$$[ES]_{t,i} = \frac{[S]_{t,i} \cdot ([E_o]_{t,i} - [EI]_{t,i})}{[S]_{t,i} + K_m} \tag{4.16}$$

$$\frac{d[P]_{t,i}}{dt} = k_{cat} \cdot [ES]_{t,i} \tag{4.17}$$

$$[ES]_{t,i} = [E_0]_{t,i} - [EI]_{t,i} - [ES]_{t,i} \tag{4.18}$$

$$\frac{d[EI]_{t,i}}{dt} = k_{on} \cdot [E]_{t,i} \cdot [I]_{t,i} - k_{off} \cdot [EI]_{t,i} - [EI]_{t,i} \cdot Rate_{dil,i} + [EI]_{syringe} \cdot Rate_{dil,i} \tag{4.19}$$

$$[EI]_{t+dt,i} = [EI]_{t,i} + \frac{d[EI]_{t,i}}{dt} \cdot dt \tag{4.20}$$

$$\frac{d[I]_{t,i}}{dt} = -k_{on} \cdot [E]_{t,i} \cdot [I]_{t,i} + k_{off} \cdot [EI]_{t,i} - [I]_{t,i} \cdot Rate_{dil,i} + [I]_{syringe} \cdot Rate_{dil,i} \tag{4.21}$$

$$[I]_{t+dt,i} = [I]_{t,i} + \frac{d[I]_{t,i}}{dt} \cdot dt \tag{4.22}$$

$$\frac{d[S]_{t,i}}{dt} = -[S]_{t,i} \cdot Rate_{dil,i} - \frac{d[P]_{t,i}}{dt} \tag{4.23}$$

$$[S]_{t+dt,i} = [S]_{t,i} + \frac{d[S]_{t,i}}{dt} \cdot dt \tag{4.24}$$

$$\frac{d[E_0]_{t,i}}{dt} = [E_0]_{syringe} \cdot Rate_{dil,i} - [E_0]_{t,i} \cdot Rate_{dil,i} \tag{4.25}$$

$$[E_0]_{t+dt,i} = [E_0]_{t,i} + \frac{d[E_0]_{t,i}}{dt} \cdot dt \tag{4.26}$$

For both inhibition and initiation experiments the k_{cat} and K_m are the catalytic rate and the Michaelis-Menten constants for TRH respectively. $[E_0]_{t,i}$ is the total

concentration of enzyme for time = t for injection i in the cell and $[I]_{t,i}$, $[E]_{t,i}$, $[S]_{t,i}$, $[EI]_{t,i}$, and $[ES]_{t,i}$ are the concentrations of free inhibitor, free enzyme, free substrate, enzyme inhibitor complex, and enzyme substrate complex in the cell at time = t for the ith injection respectively. k_{on} and k_{off} are the association rate dissociation rate of the inhibitor respectively. The dilution rate ($Rate_{dil,i}$) is the rate of dilution occurs for injection i; this is equal to $\frac{v_{inj,i}}{\tau_{inj} \cdot V_{cell}}$ during the injection and 0 otherwise. Here $v_{inj,i}$ is the volume of the ith injection τ_{inj} is the injection length V_{cell} is the volume of the cell. For ITC inhibition experiments $[I]_{syr}$ is the concentration of inhibitor in the syringe. The initial conditions for the first injection ($i = 1$) are $[E_0]_{t=1,i=1} = [E_0]_{cell}$, $[I]_{t=1,i=1} = 0$, $[S]_{t=1,i=1} = [S]_{cell}$ and $[EI]_{t=1,i=1} = 0$. For subsequent injections ($i > 1$) the initial conditions were set as $[E_0]_{t=1,i} = [E_0]_{t=N,i-1}$, $[I]_{t=1,i} = [I]_{t=N,i-1}$, $[S]_{t=1,i} = [S]_{t=N,i-1}$ and $[EI]_{t=1,i} = [EI]_{t=N,i-1}$ where N is the total time between injections and $[E_0]_{cell}/[S]_{cell}$ are the initial concentrations of enzyme/substrate in the cell (ie. $i = 1$ and $t = 0$). For ITC initiation experiments $[EI]_{syr}$, $[I]_{syr}$ and $[E]_{syr}$ are calculated via the binding polynomial using the total concentrations of enzyme and inhibitor in the syringe and the strength of the inhibitor $K_i = k_{off}/k_{on}$.[33] The initial conditions for the first injection ($i = 1$) are $[E_0]_{t=1,i=1} = 0$, $[I]_{t=1,i=1} = 0$, $[S]_{t=1,i=1} = [S]_{cell}$ and $[EI]_{t=1,i=1} = 0$. For subsequent injections ($i > 1$) the initial conditions were set as $[E_0]_{t=1,i} = [E_0]_{t=N,i-1}$, $[I]_{t=1,i} = [I]_{t=N,i-1}$, $[S]_{t=1,i} = [S]_{t=N,i-1}$ and $[EI]_{t=1,i} = [EI]_{t=N,i-1}$ where N is the total time between injections and $[E_0]_{cell}/[S]_{cell}$ are the initial concentrations of enzyme/substrate in the cell. The instantaneous heat of injection $h_i(t)$ is calculated using the enthalpy of the reaction ΔH_{cat} and the total volume of the cell according to:

$$h_i(t) = \Delta H_{cat} \cdot V_{cell} \cdot \frac{d[P]_{t,i}}{dt} \tag{4.27}$$

Prior to convolution the offset is adjusted such that the $h_i(t = 0) = 0$ and the initial portion of each transient is zero padded with ~ 500 s in order to avoid artifacts from the convolution. The instantaneous heat curve is then numerically convoluted with

an empirical response function (2.3.5) according to:

$$g_i(t) = h_i(t) \otimes f(t) \tag{4.28}$$

Where $f(t)$ is the empirical response function, $g_i(t)$ is the resulting calculated signal, and the convolution is defined according to:

$$h_i(t) \otimes f(t) = \int_0^t h_i(\tau) f(t-\tau) d\tau \tag{4.29}$$

The calculated instrument output, $g_i(t)$, was digitally resampled in second intervals to match the experimental calorimeter output. For all compound the k_{on} and K_i were floated along with ΔH_{cat} in order to account for inaccuracies in the enzyme concentration. In the case of compound 3 a stoichiometric n value was also floated (ie. $[E_0]_{cell} = n \cdot [E_0]'_{cell}$ as in ordinary binding ITC experiments) while minimizing the target function (Equation 4.30) using the MATLAB fminsearch function according to:

$$RSS = \sum_{i=1}^{M} \sum_{t=\tau_{blank}}^{N} (g_i(t) - b_i(t))^2 \tag{4.30}$$

Where $b_i(t)$ is the experimental curve generated by injection i. Note that that in most experiments the first injection was omitted from the fitting (ie. i would start at 2 in Equation 4.31 above) due to diffusion from the syringe tip. N is the time between injection, M is the total number injections and τ_{blank} is the beginning of the data analysis period which is determined using blank experiments (see 4.5.5).

4.5.8 Global Fits for ITC Kinetics

Global fits fitting routines were performed as above except with a global set of kinetic parameters. The target functions were calculated according to:

$$RSS_{total} = \frac{RSS_{inhib}}{(\frac{1}{N-\tau_{blank}} \cdot \sum_{t=\tau_{blank}}^{N} b_{1,inhib}(t))^2} + \frac{RSS_{init}}{(\frac{1}{N-\tau_{blank}} \cdot \sum_{t=\tau_{blank}}^{N} b_{1,init}(t))^2} \tag{4.31}$$

where RSS_{inhib} and RSS_{init} are the residual sum of squares of the inhibition experiment and initiation experiment respectively (Equation 4.30).

4.5.9 UV-Vis spectroscopy experiments

UV-Vis spectroscopy experiments were carried out in triplicate using a BioTek Synergy^{TM} H4 well plate reader. For the UV-Vis inhibition experiment the solution containing 80 μM carboxybenzyl-Gly-Pro-nitroanilide (ZPG-pN) and 105 nM compound 1 was combined with POP (final concentration 1 nM) ~30 s prior to the first measurement. The absorbance at 405 nm was recorded every 30 s which was converted to a concentration of p-Nitroanaline using the extinction coeffecient at 405 nm (9193 cm^{-1} M^{-1}). For UV-Vis initiation experiments POP and compound 1 were preincubated at 277 nM and 1.5 μM respectively for ~2 hours prior to being diluted to a final concentration of 2.7 nM and 15 nM into a solution containing 80 μM ZPG-pN ~10 s before the first measurement. The absorbance at 405 nm was recorded every 10 s which was converted to a concentration of p-Nitroanaline using the extinction coeffecient at 405 nm.

4.5.10 NMR spectroscopy experiments

NMR experiments were carried out using a Varian 500 MHz spectrometer in a 5 mm probe at 298 K. A DPFGSE sequence was used for water signal suppression. All samples were prepared in 20 mM phosphate buffer (pH 8.0) containing 10% D_2O. A 5 mM TRH solution was prepared and POP was added for a final concentration of 50 nM. The first spectrum was acquired 6 min after the addition of compound 5. Spectra were acquired at each 67 s time interval, 8 transients collected per spectrum. The initial concentrations in the NMR tube were 5 mM TRH, 50 nM POP and 50 nM Z-Pro-Prolinal (ZPP). The peak at ~8 ppm (TRH) was chosen for following the kinetics, as it is was the most resolved.

4.5.11 Spectroscopy Fitting Scripts

All fitting routines were performed using in house MATLAB scripts. Differential equations were integrated numerically in 0.01 s integration steps. For spectroscopic kinetics of inhibition and initiation experiments:

$$[ES]_t = \frac{[S]_t \cdot ([E_0]_t - [EI]_t)}{[S]_t + K_m} \tag{4.32}$$

$$\frac{d[P]_t}{dt} = k_{cat} \cdot [ES]_t \tag{4.33}$$

$$[ES]_t = [E_0]_t - [EI]_t - [ES]_t \tag{4.34}$$

$$\frac{d[EI]_t}{dt} = k_{on} \cdot [E]_t \cdot [I]_t - k_{off} \cdot [EI]_t \tag{4.35}$$

$$[EI]_{t+dt} = [EI]_t + \frac{d[EI]_t}{dt} \cdot dt \tag{4.36}$$

$$\frac{d[I]_t}{dt} = -k_{on} \cdot [E]_t \cdot [I]_t + k_{off} \cdot [EI]_t \tag{4.37}$$

$$[I]_{t+dt} = [I]_t + \frac{d[I]_t}{dt} \cdot dt \tag{4.38}$$

$$\frac{d[S]_t}{dt} = -\frac{d[P]_t}{dt} \tag{4.39}$$

$$[S]_{t+dt} = [S]_t + \frac{d[S]_t}{dt} \cdot dt \tag{4.40}$$

$$[P]_{t+dt} = [P]_t + \frac{d[P]_t}{dt} \cdot dt \tag{4.41}$$

Where $[E_0]_{t,i}$ is the total concentration of enzyme at time = t for and $[I]_t$, $[E]_t$, $[S]_t$, $[P]_t$, $[EI]_t$, $[ES]_t$ are the concentrations of free inhibitor, free enzyme, free substrate, product, enzyme inhibitor complex, and enzyme substrate complex in the well plate at time = t. k_{on} and k_{off} are the association rate dissociation rate of the inhibitor respectively. The initial concentrations of the various species were used as the initial conditions for the fitting scripts. For both UV-Vis inhibition and initiation experiments the k_{cat} and K_m are the catalytic rate and the Michaelis-Menten constant respectively for ZPG-pN. For NMR spectroscopy experiments the

catalytic rate and Michaelis-Menten constant for TRH were used.

For both NMR and UV-VIS spectroscopy experiments the product concentration $[P]_t$ was digitally resampled in order to match the experimental output. For UV-Vis spectroscopy the k_{on}, K_i, enzyme concentration, and intercept y_0 were floated while minimizing the target function (Equation 4.42) using the fminsearch function. according to:

$$RSS = \sum_{t=0}^{N} ([P]_{t,exp} - ([P]_{t,calc} + y_0))^2 \tag{4.42}$$

Where $[P]_{t,exp}$, and $[P]_{t,calc}$ are the experimental and calculated concentration of product at time $t = 0$ respectively. For NMR spectroscopy experiments the substrate concentration $[S]_t$ was digitally resampled in order to match the experimental output. The values of k_{on}, y_0 as well as a conversion factor S_c were floated while minimizing the target function (Equation 4.43) using the MATLAB fminsearch function according to:

$$RSS = \sum_{t=0}^{N} (S_c \cdot [S]_{t,exp} - ([S]_{t,calc} + y_0))^2 \tag{4.43}$$

4.6 Supplementary Information

4.6.1 Prolyl Oligopeptidase Enthalpy of Catalysis and Michaelis-Menten Parameters

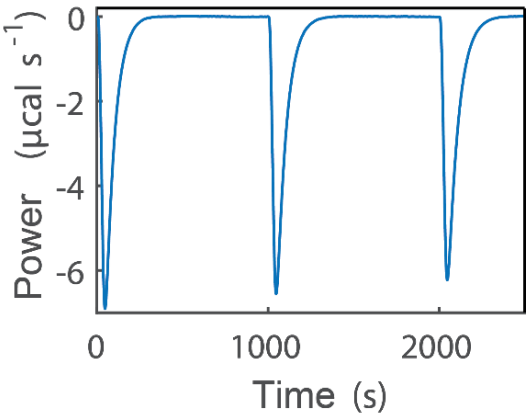

Figure 4.S1. Prolyl oligopeptidase and TRH enthalpy of catalysis. 3 injections (15 μL over 30 s) of Thyrotropin-releasing Hormone (TRH) (5.5 mM in syringe) into cell containing POP (250 nM in Cell) at 30°C in buffer described above. Experiment was carried out using a Malvern VP-ITC.

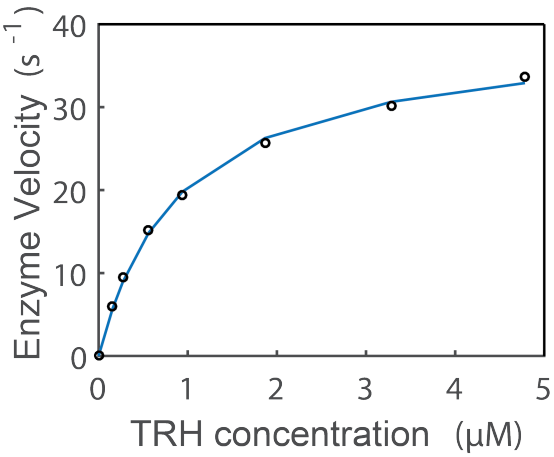

Figure 4.S2. Michaelis-Menten plot for prolyl oligopeptidase with TRH. 5 injections (8 μL, 6 μL, 15 μL, 20 μL, 50 μL, 80 μL and 90 μL over 16 s, 12 s, 30 s, 40 s, 100 s, 160 s, 180 s respectively) of Thyrotropin-releasing Hormone (TRH) (27.6 mM in syringe) into cell containing POP (2.5 nM in Cell) at 30°C in buffer described above. The enzyme velocity at several concentrations of substrate (black open circles) was extracted using the methods described in[16] and fit to Michaelis-Menten kinetics (blue curve). Experiment was carried out in Malvern VP-ITC.

Table 4.S1. Summary of prolyl oligopeptidase enzyme parameters with TRH. Determined by ITC using techniques presented by Gomez et al.[16]

ΔH_{cat}	-6.72 ± 0.06 kCal mol^{-1}
k_{cat}	42.19 s^{-1}
K_m	975 μM

4.6.2 Enthalpy of Binding in Kinetics of Inhibition and Initiation Experiments

In the kinetics of inhibition and initiation experiments performed here, the instrument measures both the heat generated by enzymatic catalysis and the heat produced due direct interaction of the inhibitor with the enzyme. In order to estimate the relative magnitudes of these two effects, the enthalpy of binding was directly measured using an ordinary ITC binding experiment at a concentration of POP significantly higher (approx. 100 to 1000-fold greater, 5 μM) than those used in

kinetics of inhibition and initiation experiments. Binding data were then modelled at the concentrations of enzyme and inhibitor and injection size and spacing used for the kinetic experiment for compound 5, with representative instrumental noise estimated from the baselines, ΔH_{bind} taken from Table 4.S2 and K_i taken as a previously reported value (0.5 nM)[27] (Figure 4.S4).

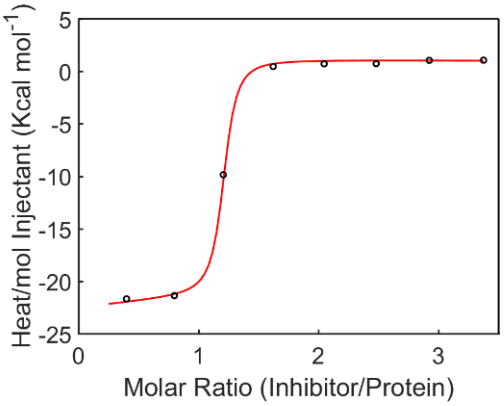

Figure 4.S3. Compound 5 prolyl oligopeptidase binding experiments. Compound 5 (90 μM) was titrated into 5 μM POP in cell using a Malvern ITC-200 calorimeter. First injection is 0.1 μL (not shown) and subsequent 8 injections are 4.3 μL. Molar ratio of compound 5/POP vs Total Heat for each injection peak (open black circles) with fit (red line).

Table 4.S2. Summary of compound 5 prolyl oligopeptidase binding parameters.

ΔH_{bind}	-22.2 ± 0.1 kCal mol^{-1}
n	0.93 ± 0.03
K_i	–

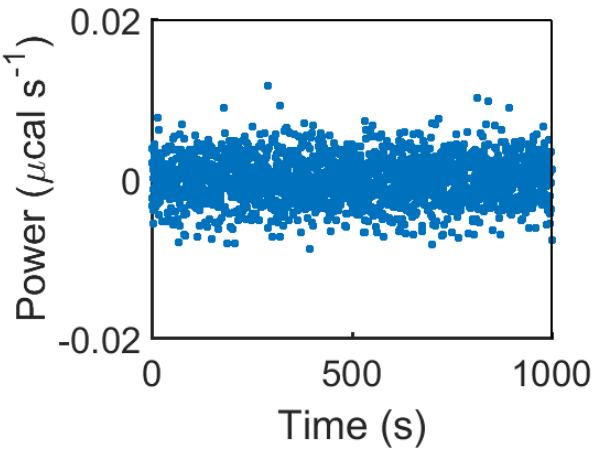

Figure 4.S4. Modelling heat of binding in kinetics of inhibition experiments. Modelled kinetics of inhibition experiment with compound 5 using only contributions from the heats of binding.

4.6.3 Supplementary Results

4.6.3.1 Fits for ITC Kinetics of Inhibition and Initiation Experiments

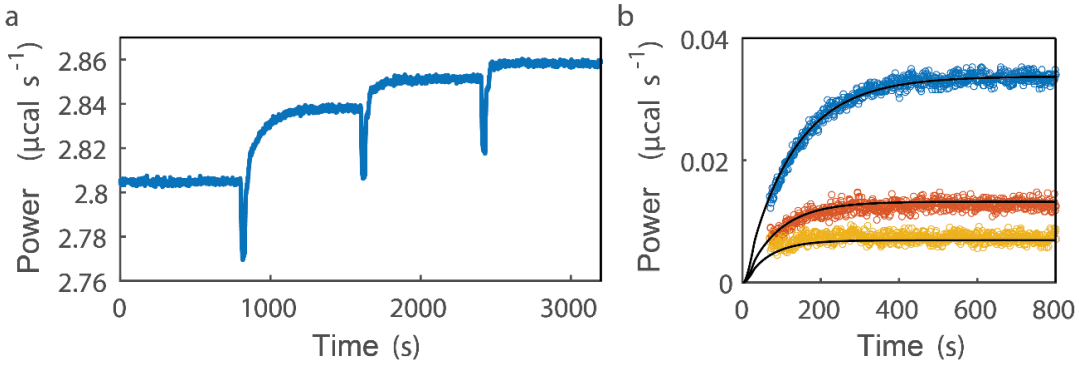

Figure 4.S5. Kinetics of inhibition experiment using compound 1. a) Baseline corrected data. 4 injections (1st injection 0.4 μL over 0.8 s, subsequent 3 injections 13 μL over 26 s) of compound 1 (7 μM in syringe) into cell containing POP and TRH (1.32 nM and 13 mM) at 30°C in buffer described above using a Malvern ITC-200. a) Overlay of injections 2 (open blue circles), 3 (open orange circles), and 4 (open yellow circles) from baseline corrected ITC kinetics of inhibition data. Fit using the kinetics of inhibition model described above (black lines). Only fitted portion of the experimental curves are shown.

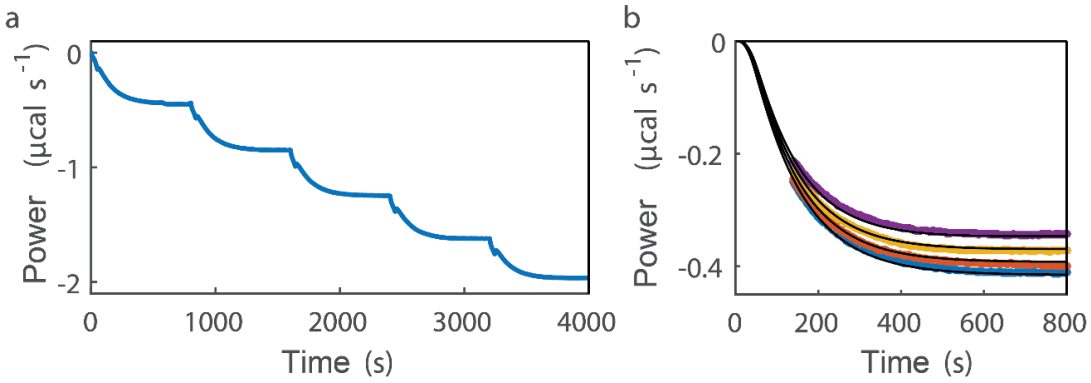

Figure 4.S6. Kinetics of initiation experiment using compound 1. a) Baseline corrected data. a) Baseline corrected data, 6 injections (1st injection 25 μL over 50 s, subsequent 3 injections 20 μL over 40 s) of pre-incubated POP and compound 1 (100 nM and 878 nM respectively in syringe) into the cell containing TRH (11 mM) at 30°C in buffer described above using a Malvern VP-ITC. b) Overlay of injections 2 (open blue circles), 3 (open orange circles), 4 (open yellow circles), 5 (open purple circles) from baseline corrected ITC kinetics of inhibition data. Fit using kinetics of inhibition model described above (black lines). Only fitted portion of the experimental curves are shown.

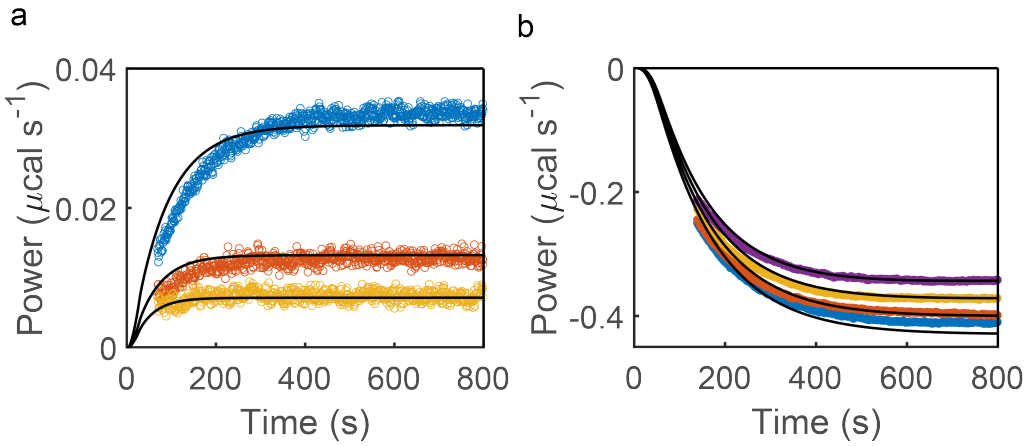

Figure 4.S7. Global fit for compound 1. Results of global fit between (a) inhibition experiment and (b) initiation experiment for compound 1.

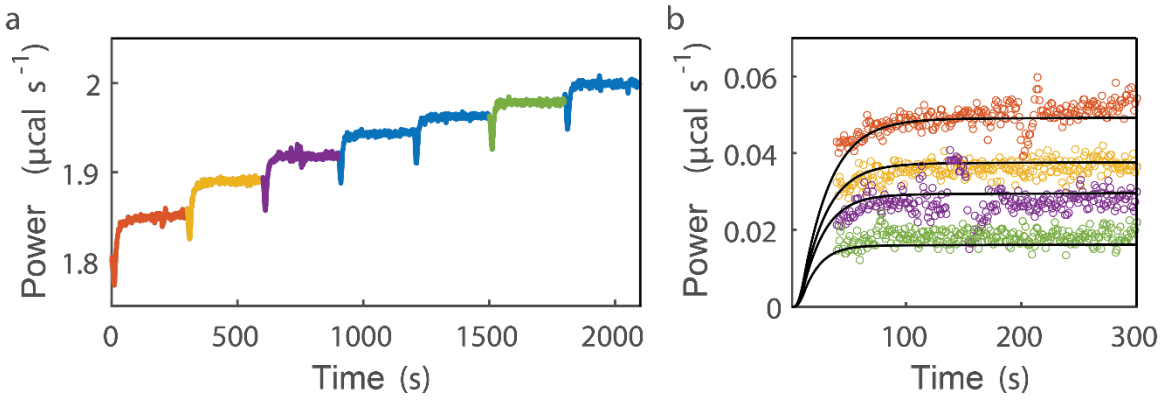

Figure 4.S8. Kinetics of inhibition experiment using compound 2. a) Baseline corrected data. 7 injections (all 4.5 μL over 9 s) of compound 2 (87.5 μM in syringe) into cell containing POP and TRH (5.4 nM and 18 mM) at 30°C in buffer described above using a Malvern ITC-200. b) Overlay of injections 1 (open orange circles), 2 (open yellow circles), 3 (open purple circles) and 6 (open green circles) from baseline corrected ITC kinetics of inhibition data. Fit using the kinetics of inhibition model described above (black lines). Only 4 curves are shown for clarity only, all injections except the first was used in the fitting routine. Only fitted portion of the experimental curves are shown.

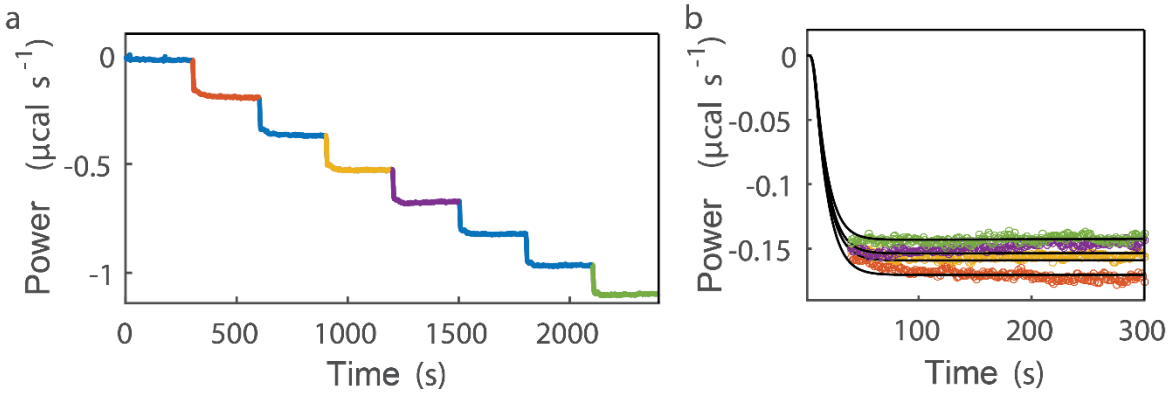

Figure 4.S9. Kinetics of initiation experiment using compound 2. a) Baseline corrected data, 8 injections (1st injection 0.2 μL over 0.4 s, subsequent 7 injections 2 μL over 4 s) of pre-incubated POP and compound 2 (200 nM and 16.2 μM respectively in syringe) into the cell containing TRH (17.3 mM) at 30°C in buffer described above using a Malvern ITC-200. b) Overlay of injections 2 (open blue circles), 3 (open orange circles), 4 (open yellow circles), 5 (open purple circles) from baseline corrected ITC kinetics of inhibition data. Fit using kinetics of inhibition model described above (black lines). Only fitted portion of the experimental curves are shown.

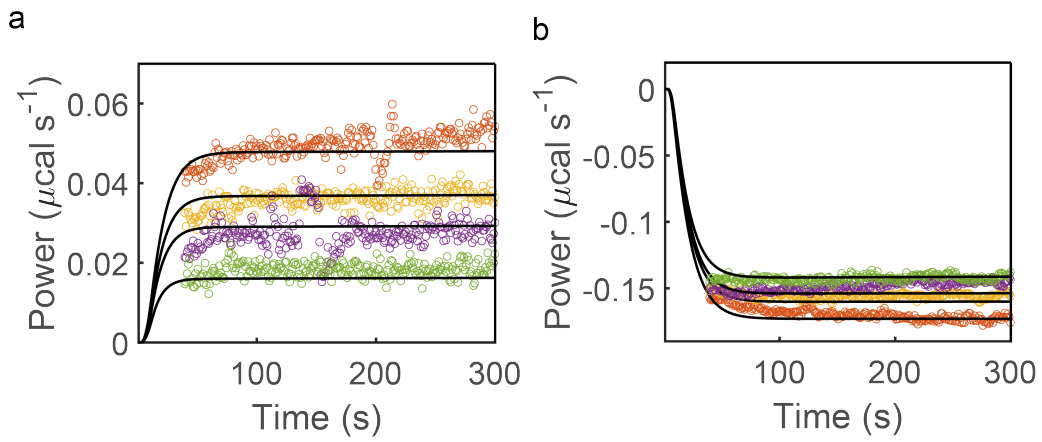

Figure 4.S10. Global fit for compound 2. Results of global fit between (a) inhibition experiment and (b) initiation experiment for compound 2.

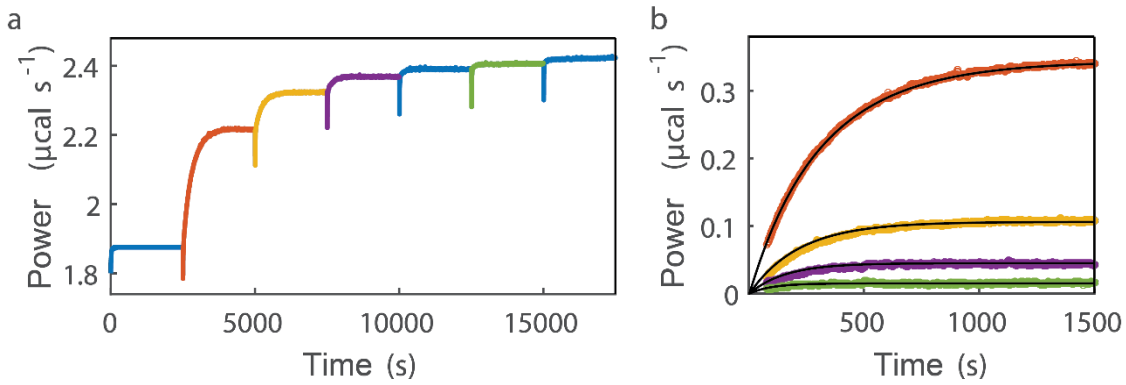

Figure 4.S11. Kinetics of inhibition experiment using compound 3. a) Baseline corrected data. 7 injections (1st injection 0.3 μL over 0.6 s, subsequent 6 injections 5 μL over 8 s) of compound 3 (462 nM in syringe) into cell containing POP and TRH (7.64 nM and 25.2 mM) at 30°C in buffer described above using a Malvern ITC-200. b) Overlay of injections 2 (open orange circles), 3 (open yellow circles), 4 (open purple circles) and 6 (open green circles) from baseline corrected ITC kinetics of inhibition data. Fit using the kinetics of inhibition model described above (black lines). Only 4 curves are shown for clarity only, all injections except the first was used in the fitting routine. Only fitted portion of the experimental curves are shown.

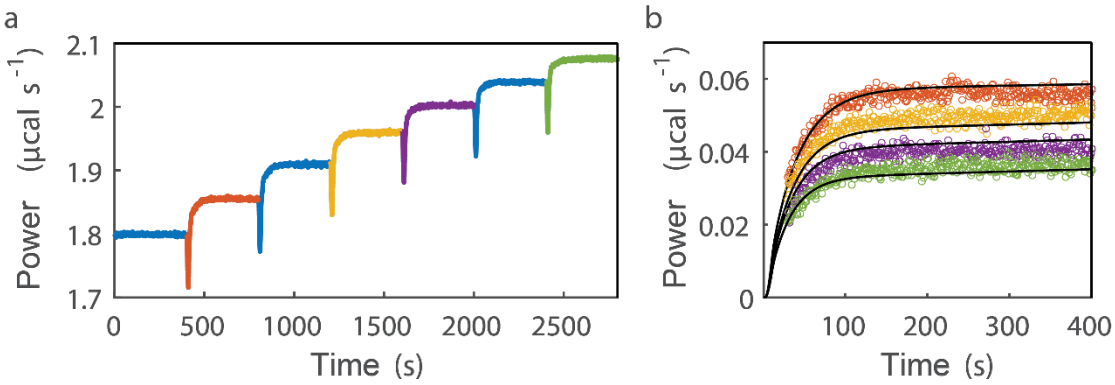

Figure 4.S12. Kinetics of inhibition experiment using compound 4. a) Baseline corrected data. 7 injections (1st injection 0.3 μL over 0.6 s, subsequent 6 injections 4 μL over 8 s) of compound 4 (500 nM in syringe) into cell containing POP and TRH (14.8 nM and 20 mM) at 30°C in buffer described above using a Malvern ITC-200. b) Overlay of injections 2 (open orange circles), 4 (open yellow circles), 5 (open purple circles) and 7 (open green circles) from baseline corrected ITC kinetics of inhibition data. Fit using the kinetics of inhibition model described above (black lines). Only 4 curves are shown for clarity only, all injections except the first was used in the fitting. Only fitted portion of the experimental curves are shown.

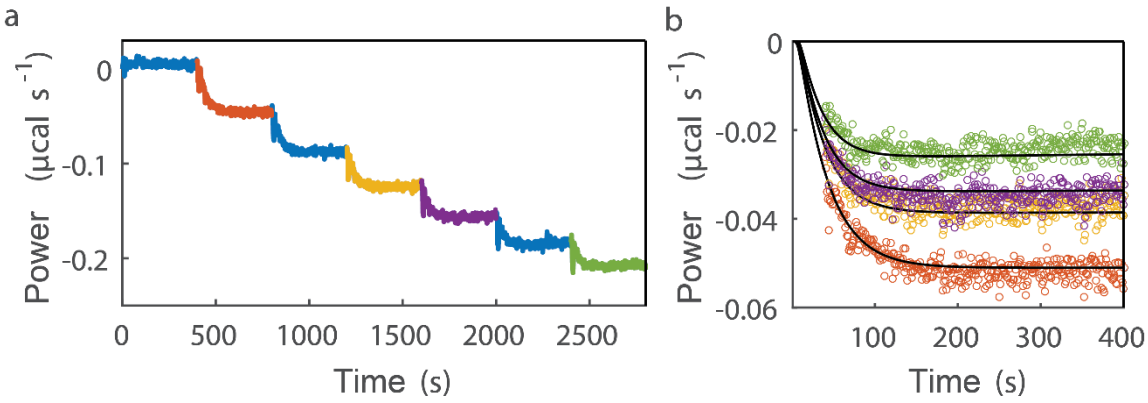

Figure 4.S13. Kinetics of initiation experiment using compound 4. a) Baseline corrected data, 7 injections (1st injection 0.3 μL over 0.6 s, subsequent 6 injections 2.9 μL over 5.8 s) of pre-incubated POP and compound 4 (88.1 nM and 500 nM respectively in syringe) into the cell containing TRH (6.9 mM) at 30°C in buffer described above using a Malvern ITC-200. b) Overlay of injections 2 (open orange circles), 4 (open yellow circles), 5 (open purple circles) and 7 (open green circles) from baseline corrected ITC kinetics of inhibition data. Fit using the kinetics of inhibition model described above (black lines). Only 4 curves are shown for clarity only, all injections except the first was used in the fitting. Only fitted portion of the experimental curves are shown.

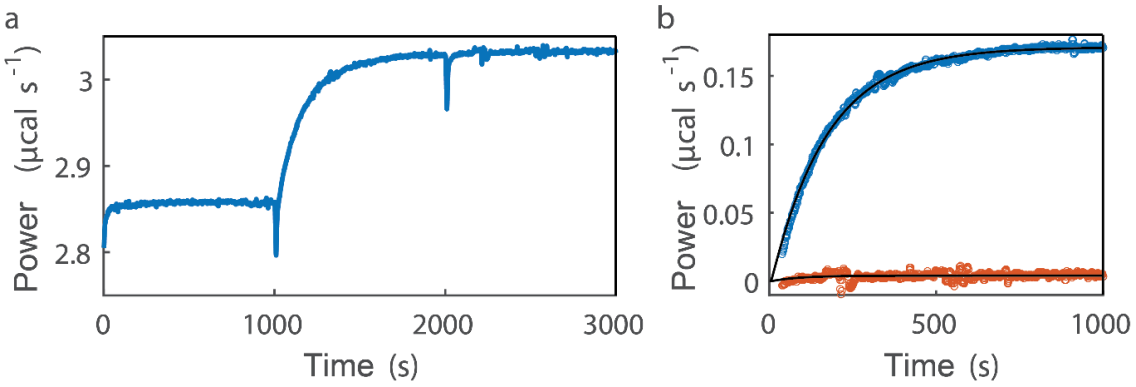

Figure 4.S14. Kinetics of inhibition experiment using compound 5. a) Baseline corrected data. 3 injections (1st injection 0.1 μL over 0.2 s, subsequent 2 injections 3.5 μL over 7 s) of compound 5 (11.7 μM in syringe) into cell containing POP and TRH (3.1 nM and 13.8 mM) at 30°C in buffer described above using a Malvern ITC-200. b) Overlay of injections 2 (open blue circles), 3 (open orange circles) from baseline corrected ITC kinetics of inhibition data. Fit using the kinetics of inhibition model described above (black lines). All injections except the first was used in the fitting routine. Only fitted portion of the curves are shown.

4.6.3.2 UV-Vis and NMR Spectroscopy Experiments

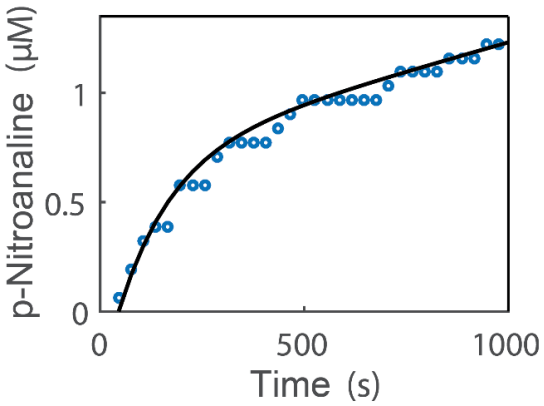

Figure 4.S15. UV-Vis inhibition experiment using compound 1. POP and colorimetric substrate ZGP-pNA (1 nM and 80 μM respectively) were spiked with compound 1 (final concentration of 105 nM). The absorbance at 405 nm was monitored as a function of time which was converted to a concentration of p-Nitroanaline (open blue circles). The data was fit using inhibition scripts described above (black line).

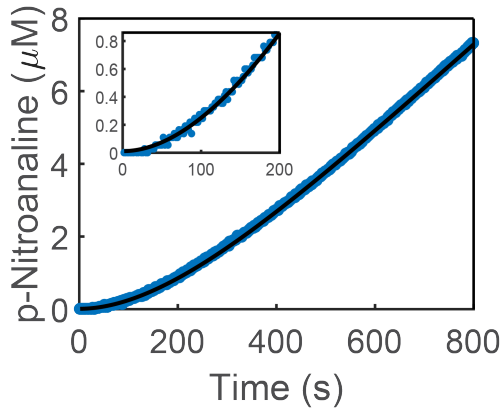

Figure 4.S16. UV-Vis initiation experiments using compound 1. POP and compound 1 at an original concentration of (277 nM and 1.5 μM respectively) are diluted 100-fold into buffer containing ZGP-pNA (80 μM). The intensity of the peak at 405 nm was monitored with time and converted to a concentration of p-Nitroanaline (open blue circles). The data was fit using initiation scripts similar to those described above (black line).

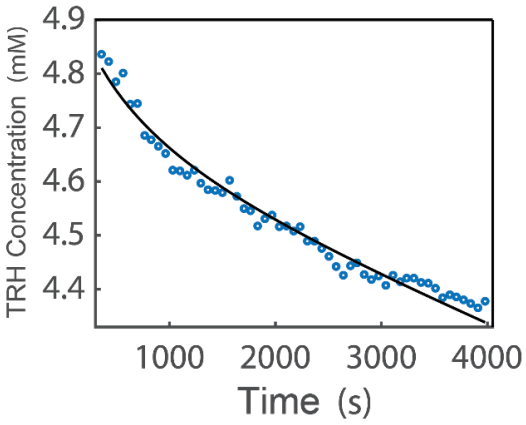

Figure 4.S17. NMR inhibition experiment using compound 5. POP and TRH (50 nM and 5 mM respectively) were spiked with compound 5 (final concentration of 50 nM). The peak corresponding to TRH at 8 ppm monitored as a function of time which was converted to a concentration of TRH (open blue circles). The data were fit using inhibition scripts described above (black line).

4.6.3.3 Statistical Analysis of Errors

Errors were calculated using residual sum of squares contour plots. This was accomplished by performing a grid search for each pair of fitted parameters for each

fit and calculating the RSS at each point. The confidence level (CL) at each RSS value was calculated as.[34]

$$CL_{i,j} = F_{CDF} \cdot \left((\frac{RSS_{i,j}}{RSS_{min}} - 1) \cdot (\frac{Dof}{P}), P, Dof \right) \tag{4.44}$$

where F_{CDF} is the F distribution cumulative density function and RSS_{min} is the residual sum of squares at the minimum found via fitting. $RSS_{i,j}$ is the RSS at the point i, j for each the i/jth pair of fitted parameters. Dof is the degrees of freedom of the fit and P is the total number of fitted parameters. The resulting %CL contour plots are shown below with the 95 %CL contour as a black dotted line, for selected pairs of parameters. Errors are shown in Table 4.1 of the main text and Supplementary Table 4.S3.

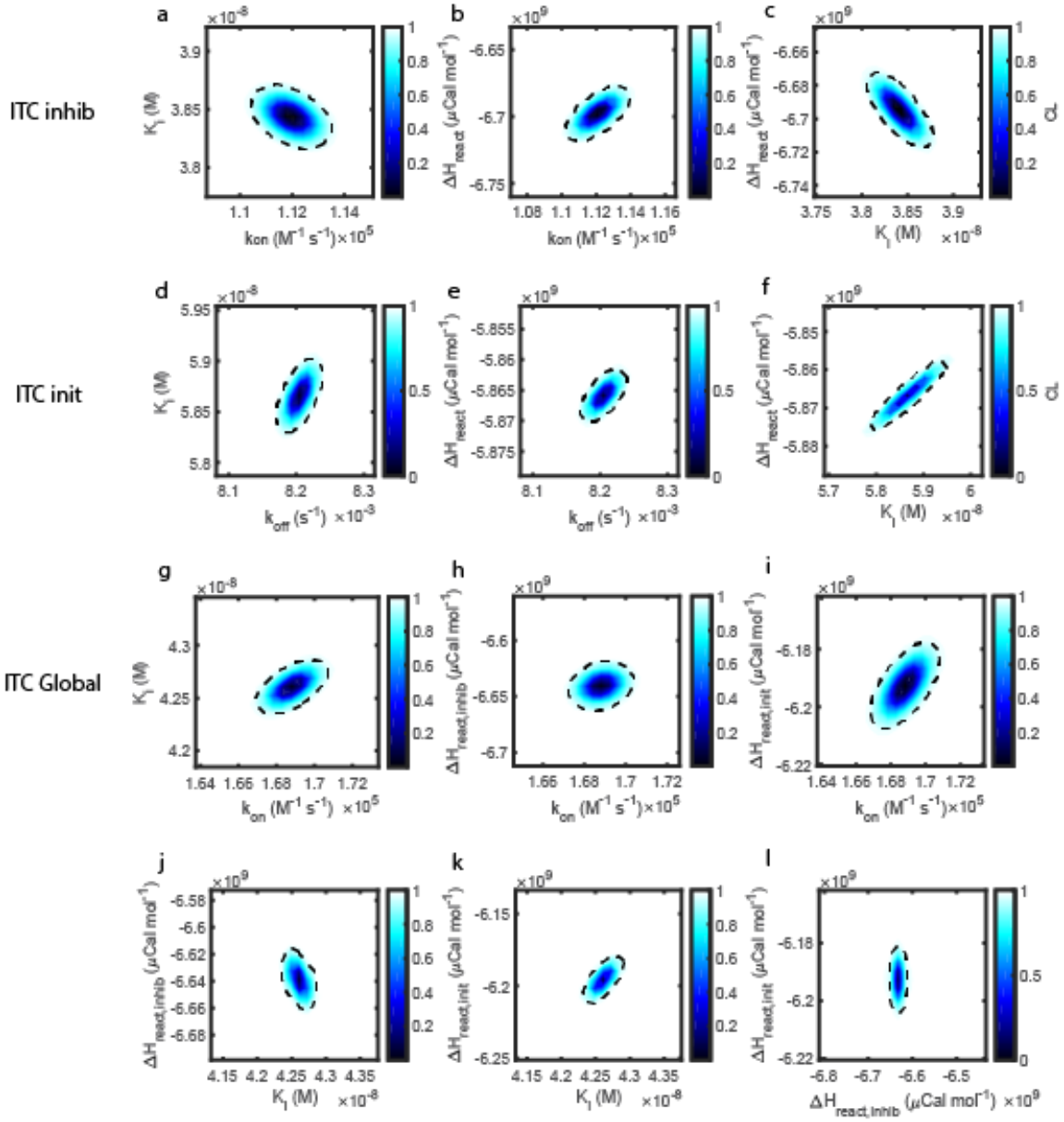

Figure 4.S18. Confidence level contour plots for ITC experiments using compound 1. Error surfaces for each pair of fitted parameters for a)-c) kinetics of inhibition experiment, d)-f) kinetics of initiation experiment and, g)-l) global fit between inhibition and initiation experiment. Dotted line highlights the 95 %CL. The largest error value at the 95 %CL is reported for each parameter.

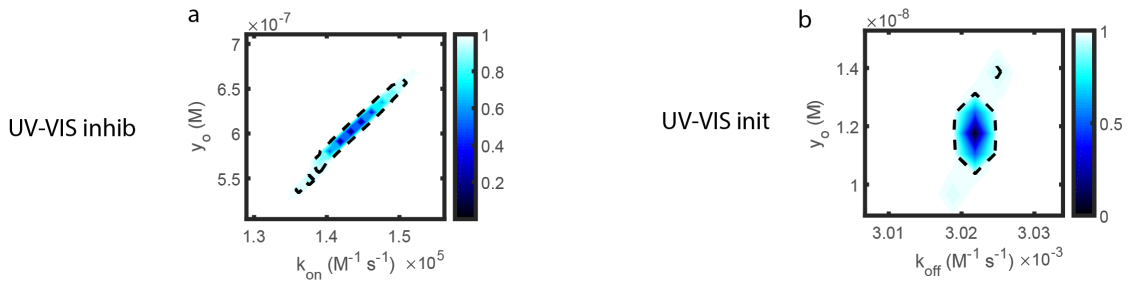

Figure 4.S19. Confidence level contour plots for UV-VIS experiments using compound 1. Error surfaces for pairs of fitted parameters for a) inhibition experiment, b) initiation experiment. Dotted line highlights the 95 %CL. The largest error value at the 95 %CL is reported for each parameter.

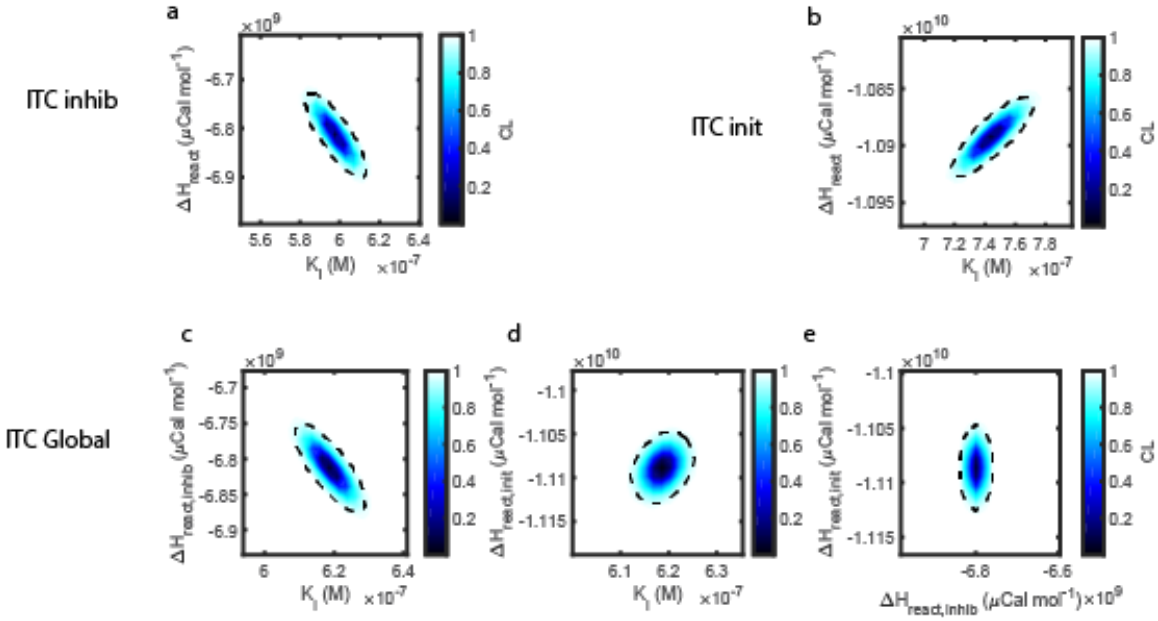

Figure 4.S20. Confidence level contour plots for ITC experiments using compound 2. Error surfaces for each pair of fitted parameters for a) kinetics of inhibition experiment, b) kinetics of initiation experiment and, c)-e) global fit between inhibition and initiation experiment. Dotted line highlights the 95 %CL. The largest error value at the 95 %CL is reported for each parameter.

ITC inhib

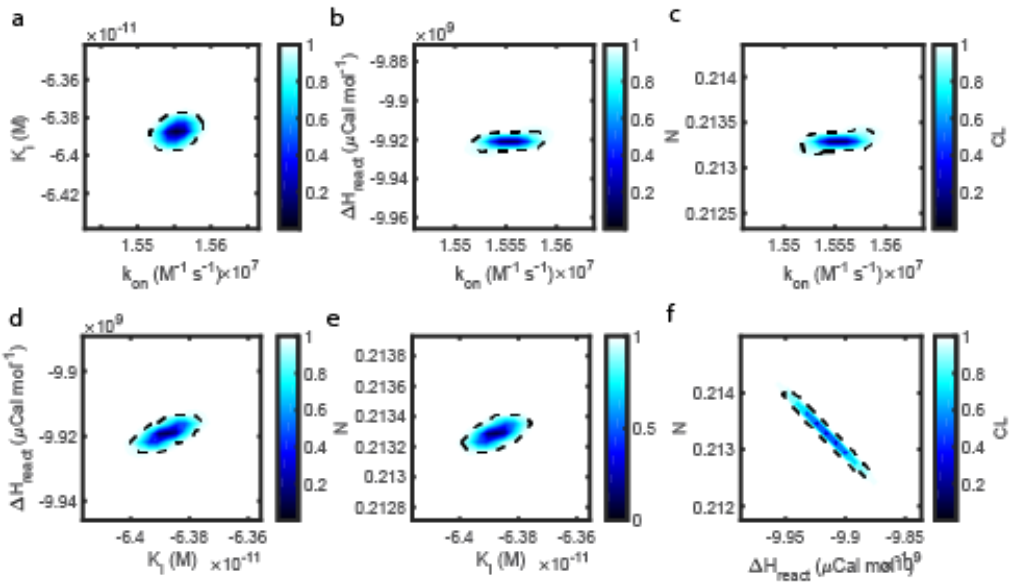

Figure 4.S21. Confidence level contour plots for ITC experiments using compound 3. Error surfaces for each pair of fitted parameters for a)-f) kinetics of inhibition experiment. Dotted line highlights the 95 %CL. The largest error value at the 95 %CL is reported for each parameter.

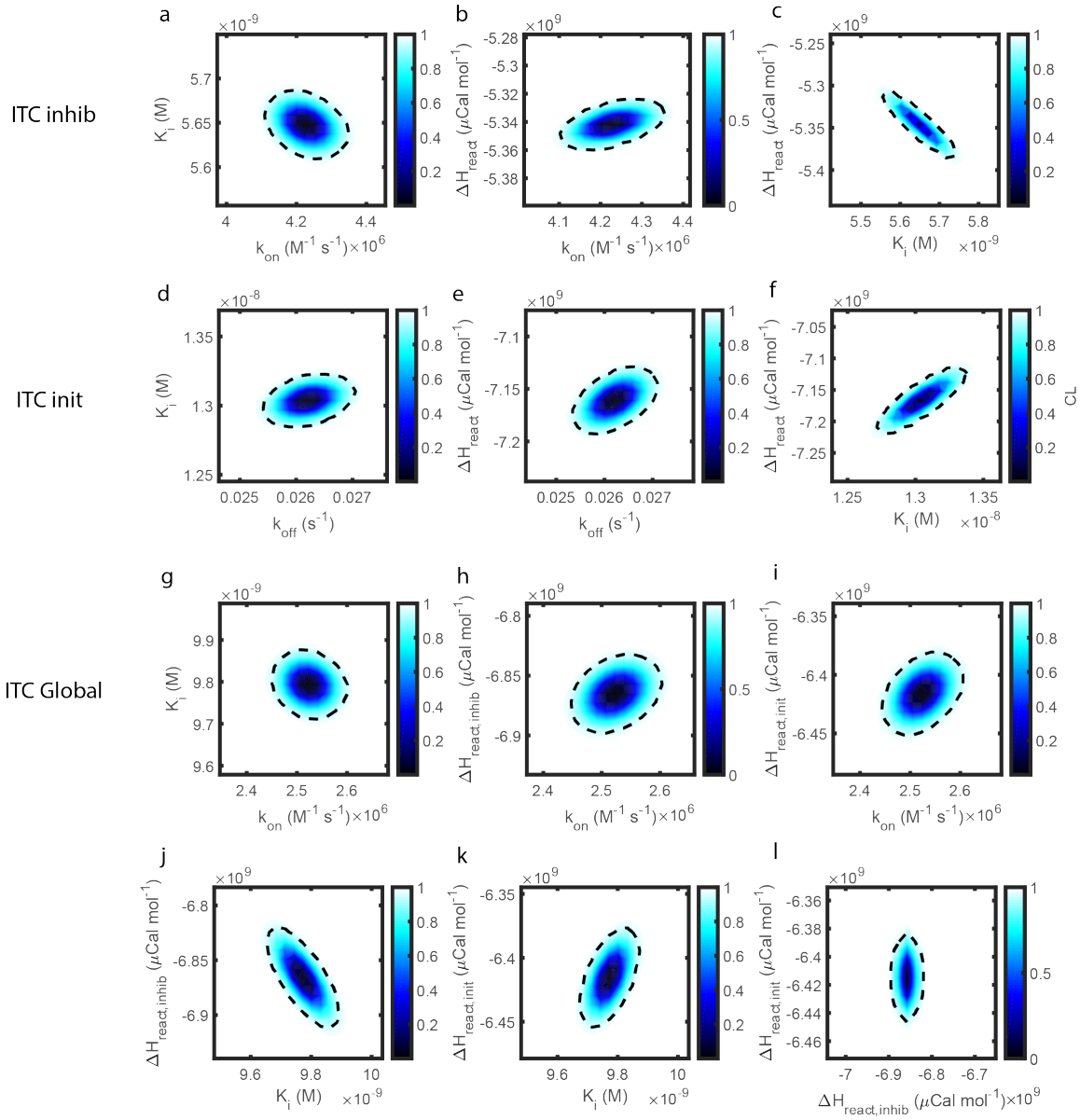

Figure 4.S22. Confidence level contour plots for ITC experiments using compound 4. Error surfaces for each pair of fitted parameters for a)-c) kinetics of inhibition experiment, d)-f) kinetics of initiation experiment and, g)-l) global fit between inhibition and initiation experiment. Dotted lines highlight the 95 %CL. The largest error value at the 95 %CL is reported for each parameter.

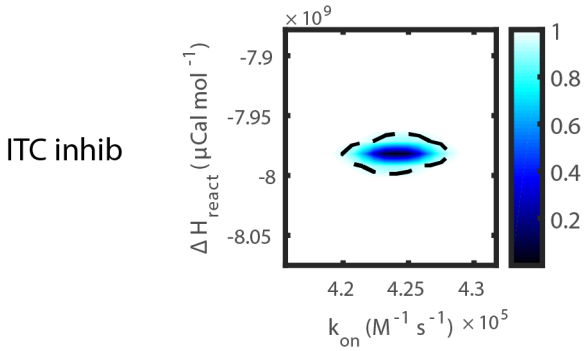

Figure 4.S23. Confidence level contour plots for ITC experiments using compound 5. Error surfaces for each pair of fitted parameters for kinetics of inhibition experiment. Dotted line highlights the 95%CL. The largest error value at the 95%CL is reported for each parameter.

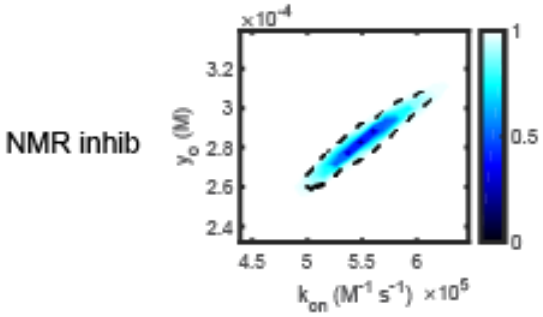

Figure 4.S24. Confidence level contour plots for NMR experiments using compound 5. Error surfaces for each pair of fitted parameters for kinetics of inhibition experiment. Dotted line highlights the 95 %CL. The largest error value at the 95 %CL is reported for each parameter.

Table 4.S3. Kinetic and thermodynamic parameters from global fits.

Cpd	Experiment	$k_{on} \cdot 10^5$ M^{-1} s^{-1}	$k_{off} \cdot 10^{-4}$ s^{-1}	K_i nM	ΔH_{cat} [a] kCal mol^{-1}
1	ITC inhib	1.68 ± 0.02	72 ± 1	42.6 ± 0.4	-6.32 ± 0.02
	& init Global				-6.18 ± 0.01
2	ITC inhib	–	–	618 ± 10	-6.79 ± 0.05
	& init Global				-11.07 ± 0.03
4	ITC inhib	25.2 ± 0.2	250 ± 8	9.72 ± 0.3	-6.85 ± 0.03
	& Global				-6.41 ± 0.02

[a] ΔH_{cat} are floated in order account for uncertainties in enzyme concentration as the magnitude of the heat flow is directly proportional to $[E_0] \cdot \Delta H_{cat}$. Since the inhibition and initiation experiments are run separately, different ΔH_{cat} correction terms can be obtained for the two experiments.

4.7 General Considerations

4.7.1 Introduction

The following is intended to assist potential users with experimental design and data interpretation and also explores the ranges of applicability for the techniques. Guidelines are given for selecting enzyme, substrate, and inhibitor concentrations, largely based on the Malvern ITC-200 instrument and the physical parameters of the POP/inhibitor system studied here (ΔH_{cat}, K_m, k_{cat}, k_{on} and K_i). We expect these guidelines to apply generally but the precise values will depend to some extent on the system under investigation and the instrument used. For POP, we estimate the upper and lower limits for measurable k_{on}, k_{off}, values to be ($8{\cdot}10^6$ and $3{\cdot}10^3$ M^{-1} s^{-1}) and (0.1 and $5{\cdot}10^{-4}$ s^{-1}) respectively. The lower limits for the K_i values are estimated to be 30 pM for inhibition experiments and 1 pM for initiation experiments respectively.

4.7.2 Instrument Parameters

4.7.2.1 Pre Injection Delay

For optimal results, it is advisable to allow the baseline to reach a steady power level prior to starting the experiment. We used long pre-injection delays of 1000-2000 s in order to ensure baseline stability.

4.7.2.2 Injection Volume

It is advisable to follow the minimum and maximum injection volume guidelines provided by the instrument manufacturer. Injections that are too large can produce artifacts due to temperature differences between the injectant and the cell contents. The largest injection size used in this study using the Malvern ITC-200 is 13 μL in the inhibition experiments with compound 1. Injections that are too small can lead to large relative errors in volume, partly due to diffusion of the injectant from the tip of the syringe between injections. We used a minimum injection size of 2 μL.

4.7.2.3 Spacing Between Injections

We recommend inter-injection spacing long enough for the signal to completely stabilize at each new plateau (according to the kinetics of the inhibitor) and to accurately evaluate the new baseline (and additional 200-300 s) after each injection.

4.7.3 Kinetic Limitations

4.7.3.1 Upper Kinetic Rate Limits

The upper and lower limits for rate constants are largely determined by the magnitude of the change in power signal, the instrument noise level, and the response time of the instrument. In order to estimate the minimum signal to noise ratio (SNR_{min}) required to extract reliable rate constants from single exponentially-decaying data,

a series of datasets were generated according to $S(t) = SNR \cdot e^{-k_{react} \cdot t} + \sigma(t)$, sampled in 1 s intervals, with $k_{react} = 0.1$ s^{-1}, SNR varying from 11 to 3.9, and values of $\sigma(t)$ drawn randomly from a Gaussian distribution with a mean of 0 and standard deviation of 1 (1000 curves for each SNR). Each curve was fit individually to $S_{fit}(t) = A \cdot e^{-k_{react} \cdot t}$ while floating the values of A and k_{react}. The relative error of k_{react} at each value of SNR was calculated as the standard deviation divided by the true value of the parameter (0.1 s^{-1}) (Figure 4.S25). We find that reliable rate constants can be extracted when the magnitude is at least 4-fold greater than the baseline noise, i.e. $SNR_{min} = 4$, which is consistent with experimental data (Figure 4.S26).

For estimating the upper kinetic limit, we take the short-timescale baseline noise to be $Q_{RMS} = 0.0017$ μCal s^{-1}. Assuming that the signal decays exponentially from the end of the injection (τ_{inj}) to the beginning of the analysis period (τ_{blank}, see above), i.e. for approximately $3 \cdot \tau_r$, where τ_r is the instrument response time, the maximum extractable rate is given by

$$k_{max} = (3 \cdot \tau_r)^{-1} \cdot ln\left(\frac{\Delta Q_{inj}}{SNR_{min} \cdot Q_{RMS}}\right) \tag{4.45}$$

The average ΔQ_{inj} over all compounds is ~0.1 μCal s^{-1} in this study, giving a rough upper limit of 0.9 s^{-1}, which corresponds to the maximum extractable dissociation rate. To estimate the maximum extractable association rate, we assume an inhibitor concentration of 11 nM (used for compound 3) giving an approximate maximum of $8.1 \cdot 10^6$ M^{-1} s^{-1} for similar systems.

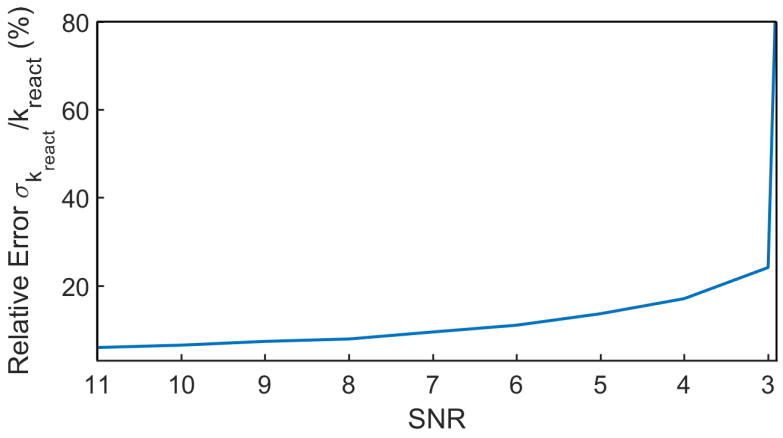

Figure 4.S25. Monte Carlo simulations of first order kinetics experiments. Relative error of the k_{react} vs the signal to noise ratio (SNR).

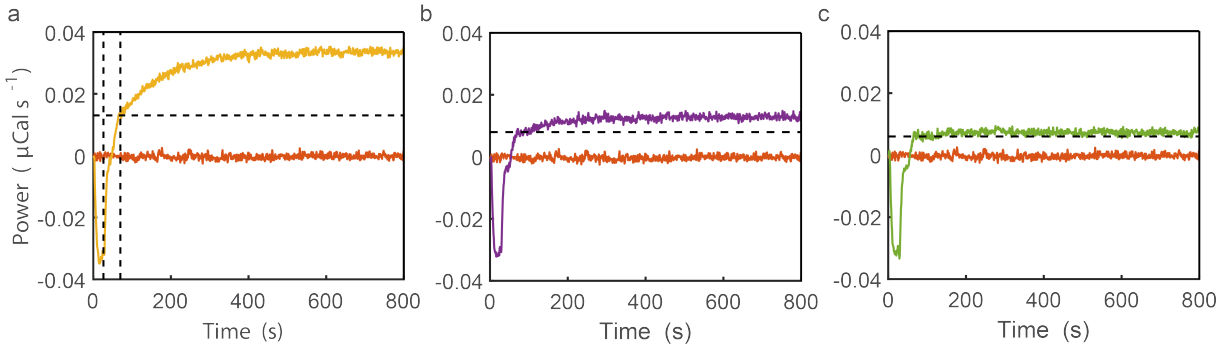

Figure 4.S26. Experimental confirmation of SNR_{min}. a) Second, b) third and c) fourth injection of kinetics of inhibition experiment using compound 1. Vertical dashed lines were placed at τ_{inj} and τ_{blank} in a). Horizontal dashed line was placed where the experimental curve passes τ_{blank} for all injections. The ΔQ_{inj} calculated as the difference between the maximum signal and the horizontal dashed line for a) is 0.029 μCal s^{-1}, b) is 0.008 μCal s^{-1} and c) is 0.0015 μCal s^{-1} making the SNR 17, 4.7 and 0.9 respectively. When individually fit the curves from panel a) and b) can be used to extract precise kinetic rates while c) cannot. This is consistent with the data form the simulations above.

4.7.3.2 Lower Kinetic Rate Limits

The lower limit for measurable kinetics is largely determined by the rate of baseline drift and the magnitude of the change in power signal. In order to estimate the

baseline drift, we performed several experiments consisting of long baseline measurements with no injections. We then calculated the root-mean-square deviation in power as a function of time according to

$$Q_{RMS}(\tau) = \sqrt{\langle \Big(Q(t) - Q(t+\tau) \Big)^2 \rangle} \tag{4.46}$$

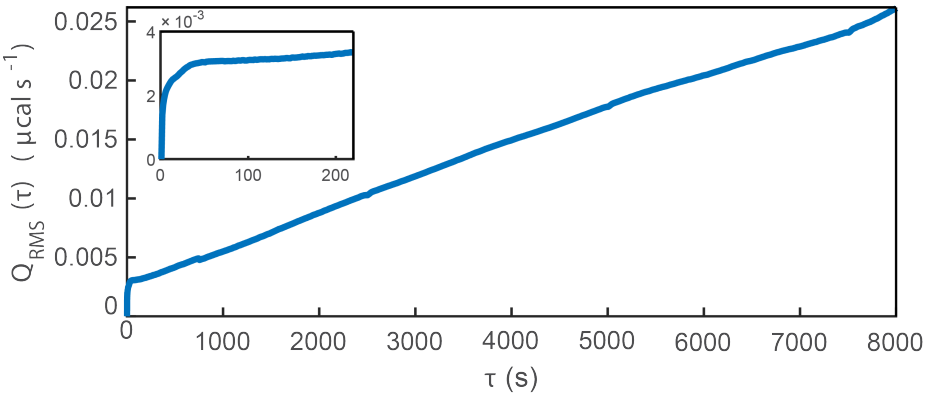

Figure 4.S27. Q_{RMS} vs. τ. 5·9000 s experiments with pre-injection delays of 2000 s with buffer described in the materials and methods section were run and analysed individually using equation 48 then averaged together. Only the first 8000 s is shown as the Q_{RMS} values become increasingly poorly defined for large τ. The inset shows first 220 s.

Q_{RMS} shows a rapid rise as short times due to random noise and fast-timescale fluctuations, followed by a more gradual increase corresponding to long-timescale drift, reaching 0.025 μCal s^{-1} after 8000 s. The kinetic ITC signals have 95% reached their new baselines after a length of time given by $4/k$. We can thus use a plot of $Q_{RMS}(\tau)$ and the magnitude of the signal, ΔQ_{total}, to estimate the longest accessible rate constants by finding the value of k_{min} which satisfies

$$Q_{RMS}\left(\tau = \frac{4}{k_{min}}\right) \cdot SNR_{min} = \Delta Q_{inj} \tag{4.47}$$

For the baseline measurements made here, Q_{RMS} appears to increases linearly with τ, the Q_{RMS} plot shown in Figure 4.S27 fits well to a line starting at $\tau = 50$ s yielding a slope and intercept of 2.89 $\cdot 10^{-6}$ and 2.99 $\cdot 10^{-3}$ respectively. Using an

average ΔQ_{inj} of 0.1 μCal $s^{-1}$and $Q_{RMS} = 0.0017$ μCal s^{-1}, this gives an approximate k_{min} of 5.26 $\cdot 10^{-4}$ s^{-1}, which corresponds to the minimum value of k_{off} and, for an inhibitor concentration of 193 nM (inhibition experiments with compound 5), this gives a minimum association rate of $2.73 \cdot 10^{3}$ M^{-1} s^{-1}.

4.7.4 Kinetics of Inhibition Experiments

4.7.4.1 Measuring Thermodynamic and Kinetic Properties for an Enzyme-Substrate Pair

It is recommended that the ΔH_{cat}, k_{cat} and K_m values are measured prior to designing experiments, for instance by the procedure of Gomez et al[16] (see 4.6.1).

4.7.4.2 Enzyme and Substrate Concentrations

Maximizing signal in inhibition experiments The sensitivity of the kinetics experiments is optimized by maximizing the changes in heat flow. In the case of inhibition experiments, this is achieved by maximizing the total heat flow due to catalysis

$$\Delta Q_{total} = \Delta H_{cat} \cdot V_{cell} \cdot \frac{k_{cat} \cdot [E_0]_{cell} \cdot [S]_{cell}}{K_m + [S]_{cell}} \tag{4.48}$$

Where ΔH_{cat} is the enthalpy of catalysis, V_{cell} is the volume of the cell, k_{cat} and K_m are the catalytic rate and Michaelis-Menten constant respectively, $[S]_{cell}$ is the total amount of substrate in the cell and $[E_0]_{cell}$ is the total amount of enzyme in the cell. This is particularly true as the signal is split into multiple ΔQ_{inj} increments. ΔQ_{total} can be optimized by maximizing the amount of enzyme and using saturating substrate concentrations. As well, when several different substrates are available, the ones with the largest $|\Delta H_{cat}|$ values are preferable. Under the experimental conditions used in this study we calculate the baseline noise level to be 0.0017 μCal s^{-1}. In the experiments presented here the smallest SNR was obtained in inhibition experiments with compound 2 (Figure 4.S8). Here the total $\Delta Q_{total} \approx 0.2$ μCal s^{-1},

$SNR \approx 67$. Split between 7 injections, this gives an average SNR per injection of just under 10.

Steady rate enzyme kinetics in inhibition experiments In order to achieve a steady baseline signal, substrate concentrations must remain either fully saturating or essentially constant at a sub-saturating level. Significant depletion of substrate over the course of an experiment it will lead to large baseline drift, making the results difficult to interpret. It is therefore important to ensure that

$$[S]_{cell} \gg \frac{k_{cat} \cdot \langle [E_0]_{cell} \rangle \cdot [S]_{cell}}{K_m + [S]_{cell}} \cdot \tau_{exp} \tag{4.49}$$

Where τ_{exp} is the total time of the experiment and angled brackets indicate the average free enzyme concentration over the course of the experiment. All of the experiments performed in this study were prepared such that the left hand side of Equation 4.49 is at 5-fold or more greater than the right hand side.

c-value and its implications for experimental design In standard ITC assays, the c-value is calculated as $\frac{K_d}{[M]}$, where K_d is the equilibrium dissociation constant and $[M]$ is the concentration of macromolecule in the cell. When designing enzyme inhibition kinetics studies, a modified c-value can be calculated as $IC_{50}/[E_0]$, as the amount of inhibitor needed to achieve 50% inhibition is not equal to the K_i, in general. For competitive inhibitors $IC_{50} = K_i \cdot (1 + \frac{[S]}{K_m})$, for uncompetitive inhibitors $IC_{50} = K_i \cdot (1 + \frac{[S]}{K_m})^{-1}$, and for noncompetitive inhibitors, $IC_{50} = K_i$. At very high c-values (greater than about 5.8), it becomes difficult to extract reliable K_i values (see 4.7.4.4). The c-value can be lowered by decreasing the concentration of enzyme and by altering concentration of substrate in the case of competitive and uncompetitive inhibitors.

4.7.4.3 Inhibitor Concentration

Tailoring inhibition kinetics The majority of the inhibition experiments performed in this study have a large excess of inhibitor compared to enzyme present in the cell. This means that the change in inhibitor concentration will be negligible throughout and during an injection making it possible to express the rate of inhibition in terms of a pseudo first order rate constant ($k'_{on} = k_{on} \cdot [I]_{cell}$) with units of s^{-1} where $[I]_{cell}$ is the concentration of inhibitor in the cell following each injection. It is therefore possible to tune the effective kinetics in the inhibition experiments by altering the concentration of inhibitor.

Decreasing inhibitor concentration For compounds with very rapid binding kinetics it is possible to decrease the inhibitor concentration such that k'_{on} is smaller than the upper kinetic rate limit (see 4.7.3.1). One difficulty with decreasing the inhibitor concentration is that it leads to a smaller change in the fractional inhibition of the enzyme and therefore a smaller signal (ΔQ_{inj}). For example, we were unable to measure the kinetics of inhibition for compound 2 due to its large K_i. High concentrations of inhibitor were required to achieve measurable ΔQ_{inj} signals, such that k'_{on} was far above the upper kinetics rate limit. In contrast, compound 4 bound much more tightly allowing much smaller concentrations of inhibitor to be used, such that k'_{on} was measurable.

Increasing inhibitor concentration In principle it is always possible to increase the inhibitor concentration such that k_{on}' is larger than the lower rate limit (see 4.7.3.2). In cases where both k_{on} and K_i are very low this may lead to K_i becoming experimentally inaccessible. Raising the concentration of a slow binding inhibitor in order to increase k'_{on} can lead to the enzyme becoming saturated with inhibitor after the first injection, as seen for compound 5.

4.7.4.4 Limitations for the K_i

Upper limit for K_i In principle, the only factor setting the upper limit for K_i (lower limit for affinity) is the magnitude of the changes in heat flow with each injection. This can be maximized by increasing the inhibitor concentration (limited by inhibitor solubility) and enzyme concentration (taking care not to overly deplete the substrate; see 4.7.4.2). For competitive inhibitors lowering the substrate concentration will help raise the c-value and increase the amount of binding with each injection, but will limit the amount of enzyme that can be used, due to substrate depletion during the experiment. In this study the highest K_i values we measured was for compound 2 (~650 nM). Lower affinities (larger K_i) are measurable but not necessarily of practical interest for drug design.

Monte Carlo simulations for the lower K_i limit The lower limit for measurable K_i values largely depends on the modified c-value (see 4.7.4.2). Note that the dependence on the c-value differs from ITC experiments performed in standard binding mode as these detect the heat released directly by binding whereas the kinetic assays detect binding indirectly as the change in heat released by catalysis. In order to map out the lower limit, we performed a Monte Carlo analysis in which data were simulated using POP enzymatic parameters, with baseline noise (0.0017 μCal s^{-1}), 1% error in the injection size (Malvern ITC-200 manual). Enzyme concentrations were set at 5 nM, substrate concentration at 25 mM, values of K_i varied from 10 nM to 10 pM, and inhibitor concentrations ranged 1 μM for high K_i simulations to 50 nM for low K_i simulations. In order save computational time a simplified (fast-limit) version of the inhibition model was used to simulate and fit data in which all injected inhibitor binds instantaneously. 1000 synthetic datasets were generated for each value of K_i. Each data set was fit individually and the relative error in K_i was calculated as the standard deviation divided by the value of the parameter (Figure 4.S28).

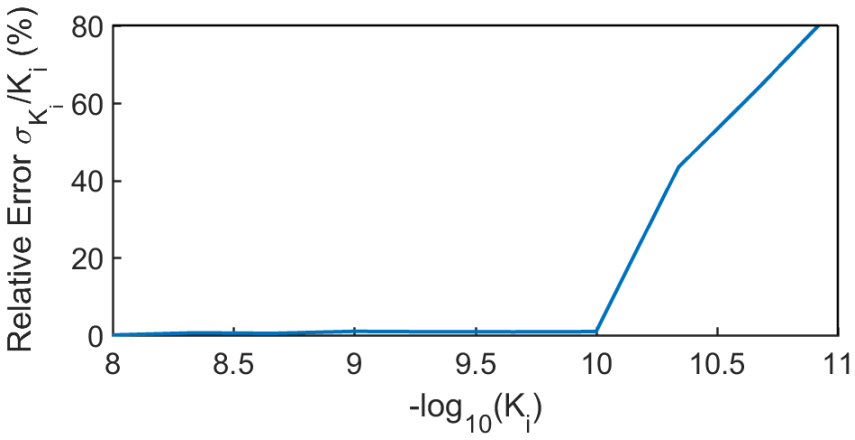

Figure 4.S28. Monte Carlo simulations of inhibition experiments. Relative error of the K_i vs the $-log_{10}(K_i)$.

Robust K_i values are obtained down to a value of about ~0.1 nM at which point the relative error begins to increase rapidly. At $-log_{10}(10.5)$ (32 pM) the relative error is approximately 50% making this an approximate lower limit measuring K_i with the kinetics of inhibition experiment Note that at the concentrations used in the simulation, this corresponds to a c-value of 5.8. Our lowest experimental K_i was 60 pM for compound 3. The estimated relative experimental error was approximately 15%, which is consistent with the errors calculated in these simulations. When measuring high affinities, it can be helpful to reduce the enzyme concentration as much as possible and to adjust the substrate concentration to increase the IC_{50}. (see 4.7.4.2).

4.7.4.5 Setting up Inhibition Experiments

1. Clean the isothermal titration calorimeter thoroughly as per manufacturer's instructions.

2. Pre-equilibrate isothermal titration calorimeter to the experimental temperature to help the baseline reach equilibrium more rapidly once the experiment is initiated.

3. Select experimental parameters – all the experimental parameters (injection

size, length etc. see 4.7.2) should be chosen at this time so that the experiment is ready to initialize.

4. Make enzyme and substrate solutions separately to ensure that substrate is not consumed prior to the experiment being initiated.

5. Load syringe with inhibitor – the inhibitor should be dissolved in a buffer that most closely matches the buffer in the cell in order to minimize dilution artifacts.

6. Mix enzyme and substrate to initiate catalysis.

7. Load the enzyme-substrate mixture into reaction cell.

8. Initiate experiment

4.7.5 Kinetics of Initiation Experiments

4.7.5.1 Measuring Thermodynamic and Kinetic Properties for an Enzyme-Substrate Pair

See 4.7.4.1

4.7.5.2 Enzyme and Substrate Concentrations

Maximizing signal in initiation experiments As for the kinetics of inhibition experiment, the total signal for a kinetics of initiation ITC experiment is maximized by using the largest concentrations of enzyme and substrate available. The magnitude of the signal can be calculated as above using Equation 4.48 (see 4.7.4.2), calculating $[E_0]_{syr} \cdot (1 - e^{\frac{-v_{inj}}{V_{cell}}})$ where v_{inj} is the total volume injected throughout the experiment.

Steady rate enzyme kinetics in initiation experiments Similarly to the kinetics of inhibition experiments, substrate concentrations must remain constant or saturating in kinetics of initiation experiments in order to keep a steady rate of catalysis (see 4.7.4.2). Equation 4.49 can once again be used, calculating $[E_0]_{cell}$ as $[E_0]_{syr} \cdot (1 - e^{\frac{-v_{inj}}{V_{cell}}})$. All of the experiments performed in this study were prepared such that the left hand side of Equation 4.49 is at a minimum over 5 times the right hand side. This introduces an upper limit for the enzyme concentration and a lower limit for the substrate concentration initiation experiments.

Substrate concentration In principle having a large substrate concentration is always advantageous in kinetics of initiation experiments, this is because it maximizes signal and ensures steady rate kinetics (see above). In the case of competitive inhibitors, high concentrations of substrate also favour enzyme-inhibitor dissociation (see 4.7.5.4).

4.7.5.3 Limitations for the K_i

Upper limit for K_i Similarly to the kinetics of inhibition experiments, the main factor setting the upper limit for K_i (lower limit for affinity) is the magnitude of the changes in heat flow with each injection. This can be maximized by increasing the concentrations of inhibitor and enzyme in the syringe, taking care not to overly deplete the substrate. For competitive inhibitors increasing the substrate concentration will help lower the c-value and increase the amount of dissociation that occurs with each injection (see 4.7.5.4). In this study the highest K_i value we measured was for compound 2 (≈675 nM). Lower affinities (larger K_i) are measurable but not necessarily of practical interest for drug design.

Monte Carlo simulations for the lower K_i limit In order to estimate the lowest K_i values measurable by this technique, we performed a Monte Carlo analysis in which

data were simulated using POP enzymatic parameters, with baseline noise (0.0017 μCal s^{-1}) and 1% error in the size in the injection (Malvern ITC-200 manual). Simulated values of K_i varied from 10 nM to 0.1 pM with enzyme concentrations ranging from 800 nM for the high K_i to 400 nM for the low K_i. Inhibitor concentrations were set to $1.2 \cdot [E_0]_{syr}$ and the substrate to 20 mM. In order save computational time a simplified (fast-limit) version of the initiation model was used to simulate and fit data in which all injected EI complex dissociates instantaneously. 1000 synthetic datasets were generated for each value of K_i. Each data set was fit individually and the relative error in K_i was calculated as the standard deviation divided by the value of the parameter (Figure 4.S29).

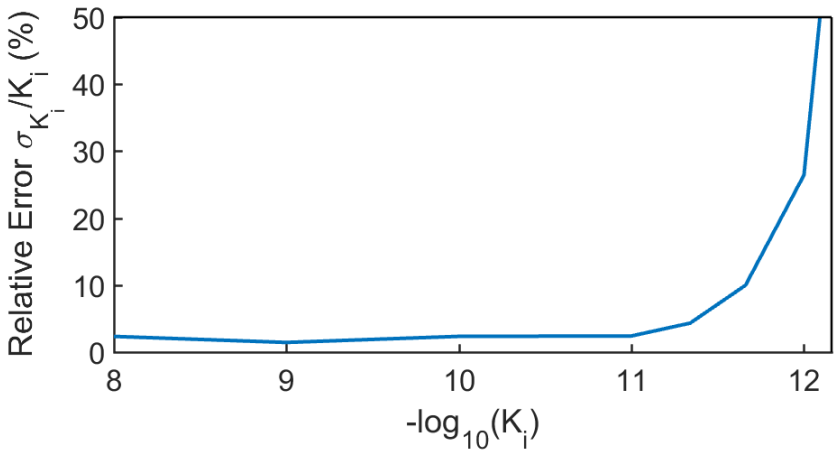

Figure 4.S29. Monte Carlo simulations of initiation experiments. Relative error of the K_i vs. the $-log_{10}(K_i)$.

K_i values are accurately reproduced down to a value of about 0.01 nM, at which point the relative error begins to increase sharply. At $\sim -log_{10}(12)$ (1 pM) the relative error is approximately 30% making this an approximate lower limit for extractable K_i using the kinetics of inhibition experiment. In this study the lowest K_i we measured was 13 nM using compound 4. This is far above the limit calculated in the simulation above. Note that the compounds that bound more tightly exhibited dissociation rates that were too slow to measure (compound 3 and 5).

4.7.5.4 Optimizing Signal due to Dissociation

Dissociation of enzyme-inhibitor complex due to dilution The magnitude of the signal in a kinetics of initiation experiment depends on the number of injected EI complexes that dissociate following an injection. Thus it is advisable to maximize the dilution factor by setting the injection volume to the minimum value recommended (see 4.7.2.2). The concentration of the inhibitor should ideally be several-fold larger than the K_i in the syringe to maximize binding and on the order of the IC_{50} or lower in the cell after the injection to ensure that dissociation occurs. Note that dilution from $100 \cdot K_i$ to $10 \cdot IC_{50}$ does not lead to much dissociation. For competitive inhibitors, maximizing the concentration of substrate increases the IC_{50} and promotes dissociation. The concentration of enzyme in the syringe is ideally at a maximum, provided that it is lower than the concentration of the inhibitor in the syringe and does not overly deplete the substrate in the cell (see 4.7.5.2).

4.7.5.5 Setting up Initiation Experiments

1. Pre-incubate enzyme and inhibitor allowing for sufficient time for the enzyme-complex to form. In our study we pre-incubate for approximately two hours.**

2. Clean the isothermal titration calorimeter thoroughly as per manufacturer's instructions.

3. Pre-equilibrate isothermal titration calorimeter to the experimental temperature to help the baseline reach equilibrium more rapidly once the experiment is initiated.

4. Select experimental parameters – all the experimental parameters (injection size, length etc. see 4.7.2) should be chosen at this time so that the experiment is ready to initialize.

5. Load syringe with the enzyme-inhibitor complex – this should be prepared in buffer that most closely matched the buffer in the cell in order to minimize

dilution artifacts.

6. Add substrate solution to reaction cell.

7. Initiate experiment.

**In the case of enzyme-inhibitor pairs with extremely slow association kinetics longer pre-incubation times may be necessary.

4.7.6 Data Analysis Workflow

1. Data extraction – only the raw output provided by the instrument (power as a function of time) is needed for analysis.

2. Baseline correction – generally data must be baseline corrected (see 4.5.4).

   (a) The last portion of each injection (see 4.7.2.3) should now be a flat horizontal line (Figure 4.4).

   (b) The injections can either be analysed as a single continuous experiment or each injection as a separate experiment with different initial conditions.

3. Blank subtraction – blank experiments can be performed (identically to actual experiments with either no enzyme or no substrate; see 4.5.5) –for determination of start-points for data analysis.

4. The kinetic trace(s) can now be fit in order to extract thermodynamic and kinetic information (see 4.5.7).

4.8 References

[1] Hao Lu and Peter J. Tonge. “Drug–target residence time: critical information for lead optimization”. In: *Current Opinion in Chemical Biology* 14.4 (2010), pp. 467–474.

[2] Per-Olof Markgren et al. “Relationships between Structure and Interaction Kinetics for HIV-1 Protease Inhibitors”. In: *Journal of Medicinal Chemistry* 45.25 (2002), pp. 5430–5439.

[3] Robert A. Copeland, David L. Pompliano, and Thomas D. Meek. “Drug-target residence time and its implications for lead optimization”. In: *Nature Review Drug Discovery* 5.9 (2006), pp. 730–739.

[4] Peter J. Tummino and Robert A. Copeland. “Residence Time of Receptor−Ligand Complexes and Its Effect on Biological Function”. In: *Biochemistry* 47.20 (2008), pp. 5481–5492.

[5] D. C. Swinney. “The role of binding kinetics in therapeutically useful drug action”. In: *Current Opinion in Drug Discovery & Development* 12.1 (2009), pp. 31–39.

[6] Robert A. Copeland. “The dynamics of drug-target interactions: drug-target residence time and its impact on efficacy and safety”. In: *Expert Opinion on Drug Discovery* 5.4 (2010), pp. 305–310.

[7] John V. Schloss. “Significance of slow-binding enzyme inhibition and its relationship to reaction-intermediate analogs”. In: *Accounts of Chemical Research* 21.9 (1988), pp. 348–353.

[8] John F. Morrison. “The slow-binding and slow, tight-binding inhibition of enzyme-catalysed reactions”. In: *Trends in Biochemical Sciences* 7.3 (1982), pp. 102–105.

[9] Elisabeth V. Schneider et al. “Structure–kinetic relationship study of CDK8/CycC specific compounds”. In: *Proceedings of the National Academy of Sciences* 110.20 (2013), pp. 8081–8086.

[10] Maris Vilums et al. “Structure–Kinetic Relationships—An Overlooked Parameter in Hit-to-Lead Optimization: A Case of Cyclopentylamines as Chemokine Receptor 2 Antagonists”. In: *Journal of Medicinal Chemistry* 56.19 (2013), pp. 7706–7714.

[11] Peter J. Tonge. “Drug–Target Kinetics in Drug Discovery”. In: *ACS Chemical Neuroscience* 9.1 (2017), pp. 29–39.

[12] Phillip A. Schwartz et al. “Covalent EGFR inhibitor analysis reveals importance of reversible interactions to potency and mechanisms of drug resistance”. In: *Proceedings of the National Academy of Sciences* 111.1 (2014), pp. 173–178.

[13] Robert A. Copeland. *Kinetics of Single-Substrate Enzyme Reactions*. Enzymes. John Wiley & Sons, Inc., 2002, pp. 109–145.

[14] Ondine Harris Callan, On-Yee So, and David C. Swinney. “The Kinetic Factors That Determine the Affinity and Selectivity for Slow Binding Inhibition of Human Prostaglandin H Synthase 1 and 2 by Indomethacin and Flurbiprofen”. In: *Journal of Biological Chemistry* 271.7 (1996), pp. 3548–3554.

[15] Jarkko I VenäLäInen et al. “Slow-binding inhibitors of prolyl oligopeptidase with different functional groups at the P1 site”. In: *Biochemical Journal* 382.Pt 3 (2004), pp. 1003–1008.

[16] Matthew J. Todd and Javier Gomez. “Enzyme Kinetics Determined Using Calorimetry: A General Assay for Enzyme Activity?” In: *Analytical Biochemistry* 296.2 (2001), pp. 179–187.

[17] Søren N. Olsen. “Applications of isothermal titration calorimetry to measure enzyme kinetics and activity in complex solutions”. In: *Thermochimica Acta* 448.1 (2006), pp. 12–18.

[18] Yi Liang. “Applications of isothermal titration calorimetry in protein science”. In: *Acta Biochimica et Biophysica Sinica* 40.7 (2008), pp. 565–576.

[19] Janice Lawandi et al. “Inhibitors of Prolyl Oligopeptidases for the Therapy of Human Diseases: Defining Diseases and Inhibitors”. In: *Journal of Medicinal Chemistry* 53.9 (2010), pp. 3423–3438.

[20] Satoshi Tanaka, Kanayo Suzuki, and Minoru Sakaguchi. “The prolyl oligopeptidase inhibitor SUAM-14746 attenuates the proliferation of human breast cancer cell lines in vitro”. In: *Breast Cancer* 24.5 (2017), pp. 658–666.

[21] Juswinder Singh et al. “The resurgence of covalent drugs”. In: *Nat Rev Drug Discov* 10.4 (2011), pp. 307–317.

[22] James G. Robertson. “Mechanistic Basis of Enzyme-Targeted Drugs”. In: *Biochemistry* 44.15 (2005), pp. 5561–5571.

[23] Stephane De Cesco et al. “Covalent inhibitors design and discovery”. In: *European Journal of Medicinal Chemistry* 138 (2017), pp. 96–114.

[24] Petr Kuzmič, James Solowiej, and Brion W. Murray. “An algebraic model for the kinetics of covalent enzyme inhibition at low substrate concentrations”. In: *Analytical Biochemistry* 484 (2015), pp. 82–90.

[25] John M. Strelow. “A Perspective on the Kinetics of Covalent and Irreversible Inhibition”. In: *SLAS DISCOVERY: Advancing Life Sciences R&D* 22.1 (2016), pp. 3–20.

[26] Razif R Gabdoulline and Rebecca C Wade. “On the protein-protein diffusional encounter complex”. In: *Journal of Molecular Recognition* 12.4 (1999), pp. 226–234.

[27] A. V. Bakker et al. “Slow tight-binding inhibition of prolyl endopeptidase by benzyloxycarbonyl-prolyl-prolinal”. In: *Biochemical Journal* 271.2 (1990), pp. 559–562.

[28] Kirk A. Vander Meulen and Samuel E. Butcher. “Characterization of the kinetic and thermodynamic landscape of RNA folding using a novel application of isothermal titration calorimetry”. In: *Nucleic Acids Research* 40.5 (2012), pp. 2140–2151.

[29] Dominique Burnouf et al. “kinITC: a new method for obtaining joint thermodynamic and kinetic data by isothermal titration calorimetry”. In: *Journal of the American Chemical Society* 134.1 (2011), pp. 559–565.

[30] Justin M. Di Trani, Nicolas Moitessier, and Anthony K. Mittermaier. “Measuring Rapid Time-Scale Reaction Kinetics Using Isothermal Titration Calorimetry”. In: *Analytical Chemistry* 89.13 (2017), pp. 7022–7030.

[31] W. Bruce Turnbull and Antonio H. Daranas. “On the Value of c: Can Low Affinity Systems Be Studied by Isothermal Titration Calorimetry?” In: *Journal of the American Chemical Society* 125.48 (2003), pp. 14859–14866.

[32] Adrian Velazquez-Campoy and Ernesto Freire. “Isothermal titration calorimetry to determine association constants for high-affinity ligands”. In: *Nat. Protocols* 1.1 (2006), pp. 186–191.

[33] Ken A. Dill and Sarina Bromberg. *Molecular driving forces : statistical thermodynamics in biology, chemistry, physics, and nanoscience*. London; New York: Garland Science, 2011.

[34] George E. P. Box, William Gordon Hunter, and J. Stuart Hunter. *Statistics for experimenters : an introduction to design, data analysis, and model building*. New York: Wiley, 1978.

Chapter 5

Conclusions

5.1 Conclusions and Contributions to Knowledge

This thesis describes several novel ITC-based methods for extracting enzyme kinetics and quantifying thermodynamic/kinetic properties of enzyme inhibitors. Each of the three research based chapters (2, 3 and 4) contains contributions to scientific knowledge that can be subdivided into different categories as follows. 1) Development of rapid techniques to assist in lead generation/optimization in drug development, 2) ITC instrument analysis including rigorous mathematical approaches for modelling isothermal titration calorimeter output and simulating errors, and 3) biophysical exploration of prolyl oligopeptidase (POP) kinetics and POP-inhibitor interactions. The following discusses the individual contributions from each chapter as they pertain to these categories.

5.1.1 Chapter 2: Measuring Rapid Time-scale Reaction Kinetics Using Isothermal Titration Calorimetry

In this research chapter we test the time resolution of several commercial calorimeters and find they are capable of sub-section accuracy indicating that, in theory, it is possible to quantitatively model rapid time-scale kinetics. While applying conventional fitting approaches to rapid enzyme kinetics we find there are systematic deviations in the shape of modelled peaks. To rectify this we performed rigorous experimental testing in order to develop the ITC empirical response model (ITC-ERM) approach for modelling peaks. Importantly, this approach allows us to quantitatively model rapid kinetics and accurately extract MM parameters. In addition, the maximum rates extractable using the ITC-ERM approach were also calculated for several common applications; enzyme catalysis and single-site binding. Furthermore, we apply the ITC-ERM approach to POP which allows for discovery of non-Michaelis-Menten kinetics at high concentrations of enzyme.

This research is the first to demonstrate the sub-second accuracy of ITC and provides a novel procedure for quantitatively modelling rapid time-scale kinetics. In principle, the ERM approach can be implemented into to any kinetic ITC appli-

cation, such as those presented in chapters 3 and 4. In addition, the experimental error of the measured response function can be used in error propagation for any experiment, as demonstrated by the error estimation simulations. Lastly, this is the first study to reveal POP's deviation from ordinary Michaelis-Menten kinetics.

5.1.2 Chapter 3: Complete Kinetic Characterization of Enzyme Inhibition in a Single Isothermal Titration Calorimetry Experiment

In chapter 3 we developed a new technique for rapidly extracting the strength and mode of enzyme inhibitors, allowing for a 5-fold reduction in time and sample relative to other ITC-based methods. In addition, we present an ERM-deconvolution procedure for extracting the instantaneous heat from ITC output data. We apply the deconvolution procedure to produce LWB plots, allowing for visual assessment of the inhibition mode. Furthermore, we explore limitations of the technique through various simulations and calculations.

This rapid ITC based technique is optimal for use in the drug design and development process. With the recent development of automated ITC instruments this technique can be easily used in screening assays as well as in lead generation and optimization. Lastly, the deconvolution technique can be used to calculate the instantaneous heat from virtually any ITC trace and therefore be applied to any technique.

5.1.3 Chapter 4: Rapid Measurement of Inhibitor Binding Kinetics by Isothermal Titration Calorimetry

The pair of techniques presented in this chapter can be used to measure the kinetics of inhibition and initiation for enzyme inhibitors. We validate the accuracy of the techniques using established methods then develop a SKR for POP inhibitors. This leads to the discovery that covalent warheads can enhance inhibition rates, further demonstrating the utility of covalent inhibitors. Furthermore, we test limitations of

the techniques through extensive simulations and calculations and provide guidelines for future users.

This study provides an ITC based method, for producing SKRs of enzyme inhibitors, which approaches the time resolution of stopped-flow experiments and possess all the inherent advantages of measuring heat. Through validation of the techniques we illustrate that calorimetric measurements are exceptionally sensitive to changes in enzyme activity compared to spectroscopic techniques. In addition, we further biophysical knowledge of POP inhibitors for guidance in future drug development efforts. Lastly, the procedures for simulating errors may be applied to other kinetic ITC applications.

5.2 Future Directions

5.2.1 Custom ITC Methodologies

ITC is capable of making measurements under experimental conditions that would be difficult or impossible using other techniques.[1,2,3,4,5,6,7] In addition, ITCs are equipped with precise injectors and can measure rapid kinetics as demonstrated in chapter 2. These features make ITC an ideal technique to use in custom applications for measuring specific properties of enzymes. Currently, in the Mittermaier lab there are custom ITC-based techniques being developed in order to elucidate novel properties of specific systems which are described below.

Aminoglycoside phosphotransferase-3'a (APH-3'a) and pantothenate kinase (PanK) are bi-substrate phosphokinases responsible for antibiotic resistance, and Coenzyme A (CoA) regulation respectively. Normally, these systems are studied using a coupled assay[8] which work by depleting one of the products, ADP, in a series of reactions that eventually lead to the depletion of NADH with a strong absorbance at 340 nm. A graduate student Yun Wang has diverted from conventional assays and started using ITC to study the catalytic activity of these systems. When using ITC to study these systems it is not necessary to use a coupled assay making it possible to

measure enzyme activity in the presence of ADP. The effect of ADP has been tested by performing multiple injections of substrate into enzyme which has led to the discovery of product inhibition and as well as product induced positive cooperativity in these systems.

There is another technique currently being developed in the Mittermaier group by Caroline Dufrense, a graduate student. In this technique enzyme is loaded into the syringe and inhibitor+substrate into the cell. When an injection is made enzyme will catalyze the reaction while becoming deactivated by inhibitor. Importantly, the total amount of heat produced by catalysis will be inversely related to the effective association rate. Therefore, by measuring the amount of heat produced by a single injection it is possible to extract the association rate of the inhibitor. Furthermore, by performing multiple injections it is possible to measure the association rate at several different concentrations of free inhibitor, allowing for full characterization of multi-step binding interactions such as covalent inhibitors of POP. Also, importantly, by using the total heat as a probe it is possible to extract the association rates of reactions that would normally occur too rapidly to measure directly.

The ITC expertise gained by the Mittermaier lab over the past few years puts the lab in a position to help other groups investigate particular systems using ITC. This means that any biochemistry laboratory or company can approach the lab with questions about specific systems that would be difficult to answer using other techniques. Members of the Mittermaier group can then assess whether the system is amenable to measurement using ITC, followed by the design, implementation, and analysis of custom ITC assays.

5.2.2 Kinetic ITC Software Development

As mentioned above there are several publicly available software packages designed for processing raw data,[9] analyzing thermodynamic data,[9,10] producing publication quality figures,[9,10] extracting MM parameters from enzyme kinetics data,[10] and quantifying binding rates.[7] One noteworthy integrated software package has been

recently developed by the Schuck lab at the National Institutes of Health.[11] The software contains three different modules, NITPIC; which allows for baseline correction of ITC data using automated peak shape analysis, SEDPHAT; software for extracting global thermodynamic parameters from sets of isotherms, and GUSSI; which allows for visualization of data and produces publication quality figures. This software package is seamless allowing for a complete data analysis; beginning with raw data and ending with publication quality figures. Similar software can be developed to help users perform and analyze the methods presented in this thesis and those currently being developed in the lab. The software can be designed in a way to make implementation of new methods simple, allowing for other members of the ITC community to add their own techniques. Eventually this can lead to an integrated software able to assist in the analysis of a wide variety of different methods for measuring kinetics. Furthermore, this software can be merged with the software produced by the Schuck lab making it even more complete.

5.2.3 Instrumentation Drawbacks and Future Design

Modern calorimeters are designed for rapidly measuring the total heat produced or absorbed by a reaction and are specifically optimized for binding applications. In addition, these calorimeters are well suited for kinetic applications as they are equipped with a stirring apparatus and a rapid compensation system. However, ITCs are not perfect and there are several instrument-derived sources of experimental artefacts that can compromise the accuracy of both thermodynamic and kinetic measurements. One source of error is diffusion of the syringe species into the sample cell both during the instrument equilibration period and in-between injections. Diffusion during the equilibration period can be worked around by ignoring the first injection during data analysis however, diffusion between injections is typically not accounted for when making thermodynamic measurements. This simplification doesn't appear to effect thermodynamic measurements however, kinetic applications are more likely to have long periods between injections allowing for more diffusion to

occur. There are two ways next generation calorimeters can circumvent this problem, 1) with different hardware such as smaller syringe tip openings, or 2) software that allows for a small withdrawal of cell solution after an injection. Fortunately, the maximum time between any injections performed in this thesis are on the same order as most thermodynamic experiments. However, when doing experiments with longer injections using the current generation of calorimeters it may be necessary to incorporate diffusion when modelling the instrument output. Another shortcoming of modern calorimeters is that the majority of the syringe contents (87.5% in the ITC-200) are not equilibrated at the same temperature as the cell. As a result of this, performing experiments far from room temperature can lead to artefacts due to mixing species of different temperatures in the cell. Amending this in future generations of instruments requires equilibrating the syringe contents at the same temperature as the cell.

5.3 References

[1] Thomas Wiseman et al. “Rapid measurement of binding constants and heats of binding using a new titration calorimeter”. In: *Analytical Biochemistry* 179.1 (1989), pp. 131–137.

[2] Apiradee Wangsakan, Pavinee Chinachoti, and David J. McClements. “Isothermal titration calorimetry study of the influence of temperature, pH and salt on maltodextrin–anionic surfactant interactions”. In: *Food Hydrocolloids* 20.4 (2006), pp. 461–467.

[3] Søren N. Olsen. “Applications of isothermal titration calorimetry to measure enzyme kinetics and activity in complex solutions”. In: *Thermochimica Acta* 448.1 (2006), pp. 12–18.

[4] Matthew J. Todd and Javier Gomez. “Enzyme Kinetics Determined Using Calorimetry: A General Assay for Enzyme Activity?” In: *Analytical Biochemistry* 296.2 (2001), pp. 179–187.

[5] Leigh Murphy et al. “An enzymatic signal amplification system for calorimetric studies of cellobiohydrolases”. In: *Analytical Biochemistry* 404.2 (2010), pp. 140–148.

[6] Hassan Rana et al. “Isothermal titration calorimetry uncovers substrate promiscuity of bicupin oxalate oxidase from Ceriporiopsis subvermispora”. In: *Biochemistry and Biophysics Reports* 5 (2016), pp. 396–400.

[7] Dominique Burnouf et al. “kinITC: a new method for obtaining joint thermodynamic and kinetic data by isothermal titration calorimetry”. In: *Journal of the American Chemical Society* 134.1 (2011), pp. 559–565.

[8] J. G. Nørby. “Coupled assay of Na+,K+-ATPase activity”. In: *Methods in enzymology* 156 (1988), pp. 116–9.

[9] Huaying Zhao, Grzegorz Piszczek, and Peter Schuck. “SEDPHAT – a platform for global ITC analysis and global multi-method analysis of molecular interactions”. In: *Methods* 76 (2015), pp. 137–148.

[10] MicroCal. *ITC Data Analysis in Origin*. 1998.

[11] Chad A. Brautigam et al. *Integration and global analysis of isothermal titration calorimetry data for studying macromolecular interactions*.